Quantitative analysis of vestibular pathways and behavior in mice: implications for understanding basic physiology and disease

Hui Ho Vanessa Chang

Department of Physiology
McGill University
Montreal, Quebec, Canada

August 2022

A thesis submitted to McGill University
in partial fulfillment of the requirements of the degree of
Doctor of Philosophy

Table of contents

List of figures

Chapter 1

Chapter 2

Chapter 3

List of tables

Appendix A

Abstract

The vestibular peripheral sensors in the inner ears provide head motion information to the brain to generate reflexes for gaze and postural stabilization and to contribute to self-motion perception. The system also possesses impressive adaptive capability as it interacts with various parts of the brain, including the cerebellum and its efferent pathways in the brainstem. Current knowledge of the vestibular system is based on experimental approaches using a wide range of animal models, from fishes to nonhuman primates. Specifically, mouse models have been widely used given their accessibility and abundant genetic resources. Thus, studies presented in the thesis used a mouse model and aimed at investigating: 1) signals relayed from the vestibular organs to ascending vestibular pathways that contribute to self-motion perception, (2) effects of spinocerebellar ataxia type 6 on vestibular functions, and finally, (3) functional roles of the efferent vestibular system in mice.

First, I studied signals projecting through the nucleus prepositus hypoglossi to the dorsal tegmental nucleus in mice. This anatomical projection originating from the vestibular organs was proposed to provide the vestibular signal to the head direction network, which then generates an estimate of spatial orientation. To test this view in mice, I designed experimental setups, including acute implants of high-density silicon Neuropixel probes. Using the setups, I demonstrate that mouse nucleus prepositus hypoglossi neurons predominately encode eye position and velocity. This finding is consistent with the role of the nucleus prepositus hypoglossi as the velocity-to-position neural integrator in other species like nonhuman primates.

The second focus of my thesis was to identify vestibular dysfunctions and possible neural mechanisms underlying vestibular dysfunctions in a mouse model of spinocerebellar ataxia type 6 (SCA6). I found this mouse model displays vestibular deficits such as reduced gain of the vestibulo-ocular reflex (VOR) and impaired VOR learning. I then found that Purkinje cells in the flocculus of the cerebellum also fire less regularly in the mouse model

of SCA6. These results reveal the widespread effect of SCA6 in the mouse mutant, and loss of firing precision may give rise to abnormal phenotypes.

Finally, I studied vestibular functions in mice lacking an α9 subunit of the nicotinic acetylcholine receptor (nAChRs) to understand the functional roles of the mammalian efferent vestibular system as α9 containing nAChRs are widely expressed in the efferent system. I first quantified VOR responses of α9 knockout mice and found there is no effect of loss of the α9 subunit on gaze stability. However, when α9 knockout mice were tested for their ability to maintain balance and posture, the mouse mutant showed impaired posture with altered head movement dynamics. These results suggest the loss of the α9 subunit predominantly results in impairments in postural rather than gaze stability.

Taken together, the results of my thesis strengthen the current understanding of the functional roles of nucleus prepositus hypoglossi and sensory processing in ascending vestibular pathways. By demonstrating that mouse nucleus prepositus hypoglossi predominantly encodes eye movements, it fills a gap between literature in the field of navigation and oculomotor functions. My findings also provide insight into pathophysiological alteration underlying SCA6 and the functional roles of the mammalian efferent vestibular system.

Résumé

Les capteurs vestibulaires périphériques situés dans les oreilles internes fournissent des informations sur les mouvements de la tête au cerveau afin de générer des réflexes de stabilisation du regard et de la posture et de contribuer à la perception des mouvements de soi. Le système possède également une impressionnante capacité d'adaptation car il interagit avec diverses parties du cerveau, notamment le cervelet et ses voies efférentes dans le tronc cérébral. Les connaissances actuelles sur le système vestibulaire reposent sur des approches expérimentales utilisant un large éventail de modèles animaux, des poissons aux primates non humains. Plus précisément, les modèles de souris ont été largement utilisés en raison de leur accessibilité et de l'abondance de leurs ressources génétiques. Ainsi, les études présentées dans la thèse ont utilisé un modèle de souris et ont eu pour but d'étudier: 1) les signaux relayés des organes vestibulaires aux voies vestibulaires ascendantes qui contribuent à la perception du mouvement propre, 2) les effets de l'ataxie spinocérébelleuse de type 6 sur les fonctions vestibulaires, et enfin, 3) les rôles fonctionnels du système vestibulaire efférent chez la souris.

Tout d'abord, j'ai étudié les signaux se projetant à travers le noyau prépositus hypoglossi vers le noyau tegmental dorsal chez la souris. Cette projection anatomique provenant des organes vestibulaires a été proposée pour fournir le signal vestibulaire au réseau de direction de la tête, qui génère ensuite une estimation de l'orientation spatiale. Pour tester ce point de vue chez les souris, j'ai conçu des montages expérimentaux, y compris des implants aigus de sondes Neuropixel en silicium à haute densité. À l'aide des configurations, je démontre que les neurones hypoglossi prépositus du noyau de la souris codent principalement la position et la vitesse des yeux. Cette constatation est cohérente avec le rôle du nucleus prepositus hypoglossi en tant qu'intégrateur neuronal de la vélocité à la position chez d'autres espèces comme les primates non humains.

Le deuxième axe de ma thèse consistait à identifier les dysfonctionnements vestibulaires et les éventuels mécanismes neuronaux sous-jacents aux dysfonctionnements vestibulaires dans un modèle murin d'ataxie spinocérébelleuse de type 6 (SCA6). J'ai

découvert que ce modèle de souris présente également des déficits vestibulaires tels qu'un gain réduit du réflexe vestibulo-oculaire (VOR) et une altération de l'apprentissage du VOR. J'ai ensuite découvert que les cellules de Purkinje dans le flocculus du cervelet émettent également des signaux moins réguliers dans le modèle de souris SCA6. Ces résultats révèlent l'effet généralisé de SCA6 chez le mutant de souris, et la perte de précision de tir peut donner lieu à des phénotypes anormaux.

Enfin, j'ai étudié les fonctions vestibulaires chez des souris dépourvues de la sous-unité α9 du récepteur nicotinique de l'acétylcholine (nAChRs) afin de comprendre les rôles fonctionnels du système vestibulaire efférent des mammifères, les nAChRs contenant α9 étant largement exprimés dans le système. J'ai d'abord quantifié les réponses VOR des souris knockout α9 et j'ai constaté qu'il n'y a pas d'effet de la perte de la sous-unité α9 sur la stabilité du regard. Cependant, lorsque les souris knockout α9 ont été testées pour leur capacité à maintenir l'équilibre et la posture, la souris mutante a montré une posture altérée avec une dynamique de mouvement de la tête altérée. Ces résultats suggèrent que la perte de la sous-unité α9 entraîne principalement des altérations de la stabilité posturale plutôt que de la stabilité du regard.

Les résultats de ma thèse renforcent la compréhension actuelle des rôles fonctionnels du noyau prépositus hypoglossi et du traitement sensoriel dans les voies vestibulaires ascendantes. En démontrant que le noyau prépositus hypoglossi de la souris encode de manière prédominante les mouvements oculaires, il comble un vide dans la littérature dans le domaine de la navigation et des fonctions oculomotrices. Mes résultats permettent également de mieux comprendre l'altération physiopathologique qui sous-tend le SCA6 et les rôles fonctionnels du système vestibulaire efférent des mammifères.

Acknowledgements

First and foremost, I would like to thank my supervisor, Dr. Kathleen Cullen, who not only trained me to be a better scientist but also helped me grow as a better person. There have been many challenges I faced over the last 7 years both professionally and personally. Without her continuous guidance and support, I would not have made it this far. She believed in me and rather than leading the way, she let me set my own path with patience. Her unparalleled passion and determination will always be my inspiration in my future endeavors.

I am also grateful that I had a chance to collaborate with Dr. Alanna Watt. She has always provided me with fresh insight, feedback, and encouragement on my research projects. I can say without a doubt that recording Purkinje cells in $SCA6^{84Q/84Q}$ mice was the most joyful experiment of my thesis. My experiment with $SCA6^{84Q/84Q}$ mice would not have been possible without Dr. Sriram Jayabal, an *in vitro* wizard. His love and passion for the mice and the project was highly contagious. I also thank Dr. Anna Cook for her help with the absolutely beautiful imaging of Purkinje cells.

A "thank you" cannot encapsulate how grateful I am to work with such amazing lab mates. Omid Zobeiri, soon to be Dr. Zobeiri, you are not my lab mate, you are my best friend, brother, mentor and therapist. Academically, your exceptional critical thinking, analytical and coding skills have saved me on countless occasions. You were always there for me to lend your shoulder after failed experiments (many times) and you helped me stay strong and grounded. Big thanks to Dr. Ran Wei, who always provided me great advice and fed me well. Aamna Lawrence for being the best partner in the lab. Soon to be Dr. Natasha Hughes for bringing a coherent system to our mouse colony and bringing vitality into Team Mouse. Pum Wiboonsaksakul for his eagle eyes—his attention to detail amazed me every single time. Many thanks to Subhi, Tobias, Brandie, Matt, Edward –members of Team Mouse always full of encouragement, positivity and fun. I would like to thank all the rest of past and present members of the Cullen lab for their support and feedback: Diana, Alexis, Ken, Dawoon, Jie, Lydia, Adrien, Amy, Lin, Erez, Dr. Sung Kwang Hong, Olivia, Oliver and Robyn.

I would also like to thank the members of my committee, Drs. Melissa Vollrath, Maurice Chacron and Erik Cook for their helpful feedback, encouragement and guidance. I was proud be a McGill Student because of them.

Reaching all the milestones of my PhD studies would not be possible without the help from Rosie from the physiology department. Thank you for being so patient with me.

My experiments setup would not have been happened without the exceptional craftmanship of Walter Kucharski, Bill Griffith, and Daren Ayres. I would also have been left with electrical and mechanical noises if Dale Roberts had not been there for me.

I would not have completed this thesis if weren't for the love and support of my family and friends. My parents who believed in me even I was doubting myself, Craig (for literally everything: love, support, mentorship and even proofreading my draft!), Elaine (my partner in crime), Rojhat (I would not have been able to finish this thesis without pide), Hugues (for helping me to stay reasonable and always helping me seek for solutions together). Love and support from all of you has meant the world to me.

Lastly, I would also like to thank the reviewers of this thesis and reviewers for previously published manuscripts for insightful feedback and constructive criticism.

- Vanessa

Contribution of authors

Chapter 2 contains a manuscript in preparation for submission: Chang HHV, Verdone, BM, Cullen KE. The mouse nucleus prepositus relays eye movement information to head direction network during navigation. For this study, I performed the surgery to implant probes, performed neural and behavioral recording and analyzed the data. I prepared a first draft of the manuscript (text and figures). My thesis supervisor, Dr. Kathleen Cullen, provided guidance and instruction through the different stages of the study, including experimental design, data analysis, interpretation of the data, and preparation of the manuscript.

Chapter 3 contains a manuscript submitted for publication: Chang HHV, Cook AA, Watt AJ, Cullen KE. Loss of flocculus Purkinje cell firing precision leads to impaired gaze stabilization in a mouse model of spinocerebellar ataxia type 6 (SCA6). For this study, I performed neural and behavioral recording and analyzed the data. Dr. Anna Cook performed immunohistochemistry and performed imaging. I prepared a first draft of the manuscript (text and figures). Dr. Anna Cook and Dr. Alanna Watt edited the manuscript. My thesis supervisor, Dr. Kathleen Cullen, provided guidance and instruction through the different stages of the study, including experimental design, data analysis, interpretation of the data, and preparation of the manuscript.

Chapter 4 contains a published manuscript: Chang HHV, Morley BJ, Cullen KE. Loss of alpha-9 nicotinic acetylcholine receptor subunit predominantly results in impaired postural stability rather than gaze stability. For this study, I performed behavioral recording and analyzed the data. I prepared a first draft of the manuscript (text and figures). Dr. Barbara Morley provided the animal model and edited the manuscript. My thesis supervisor, Dr. Kathleen Cullen, provided guidance and instruction through the different stages of the study, including experimental design, data analysis, interpretation of the data, and preparation of the manuscript.

Appendix A contains a published manuscript: Ono, K et al. Retinoic acid degradation shapes zonal development of vestibular organs and sensitivity to transient linear accelerations. For this study, I performed behavioral recording including balance beam and OVAR. I did initial data segmentation of OVAR data and analyzed balance beam data. I contributed to writing the result section of the manuscript.

Contribution to original knowledge

Chapter 2

I. Demonstrated that that mouse nucleus prepositus hypoglossi neurons predominately encode eye position and velocity.
II. Showed the novel experimental design for acute Neuropixel recording.
III. Demonstrated that that mouse nucleus prepositus hypoglossi neurons showed amplitude-dependent nonlinear response.

Chapter 3

I. Demonstrated that VOR and OKR gains were reduced in SCA6^{84Q} mice but nystagmus dynamics are comparable between wild-type and SCA6^{84Q} mice.
II. Demonstrated that VOR learning is impaired in SCA6^{84Q} mice.
III. Demonstrated that firing precision is altered in both anesthetized and awake SCA6^{84Q} mice.

Chapter 4

I. Demonstrated that VOR and OKR responses are normal in α9(-/-) mice and nystagmus dynamics are not changed in α9(-/-) mice.
II. Demonstrated that α9(-/-) mice showed impaired postural control on rotarod and balance beam and head movement dynamics are different from wild-type during the two tasks.

Chapter 1
General introduction

1.1 Overview and conceptual framework

Our brains process and integrate different types of sensory information, such as visual and auditory information, to respond to the challenges of our daily lives. The vestibular system provides our brains with information about the motion and orientation of the head in space. The information furnished by the vestibular system is necessary for gaze and postural stabilization and the computation of spatial orientation, thereby providing us with our subjective sense of orientation and self-motion (reviewed in Angelaki and Cullen, 2008; Cullen, 2012). Given the dynamic nature of head motion during everyday activities, the vestibular system also possesses impressive adaptive capability as it interrelates with many different brain regions, such as the cerebellum.

Our knowledge of the vestibular system, especially basic principles underlying vestibular processing, pathologies, and potential treatments, has benefitted from various animal models, from fishes to nonhuman primates. Specifically, mouse models have been widely used in the systematic investigation of vestibular functions, given their accessibility and technological advances that enabled the generation of genetically engineered mouse models of human disease. Accordingly, studies in this thesis were aimed at investigating the functions of three different vestibular pathways using a mouse model: (1) ascending vestibular pathways that contribute to spatial orientation, (2) the vestibulo-cerebellar pathway, and (3) the efferent vestibular pathway. In *Chapter 2* of this thesis, I test whether mouse nucleus prepositus hypoglossi (NPH) conveys vestibular information to the head direction (HD) cell network to generate a directional signal. The focus of *Chapter 3* is to identify vestibular dysfunctions and a potential underlying neural mechanism in a mouse model of spinocerebellar ataxia type 6 (SCA6). Finally, the functional role of the mammalian efferent vestibular system implicated by a mouse model lacking an α9 subunit of the nicotinic acetylcholine receptor (nAChRs) is addressed in *Chapter 4*.

To provide context for the studies presented in *Chapters 2-4*, this introductory chapter begins with an overview of the vestibular periphery, describing the vestibular sensory organs, vestibular hair cells, and primary afferents. Next, I briefly review the central circuitry that mediates the vestibulo-ocular reflex (VOR) and vestibulo-spinal reflex (VSR), and spatial orientation. Then, I will summarize the role of the nucleus prepositus hypoglossi (NPH) in the generation of eye movements. Following this, I describe in more detail the ascending vestibular pathway to the head direction (HD) cell network and the proposed role of the NPH in the generation of an HD signal. For the second section of this chapter, I describe the pathways and functions of the vestibulocerebellum. I then introduce spinocerebellar ataxias, specifically type 6, and mouse models matching human mutation associated with SCA6. Finally, I review the anatomy of the mammalian efferent vestibular system and its proposed functional roles.

1.2 The vestibular periphery

The periphery vestibular apparatus is located in the inner ear within the temporal bone. The apparatus consists of a bony labyrinth and a membranous labyrinth. The bony labyrinth includes the cochlea, the vestibule, and the semicircular canals and is filled with a sodium-rich fluid known as perilymph. The membranous labyrinth is suspended within the bony labyrinth and contains a potassium-rich fluid known as endolymph. The vestibular apparatus has five organs: three semicircular canals consisting of three nearly orthogonally arranged canals (the anterior, lateral, and posterior) and two otolith organs –utricle and saccule (**Fig 1.1**).

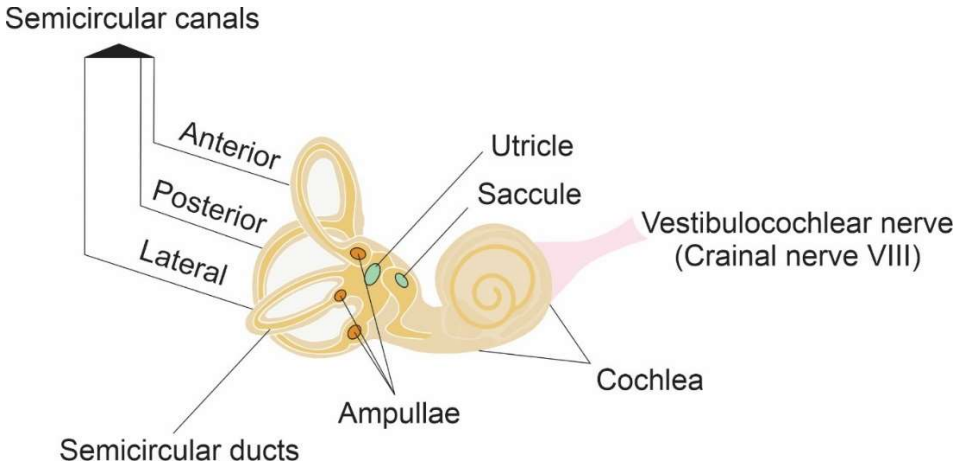

Figure 1.1: Bony and membranous labyrinths. The bony labyrinth includes the cochlea, the vestibule, and the semicircular canals. The membranous labyrinth is located within the bony labyrinth and consists of two otolith organs (the utricle and saccule) and the lateral, anterior, and posterior semicircular ducts.

1.2.1 Hair cells and primary afferents

Each vestibular organ has a neuroepithelium that comprises its receptor cells as referred to as hair cells. Hair cells are innervated by afferent nerves (cranial nerve VIII) that project to the brain and efferent nerves from the brain. Hair cells contain cross-linked actin filaments known as stereocilia and are organized in a row by length, with the tallest stereocilium connected to a single eccentrically-placed kinocilium.

Head motion results in the bending of stereocilia as the endolymph lags due to its inertia. This bending of the stereocilia results in the opening and closing of potassium channels on the hair cells. Deflection towards the kinocilium leads to an influx of potassium, resulting in a depolarization of the hair cells and the opening of calcium channels allowing neurotransmitter release into the synapse with vestibular afferent nerve fibers. In contrast, bending away from the kinocilium leads to the closing of the channels resulting in hyperpolarization and a decrease in neurotransmitter release. There are two types of hair cells in the neuroepithelium: type I with a calyx ending and type II with a bouton ending. Type I hair cells are preferentially innervated by irregular afferents with a broad distribution of interspike intervals at rest. In contrast, type II hair cells are mainly innervated by regular afferents characterized by lower variability of resting discharge (Fernández et al., 1988, 1990,1995). Most vestibular afferents terminate at the vestibular nuclei in the brainstem and send projections to the nodulus/uvula of the cerebellum. Quantification of individual vestibular afferent responses during sinusoidal motion stimulus is further

characterized according to their regular vs. irregular afferent activity dynamics. Irregular afferents have greater sensitivity and phase lead in response to head motion compared to regular afferents. However, regular afferents transmit twofold more information than irregular afferents and have a lower detection threshold (reviewed in Cullen, 2012;2019). Thus, irregular afferents are better optimized for encoding more robust natural vestibular stimuli, whereas regular afferents are better at encoding the detailed time course of the vestibular stimulus. Consistent with this, regular afferents are thought to predominantly synapse to the subclass of neurons in the vestibular nuclei that mediate vestibulo-ocular reflex (VOR) (reviewed in Cullen, 2012). Generation of the VOR requires a detailed time course of head motion stimulus to generate compensatory eye movements over a wide range of head movements. In addition, irregular afferents project to neurons in the vestibular nuclei that project to the spinal cord, vestibular cerebellum, and thalamus for ensuring balance and maintaining posture (Marlinski and McCrea, 2009; Meng et al., 2007).

1.2.2 Semicircular canals

The semicircular canals detect angular acceleration of the head. This nearly orthogonally arranged structure allows detection of head rotation in the pitch, roll, and earth-vertical axes—each canal (horizontal, anterior, and posterior) senses movement in its specific plane. A protrusion at the end of each canal – the ampulla – contains the sensory neuroepithelium called crista. It is overlayed with a gelatinous substance known as the cupula. Rotation of the head causes endolymph motion that shifts the cupula resulting in bending of the hair cells in the opposite direction of the head rotation (**Fig 1.2**; see green inset). Because of the small diameter of the canals and the viscosity of the endolymph, the canal transmits angular head velocity rather than encoded angular acceleration (Oman et al., 1987; Rabbitt et al., 2004).

1.2.3 Utricle and the saccule

The utricle and saccule monitor linear acceleration and the orientation of the head with respect to gravity. Each organ has a sensory neuroepithelium known as the macula. The macula of the utricle senses translational motion in the horizontal plane, while the macula of the saccule senses the motion in the vertical plane. The hair cells in the macula sit within the otolithic membrane – a gelatinous matrix embedded with calcium carbonate stones called otoconia. Translational movement or tilting of the head leads the otoconia to lag because of the inertial mass

and causes the otolithic membrane to shift relative to the underlying epithelium. This results in the bending of the hair cells (**Fig 1.2**; see brown inset). The stereocilia in the macula are oriented in relation to a curvilinear line called the striola. In the utricle, the hair cells are oriented toward the striola, whereas in the saccule, they are oriented away from the striola. This leads to an intricate response pattern to head tilt within the otoliths.

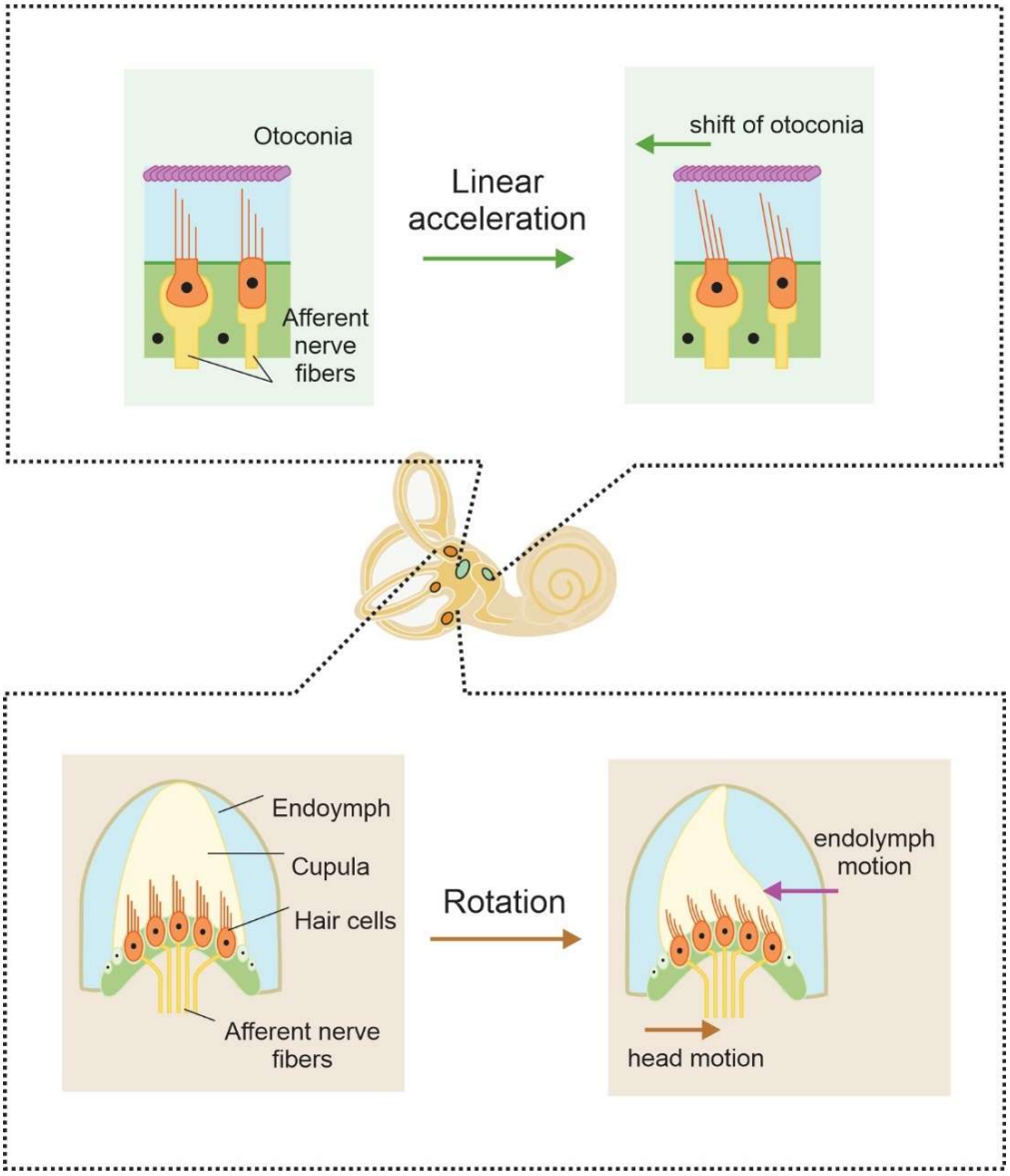

Figure 1.2: Hair cell activation during head motion. Linear acceleration or tilting of the head causes otoconia to lag and a shift to occur between the otolithic membrane and epithelium. This results in the bending of the hair cells embedded in the epithelium. Rotational acceleration of the head causes endolymph motion that pushes on the cupula, bending the hair cells in the opposite direction.

1.3 Central vestibular pathways for reflexes and perception

As mentioned above, the vestibular afferents project to the vestibular nuclei in the brainstem. The vestibular nuclei in the brainstem are the first signal processors of vestibular input and consist of four nuclei: medial, superior, lateral, and inferior. The medial vestibular nucleus located in the medial column of the nuclei receives afferents from the crista of the horizontal canals. The superior vestibular nucleus receives inputs from superior and posterior semicircular canals. The lateral vestibular nucleus receives afferent information from the crista, the maculae, and the vestibulocerebellum. The inferior vestibular nucleus receives inputs from the maculae of both the utricle and the saccule. The vestibular nuclei can be further classified according to the behaviors they mediate (i.e., eye-sensitive or vestibular-only neurons (VO))

1.3.1 Vestibulo-ocular reflex pathway

The vestibulo-ocular reflex (VOR) generates eye movements that are equal in magnitude but opposite in direction to head motion ensuring a stable gaze over a wide range of unexpected head movements (Huterer and Cullen, 2002). There are two types of VOR responses: the angular VOR (aVOR) and the translational VOR (tVOR). The angular VOR (aVOR) is the response evoked to rotational head movement. In mice and humans, rotational head motion during activities can power up to 20 Hz (Carriot et al., 2014; 2017). The aVOR has a fast response time of 5 ms in nonhuman primates (reviewed in Cullen, 2012). The VOR pathway is mediated by a three-neuron arc: vestibular afferents send projections to neurons in the vestibular nuclei which then directly project to extraocular motoneurons (in the abducens, trochlear, and oculomotor nuclei) (**Fig 1.3**; Lorente de Nó, 1933). This 5 ms latency can be explained by the simplicity of this pathway. The translational VOR (tVOR) is evoked by translational head movements. The tVOR is not as effective as the aVOR in stabilizing gaze (Paige and Seidman, 1999). It has a latency of >10 ms and is not fully compensatory compared to the aVOR (Angelaki and McHenry, 1999). This is because the tVOR is mediated by more complex polysynaptic pathways contrary to the direct three-neuron-arc.

The VOR has the remarkable capability of adjusting to maintain gaze stability, such as changes in the size of the head or for myopia. Sadeghi et al. (2006) showed that the VOR exhibited close to complete compensation within 1 week after unilateral lesion. Under normal conditions, VOR gain (eye velocity/head velocity) – a measure to test the efficacy of the reflex – is ~1.

However, a mismatch between visual and vestibular stimuli leads to VOR adaptation. For example, a decrease in VOR gain can be achieved by having a subject be trained with visual stimuli rotating in the same direction as the head. An increase in VOR gain can be induced when the visual stimulus rotates in the opposite direction to the head motion. The floccular complex of the cerebellum is crucial for VOR adaptation. It is believed that an error signal, the motion of images on the retina (i.e., retinal slip) that is conveyed by the climbing fiber input, triggers synaptic plasticity that leads to VOR adaptation (Ito, 1972; Miles and Lisberger, 1981).

The VOR is less efficient in compensating for low-velocity head movements. Thus, it works in concert with the optokinetic reflex (OKR), which compensates for retinal slip (the relative motion of the visual world across the retina) at low-velocity below 0.1 Hz and constant velocity head movements (Goldberg et al., 2012). Initial OKR response is generated by the cortico-pontine-floccular circuit. Cortical areas such as the middle temporal (MT), medial superior temporal (MST) area, and the frontal eye fields (FEF) send projections to the pontine nuclei, which in turn project to the cerebellar flocculus. Floccular Purkinje cells projects to premotor neurons in the vestibular nuclei that project directly to extraocular motoneurons. The slower build-up of eye velocity is followed by initial eye OKR velocity rise, and it is mediated by subcortical pathways (reviewed in Cullen, 2016). Briefly, neurons sensitive to visual motion in the nucleus of the optic tract and the accessory optic nuclei send projections to premotor neurons in the vestibular nuclei and the nucleus prepositus hypoglossi (NPH), which then project directly to the extraocular motoneurons.

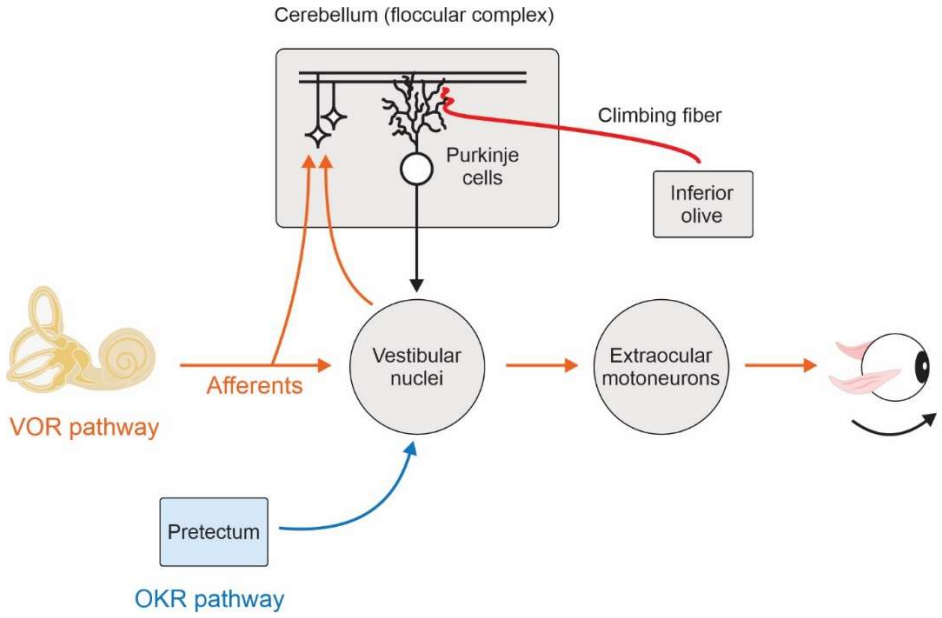

Figure 1.3: Vestibulo-ocular reflex (VOR) and optokinetic reflex (OKR) neuronal circuit. The pretectum targets the same premotor cells in the vestibular nuclei that mediate the VOR.

1.3.2 Vestibulo-spinal reflex pathway

The vestibular system also mediates vestibulo-spinal reflexes to maintain postural stability. There are two descending vestibulo-spinal pathways: the lateral vestibulo-spinal tract (LVST) and the medial vestibulo-spinal tract (MVST). The MVST tract, which is originated in the medial and inferior vestibular nuclei, stabilizes the head in space during unanticipated passive head motion by activating the neck musculature. The MVST is primarily driven by information from the semicircular canals. This reflex which includes pathways from the vestibular periphery to the cervical spinal cord, is referred to as the vestibulo-collic reflex (VCR) (reviewed in Goldberg and Cullen, 2011). In animals with smaller oculomotor ranges, such as barn owls and cats, the VCR makes a significant contribution to the stabilization of gaze that complements the VOR (barn owl:Money and Correia, 1972; cat: Goldberg and Peterson, 1986; frog: Dieringer, 1987; pigeon: Gioanni, 1988; Haque and Dickman, 2005; guinea pig: Shanidze et al., 2012). The LVST is originated in the lateral vestibular nucleus and primarily driven by otolith inputs. It projects ipsilaterally to many levels of motor neurons in the spinal cord to coordinate different muscle groups in trunks and limbs to ensure the maintenance of posture.

1.3.3 Ascending vestibular pathways

There are two main ascending vestibular pathways to cortical areas: the anterior and posterior pathways. The anterior pathway consists of projections from the vestibular nuclei through the nucleus prepositus hypoglossi (NPH) to the network of areas containing head direction (HD) cells, such as the anterior dorsal thalamus (ADN). This pathway then reaches the retrosplenial cortex and the entorhinal cortex and is thought to contribute to our sense of direction. The posterior pathway projects to the ventral posterior lateral nucleus of the thalamus (VPL), then onto the somatosensory cortex and the parieto-insular vestibular cortex. This pathway is believed to contribute to a perception of self-motion (**Fig 1.4**) (reviewed in Taube and Cullen, 2017). The anterior pathway, particularly the projection between the NPH and the HD network, will be investigated in *Chapter 2* of this thesis.

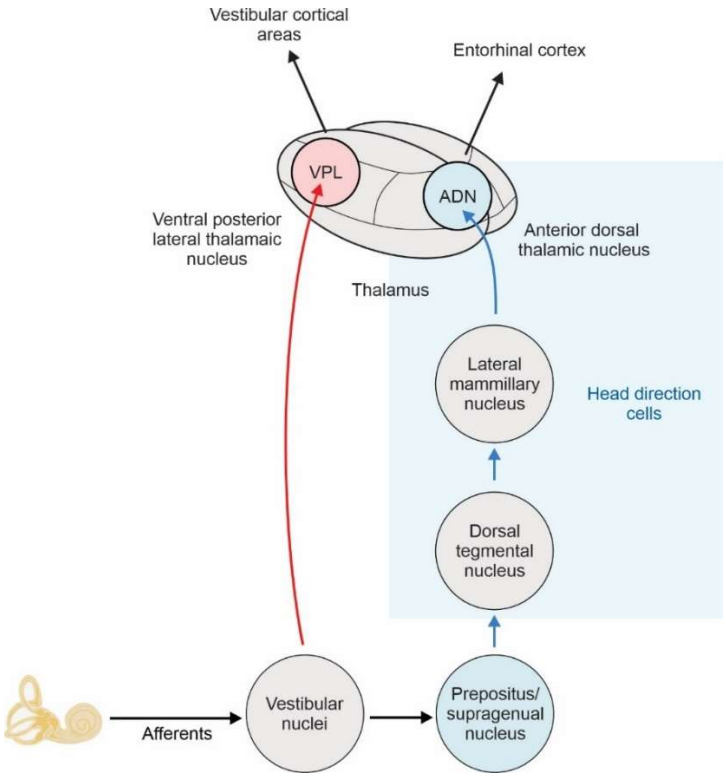

Figure 1.4: Two vestibular thalamocortical pathways. The anterior pathway goes through the nucleus prepositus and supragenual nucleus to the head direction network (blue box). The posterior pathway project from the vestibular nuclei to the ventral posterior lateral nucleus (red arrow).

1.4 The nucleus prepositus hypoglossi (NPH)

Anatomically, the nucleus prepositus hypoglossi (NPH) is located between the hypoglossal nucleus and the abducens nucleus in the brainstem. Decades of anatomical and physiological studies have confirmed the involvement of the NPH in controlling eye movements. For example, many of the cells in the NPH send projections to the extraoculomotor nuclei, and their firing rates modulate in response to eye movements. In addition, lesions of the NPH lead to oculomotor control deficits such as the inability to hold the eccentric gaze. I will review the findings of this research in the section below (section 1.4.1). Alternatively, a different view is that the NPH encodes a head motion signal which it then transmits to the head direction (HD) network, where it is integrated to provide a reference to establish higher-order spatial representations of head direction (Bassett and Taube, 2001; Sharp et al., 2001), I will review the studies used in support of this second view below (section 1.4.2). Notably, the proposal that the NPH transmits a head motion signal to the HD network is based on anatomical connectivity; there is no direct electrophysiological evidence for this view.

1.4.1 NPH in the generation of eye movement

Overcoming the viscoelastic properties of the orbital plant requires the eye velocity commands to be integrated into a tonic "step" signal to hold the eye steady at its position after horizontal saccades (Robinson, 1970). The NPH receives projections from burst neurons in the paramedian pontine reticular formation (PPRF). It is considered a neural integrator as it integrates the velocity signals from PPRF and provides the step signals to the abducens nucleus and the oculomotor nucleus (**Fig 1.5**; reviewed in McCrea and Horn, 2006). Indeed, lesions and inactivation of the NPH led to an inability to maintain an eccentric gaze (Godaux et al., 1993; Godaux and Cheron, 1996; Kaneko, 1997; Arnold et al., 1999; Cannon and Robinson, 1987). The NPH also receives inputs from the vestibular nuclei, and lesions and inactivation of the NPH result in gaze instability in the horizontal plane (Godaux et al., 1993; Mettens et al., 1994; Büttner and Grundei, 1995; Kaneko, 1997; Arnold et al., 1999).

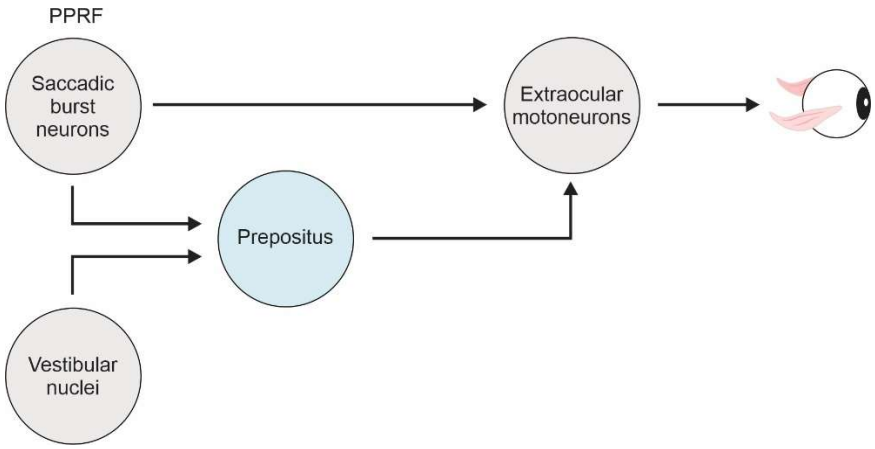

Figure 1.5: The premotor pathway for controlling horizontal eye movements involving the nucleus prepositus. *Abbreviation:* PPRF, paramedian pontine reticular formation. The NPH receives projections from burst neurons in the PPRF and the VN. It then projects to extraocular motoneurons.

1.4.2 NPH inputs in the generation of a head direction (HD) signal

The neural circuit of head direction (HD) signal generation includes projections from the vestibular nuclei through the NPH and the supragenual nucleus (SGN) to the dorsal tegmental nucleus (DTN). From the DTN, the pathway projects to the lateral mammillary nucleus (LMN) and the anterior dorsal thalamus (ADN) (reviewed in Taube and Cullen, 2017). HD cells, which fire in relation to the animal's directional heading in the horizontal plane, have been found in the DTN (Dumont et al., 2016), the LMN, and the ADN (reviewed in Taube 1998; 2007). Based on this pathway connectivity, it has been proposed that the angular head velocity information from early vestibular pathways is sent to the DTN via the NPH. For example, vestibular manipulations such as lesions, inactivation, and occlusions of the semicircular canals all resulted in disruption of the HD signal (reviewed in Clark and Taube, 2012; Yoder and Taube, 2014). Importantly, lesions of the NPH also have been shown to disrupt the HD signal in the ADN (Butler et al., 2017). However, the proposed role of the NPH in relaying vestibular information is complicated by the fact that the NPH is involved in controlling eye movements, as mentioned above. Accordingly, in *Chapter* 2 of this thesis, I test whether NPH neurons in mice also encode eye movement information, head movement information, or some combination of the two during changes in the directional heading (i.e., head rotations).

1.5 Vestibulocerebellum

The vestibulocerebellum is a group of areas in the cerebellum associated with multimodal information, including vestibular, visual, and eye-related signals. It consists of five main regions of the cerebellum: (1) the nodulus (lobule X) and ventral uvula (lobule IX), (2) the flocculus and ventral paraflocculus, (3) the oculomotor vermis of the posterior lobe, (4) lobules I and II of the anterior lobe, and (5) the deep cerebellar nuclei (**Fig 1.6A**)

Both vestibular primary and secondary afferents project directly to the cerebellum. Specifically, vestibular primary afferent fibers originating from the vestibular end organs send collateral to the deep cerebellar nuclei. The vestibular afferent fibers also terminate as mossy fibers in the ipsilateral nodulus and ventral uvula, lobules I and II of the anterior lobule and posterior lobules. (reviewed in Barmack and Yakhnitsa, 2013). Secondary vestibular afferents from the vestibular nuclei project to the regions mentioned above and the flocculus and ventral paraflocculus. The ipsilateral cerebellum has efferent projection to bilateral vestibular nuclei (**Fig 1.6B**;reviewed in Voogd and Bigare, 1980).

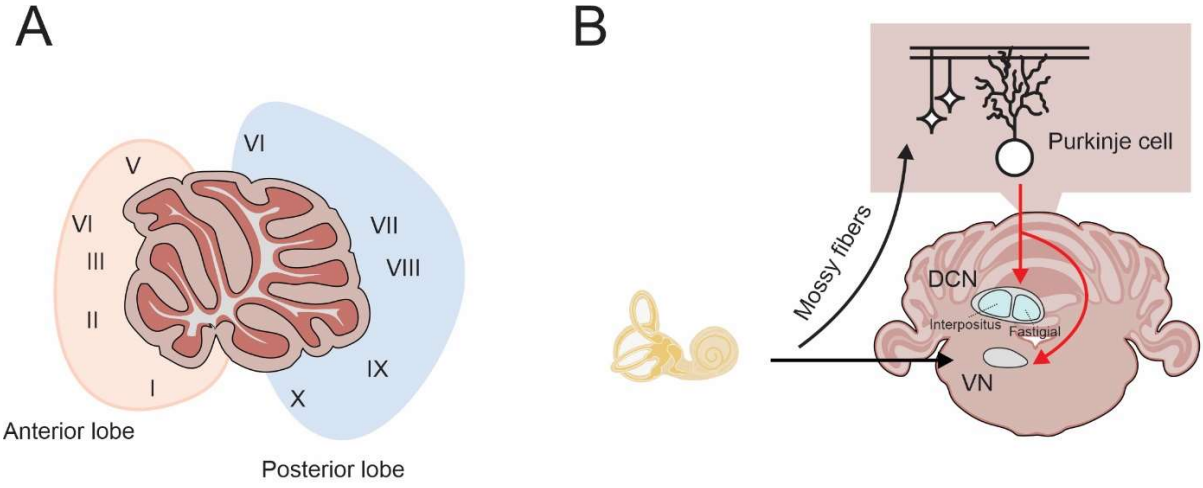

Figure 1.6:Organization of the adult mouse cerebellum and vestibulocerebellar pathway. *Abbreviation:* DCN, deep cerebellar nuclei; VN, vestibular nuclei. (A) The cerebellum is divided into anterior, posterior, and flocculonodular (not shown) lobules and their subdivisions. (B) Vestibular information is carried to the cerebellum via mossy fibers. Purkinje cells project to the fastigial and interposed nuclei and the vestibular nuclei.

1.5.1 Flocculus and ventral paraflocculus

The floccular complex consists of the flocculus and ventral paraflocculus. The complex plays a critical role in the generation, and the plasticity of the VOR, OKR, and smooth-pursuit eye movements as vestibular, eye movement, and visual image motion information converge on the complex (Nagao, 1992; Nagao and Kitazawa, 2003). The floccular complex receives most of its vestibular information from mossy fiber projections that originated in the vestibular nuclei (Highstein et al., 1987; Langer et al., 1985; Osanai et al., 1999; Voogd et al., 1996). The efferent vestibular system (EVS) in the brainstem also sends efferent projections to the floccular complex (Shinder et al., 2001). Eye-movement-related information is sent to the complex from the vestibular, reticular, and perihypoglossal nuclei and nucleus reticularis tegmenti pontis (NRTP) (Mustari et al., 1988; Buttner-Ennever and Horn, 1996). Visual image motion information is relayed to the complex via climbing fiber from the inferior olive (Maekawa and Simpson, 1973).

Floccular simple spike activity is modulated in response to optokinetic and vestibular stimulation and smooth-pursuit eye movements (Graf et al., 1988; Waespe and Henn, 1981; Stone and Lisberger, 1990a,b). The climbing fiber-driven response (i.e., complex spikes) is sensitive to retinal image motion during optokinetic stimulation and smooth-pursuit eye movements (OKN: Frens et al., 2001; Ghelarducci et al., 1975; Graf et al., 1988; Waespe et al., 1981; smooth-pursuit: Stone and Lisberger 1990; Kahlon and Lisberger, 2000). The complex spike activity also modulates in response to vestibular stimulation (DeZeeuw et al., 1995; Ghelarducci et al., 1975). Notably, both simple and complex spike activity respond to changes in modulation following VOR learning (Blazquez et al., 2003; Lisberger, 1994; Miles et al., 1980; Raymond and Lisberger, 1996; Watanabe, 1984). Indeed, the adaptive capability to modify VOR gain was lost when monkeys were given bilateral lesions in the floccular region (Ito et al., 1974; Lisberger et al., 1984; Robinson, 1976).

1.5.2 Nodulus and ventral uvula

Each lobule receives projections from all of the semicircular canals and the otolith organs. The nodulus and ventral uvula get predominant input from the posterior canals and saccule (Korte and Mugnaini, 1979; Maklad and Fritzsch, 2003). Most vestibular nuclei also send projections to the nodulus and ventral uvula (Barmack and Shojaku, 1992; Barmack et al., 1992; Shojaku et al., 1991). These regions are sensitive to static and rotational roll and tilt, suggesting inputs from

otolith organs and anterior or posterior canals (otolith: Barmack and Shojaku, 1995; Marini et al., 1976; Sheliga et al., 1999; Yakusheva et al., 2007; semicircular canals: Fushiki and Barmack, 1997; Sheliga et al. 1999). However, these regions show more robust responses during translational motion in comparison to pitch or roll rotations (Yakusheva et al., 2007). The nodulus and ventral uvula are critical structures for controlling the time course and spatial orientation of velocity storage (i.e., prolonging vestibular response) as electrical stimulation in these regions altered both the time course and spatial orientation. (Precht et al., 1976; Angelaki and Hess, 1995; Wearne et al., 1996;1998).

1.5.3 Anterior and posterior lobes and deep cerebellar nuclei

Lobules I to V of the anterior lobe and lobules VI and VII (also referred to as oculomotor vermis) of the posterior lobe receive primary and secondary vestibular inputs. Lobules I to V are sensitive to vestibular and neck proprioceptive signals (Manzoni et al., 1998;1999;2004). These cerebellar lobules mediate vestibulospinal reflexes and the integration of vestibular and proprioceptive information. Oculomotor vermis (lobules VI and VII), as its name suggests, contributes to visual-vestibular processing (Sato and Noda, 1992; Suzuki and Keller, 1982; 1988). Indeed this region receives eye-movement signals from other brainstem regions such as the nucleus prepositus hypoglossi, dorsolateral pontine nuclei (DLPN), and NRTP (Belknap and McCrea, 1988; Brodal. 1979; Yamada and Noda, 1987; reviewed in Their and Möck, 2006).

The deep cerebellar nuclei consist of the fastigial, interpositus, and dentate nuclei. The fastigial nucleus is the most closely related to the vestibular system as it receives both primary and secondary vestibular inputs. The fastigial nucleus plays a critical role in transmitting cerebellar signals to vestibulo-spinal pathways to mediate postural reflexes and balance (Gruart and Delgado-Garcia, 1994). The region can be further classified into two areas in which neurons encode either head motion or eye movements. Specifically, neurons in the rostral portion of the fastigial nucleus are sensitive to head rotations in the dark and insensitive to eye movement (Buttner et al., 1991; Gardner and Fuchs, 1975; Siebold et al., 1997; Brooks and Cullen, 2013), while the caudal fastigial nucleus responds more robustly to pursuit and saccadic eye movements (Buttner et al., 1991; Fuchs et al., 1993; Gardner and Fuchs, 1975).

1.6 Spinocerebellar ataxia type 6 (SCA6)

Spinocerebellar ataxias (SCAs) are a group of autosomal dominant neurodegenerative disorders that are characterized by progressive motor incoordination. Some SCAs present with progressive ataxia alone, and others accompany additional progressive neurological deficits such as slurred speech or oculomotor abnormalities (reviewed in Solodkin and Gomez, 2012). Currently, there are 46 genetically distinct subtypes of SCAs registered, and they fall into two categories based on their genetic mutations: (1) SCAs that are caused by microsatellite repeat expansions, and (2) SCAs caused by point mutations (reviewed in Ashizawa et al., 2018; Klockgether et al., 2019). SCAs caused by microsatellite repeat expansion can be further categorized into ones caused by polyglutamine (polyQ)-coding CAG repeat expansions and those caused by non-protein-coding repeats. For example, SCA1-3,6,7, and 17 are called polyglutamine SCAs because they are caused by CAG repeat expansion mutation encoding stretches of pure glutamine. (reviewed in Klockgether et al., 2019). To date, polyglutamine SCAs are the most prevalent forms of SCAs (Schols et al., 2004). Given distinct genetic causes to each subtype, SCAs show a broad heterogeneous spectrum in their pathology, ranging from relatively pure cerebellar involvement (i.e., SCA6) to broader degeneration in other parts of the brain, the spinal cord, and even peripheral nerves (i.e., SCA1-3) (reviewed in Klockgether et al., 2019).

Among subtypes of SCAs, SCA6 is characterized by late-onset, progressive ataxia, dysarthria, and nystagmus. Initially, SCA6 patients experience unsteady gait and imbalance, and eventually, all patients have gait ataxia, upper limb incoordination, and dysarthria (Solodkin and Gomez, 2012). Most SCA6 patients also report visual disturbances such as nystagmus (Gomez et al., 1997). SCA6 is one of the polyglutamine SCAs caused by a CAG repeat expansion in exon 47 of the *CACNA1A* gene, which encodes the α1A ($Ca_v2.1$) subunit of the P/Q-type voltage-gated calcium channel (Zhuchenko et al., 1997). SCA6 is distinct from other polyglutamine SCAs such as SCA1,2 and three as the size of the CAG repeat expansion is relatively small (20-33), and the calcium channel protein expressing the polyglutamine tract has a restricted expression to cerebellar Purkinje cells (Ishikawa et al., 1999; Restituito et al., 2000). Indeed, neuropathological studies and MRI scans have shown profound loss of Purkinje cells and cerebellar atrophy in SCA6. (Solodkin and Gomez, 2012). Currently, there is no cure for SCA6, and treatment to date is symptomatic to treat ataxic episodes. There are efforts to develop treatments that are still experimental. Understanding a link between pathological alterations (i.e., PC intrinsic firing deficits) that arise

from mutation and deficits in cerebellar-related behavior would be a key to developing treatment strategies.

Mouse models have facilitated advancement in understanding pathophysiologic mechanisms of human diseases and potential treatment. Indeed, several different mouse models of SCA6 have been generated to date, and mainly there are two types. Watase et al. (2008) generated the mouse mutant strain by knocking in the C-terminal regions from the human *CACNA1A* locus with polyQ repeats into the mouse *Cacna1a* locus. The mice bearing a polyQ repeat size of 30, which leads to SCA6 in humans, did not display any ataxic behavior. However, knocking in hyperexpanded polyQ repeat size of 84 resulted in ataxia in mice at 7 months of age (Watase et al., 2008). In these $SCA6^{84Q/84Q}$ mice, Purkinje cell degeneration was observed at 22 months of age which lags behind the manifestation of ataxia in SCA6. Another mouse model that has been developed is the mouse model with overexpression of α1ACT fragments with 27 polyQ repeats ($SCA6^{CT\text{-}27Q}$ mice) (Mark et al., 2015). These $SCA6^{CT\text{-}27Q}$ mice, similar to $SCA6^{84Q/84Q}$ mice, have an ataxic phenotype at 8 months of age. However, Purkinje cell degeneration precedes ataxia in $SCA6^{CT\text{-}27Q}$ mice (~4 months of age) (Mark et al., 2015). In *Chapter 3*, I utilize $SCA6^{84Q/84Q}$ mice to investigate the potential underlying neural mechanism for ataxia and oculomotor abnormalities seen in these mice.

1.6.1 P/Q channels and Purkinje cell firing precision

The *CACNA1A* gene in which polyglutamine expansion mutation occurs, encodes two proteins: (1) the full-length P/Q channels (Usowicz et al., 1992; Catterall, 2000) and the C-terminus of the P/Q channel, α1ACT (Du et al., 2013). P/Q channel is comprised of the pore-forming α1A subunit and other auxiliary subunits such as β, α2δ, and γ (Miller, 1992). The polyQ repeat expansion is located at the C-terminus of the α1A subunit. The P/Q channels display a widespread expression throughout the brain, with a higher level of the P/Q channels expressed in the Purkinje cells and granule cells of the cerebellum compared to other regions of the brain (Hillman et al., 1991; Mintz et al., 1992; Kulik et al., 2004; Mori et al., 1991; Westenbroek et al., 1995). Genes encoding α1A subunit generate protein isoforms containing polyQ repeats that are found in SCA6. These isoforms encode the entire exon 47 that is highly expressed in Purkinje cells in the cerebellum (Zhuchenko et al.,1997; Restituito et al., 2000). P/Q channels are colocalized with two types of calcium-activated potassium channels, BK and SK2, and together they activate

potassium channels (Indriati et al., 2013). ~90% of the total calcium channels in the Purkinje cells are P/Q type channels (Mintz et al., 1992).

Suggested by high expression in the cerebellum, P/Q type channels play a crucial role in the proper functioning of the Purkinje cells as they ensure the calcium-induced neurotransmitter release. Indeed, *CACNA1A* variants also underlie two additional neurological disorders, namely, familial hemiplegic migraine type 1 (FHM1) and episodic ataxia type 2 (EA2) (Ophoff et al., 1996). FHM1 patients experience severe migraines with an aura, and some of them have cerebellar dysfunctions ranging from nystagmus to progressive ataxia (Ducros et al., 2001; Terwindt et al., 1996). EA2 is characterized by ataxia, limb incoordination, nystagmus, and slurred speech (Denier et al., 1999). Mutations in the *CACNA1A* gene also give rise to mouse mutant models that manifest ataxic symptoms. For example, amino acid substitutions in the *CACNA1A* gene generated the *tottering* (Fletcher et al., 1996), the *rolling Nagoya* (Mori et al., 2000), and the *rocker* (Zwingman et al, 2001) mice. Splice site mutation in the gene resulted in the generation of the *leaner* mice (Fletcher et al., 1996). Together, these collectively suggest altered P/Q type channel function is associated with ataxia and other cerebellar dysfunctions.

Altered P/Q channel function implicates changes in synaptic transmission and the intrinsic properties of Purkinje cells (Jun et al., 1999; Matsushita et al., 2002; Cao and Tsien, 2005; Tottene et al., 2009; Walter et al., 2006). Purkinje cells exhibit highly spontaneous pacemaker firing properties at rest (Strick, 1985). This regular firing of Purkinje cells is mediated by synaptic input and the intrinsic properties of Purkinje cells (Raman and Bean, 1999; Womack and Khodakhah, 2002; Swensen and Bean, 2000). P/Q type channels, along with calcium-activated and voltage-gated potassium channels, are required for the firing precision of Purkinje cells (Womack and Khodakhah, 2002; Womack and Khodakhah, 2003). Indeed, blocking the P/Q type channel leads to a loss of firing precision of Purkinje cells. Additionally, such loss of firing precision of Purkinje cells was found in mouse models of EA2, which exhibit ataxic phenotype on rotorod (Walter et al., 2006). These findings highlight the importance of P/Q type channels in maintaining pacemaker properties of the Purkinje cells and point to the possible underlying pathophysiologic mechanism of ataxia.

1.7 The efferent vestibular system (EVS)

The efferent system innervates peripheral sensors and modulates their afferent activity. The efferent vestibular system (EVS) arises from the brainstem, and it synapses with vestibular hair cells and afferents (Gacek, 1960). In every vertebrate class, the location of the efferent cell bodies and their dendritic morphology differs between species. In mammals, the majority of the efferent cell bodies (~300 neurons) are clustered in the brainstem and known as group *e,* and these group *e* neurons are located dorsal to the genu of the facial nerve and medial to the VI (abducens) nucleus. These neurons project bilaterally to the peripheral vestibular system (**Fig 1.7A**;reviewed in Holt et al., 2011; Mathews et al., 2017; Cullen and Wei, 2021).

1.7.1 Synaptic physiology of the EVS

Artificial activation of the EVS via electrical stimulation results in an increase in afferent firing rate in all mammalian species. This excitatory effect is more pronounced (an order of magnitude) in irregular afferents (Goldberg and Fernàndez, 1980; Highstein and Baker, 1985; Boyle and Highstein, 1990; Boyle et al., 1991, 2009; McCue and Guinan, 1994; Marlinski et al., 2004; Sadeghi et al., 2009; Rabbitt et al., 2010). This efferent-mediated afferent activation is dependent on acetylcholine (ACh) (reviewed in Goldberg et al., 2012). Localized around the efferent nerve terminals, ACh is the main neurotransmitter of the EVS and hyperpolarizes hair cells via nicotinic receptors and calcium-activated potassium (SK) channels. The nicotinic ACh receptors that mediate hyperpolarization of hair cells are α9 subunit-containing nicotinic acetylcholine receptors (α9*nAChRs) (reviewed in Poppi et al., 2020). Briefly, activation of α9*nAChRs results in an influx of calcium and is coupled to the SK channels. A consequent efflux of potassium is then followed, hyperpolarizing the hair cells. This leads to a reduction in calcium release through other calcium channels and inhibits glutamate release onto afferents (Im, 2012; Kong et al., 2008; Turcan et al., 2010). α9*nAChRs subunits are often found to form heteromeric receptors with α10 subunits (Elgoyhen et al., 2001). In mammalian vestibular hair cells, the presence of α9 and α10 subunits were confirmed by molecular biological and immunohistochemical data. Specifically, α9 subunits are localized to type II hair cells (Cristobal et al., 2005; Kong et al., 2006). This ACh-mediated hyperpolarization of vestibular hair cells is believed to lead to excitation of vestibular afferent activity by uncoupling α9*nAChRs with SK channel as the application of SK channel antagonists led to depolarization (Parks et al., 2017).

However, the prevailing view is that the fast component of excitation (time constant of 10-100ms) of afferents is mediated through a different type of nAChRs identified as α4/β2-containing nAChRs and the slow component (time constant of 20-40s) is mediated by muscarinic acetylcholine receptors (mAChRs) (reviewed in Jordan et al., 2013; Goldberg and Fernandez, 1980).

In addition to the presence of acetylcholine receptors, other substances co-expressed in the EVS include adenosine-5'-triphosphate (ATP), calcitonin gene-related peptide (CGRP), γ-aminobutyric acid (GABA), dopamine (DA), nitric oxide (NO), and enkephalins (**Fig 1.7B**;reviewed in Holt et al., 2011). Among those, CGRP is the most abundantly expressed in vestibular efferents within the central nervous system (reviewed in Holt et al., 2011; Soto and Vega, 2010; Yamashita et al., 1993). CGRP is co-expressed with choline acetyltransferase (CHAT), catalyzes the synthesis of (ACh), and thus is believed to influence ACh activity.

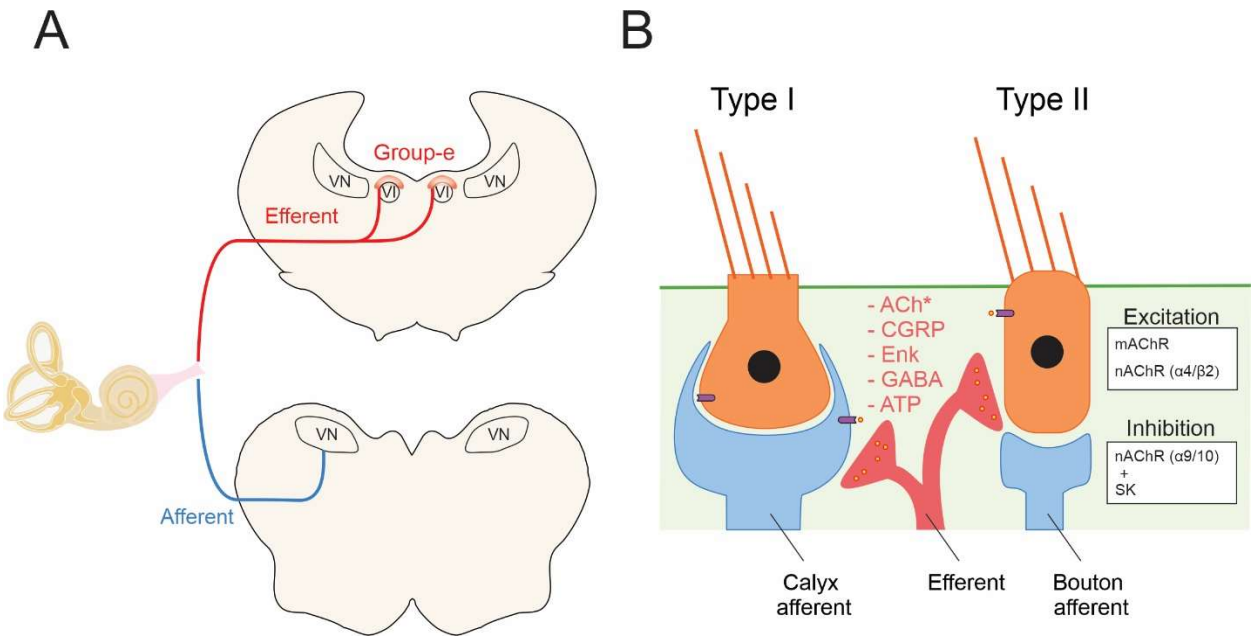

Figure 1.7: Schematic of vestibular efferent and afferent projections in the central nervous system and in the vestibular sensory epithelium. (A) Cell bodies of efferents innervating the mammalian vestibular sensory epithelium are located in separate nuclei called "group-e". (B) *Abbreviation:* PPRF, paramedian pontine reticular formation. (B) Efferent synapses are predominantly cholinergic (ACh). Other neuromodulators such as CGRP, Enk, GABA, and ATP are also present at the synapses.

1.7.2 Function of the mammalian vestibular efferent system

Despite decades of research, the functional role of the EVS in natural conditions is poorly understood. There is evidence in nonmammalian species such as fish and tadpoles that the EVS functions to differentiate between active and passive motion. In this view, the EVS sends motor-related information to the peripheral vestibular system, which in turn modulates outputs from the semicircular canal and otolith organs. This modulatory effect extends their head motion coding range during an active motion to avoid inhibitory cut-off and/or saturation (reviewed in Goldberg, 2000; Mathews et al., 2017). Consistent with this view, studies in toadfish have demonstrated an increase in firing rate and a decrease in vestibular sensitivity during active motion (Boyle and Highstein, 1990; Rabbitt et al., 1995).

In contrast, in mammals, the EVS does not play a role in differentiating between active and passive motion. Evidence to date in nonhuman primates (i.e., rhesus monkeys) showed neither semicircular canal nor otolith afferent responses are altered during active head movements (Cullen and Minor, 2002; Sadeghi et al., 2007; Jamali et al., 2009; Mackrous et al., 2019). Mackrous et al. (2022) further proved that during active walking conditions, both semicircular canal and otolith afferent responses were unchanged. Thus, the mammalian EVS does not encode head motion in a context-dependent manner as in nonmammalian species.

The mammalian EVS has also been thought to play a role in the plasticity and compensation of vestibular pathways. Recent studies suggest that α9 nAChRs may play a role in vestibular compensation following unilateral labyrinthectomy (Eron et al., 2015; Hübner et al., 2017). For example, VOR adaptation efficacy was reduced to ~70% in α9 nAChR knockout mice (Hübner et al., 2015). α9 nAChR knockout mice also showed poorer functional recovery (i.e., VOR) compared to wild-type mice following unilateral labyrinthectomy (Hübner et al., 2017). In contrast, the EVS does not appear to play a major role in the plasticity and compensation of vestibular pathways in rhesus monkeys; the resting firing rates of vestibular afferents between passive and active head and eye movements were not different even after labyrinthectomy (Cullen and Minor, 2002; Jamali et al., 2009; Sadeghi et al., 2007; Mackrous et al., 2019; Mackrous et al., 2022). In addition, both firing rate and head velocity sensitivity of both semicircular and otolith afferents were unchanged following VOR adaptation using a dove prism (Miles and Braitman, 1980). Together, the role of mammalian EVS in plasticity and compensation is still the subject of debate. Finally, it has been postulated that the EVS plays a modulatory role in shaping functional

efficacy during development (i.e., central vestibular functions and afferent nerve response) (Holt et al., 2011). Indeed, CGRP null mice showed significant attenuation in the efficacy of their VOR response (Luebke et al., 2014). In addition, α9 nAChR knockout mice also showed lower VOR gain (Hubner et al., 2015). Further experiments are needed to test this proposal as well as determine whether it generalizes across mammalian species, including primates.

1.8 Summary of research goals

The overall goal of my thesis was to perform a quantitative analysis of vestibular pathways and behaviors in mice to further understand the basic physiology of the system. Three vestibular pathways I investigate in my thesis are: (1) ascending vestibular pathways that contribute to spatial orientation, (2) the vestibulo-cerebellar pathway, and (3) the efferent vestibuar pathway. The methods and results presented in this thesis provide novel approaches and designs for vestibular phenotyping and high-density neural recording.

In *Chapter* 2, I characterize the responses of mouse NPH neurons to eye movements and/or head motion. Specifically, I test the hypothesis, based on anatomical studies, that the NPH conveys vestibular information to the HD network. Here I present a novel mount design using a high-density silicon probe, Neuropixel.

In *Chapter* 3, I investigate the underlying neural mechanism in ataxia, and oculomotor abnormalities observed in a mouse model of spinocerebellar ataxia type 6 (SCA6). I test VOR responses and VOR adaption in SCA6 mice and determine whether that are any alterations in the firing properties of Purkinje cells that may explain dysfunctions.

Finally, in *Chapter* 4, I investigate the functional role of the mammalian efferent vestibular system (EVS) using a mouse model lacking a subunit of one of the main neurotransmitters of the EVS—the nicotinic acetylcholine receptor (nAChRs). I quantify gaze and postural stability in the mouse mutant model and determine to what extent gaze and postural control performances are affected by the compromised EVS.

Chapter 2

The mouse nucleus prepositus relays eye movement information to head direction network during navigation

2.1 Abstract

The vestibular system plays a crucial role in our everyday life as it ensures gaze and postural stabilization and the sense of self-motion by detecting the head motion in space. Previous work done in rodents (i.e., mice and rats) has led to the view that the nucleus prepositus hypoglossi (NPH) and the supragenual nucleus (SGN) in brainstem relay vestibular information (i.e., angular head velocity) from the vestibular system to the head direction (HD) network. However, the NPH has also been long-known to comprise the oculomotor integrator, which plays an essential role in gaze control and stabilization. To date, however, it remains unknown whether neurons in the NPH of rodents encode eye-related and/or head-related movement signals. To address this, we simultaneously recorded eye movements and the activity of NPH neurons during conditions which involves only eye movements versus both eye and head movements. We found that a dynamic eye movement-based model can characterize neuronal responses while mice generated eye movements in the absence of head motion. In addition, the same eye movement-based model can accurately describe responses during head rotations. Thus, our results demonstrated NPH neurons of mice primarily encode eye-related information even during head rotations. Notably, mouse NPH neurons also demonstrated a nonlinear response dependent on the amplitude of eye movements. Overall, our results provide the first evidence that mouse NPH neurons primarily encode eye movements rather than head movements. Thus, our findings suggest that NPH neurons relay an eye-related rather than head-related signal to the HD network.

2.2 Introduction

Knowledge of location and direction within the environment is crucial aspects of successful navigation. This spatial knowledge dominantly comes from visual cues but nonvisual cues such as vestibular, motor proprioceptive information also contribute especially when visual cues are absent (reviewed in Yoder and Taube, 2014) Monitoring these nonvisual cues, referred to as path integration, allows the estimation of linear and angular displacement of the head therefore providing a rapid updating of the animal's orientation (reviewed in Clark and Taube, 2012). These spatial cues are processed in a complex and interconnected network of spatially selective cells found throughout the brain such as place cells, grid cells and head directions cells. (place cells: O'Keefe, 1976; O'Keefe and Dostrovsky, 1971; grid cell: Fyhn et al., 2004; Hafting et al., 2005; Head direction cells: Ranck 1985; Taube et al., 1990; Taube, 2007).

One fundamental component of this network is head direction (HD) cells and these cell fire as a function of the animal's directional heading independent of animal's location and behavior (reviewed in Taube, 1998). The prevailing model that accounts for HD cell firing is continuous ring attractor network (reviewed in Knierim et al., 2012). This view proposes that the network receives inputs from cells sensitive to angular head velocity and HD cells in the network with preferred firing directions share excitatory connections with one another. The local area of activity is then moved around the ring to different directional heading. Given that the vestibular system conveys angular head velocity information, it has been inferred that the system sends the self-motion cues to update the ring attractor network. Indeed, previous studies involving lesions, inactivation and occlusions of the vestibular periphery all resulted in loss of head direction activity in anterior dorsal nuclei in thalamus and post subiculum (reviewed in Yoder and Taube, 2014; Clark and Taube, 2012). Anatomically, vestibular system also connects to the HD network via the supragenual nucleus (SGN) and the nucleus prepositus hypoglossi (NPH) which send projections to the dorsal tegmental nucleus and lateral mammillary nuclei where the HD signal originates (Hayakawa and Zyo, 1985; Liu et al., 1984; Mehlman et al., 2021).

However, electrophysiological evidence is lacking in support for this hypothesis that the vestibular system sends angular head velocity to the HD network. Though lesion in the NPH, a structure that is implicated to relay the vestibular signal to the HD network, led to disruption in HD signal (Butler and Taube, 2015), the finding is complicated by that fact that NPH controls eye movement (reviewed in McCrea and Horn, 2006). For decades, the role of NPH has been

established as an oculomotor integrator. In various animal models including goldfish, cats, and monkeys, the NPH is implicated to control eye movements such as vestibulo-ocular reflex (VOR), optokinetic nystagmus (OKN), pursuit and saccades (monkey: Cullen et al., 1993; McFarland and Fuchs, 1992; Cat: Escudero et al., 1996; Lopez-Barneo et al., 1982) Indeed, to date, most HD cell experiments have been done in rodent, rat in particular, and eye position was never measured in these experiments. Accordingly, it is important to perform systematic tests to find out what input goes into the HD network from the vestibular system and if gaze direction contributes to the HD system.

Accordingly, in the present study, we performed electrophysiological experiments to test whether mouse NPH also encodes angular head velocity. As mentioned above, most HD cell experiment were conducted without measuring eye movement. Thus, we recorded the activities of individual NPH neurons in mice while simultaneously measuring eye movement. We specifically tested whether NPH neurons encode eye movements by comparing neuronal responses during conditions which involves only eye movements versus both eye and head movements. Our results show neuronal responses of mouse NPH neurons to eye movement could account for responses during head rotations indicating that the nucleus prepositus predominantly encodes eye movements. Mouse nucleus prepositus also show nonlinear responses that are dependent on the amplitude of eye movements. Together, our results suggest that eye-related information is predominantly encoded in the mouse NPH.

2.3 Methods

2.3.1 Animals

Five male C57BL/6J (The Jackson Laboratory) adult mice were included in this study. All procedures were conducted under approved animal protocols at Johns Hopkins University.

2.3.2 Head-post implantation and craniotomy

Mice were anesthetized with isoflurane 2% in oxygen. A 1.5 mm-diameter craniotomy was performed. A custom-build head-post was cemented on the skull. Bupivacaine 0.5%) was given to mice before and after the surgery. Care was provided to avoid hypothermia and dehydration.

2.3.3 Electrophysiological recording

Neural activity of mouse NPH neurons were collected using either tungsten electrodes (8-10 MΩ impedance, FHC) or Neuropixel probes (IMEC). To locate the nucleus prepositus, we first located the abducens nucleus based on the characteristic discharge of its neurons to ipsilateral eye position/velocity during the SEP and OKR conditions and burst of action potentials for ipsilaterally directed saccades/quick phases (Stahl and Thumser 2012). We then mapped the nucleus' anterior-posterior and medial-lateral boundaries, verifying that its center comprised at 200-250 μm of this characteristic activity along a single-recording track. All the prepositus neurons in this study were then identified at a location ~200 μm posterior to the center of the abducens nucleus, which assured that they were not part of the abducens nucleus.

Tungsten electrodes were used with a custom-built microdrive. For acute usage of Neuropixel probes, an implant assembly was developed. This assembly allowed flexible positioning of the probe and retraction after experiments. The assembly consisted of two parts: a probe holder and a skull connector (**Fig 1A**). The probe holder had a slot where 2/3 of the dovetail rail on the back of the Neuropixel probe can be slid into. A set screw on the probe holder secured the probe holder and probe assembly in place. The rest of the dovetail rail on the Neuropixel probe was then attached to a stereotaxic adapter. The probe and its holder were lowered to the skull connector. The skull connector was cemented on the animal's skull where the craniectomy was. The depth of the probe in the brain when the probe and its holder touched the base of the skull connector was ~4.5mm. The probe holder was then fixed to the skull connector by tightening six screws on the skull connector against the probe holder. For extra security, removable glue was added on the top of the

probe holder. Finally, the probe was released from the stereotaxic adaptor and the animal was moved to the experimental setup. To retract a Neuropixel probe (**Fig 1B)**, the stereotaxic adaptor was reattached to the dovetail. Once the glue and screws on the skull connector were removed, the probe holder and the probe were lifted from the brain. Single-unit activity from tungsten electrodes was recorded through a Plexon system at a sampling rate of 20kHz for offline analysis. Neural data from Neuropixel probes was collected with SpikeGLX (Bill Karsh, https://github.com/billkarsh/SpikeGLX) at a sampling rat of 30kHz.

2.3.4 Recording setup

Eye and head movements were simultaneously recorded with neural activity. The animal was placed in a bodytube and was head-fixed. The animal was then placed in the rotating turntable surrounded by a drum with vertical black and white stripes (**Fig 2**). Head movements of the animal (whole-body rotation) was measured using a gyroscope on the turntable (MPU-9250, SparkFun Electronics). Two systems were used to measured eye movements: (1) a magnetic eye tracking system and (2) a mini camera system. For a magnetic tracking system, a small magnet (0.75 x 2mm; SuperMagnetMan) was implanted in on the eye. An angular magnetic field sensor (HMC1512, Honeywell) was affixed to the head directly above the implanted magnet. The rotation of the eye was then picked up by the sensor. For a mini camera system, a mini camera (Amazon) was positioned directly in front of one eye. The camera was secured in place by inserting the connector on the mini camera holder into its matching connector on the animal's head. Both systems encoded eye movements robustly.

2.3.5 Behavioral paradigms

Responses of nucleus prepositus were tested in three different paradigms. Each condition evoked either combined or dissociated head and eye movements (**Fig 3**).

During static eye position (SEP), the turntable was rotated through a series of steps to drive the eye at different eccentric positions in the orbit (range of ~20 degrees). Only the segments where both head and eye were stable were used for the analysis (Beraneck and Cullen, 2007).

Visually-evoked eye movements during optokinetic reflex (OKR) condition were generated by rotating the striped drum surrounding the animal. The turntable where the animal was

positioned remained stationary. The testing stimuli used were 0.5 Hz rotations at a velocity of 40 deg/s and 0.2 Hz rotations at a velocity of 20 deg/s.

During vestibulo ocular reflex (VOR) paradigm, the turntable was rotated while the striped drum remained stationary. This paradigm involves combined head and eye movements. The testing stimuli used were 0.5 Hz rotations at a velocity of 40 deg/s and 0.2 Hz rotations at a velocity of 12 deg/s.

2.3.6 Data analysis

Raw spike signals were imported into MATLAB (The MathWorks, Natick, MA) and analyzed using custom written algorithms. Data collected with Neuropixel probes were first sorted with Kilosort spike sorting software (Pachitariu et al., 2016) and curated using phy (https://github.com/kwikteam/phy).

All neurons were selected based on their modulation to ipsilateral eye position and velocity. Eye position and velocity sensitivities were computed using a linear firing rate estimation model described previously (Sylvestre and Cullen, 1999). For each model fit, we determined the estimated coefficients as well as the variance accounted for the resultant best fit: VAF={1-[var($\widehat{FR}(t)$)/var(FR)]}, where $\widehat{FR}(t)$ is the neuron's estimated firing rate and FR is actual firing rate. A VAF value of 1 indicates a perfect fit to the data and zero indicates a fit that is equivalent to the neuron's mean firing rate.

For each model coefficient that are computed in the analysis of neuronal responses during SEP, OKR and VOR paradigms, 95% bootstrap confidence intervals were computed as previously reported (Dale and Cullen, 2013). Specifically, 2,000 new data sets were generated by randomly sampling with replacements from the original data segments. Coefficient values were estimated for the 2,000 iterations. Distributions were generated for each coefficient and were checked to see if they overlap with zero.

2.3.7 Statistical analysis

Data are reported as the mean ± SEM. Non-parametric Wilcoxon test was performed to test significance. Prism 9 (GraphPad) was used for statistical analyses.

2.4 Results

The goal of this study was to establish whether neurons in the mouse nucleus prepositus hypoglossi (NPH) contribute to head-motion signaling. To address this question, we first characterized the firing rate of single NPH neurons while mice generated eye movements in the head-restrained condition (i.e., static eye position (SEP) and optokinetic response (OKR) conditions) and fit a dynamic eye movement-based model of neuronal responses. Next, we rotated the mouse relative to space to activate the vestibular system and recorded the activity of the same NPH neurons as well as the eye movements generated by the vestibulo-ocular reflex (VOR). We then assessed whether the same eye movement-based model that described a given neuron's activity during eye movements made in the absence of head motion (i.e., SEP and OKR) could also be used to accurately predict its firing rate during head rotations (i.e., VOR). Finally, to directly address the latter question, we adapted our initial stimulation protocols so that the eye movements evoked by visual stimulation during OKR and vestibular stimulation during VOR were comparable in their dynamics.

2.4.1 Responses of nucleus prepositus neurons in conditions where the eye but not the head moves

All NPH neurons recorded in this study were robustly modulated by ipsilateral eye position and eye velocity during head-restrained conditions, consistent with prior characterizations of burst-tonic prepositus neurons in nonhuman primates (Cullen et al., 1993; McFarland and Fuchs, 1992; Dale and Cullen, 2013). Figure **4A** shows the responses of an example neuron while the mouse generated eye movements in the SEP condition: the neuron fired a burst of action potentials for ipsilaterally directed saccades (red arrow) and sustained tonic firing rates that varied linearly with eye position.

To quantify the eye position sensitivity and resting discharge of a given neuron, we used a VAF criterion to find the best fit of the following eye-based model to the neuronal response:

$$\widehat{FR}(t) = bias + kE(t) \qquad \text{(Eq. 1)}$$

where $\widehat{FR}(t)$ is the neuron's estimated firing rate; *bias* is the resting discharge; *k* is the sensitivity to eye position (spike/s)/(deg); $E(t)$ is the eye position. The fit obtained using this approach is illustrated in Figure **4A** for the example neuron, where the superimposed model fit (red trace) well approximates the example NPH neuron's actual firing rate. Overall, this model well described

NPH neuron firing rates during SEP; across our population of neurons, the mean population VAF for Eq. 1 was 0.51±0.07.

Figure **4B** shows the responses of this same example neuron while the mouse generated eye movements in the OKR condition. Optokinetic reflex eye movements were evoked in the absence of head motion by sinusoidally (about the earth-vertical axis) rotating a striped drum around the stationary mouse (see Methods). These eye movements function to move the eye in the direction of the striped drum's rotation in order to stabilize the visual world relative to the retina. In response to OKR movements, NPH neurons demonstrated an increase in firing rate for ipsilaterally directed eye movements that led eye position but lagged eye velocity. To quantify the eye position sensitivity, eye velocity sensitivity, and resting discharge of a given neuron in this condition, we added the eye velocity term to the eye-based model in Eq. 1 and then again used a VAF criterion to find the best fit of the following eye-based model to the neuronal response:

$$\widehat{FR}(t) = bias + kE(t) + r\dot{E}(t) \qquad \text{(Eq. 2)}$$

Where r is the sensitivity to eye velocity (spike/s)/(deg/s); $\dot{E}(t)$ is the eye velocity.

The fit obtained using this approach is illustrated in Figure **4B** for the example neuron, where the superimposed model fit (red trace) again well approximates the example NPH neuron's actual firing rate. Overall, this model well described NPH neuron firing rates during OKR; across our population of neurons, the mean population VAF for Eq. 1 was 0.54±0.05.

Figures **4C-E** compare the firing rate bias and eye movement sensitivities during the SEP and OKR conditions across our population of NPH neurons. The firing rate bias estimated in the OKR and SEP conditions using Equations 2 and 1, respectively, were not significantly different (**Fig 4C**; 53.78±8.4 spike/s for SEP; 46.94 ±9.7 spike/s for OKR). The average eye position sensitivity (*k*) estimated for OKR was generally greater than that estimated in the SEP condition, but they were not significantly different (**Fig 4D**; 4.0 ±0.9 vs. 6.0 ±1.1 (spike/s)/(deg), *P*=0.084). Finally, across the population, the estimated eye velocity sensitivity (*r*) for OKR was 3.4 ±0.8 (spike/s)/(deg/s). No eye velocity estimate was obtained from the SEP condition since this condition evoked static rather than dynamic changes in eye position (see Methods). For each model estimate, we computed 95% confidence intervals using a non-parametric bootstrap approach (See Methods). The 95% bootstrap confidence intervals for the eye position sensitivity and eye velocity sensitivity did not overlap with zero, indicating that two terms contributed significantly to the best estimate of NPH neuron firing rates.

2.4.2 Eye-based models also well describe neuronal firing rates during passively applied head movements in the VOR condition

We next tested whether the same eye movement-based model that described a given neuron's activity during eye movements made in the absence of head motion (i.e., SEP and OKR) could also accurately predict firing rates during head rotations. To do this, we recorded the activity of the same NPH neurons as we rotated the mouse relative to space to activate the vestibular system. VOR eye movements are evoked in response to such head rotations, thus we specifically addressed a given neuron's sensitivity to eye movement could account for its modulation during head rotations.

Figure **5A** shows the responses of the same example neuron shown in Figure **4**, while the mouse generated VOR eye movements in response to the head motion (vestibular stimulation). These eye movements function to move the eye in the direction *opposite* to that of ongoing head motion in order to stabilize the visual world relative to the retina. As for SEP and OKR movements, NPH neurons demonstrated an increase in firing rate for ipsilaterally directed eye movements (i.e., compensatory eye movements evoked by contralateral head motion) that led eye position but lagged eye velocity. Additionally, most neurons generated a burst of activity (red arrow) for ipsilaterally directed saccadic quick phases of the VOR response. To quantify the eye position sensitivity, eye velocity sensitivity, and resting discharge of a given neuron during the compensatory VOR eye movements evoked by head rotations, we again applied a VAF criterion to Eq. 2 to find the best fit. The firing rate estimate obtained using this approach is illustrated in Figure **5A** for the example neuron (red trace) again well approximates the example NPH neuron's actual firing rate. Overall, an eye movement-based model well-described NPH neuron firing rates during OKR; across our population of neurons, the mean population VAF for Eq. 2 was 0.59 ± 0.04. In addition, the 95% bootstrap confidence intervals of eye position and eye velocity coefficients did not overlap with zero.

We then compared values of *bias*, *k*, and *r* coefficients estimated in the VOR condition to those estimated in the OKR and SEP conditions to determine whether the same eye-based model can be used to predict NPH neuron firing rates across conditions. Overall, the firing rate bias (*bias*) estimated for the VOR condition (60.8 ±12.9 spike) was comparable to that estimated for the OKR and SEP conditions (**Fig 5B**). In contrast, the eye position sensitivity (*k*) estimated for the VOR condition (3.0 ±0.9 (spike/s)/(deg)) was comparable to that estimated for the SEP condition but

significantly lower than that estimated for the OKR condition (**Fig 5C**; *P*=0.049). Likewise, the eye velocity sensitivity (*r*) estimated in the VOR condition (0.7±0.1 (spike/s)/(deg/s)) was also significantly lower compared to that estimated for the OKR paradigm (**Fig 5D**; *P*= 0.002).

Previous studies have shown that eye position and velocity sensitivities of neurons in the extraocular motor nuclei - to which NPH neurons directly project - decrease systematically as a function of peak eye velocity generated during eye movement behaviors (Sylvetre and Cullen 1999; Stahl and Thumser 2012). Thus, we hypothesized that the eye movement sensitivities of NPH neurons might demonstrate a similar relationship. To test this proposal, we first compared the amplitude of eye movements generated during VOR and OKR paradigms for which stimuli were sinusoidal rotations (0.5Hz, +/- 40 deg/s) of the vestibular motion platform versus visual surround, respectively (**Fig 5E**). On average, visual field stimulation (0.5Hz, +/- 40 deg/s) applied in the OKR condition evoked an eye movement response of 7.0 ±1.1 deg/s. In contrast vestibular motion platform stimulation (0.5Hz, +/- 40 deg/s) produced a significantly greater eye movement response (**Fig 5F;** 35.7 ±5.0 deg/s; *P*= 0.002).

2.4.3 An eye-movement based model can predict firing rates during passive head motion if eye amplitudes are matched

Based on our above analysis, we next posited that: If the amplitudes of the eye movements evoked in the OKR and VOR conditions were matched (rather than the amplitudes of the stimuli themselves), then eye movement sensitivities would be comparable across the two conditions. To investigate this possibility, we used a stimulation frequency that produced a relatively large OKR response while still being of high enough frequency to evoke a robust VOR response. In mice, the VOR is most effective for head motion at frequencies above >0.2 Hz, while the OKR reflex is most effective at lower frequencies, particularly below 0.2 Hz (see Luebke et al., 2014). Accordingly, we choose a 0.2 Hz stimulus frequency at this transition zone. Specifically, in the matched OKR condition, we sinusoidally rotated the visual field at 0.2Hz, with a peak velocity of +/- 20 deg/s (**Fig 6A)**. To evoke an eye movement of a comparable amplitude in the matched VOR condition, we sinusoidally rotated the vestibular motion platform at 0.2Hz, with a peak velocity of +/- 12 deg/s (**Fig 6B)**. As illustrated in **Figure 6C**, the amplitudes of the eye movements generated in these two conditions were consistently comparable across trials (12.6 ±1.7 deg/s for OKR; 11.3 ±1.1 deg/s for VOR).

We next directly tested our above hypothesis: If the amplitudes of the eye movements evoked in the OKR and VOR conditions were matched (rather than the amplitudes of the stimuli themselves), then NPH neuron eye movement sensitivities would be comparable across the two conditions. To do this, we recorded an additional population of NPH neurons (n=15) in the matched OKR and VOR conditions. Figures **6D-F** compare the firing rate bias and eye movement sensitivities during the matched OKR and VOR conditions across our population of NPH neurons, with the original SEP estimates also included for comparison.

Overall, the firing rate bias (*bias*) estimated in the matched OKR and VOR conditions was not significantly different from each other or from that estimated for the SEP condition (**Fig 6D**; 54.5 ±7.4 versus 58.7 ±7.3 spike/s for OKR versus VOR). Additionally, and importantly, the eye position sensitivities (*k*) estimated for the matched OKR and VOR conditions were also comparable (**Fig 6E**; 3.4 ±0.6 versus 4.0 ±0.8 (spike/s)/(deg) for OKR versus VOR), and not significantly different from that estimated for the SEP condition. Finally, across the population, the estimated eye velocity sensitivities (*r*) for the matched OKR and VOR conditions were also comparable (**Fig 6F**; 0.9 ±0.2 versus 1.2 ±0.2 (spike/s)/(deg/s)). Thus, consistent with our hypothesis, NPH neuron eye movement sensitivities were comparable across the OKR and VOR conditions when the amplitudes of the evoked eye movements were matched. Thus, the same eye movement-based model that describes NPH neuron activity during eye movements made in the absence of head motion (i.e., OKR) could also be used to accurately predict its firing rate when the head moves and there is vestibular stimulation (VOR).

2.4.4. The variance in the firing rate during the VOR paradigm did not respond to head motion

So far, we have shown when amplitudes of the eye movements are in the same range, NPH neurons similarly encode eye position and velocity sensitives made in the absence or presence of head motion. Indeed, an eye movement-based model equally described NPH neuron firing rates in the matched OKR and VOR conditions; across our population of neurons, the mean population: VAFs for Eq. 2 were 0.58 ± 0.05 versus 0.58 ± 0.03, respectively.

To explicitly address the implications of this finding regarding the question of eye versus head movement coding by mouse NPH neurons during the VOR condition, we next directly compared: (1) the VAF obtained from the eye-based model (i.e., Eq 2) optimized to estimate the

neuron's firing rate directly (i.e., *VOR FR estimate*) and (2) with that obtained using the model prediction estimated from the same neuron's response in the matched OKR condition (*VOR FR prediction*) (**Fig 7A**). Consistent with the proposal that neurons predominately encode eye and not head velocity, we found that the VAF obtained from the OKR eye-based model fit with close to the same precision as that obtained from optimizing the model to directly fit the VOR dataset (0.58 ± 0.03 versus 0.59 ± 0.04, respectively). Again, this suggests the same eye-based model estimated during the OKR condition could be used to accurately predict the firing rates for the fixed head movements.

Finally, we examined the possibility that, during the VOR paradigm, the firing rate residual relative to our eye-based models might encode head motion. To do this, we computed the residual for both of our model fits: the *VOR FR estimate* and *VOR FR prediction* ($\widehat{FR}residual$**; Fig 7A**). To then determine whether there was any sensitivity to head velocity (g) we used a VAF criterion to find the best fit of the following head-based model to the residual firing rates:

$$\widehat{FR}residual(t) = bias + g\dot{H}(t) \quad (3)$$

Where g is the sensitivity to head velocity (spike/s)/(deg/s); $\dot{H}v(t)$ is the head velocity.

Generally, the residual firing rates from both model fits did not show significant modulation to head velocity as demonstrated by the mean population VAF for VOR *FR estimate* (0.024 ±0.006) and *VOR FR prediction* (0.031 ±0.01) **(Fig 7B**). Importantly, the 95% bootstrap confidence intervals for the head velocity coefficient estimated from both models overlapped zero. Similar results were obtained from models of the residual that includes head position / acceleration terms in addition to head velocity. Addition of head position / acceleration terms increased population mean VAF only by 0.09 and 0.02 respectively (mean VAF with position term: 0.11 ± 0.03; mean VAF with acceleration term: 0.046 ± 0.01). The 95% bootstrap confidence intervals for each coefficients spanned again zero. Thus, taken together, these results suggest that NPH neurons predominately encode eye position and velocity, but negligible head movement information.

2.4.5 NPH neuronal responses display amplitude-dependent non-linearities

Finally, our results above suggest that eye movement sensitivities of NPH neurons decrease with increasing movement amplitude. To better understand this nonlinearity, we plotted the

sensitivities of neurons as function of peak movement velocity across paradigms. Specifically, **Figure 8A-C** superimposes the population-averaged coefficients estimated using Eq. 2 for each of the conditions. This data set includes, i) VOR, 0.5Hz, +/- 40, ii) OKR, 0.5Hz, +/- 40, iii) VOR, 0.2Hz, +/- 12 and iv) OKR, 0.2Hz, +/- 20, as well as bias and eye position sensitivities computed during the static SEP condition (where peak velocity = 0 deg/s). Notably, the coefficient estimates in our eye-based models exhibited similar trends as a function of eye velocity to those reported previously for extraocular motoneurons and NPH neurons in rhesus monkeys (Sylvestre and Cullen 1999, 2003) as well as extraocular motoneurons in mouse (Stahl and Thumser 2012). Estimated eye-position and eye-velocity sensitivities decreased with increasing eye velocity whereas bias estimates increased with increasing eye velocity. Thus, these data emphasize that NPH neuronal responses display significant amplitude-dependent non-linearities. As considered in the discussion, these trends likely to reflect nonlinearities that are intrinsic to the extraocular muscles.

2.5 Discussion

Summary

The results of this study demonstrate that mouse nucleus prepositus neurons predominantly encode eye movement related information (i.e., eye position and velocity) during head rotations. Specifically, we first recorded responses of NPH neurons during eye movements made in the absence of head motion (i.e., SEP and OKR). We found that the eye movement-based model characterized by bias, eye-position, and eye-velocity terms can accurately described a given neuron's firing rate during those conditions. We then characterized firing rates of each given NPH neuron during head rotations (i.e., VOR) and found that same eye movement-based model based on these bias, eye-position, and eye-velocity terms could be used to predict its firing rate, indicating that neurons did not display significant modulation to head-motion. We further found that NPH neurons demonstrate significant nonlinearities in their encoding of eye movement. Notably, neuronal sensitivities decreased with increasing eye movement amplitude. Taken together, our findings establish that that mouse NPH neurons mainly convey eye-related information.

2.5.1 Comparison with quantitative analysis of the NPH neurons in other species

Prior studies have reported quantitative analyses of NPH neuron sensitivities to eye movements in other species, most notably cat and monkey (cat: Escudero et al., 1996; Lopez-

Barneo et al., 1982; Delgado-Garcia et al., 1989; monkey: McFarland and Fuchs, 1992; Sylvestre et al., 2003; Dale and Cullen, 2013). Here, NPH neuronal responses were characterized during different classes of eye movements including static fixation, smooth eye movements, and saccades. Consistent with these prior studies, here we found that NPH neurons significantly encoded both eye position and eye velocity (monkey: Dale and Cullen, 2013; cat; Escudero et al., 1996; Delgado-Garcia et al., 1989). Overall, we found that NPH neuronal eye position sensitivity was, on average, 3.6 ± 2.9 spike/s/deg during fixation. This value is similar to that previous reported in both cat and monkey models (3.4 ± 2.6 (Escudero et al., 1996) versus 3.2 ± 2.0 spike/s/deg (Sylvestre et al., 2003, Dale and Cullen 2013), respectively. Prior studies in monkey also estimated sensitivities to both eye position and velocity during visual tracking movements, specifically recording neuronal responses during smooth pursuit. Because mice do not generate smooth pursuit, here we instead quantified neuronal eye velocity sensitives response visual tracking movements made during OKR. On average, we obtained vales that were lower (0.9 ±0.2 spike/s/deg) to these reported in monkey (~0.5 ± 0.2 (spike/s)/(deg/sec), Sylvestre et al., 2003, Dale and Cullen 2013). Interestingly, the head related sensitivities of vestibular afferents and vestibular nuclei neuron are also substantially less in mice compared to monkey (Beraneck and Cullen, 2007). I speculate that the lower sensitivities in premotor oculomotor and vestibular pathways in the mouse are more energy efficient but come at the cost of performance. Further studies will be required to determine whether evolutionary pressure for increased accuracy of motor performance underlies the differences observed across species.

2.5.2 Amplitude-dependent response nonlinearities in mouse prepositus neurons

Our analysis of NPH neural eye movement sensitivities further revealed an amplitude-dependent nonlinearity in the responses of prepositus in the mouse. Specifically, as the amplitude of eye movements became larger, firing rate modulation failed to increase proportionately, causing both *k* and *r* to decrease. A similar result has been reported for the eye movement sensitivities of NHP neurons in monkey (Dale and Cullen 2013). Thus, overall, comparison with the existing literature suggests that NPH neurons generally share similar strategies of encoding eye velocity sensitivity across species. Interestingly, NPH neurons target extraocular motoneurons in the abducens neurons, and prior single unit recording studies have also established that abducens neurons demonstrate a comparable amplitude-dependent response nonlinearity across species

including mouse (monkey: Sylveste and Cullen 1999; rabbit: Stahl and Simpson, 1995; mouse: Stahl and Thumser, 2012). While the source of the nonlinearity is unclear, it has been speculated that this amplitude-dependent encoding of eye movements by prepositus and abducens neurons accounts for the nonlinear relationship between firing rate and muscle tension (Sylvestre and Cullen, 1999).

2.5.3 Implications regarding the functional role of descending NPH pathways

Anatomical, neurophysiological and lesion studies in a wide range of species have established that the NPH plays a vital role in the control of eye movements. Anatomically, the NPH sends descending projections to the extraocular motor nuclei and some areas of the reticular formation (monkey: Belknap and McCrea, 1988; Robinson et al., 1994; cat: Langer et al., 1986; McCrea and Baker. 1985; rat: Iwasaki et al., 1999). Additionally, NPH neurons send projections to brain regions including the vestibular nuclei and play a role in matching the dynamics of the motor commands that generate the vestibulo-ocular reflex (VOR) and optokinetic nystagmus to the biomechanical requirements of the eye (monkey: Belknap and McCrea, 1988; Carleton and Carpenter, 1983; cat: McCrea and Baker. 1985; rabbit: Arts et al., 2000; Barmack et al., 1993). Additionally, as reviewed above, NPH neurons robustly encode eye position across species including monkeys and cats, as well as mice as shown in the present study. Further, lesions to the NPH result in the inability to hold the eye position following ipsilateral saccades (monkey: Cannon and Robinson, 1987; Kaneko, 1997; cat: Cheron et al., 1986a) and reduced VOR and OKR gains after the lesion (monkey: Kaneko, 1999: cat: Cheron et al., 1986a and b). In this context, both the eye movement related responses and connectivity of the nucleus prepositus are consistent with its role as an essential component of the neural integrator that generates eye-position signals for the VOR and saccades (Cannon and Robinson, 1987). Indeed, despite difference in reliance on visual information between species, our results support a common role of the NPH in ocular motor control that is conserved across mammalian species.

2.5.4 Implications regarding the functional role of the ascending NPH pathway to the HD network

The NPH also sends ascending projections to the dorsal tegmental nucleus (DTN), which in turn projects the head direction cell network via the lateral mammillary nuclei (LMN) (Blair et

al., 1999; Bassett et al., 2007). In addition, the NPH receives direct inputs from the vestibular nuclei (reviewed in McCrea and Horn, 2006). Most computational models that account for the tuning of HD cells to head direction are based on continuous ring attractor networks, which receive input from cells sensitive to angular head velocity (Skaggs et al., 1995; Zhang, 1996; Redish et al., 1996). Accordingly, the connectivity between the vestibular nuclei, NPH, and DTN have led to the proposal that the NPH transmits vestibular information to the HD network (Blair et al., 1999; Bassett et al., 2007). Specifically, the prevailing view is that that the vestibular nuclei relay head motion information via the NPH, and smaller nearby supragenual nucleus (SGN) to the DTN (reviewed in Yoder and Taube, 2014; Cullen and Taube 2017). In support of this view, is the finding that partial and complete lesions of the NPH can disrupt direction-specific firing in anterodorsal thalamus (ADN) (Butler and Taube, 2015).

However, as noted above, it has been well established that NPH lesions produce profound impairments in oculomotor control (Cannon and Robinson, 1987; Kaneko, 1997; Cheron et al., 1986a). Specifically, lesions to the NPH will produce gaze instability that will in turn ultimately lead to HD cell instability given that their tuning is anchored to visual cues (Goodridge and Taube, 1995; Zugaro et al., 2003). I therefore speculate that increased gaze instability is the primary cause of the unstable HD cell firing observed after the targeted lesion of the NPH (Butler and Taube, 2015). Likewise, increased gaze instability is a probable cause of the unstable HD cell firing after lesions to the peripheral vestibular system which also results in gaze instability (reviewed in Yoder and Taube, 2014; Cullen and Taube 2017).

To determine conclusively the functional contribution of the NPH to the HD signal, future work examining HD cell firing with simultaneous recordings of both eye and head movement are needed. My thesis research had emphasized that we did not identify a subpopulation of NPH neurons that showed sensitivity to head as well as eye movements. Specifically, using an extended firing rate estimation model with head velocity term (Eq.3), we confirmed that head movement sensitivity is not significantly different from zero consistent with prior finding in monkeys (see also, Dale and Cullen, 2013). Accordingly, I assert that the NPH input to the DTN predominantly encodes eye movements.

Finally, lesions of the SGN also lead to instability in the direction-specific firing of HD cells (Clark and Taube, 2012). In this context, it is interesting that a recent anatomical study reported denser projections from the SGN to the DTN compared to those arising from the NPH

indicating the importance of the SGN in processing of the HD signal (Mehlman et al., 2021). Interestingly, the same study found that the majority of individual NPH neurons project either the DTN or abducens, but rarely to both structures. Given that different cells preferentially project to the DTN versus abducens, these authors raise the question as to whether a small subpopulation of NPH neurons, encoding head motion information based on inputs from the vestibular nuclei, might selectively target the DTN. While this question is open, it is premature to argue that a this is the case. In fact, even neurons in the vestibular nuclei do not solely encode head motion information but integrate vestibular signals with proprioceptive, eye movement and head/body motor signals. A more likely alternative possibility is that the NPH relays eye-related information to the HD cell network, such that eye movement information contributes to the direction-specific firing of HD cells. Future studies involving the recording of DTN-recipient NPH neurons will be required to distinguish between these possibilities.

2.5.5 Future directions

During navigation, animals navigate the environment while making a wide range of voluntary head movements. My current study did not include a condition in which we recorded the activity of nucleus prepositus neurons while animals made voluntary head movements. If neural sensitivities to eye movements could account for a given NPH neuron's firing modulation during voluntary head rotations, this would further support my main conclusions. Indeed, in nonhuman primate model, an eye-based model estimated during smooth pursuit could describe firing rates of neurons during voluntary head movements (Dale and Cullen, 2013). Accordingly, I developed a training protocol for mice that evokes robust voluntary head movements in 16 days (See **Fig 9**). Future efforts to incorporate this voluntary head movement condition will allow more physiologically realistic assessment of eye movement encoding in prepositus neurons.

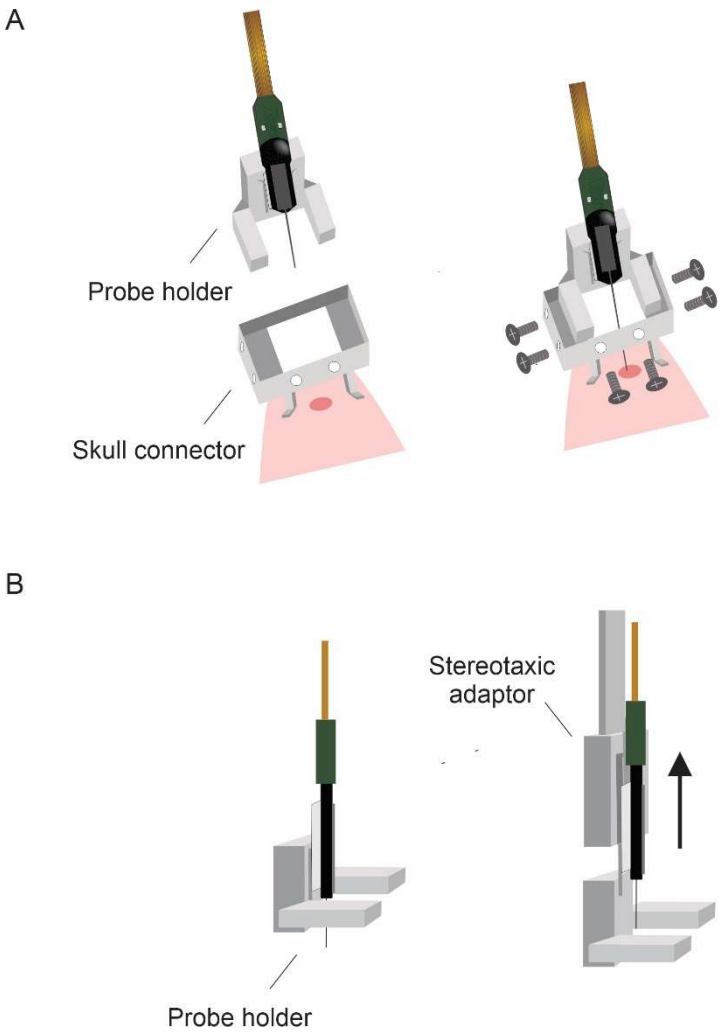

Figure 1. **Schematic of an implant assembly of Neuropixel probes**. **(A)** the dovetail rail of a probe was slid into the probe holder and was fixed with a screw. The probe and its probe holder were lowered to skull connector (cemented on the skull) and the assembly was fixed with screws and removable glue. **(B)** To retract the probe, the stereotaxic adaptor was attached to the dovetail rail of the probe. The probe was then released from the probe holder and retracted.

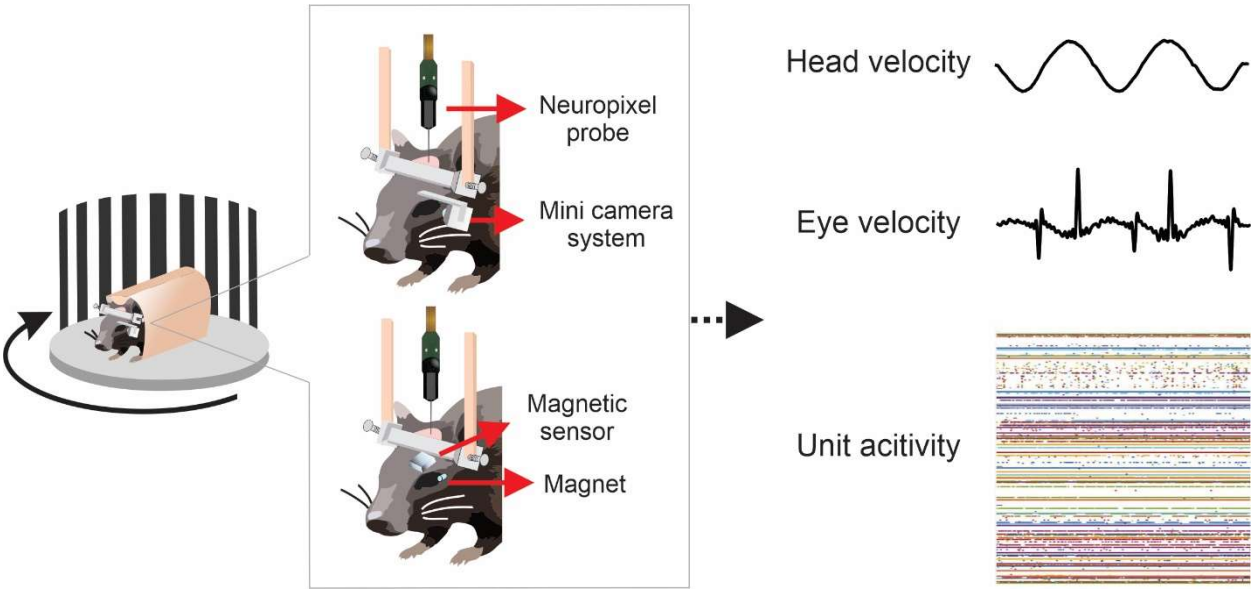

Figure 2. **Schematic representation of the experimental setup**. During the experiment, animals were placed in a plastic tube at the center of a turntable surrounded by a striped drum. Eye movements were simultaneously recorded by either a mini camera system or magnetic eye-tracking system. Head movements were also measured using a gyroscope on the turntable

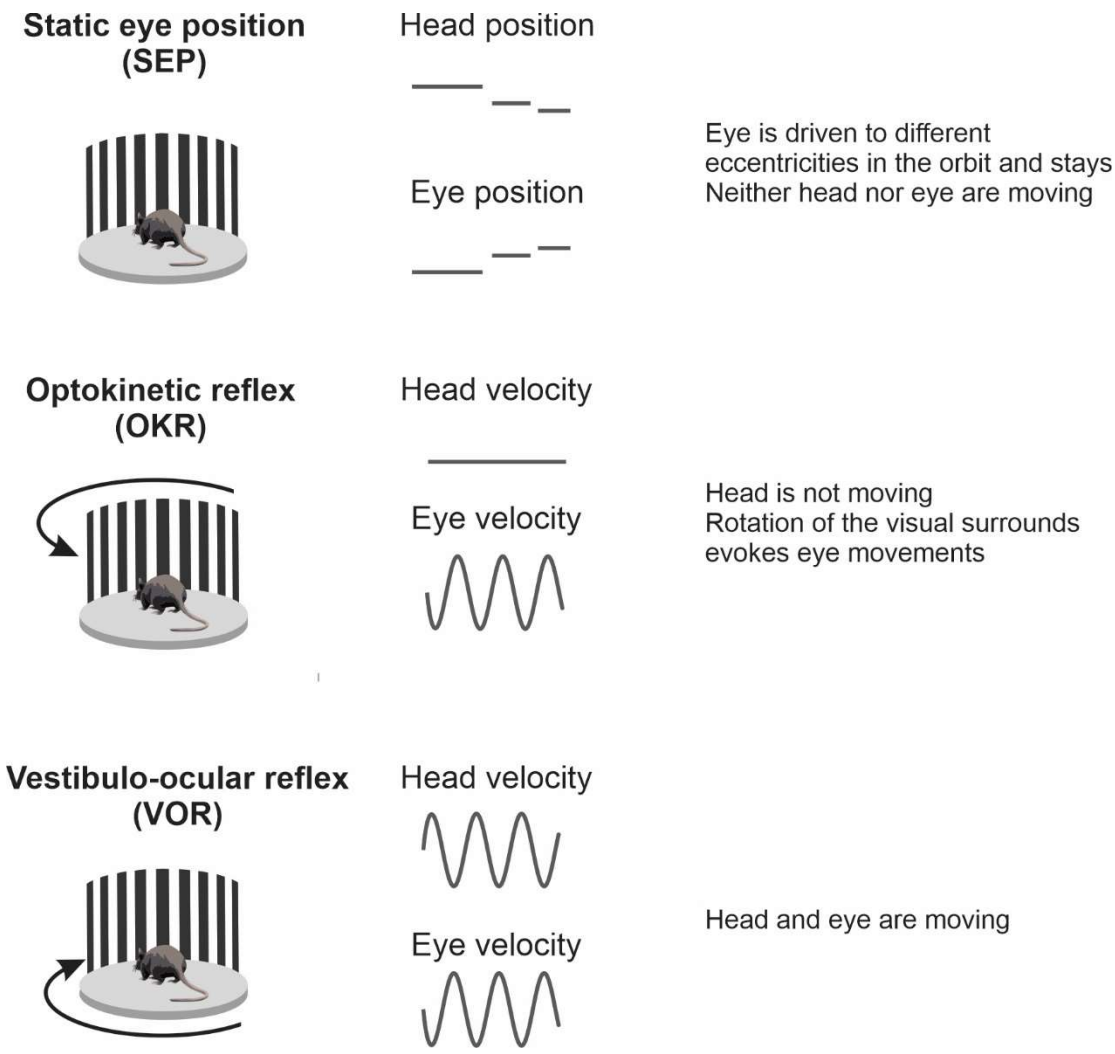

Figure 3. **Behavioral paradigms tested. (Top)** During the static eye position (SEP) paradigm**,** mice were rotated through a series of steps, driving the eye to different eccentric positions. Only the segments where neither the head nor the eye were moving were selected for the analysis. **(Middle)** Rotation of the striped drum evoked eye movements in mice during the optokinetic reflex (OKR) paradigm. **(Bottom)** Both head and eye were moving during the vestibulo ocular reflex (VOR) paradigm.

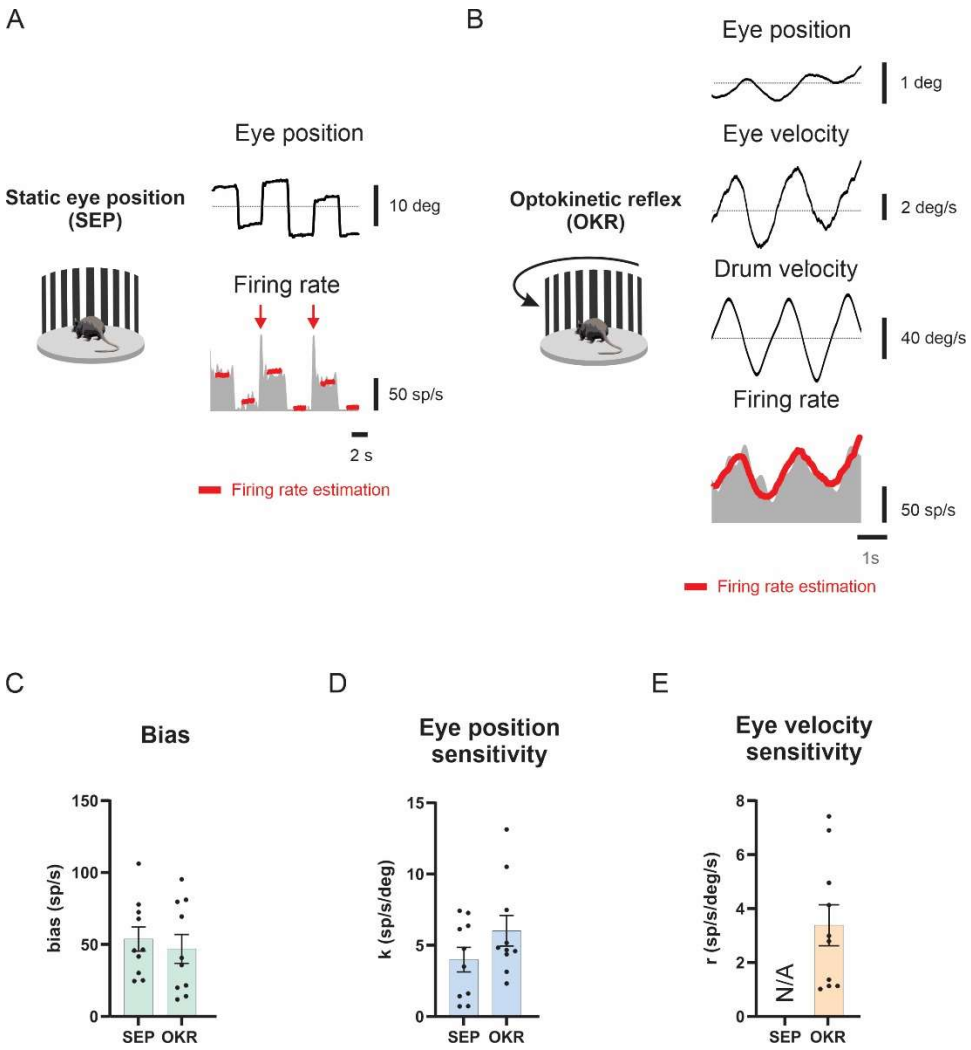

-

Figure 4. **Activity of a typical nucleus prepositus neuron during SEP and OKR paradigms**. (A) The example neuron's response during the SEP paradigm and (B) the OKR paradigm. Red lines represent the firing rate estimation. Read arrows indicate ipsilaterally directed saccades. Traces toward the top of the page correspond to the neuron's ipsilateral direction. Population summary of (C) *bias*, (D) eye position sensitivity (*k*) and (E) eye velocity sensitivity (*r*) values from SEP and OKR paradigms (N=10).

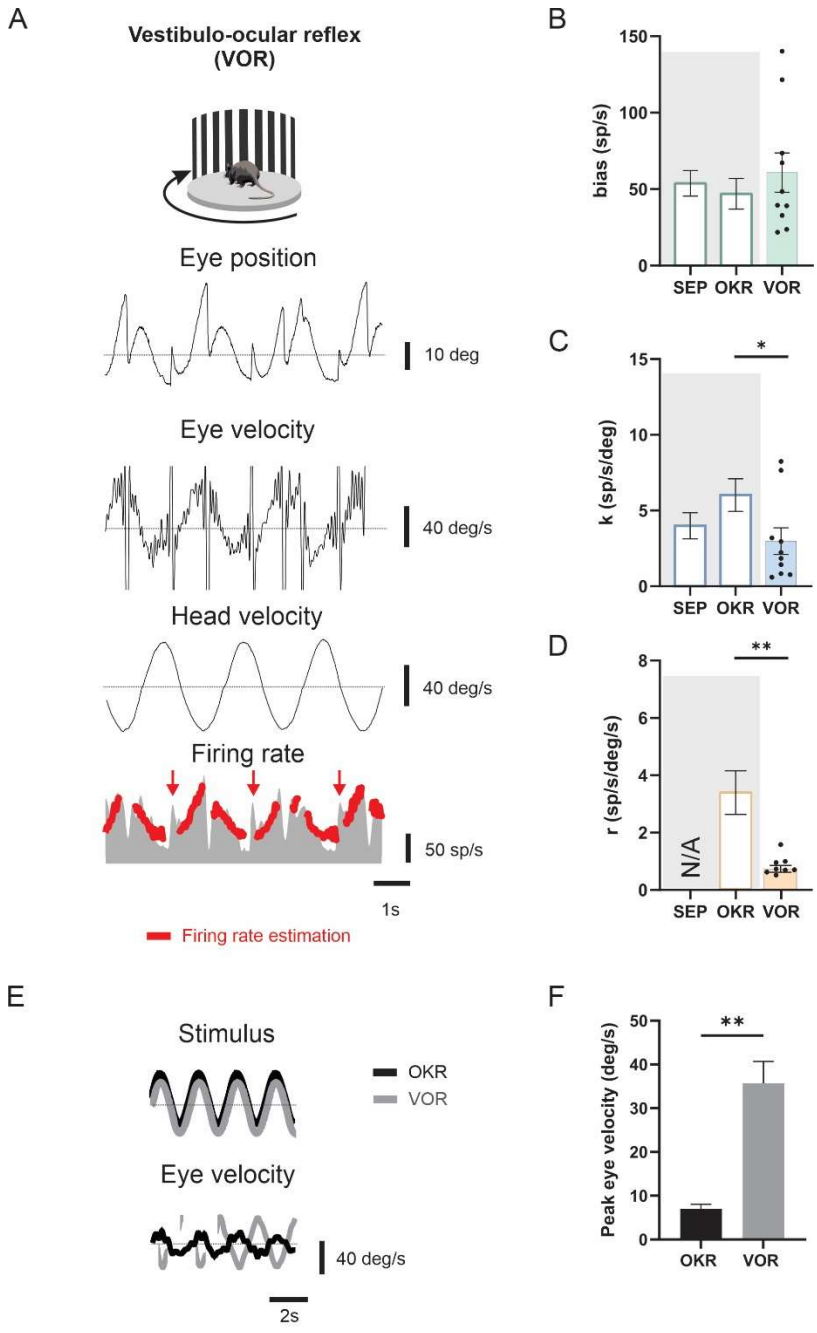

Figure 5. **Eye sensitivities during the VOR paradigm.** (A) The example neuron's response during the VOR paradigm. Red lines represent the firing rate estimation. Traces toward the top of the page correspond to the neuron's ipsilateral direction. . Read arrows indicate ipsilaterally directed saccades. Population summary of (B) *bias*, (C) eye position sensitivity (*k*) and (D) eye velocity sensitivity (*r*) values from SEP, OKR and VOR paradigms (N=10). (E) The stimuli tested and observed eye velocity from OKR and VOR paradigms. (F) Peak eye velocity during OKR and VOR paradigms. Comparisons were made with Wilcoxon paired t-test. *P<0.05, **P<0.01.

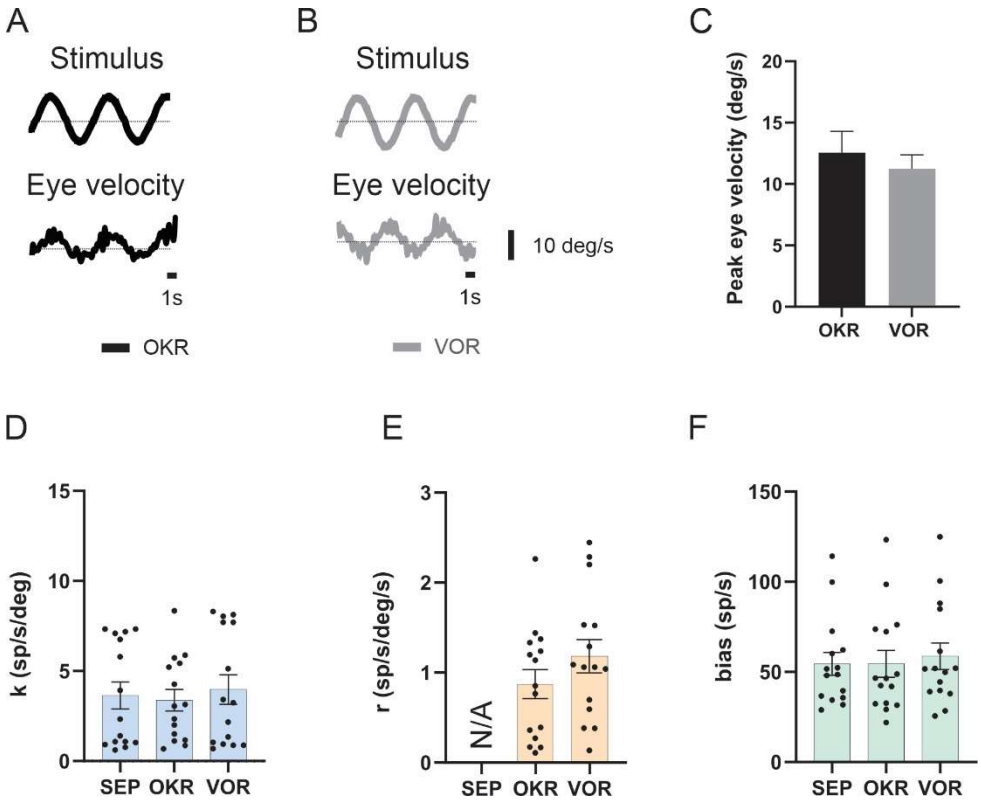

Figure 6. **Eye sensitivities are comparable across all paradigms when the eye amplitudes are matched.** (A) The stimulus tested and observed eye velocity from OKR paradigm. (B) The stimulus tested and observed eye velocity from VOR paradigm. (C) Peak eye velocity during OKR and VOR paradigms. Population summary of (D) *bias*, (E) eye position sensitivity (*k*) and (F) eye velocity sensitivity (*r*) values from SEP, OKR and VOR paradigms (N=15).

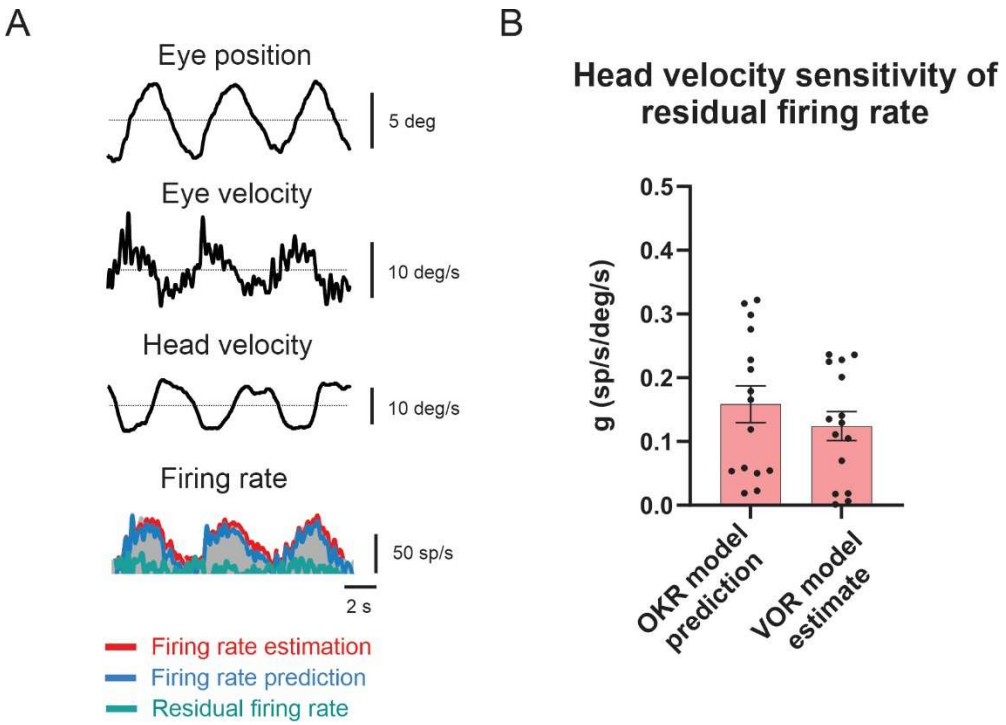

Figure 7. **Head motion is not encoded in the prepositus neurons**. (A) Firing rate estimation from VOR paradigm (red line), predicted firing rate by the model derived from the OKR paradigm (blue line) and residual firing rate (actual firing rate- predicted firing rate). (B) Population summary of the head velocity sensitivity (*g*) for residual firing rates from both of model fits: *VOR model estimate* and OKR *model prediction*.

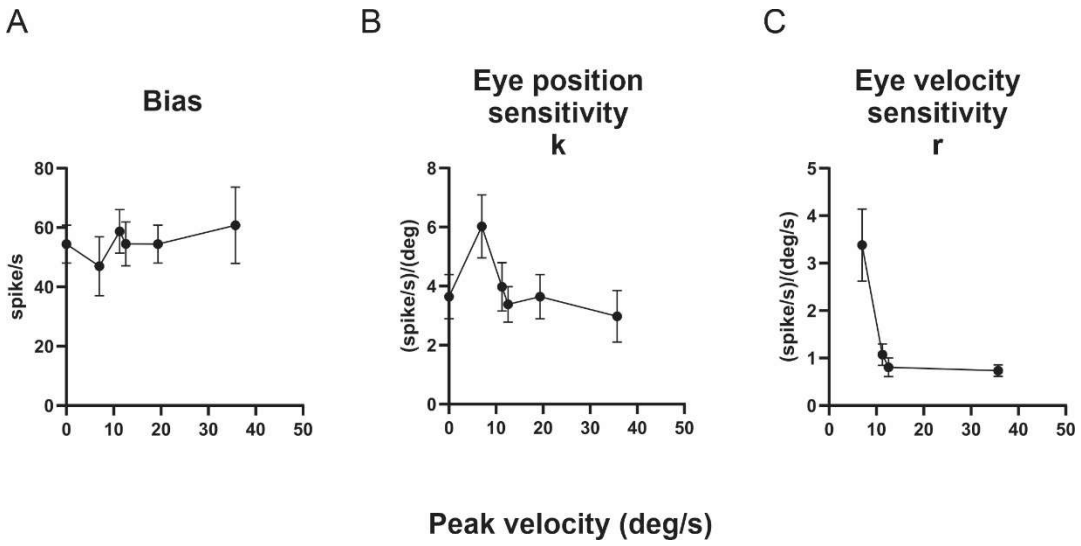

Figure 8. **Eye position and velocity coefficients and bias as a function of the peak eye velocity.** Population summary of (A) *bias*, (B) eye position sensitivity (*k*) and (C) eye velocity sensitivity (*r*) values from SEP, OKR and VOR paradigms with different peak eye velocities.

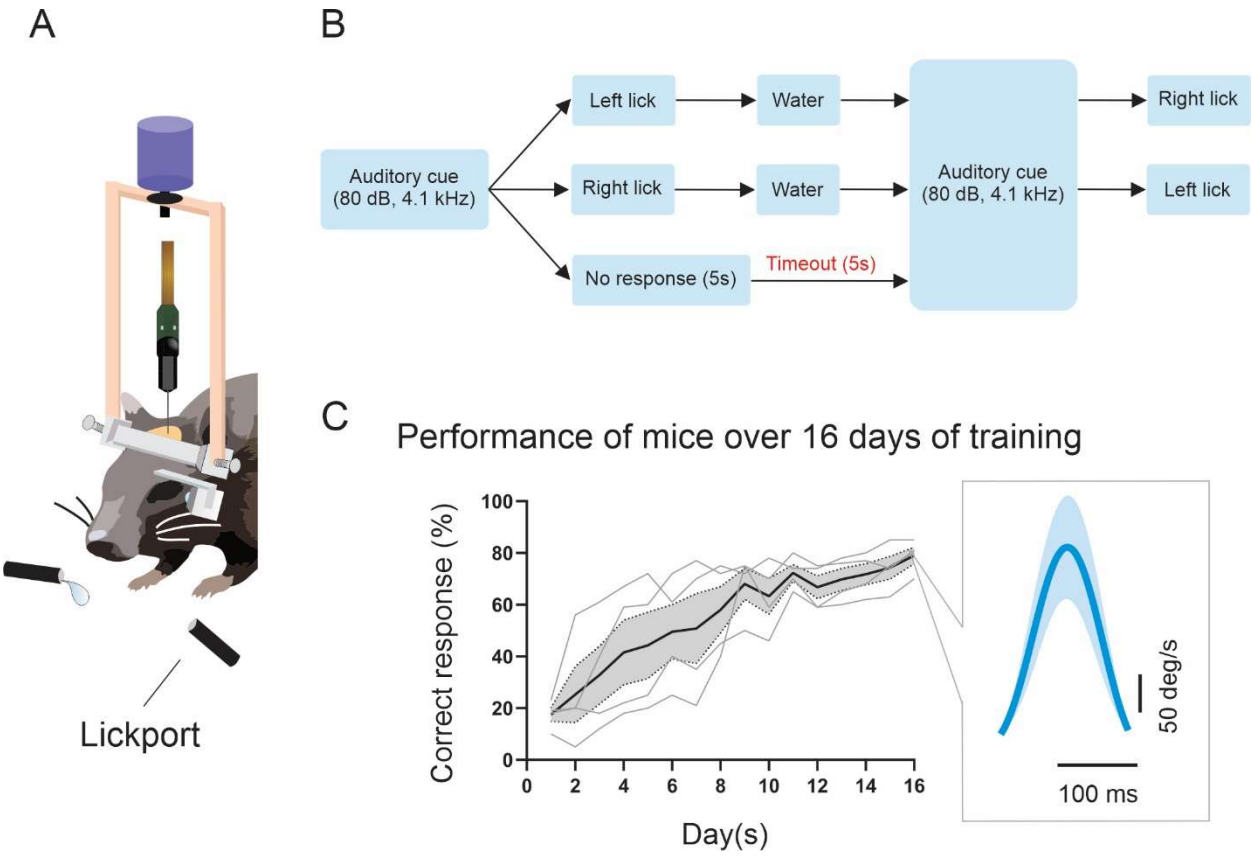

Figure 9. **Training protocol for evoking voluntary head movements in mice**. **(A)** A schematic of the experimental setup. Mice was head-restrained so that they were free to move their heads in yaw-axis. Dual lickports were positioned to the left and right side of mice. **(B)** A block-diagram of the possible events in a single trial. **(C)** Performance of example mice (n=4) over 16-day-period. Black line is the average of 4 mice (grey lines). Shaded area indicates SEM. (Inset) An example of head movement made after 16 days of training.

Chapter 3

Loss of flocculus Purkinje cell firing precision leads to impaired gaze stabilization in a mouse model of spinocerebellar ataxia type 6 (SCA6)

3.1 Abstract

Spinocerebellar Ataxia Type 6 (SCA6) is a mid-life onset neurodegenerative disease characterized by progressive ataxia, dysarthria, and eye movement impairment. This autosomal dominant disease is caused by the expansion of a CAG repeat tract in the *CACNA1A* gene that encodes the α1A subunit of the P/Q type voltage-gated Ca^{2+} channel. Mouse models of SCA6 demonstrate impaired locomotive function and reduced firing precision of cerebellar Purkinje in the anterior vermis. Here, to further assess deficits in other cerebellar-dependent behaviors, we characterized the oculomotor phenotype of a knock-in mouse model with hyper-expanded polyQ repeats ($SCA6^{84Q}$). We found a reduction in the efficacy of the vestibulo-ocular reflex (VOR) and optokinetic reflex (OKR) in SCA6 mutant mice, without a change in phase, compared to their litter-matched controls. Additionally, VOR motor learning was significantly impaired in $SCA6^{84Q}$ mice. Given that the floccular lobe of the cerebellum plays a vital role in the generation of OKR and VOR calibration and motor learning, we investigated the firing behavior and morphology of floccular cerebellar Purkinje cells. Overall, we found a reduction in the firing precision of floccular lobe Purkinje cells but no morphological difference between $SCA6^{84Q}$ and wild-type mice. Taken together, our findings establish that gaze stabilization and motor learning are impaired in $SCA6^{84Q}$ mice and suggest that altered cerebellar output contributes to these deficits.

3.2 Introduction

Spinocerebellar ataxias (SCAs) are a group of autosomal-dominant neurodegenerative disorders. SCAs display a highly heterogenous genotype-phenotype spectrum, but the unifying clinical symptoms observed across all SCAs include the loss of balance, gait ataxia, and slurred speech (reviewed in Klockgether et al., 2019). One subtype of SCA, SCA6, is characterized by a late-onset ataxia with a relatively slow progression rate. Prior studies have reported cerebellar atrophy and Purkinje cell loss in the cerebellar hemispheres and vermis of SCA6 patients (Gomez et al., 1997; Schols et al., 1998; Ishikawa et al., 1999; Sasaki et al., 1998; Yang et al., 2000; Murata et al. 1998; Satoh et al. 1998; Butteriss et al. 2005; Lukas et al. 2006). In addition to their balance and gait deficits, patients with SCA6 generally display oculomotor abnormalities such as nystagmus (reviewed in Solodkin & Gomez, 2012).

SCA6 is categorized as a polyglutamine SCA because it results from an expansion of a CAG repeat within the gene CACNA1A that, in turn, produces a polyglutamine (polyQ) expansion (Zhuchenko et al., 1997). The CACNA1A gene encodes the αA subunit of P/Q-type voltage-gated calcium channels. Notably, these channels are highly expressed in the cerebellum and are required for spontaneous firing properties of Purkinje cells (Hillman et al., 1991; Westenbroek et al., 1995; Womack et al., 2004). Several mouse models that mimic the disease-causing mutation have been developed to understand the underlying pathophysiology, with the ultimate goal of developing treatments for patients with SCA6 (Watase et al., 2008; Unno et al., 2012; Du et al., 2013; Mark et al., 2015). Mouse models include the CT-longQ27^{pc} mutant in which pathological C-terminus fragments of the αA subunit of P/Q channel are overexpressed and the SCA6^{84Q} knock-in models characterized by hyper-expanded polyQ repeats. Both models display a progressive ataxic phenotype, which begins when the animal is 7- to 8-months-old (Mark et al., 2015; Jayabal et al., 2015; Jayabal et al., 2016). Purkinje cell degeneration was observed prior to the onset of ataxic behavior in CT-longQ27^{pc} mice (Mark et al., 2015). On the other hand, the phenotype precedes Purkinje cell degeneration in SCA6^{84Q} mice (Jayabal et al., 2015). Previous studies have recorded from Purkinje cells in the cerebellar vermis in each of these two SCA6 mouse models and found a reduction in firing precision compared to wild-type mice (Mark et al., 2015; Jayabal et al., 2016).

Importantly, studies of these two SCA6 mouse models to date have focused on quantifying and understanding their resultant ataxic phenotypes. However, the SCA6 mutation affects P/Q-

channels throughout the entire cerebellum, including the vestibulocerebellum (Gomez et al., 1997). Thus, we predicted that other cerebellar-dependent behaviors would also be impaired. Notably, the cerebellum plays a crucial role in optimizing eye movement control for gaze stability. In particular, the vestibulo-ocular reflex (VOR) and optokinetic reflex (OKR) generate compensatory eye movements that stabilize the visual field on the retina. The flocculus of the cerebellum modulates VOR and OKR. In addition, the flocculus is involved in oculomotor learning, for example, calibrating the amplitude (gain) and direction of the VOR. Hence, we hypothesized that VOR and OKR responses and VOR motor learning may be affected in a mouse model of SCA6.

To test this hypothesis, we recorded eye movements in SCA6^{84Q} and wild-type mice. We first quantified VOR and OKR responses and found that the gains of both reflexes were significantly reduced in SCA6^{84Q} compared to wild-type (WT) mice. In contrast, analysis of the relationship between vestibular quick phase amplitude and peak velocity revealed no differences, indicating that the observed VOR and OKR deficits were not the result of nontarget effects at the level of the extraocular motoneurons and/or their innervations. We next evaluated VOR motor learning to determine whether SCA6^{84Q} mice also demonstrated deficits during this cerebellar-dependent task. We found that VOR motor learning was indeed significantly impaired in SCA6^{84Q} mice by ~ 50%. Finally, because the floccular lobe of the cerebellum plays a key role in the generation of VOR, OKR, and VOR motor learning, we examined whether the firing behavior and morphology of floccular Purkinje cells were altered in SCA6^{84Q} mice. In vivo recordings revealed altered firing precision in both anesthetized and awake SCA6^{84Q} mice, but no detectable changes in morphology were found. Taken together, our results establish that gaze stability and cerebellar-dependent VOR motor learning are impaired in SCA6^{84Q} mice. We suggest changes in the firing properties of floccular Purkinje cells contribute to these observed deficits in gaze stability.

3.3 Methods

3.3.1 Animals

We used a knock-in mouse model of SCA6 with a humanized 84 CAG repeat expansion mutation at the *CACNA1A* locus (SCA684Q). We bred heterozygous mice (Jackson laboratories, Bar Harbor, Maine; strain: B6.129S7-Cacna1atm3Hzo/J; stock number: 008683) to obtain litter-matched SCA684Q/84Q and wild-type control mice. Genotyping was performed using primer sequences published by Jackson laboratories for this strain. All animal procedures were approved by the Johns Hopkins University and McGill University Animal Care Committees and were in accordance with the regulations established by the Canadian Council on Animal Care.

3.3.2 Quantification of VOR and OKR

Surgical techniques and experimental setup have been previously described (Beraneck and Cullen, 2007). Eye movement data were collected using an infrared video system (ETL-200, ISCAN system). The rotational velocity of the turntable (head velocity) was measured using a MEMS sensor (MPU-9250, SparkFun Electronics). Eye movements during OKR were evoked by sinusoidal rotations of a visual surround (vertical black and white stripes, visual angle width of 5°) placed around the turntable at frequencies 0.2, 0.4, 0.8, 1 and 2 with peak velocities of ±16◦/s. To record VOR responses, the turntable was rotated at sinusoidal frequencies 0.2, 0.4, 0.8, 1, and 2 Hz with peak velocities of ±16◦/s in both light and dark. In the light condition, the visual surround remained stationary, whereas, in the dark condition, both the visual surround and turntable rotated in phase. Head and eye movement signals were low-passed filtered at 125 Hz, and sampled at 1kHz. Eye position data were differentiated to obtain velocity traces. Cycles of data with quick phases were excluded from the analysis. Least-square optimization determined the VOR and OKR gains and phases plotted as mean ± standard error of the mean (SEM) against all frequencies for all mice.

3.3.3 In vivo single-unit recording data acquisition and analysis

The extracellular activity was obtained with glass micropipettes filled with 2M NaCl (Sutter Instrument). The electrode was advanced into the left flocculus using a manipulator (Narishige International, Amityville, NY). Signals were amplified and band-pass filtered (400Hz-5000Hz). The single-unit activity was recorded using a Plexon system at a sampling rate of 20kHz for offline analysis. Raw spike signals were imported in MATLAB (The MathWorks, Natick, MA) and analyzed. The spike timing precision was quantified using a coefficient of variation (CV). CV

is calculated using the formula, $CV = \frac{\sigma ISI}{\mu ISI}$, where σ and μ are the standard deviation and mean of the inter-spike intervals (ISI). In addition to CV and frequency of simple spikes, the CV2, which measures short-scale regularity in spike trains, was also calculated where $CV2 = \frac{2|ISI_{n+1} - ISI_n|}{(ISI_{n+1} - ISI_n)}$.

3.3.4 Immunohistochemistry

Mice were deeply anesthetized with intraperitoneal injection of 2,2,2-tribromoethanol (Avertin) prior to intracardiac perfusion with an initial flush of ice-cold phosphate-buffered saline (PBS, 0.1M, pH 7.4) with 5.6 μg/mL heparin salt. This was followed by perfusion with 40 mL of 4% paraformaldehyde (PFA) in phosphate buffer (PB, pH 7.4) before removal of the brain which was post-fixed in 4% PFA at 4°C for 24 hours. Brains were stored in PBS with 0.5% sodium azide at 4°C until sectioning. 100 μm thick coronal slices of cerebellar tissue containing the flocculus were prepared using a Vibratome 3000 sectioning system (Concord, ON, Canada).

Immunohistochemistry was performed on free floating slices. Briefly, slices were incubated for 30 minutes in blocking solution with 5% bovine serum albumin (BSA), then washed and incubated for 3 days with anti-calbindin (CB300, Swant, Burgdorf, Switzerland) primary antibody in blocking solution followed by a 90-minute incubation with AlexaFluor 488 anti-mouse (715-545-150, Jackson Immunoresearch, West Grove, USA) secondary antibody in blocking solution. After a final wash in PBS and Triton X, slices were mounted using ProLong Gold Antifade mounting medium (ThermoFisher Scientific, Waltham, USA) and stored protected from light at 4°C.

3.3.5 Image acquisition and analysis

Imaging was performed using an LSM800 confocal microscope (Zeiss), using Zeiss Zen software for image acquisition. Image analysis was performed in FIJI (ImageJ; US National Institutes of Health). Molecular layer height measurements were taken at 4 points along the molecular layer and pooled. Purkinje cell density was calculated by first measuring the length of the Purkinje cell layer and then counting the number of visible Purkinje cell somas along the previously measured length.

3.3.6 Statistical analysis

Data are reported as the mean ± SEM. Two-way repeated-measures ANOVA followed by Bonferroni *post hoc* comparison tests was used to test significance for the following data: (1) the VOR/OKR data across frequencies and; (2) VOR learning across frequencies. For the main sequence analysis, the extra sum-of-squares *F* test was used to compare two slopes. Non-parametric Mann–Whitney *U*-test was performed to test significance for (1) percent change in VOR learning, (2) firing rate, CV, and CV2 comparison and 3) Floccular morphology comparisons. Prism 9 (GraphPad) or MATLAB was used for statistical analyses.

3.4 Results

3.4.1 VOR and OKR gains are reduced in SCA6^{84Q} mice

To test whether these mice show deficits in oculomotor control, we first quantified the VOR responses of SCA6^{84Q} mice during rotation about an earth vertical axis. To measure VOR responses, head restrained mice were rotated at 0.2, 0.4, 0.8, 1, and 2 Hz with 16◦/s peak velocity in the dark (referred to as VORd). We quantified the dynamic properties of VORd by computing the gain and phase for each testing frequency. Litter-matched wild-type control mice displayed robust compensatory eye movements, which increased as a function of frequency. In contrast, SCA6^{84Q} mice showed significantly reduced VOR gain at high frequencies (**Fig 1A**) compared to wild-type mice (wild-type vs. SCA6^{84Q} gains at 0.8 Hz, p=0.021; at 1 Hz, p=0.005; at 2 Hz, p=0.008). At the highest frequency tested (at 2 Hz), we found a 28% decrease in VORd gain of SCA6^{84Q} mice. In contrast, there was no difference in the VOR phase between the two groups of mice (**Fig 1B**). We next quantified optokinetic eye movement responses (OKR) generated in response to a moving visual scene. Gains at 0.2 and 0.4 Hz were also significantly reduced in SCA6^{84Q} mice without changes in the response phase (**Fig 1C and D**; wild-type vs. SCA6^{84Q} gains at 0.2 Hz, p=0.0046; 0.4 Hz, p=0.042). Finally, VOR gain was also quantified in a lit environment (referred to as VORl), where VOR functions in concert with OKR. VOR gains of SCA6^{84Q} mice were significantly reduced at all testing frequencies with no change in the phase response (**Fig 1D and E**; wild-type vs. SCA6^{84Q} gains at 0.2 Hz, 0.4 Hz, 0.8 Hz, and 1 Hz, p<0.01, 2 Hz, p=0.021). Thus, we found that, as we hypothesized, eye movements evoked by VOR and OKR testing were altered in homozygous SCA6^{84Q} mice relative to their litter-matched controls.

3.4.2 Nystagmus dynamics are comparable between wild-type and SCA6^{84Q} mice

One possible alternative explanation for the marked deficits in the VOR and OKR gains of SCA6^{84Q} mice is that they reflect non-targeted effects, occurring at the level of extraocular motoneurons and/or their innervations of extraocular muscles. To rule out these possibilities, we analyzed the dynamics of quick phases generated during VOR testing, which are produced by a premotor saccadic circuit largely separate from that producing the compensatory VOR (i.e., slow phase) (for review, see Cullen and Van Horn, 2011). In agreement with previous studies (McMullen et al., 2004, Luebke et al., 2014), quick phase amplitudes were proportional to quick phase peak velocities in wild-type control mice (**Fig 2,** blue symbols). Moreover, we found that this relationship, called the main sequence, was comparable (**Fig 2,** red symbols; p = 0.28) for SCA6^{84Q} mice suggesting that the VOR and OKR gain deficits were not the result of a processing impairment at the level of the extraocular motoneurons and/or their innervations. Interestingly, this result is consistent with prior reports of normal saccade velocities in reported in SCA6 patients (Buttner et al., 1998).

3.4.3 VOR learning is impaired in SCA6^{84Q} mice

The floccular region of the cerebellum is known to play a crucial role in calibrating VOR responses. In SCA6 patients, most of the cerebellum is affected, including the floccular lobe. Thus, we hypothesized that the flocculus of the SCA6^{84Q} mice would also be affected by the mutation, and robust VOR adaptive changes would be affected. To test if SCA6^{84Q} mice show a VOR learning deficit, we carried out a 30-minute-long VOR gain-down training with both wild-type and SCA6^{84Q} mice (**Fig 3A**). Head restrained mice were placed in the turntable that rotates together with the visual field, so the target VOR gain is 0. The training stimulus was 2 Hz with a peak velocity of 16 ◦/s. The learning acquired was assessed by quantifying change in the VOR gain after training. At the testing frequency where we expected the most significant gain decrease (2 Hz), there was an average of 46.2±5.0% decrease in VOR gain after training (**Fig 3B and C**). In contrast, SCA6^{84Q} mice showed an average of 21.6±5.0% decrease in VOR gain after training (**Fig 3C and D**; percent change difference at 0.4 Hz, p=0.035; 0.8 Hz, p=0.0012; 1 Hz, p=0.0012; 2Hz, p=0.0082), indicating that the SCA6^{84Q} mice were less able to adapt their eye movements to stabilize their gaze and thus have deficits in VOR learning, likely due to alterations in the floccular region of the cerebellum.

3.4.4 Firing precision is altered in SCA6^{84Q} mice

Attenuated VOR/OKR gains and impaired VOR learning in SCA6^{84Q} mice lead us to speculate that altered neuronal firing in the flocculus may explain such deficits. Notably, a reduction in Purkinje cell firing rate and precision has been reported in the anterior vermis of SCA6^{84Q} mice, and are associated with ataxia (Jayabal et al., 2016). We thus hypothesized that floccular Purkinje cells in SCA6^{84Q} mice might demonstrate comparable changes. To test this, we performed single-unit recordings in the flocculus of both anesthetized and awake mice (**Fig 4A-B**). We found that in the anesthetized state, Purkinje cell simple spike firing rate was significantly increased in SCA6^{84Q} mice compared to wild-type mice (p=0.0218; **Fig 4C**). Additionally, the coefficient of variation (CV) of the inter-spike intervals (**Fig 4D**) in SCA6^{84Q} mice was significantly higher in SCA6^{84Q} mice, indicating reduced firing precision in SCA6^{84Q} mice (p=0.0002). We also computed CV2 (see Methods) as it takes into account the presence of burst firing and pauses that are more characteristic of in vivo recordings (Jayabal et al., 2016; Holt, 1996). This measure likewise indicated increased firing irregularity in SCA6^{84Q} mice compared to wild-type controls (p=0.0002; **Fig 4E**). Interestingly, in awake mice, floccular Purkinje cell simple spike firing rates were significantly lower in SCA6^{84Q} mice compared to wild-type control cells (p=0.0083; **Fig 4F**). However, both CV and CV2 values of SCA6^{84Q} mice remained higher than wild-type mice in awake mice, indicating a reduced firing precision consistent with our observations from anesthetized mice (CV, p=0.004; CV2, p=0.0387; **Fig 4G and H**). Together, these findings suggest that loss of firing precision in the floccular lobe may contribute to VOR/ OKR and learning deficits in SCA6^{84Q} mice.

3.4.5 Flocculus morphology appears normal in SCA6^{84Q} mice

Given the changes in the firing properties of Purkinje cells in the flocculus and the behavioral changes in OKR and VOR, we wondered whether the morphology of the Purkinje cells in the flocculus would be altered in SCA6. Molecular layer height has been shown to be altered in other mouse models of ataxia, and in some cases is restricted to specific regions of the cerebellum (SCA1: Chopra et al., 2020; SCA2: Koeppen, 2005; SCA17: Rolfs et al., 2003). Similarly, Purkinje cell loss is seen in multiple mouse models of ataxia, particularly at advanced disease stages, and can also be region specific (Chopra et al., 2020; Blot et al.,2021 Stoyas et al., 2020; Lariviere et

al., 2015; Toscano-Marquez et al., 2021). We have previously shown that the molecular layer height and Purkinje cell density in lobules 3 and 9 of SCA6 mice are unchanged at disease onset, even when behavioral and Purkinje cell firing deficits are present (Jayabal et al., 2015). Indeed, we only observed changes in Purkinje cell density and molecular layer height at a much more advanced disease stage of 2 years of age, when Purkinje cell loss was also observed (Jayabal et al., 2015). However, given that we identified Purkinje cell firing and behavioral deficits specific to the flocculus in SCA6, we wondered whether Purkinje cell morphology could be altered in a region-specific manner in the flocculus at disease onset.

We performed immunohistochemistry with anti-calbindin antibody to label Purkinje cells in the flocculus of litter-matched wild-type and $SCA6^{84Q}$ mice at 7.5-8 months. This labelled Purkinje cells in the flocculus of both wild-type and $SCA6^{84Q}$ mice (**Fig 5A**) and allowed visualization of the morphology of the flocculus. The flocculus appeared normal in $SCA6^{84Q}$ mice, and analysis of both molecular layer height and Purkinje cell density showed no significant differences between wild-type and $SCA6^{84Q}$ mice (**Fig 5B and C**, molecular layer height median wild-type 115.9µm, $SCA6^{84Q}$ 112.2µm, p=0.30; Purkinje cell density median value wild-type 3.1 cells/ 100µm, $SCA6^{84Q}$ 3.0 cells/ 100µm, p=0.33). Thus, Purkinje cell morphology in the flocculus appears normal at disease onset. Any differences in behavior or Purkinje cell firing appear to be arising from other changes in Purkinje cell function, similar to what we have previously observed in other regions of the cerebellum in $SCA6^{84Q}$ mice (Jayabal et al., 2015, 2016).

3.5 Discussion

Summary

To date, studies of SCA6 mouse models mainly focused on deficits in motor behaviors (Mark et al., 2015; Jayabal et al., 2015). Here we show that knock-in mouse models of SCA6 with hyper-expanded polyQ repeats show a reduction in VOR and OKR responses as well as an impairment of VOR motor learning. To our knowledge, this is the first study to establish that $SCA6^{84Q}$ mice have oculomotor deficits and impaired VOR learning. Because the flocculus of the cerebellum plays a key role in the generation of VOR and OKR responses, we determined whether there were changes in the flocculus of $SCA6^{84Q}$ mice relative to their litter-matched controls. We identified changes in the firing activity of floccular Purkinje cells in $SCA6^{\mathbf{84Q}}$ mice that are

consistent with impaired VOR/OKR response and VOR learning. However, quantification of Purkinje cell density and molecular layer height in the flocculus, showed no changes in SCA6$^{\mathbf{84Q}}$ mice, suggesting that Purkinje cells are not dying and have normal gross morphology at this age. Taken together, our findings suggest that mutations of the *CACNA1A* gene in SCA6^{84Q} mice lead to changes in the firing properties of floccular Purkinje cells leading to impaired gaze stabilization.

3.5.1 Comparison of oculomotor deficits in SCA6 patients and a mouse model of SCA6

Clinical studies in human subjects have reported oculomotor deficits in SCA6 patients. While SCA6 patients generally have normal saccade velocities that fall on the main sequence, their smooth pursuit and optokinetic nystagmus gains are severely reduced (Gomez et al., 1997; Buttner et al., 1998). Reports regarding the VOR in SCA6 patients, however, show less consensus. Some studies have reported normal gains (Takeichi et al., 2000; Buttner et al., 1998), while others have reported both increases (Gomez et al., 1997) and decreases (Yu-Wai-Man et al., 2009; Weist et al., 2001) in VOR gains. Huh et al. (2015) has suggested that such discrepancy can be due to difference in stimuli and severity of the disease.

Our present experiments in SCA6^{84Q} mice similarly reveal that rapid eye movements fall on the main sequence while OKR gain is significantly reduced in SCA6^{84Q} mice. In our mouse model of SCA6, we found that VOR gain was reduced (by 28% at 2 Hz). Because the cerebellum plays a vital role in visually-induced motor learning, we predicted that VOR motor learning would also be impaired in SCA6^{84Q} mice. Consistent with our prediction, VOR motor learning was also significantly impaired in SCA6^{84Q} mice compared to their littermate controls (21.6% vs. 46.2% learning at 2 Hz, respectively). To date, no study to our knowledge has tested VOR learning in SCA6 patients. Nevertheless, given the cerebellum's essential role in VOR motor learning, we speculate that these patients will show deficits similar to those reported here for SCA6^{84Q} mice.

3.5.2 SCA6 in relationship with other CACNA1A mutant mice

SCA6 is not the only disease that affects the P/Q channel alpha subunit: deletion mutations of the same gene underlie episodic ataxia type 2 (EA2) in patients, which also demonstrate gaze impairments (Lemos and Manto 2022). Missense mutations in domain II and III and split-site of

the *CACNA1A* gene have led to the generation of three specific mutant mouse strains: tottering (cacna1a^{tg}), rocker (cacna1a^{rkr}), and leaner mice (cacna1a^{tg1a}) respectively (reviewed in Pietrobon, 2002), which have no clinical analog. Interestingly, these mutant stains also demonstrate impaired gaze stabilization (Stahl, 2004; Stahl et al., 2006; Katoh et al., 2006). For example, all three of these *CACNA1A* mutant strains show reduced gains of optokinetic (OKR) and vestibulo-ocular (VOR) reflexes as well as impaired VOR learning similar to the SCA6 model mice tested in the present study (Stahl, 2004; Stahl et al., 2006; Stahl and Thumser, 2014; Katoh et al., 2006).

The oculomotor impairments reported for SCA6^{84Q} mice in the present study were linked to the observed increased irregularity in floccular Purkinje cell simple spike firing (i.e., **Fig 4**).-We have likewise previously demonstrated a relationship between ataxic behavior in SCA6^{84Q} mice and increased irregularity in anterior vermis Purkinje cell simple spike firing (Jayabal et al. 2016). Further, another SCA6 mouse mutant (CT-longQ27^{pc}) also displays decreased Purkinje cell simple spike firing regularity (Mark et al., 2015). Deletion mutations of *CACNA1A* also show impairment in firing regularity in cerebellar vermis (Walter et al., 2006; Alvina & Khodakhah, 2010), and when firing regularity is restored, is associated with a reduction of ataxia. Interestingly, floccular Purkinje cells of rocker and tottering mutant mice also showed increased firing irregularity scaled with the severity of the oculomotor deficit (Stahl and Thumser, 2014). Together, these results suggest that impairments in Purkinje cell firing precision of SCA6 mice contribute to both oculomotor and gait deficits.

3.5.3 Morphological changes of Purkinje cell in anterior vermis and flocculus

Histological and resonance imaging (MRI) analyses of the brains of SCA6 human patients have demonstrated the loss of Purkinje cells, and cerebellar atrophy is most prominent in the vermis of the cerebellum and, to a lesser extent, the cerebellar hemispheres (Morphology: Gomez et al., 1997; Ishikawa et al., 1999; Yang et al., 2000; MRI: Sasaki et al., 1998; Murata et al. 1998; Satoh et al. 1998; Butteriss et al. 2005; Lukas et al. 2006). In this context, it is notable that our studies have identified both motor control and oculomotor dysfunctions in 7-month-old SCA6^{84Q} mice (i.e., Jayabal et al., 2015 and present study), but found no significant morphological changes in Purkinje cells in either the anterior vermis or the flocculus. Thus, our findings suggest a minimal contribution of cell loss to the impairments observed in this early disease stage in SCA6^{84Q} mice.

It is generally believed that cerebellar cell loss follows a trend; the zebrin-positive flocculonodular lobules of cerebellum are considered to be more resistant to neurodegeneration as compared to anterior cerebellum (Slemmer et al., 2007). Additionally, in a mouse model of ARSACS, both the zebrin identity and anterior-posterior location of Purkinje cells determined their susceptibility to disease insult, both at the level of Purkinje cell loss and loss of innervation to the cerebellar nuclei (Toscano-Marquez et al., 2021). Moreover, higher levels of sphingosine kinases, which are also thought to be protective against neurodegeneration, have been reported in the flocculonodular lobules compared to the anterior vermis (Blot et al., 2021). Indeed, changes in flocculus of SCA6 patients are relatively moderate compared to the cerebellar atrophy and Purkinje cell loss reported in the vermis (Gomez et al., 1997; Ying et al., 2015). Thus, given that several different factors appear to combine to maintain Purkinje cells in the flocculus versus vermis, we speculate that the onset of oculomotor deficits generally follows that of ataxia symptoms in SCA6 human patients. Future studies focused on the quantification of gait kinematics versus oculomotor function in patients will be required to fully understand the relative time course of SCA6 symptoms.

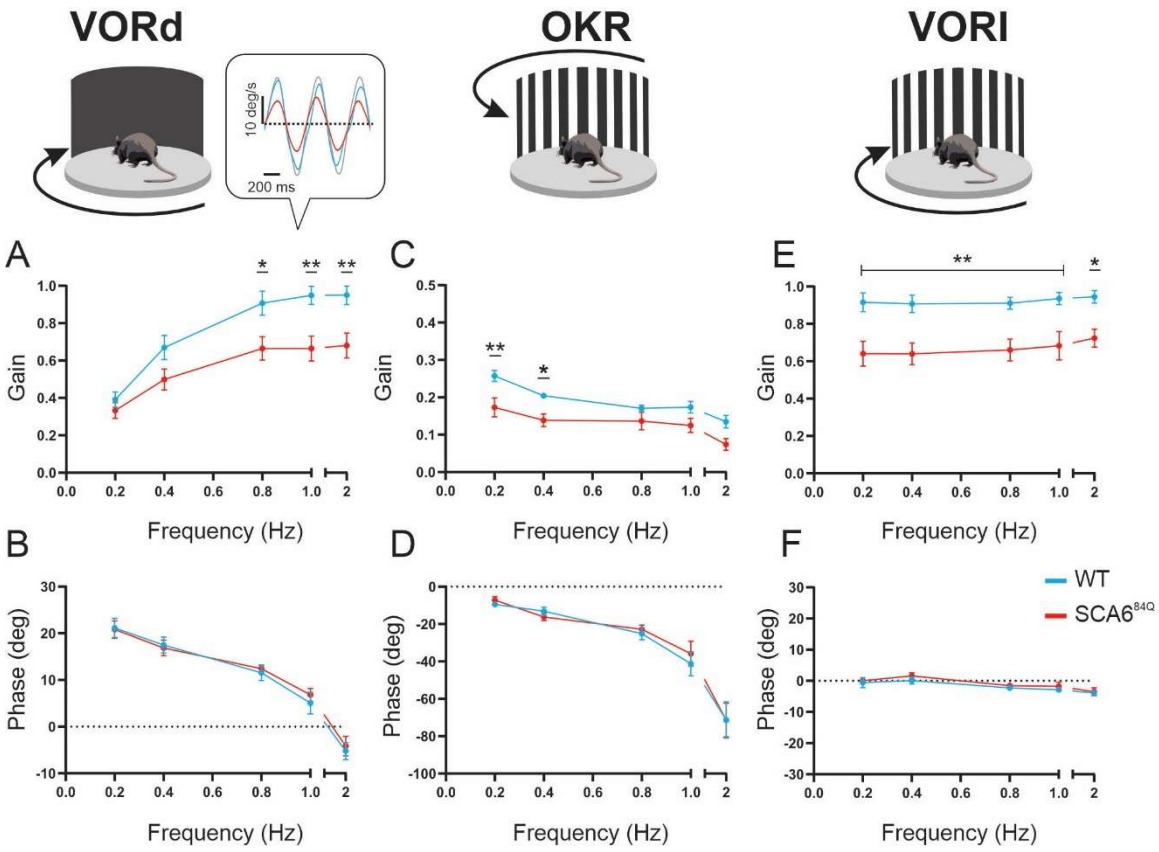

Figure 1. VOR and OKR gains were reduced in SCA6^{84Q} mice. (A and B) VORd gain and phase (mean±SEM) plotted as a function of frequency for SCA6^{84Q} mice (n=8) and wild-type (WT) mice (n=7). VOR gains at 0.8, 1 and 2 Hz were significantly reduced in SCA6^{84Q} mice. There was no change in phase between two groups. Inset, examples of eye- and head-velocity (grey) traces for WT (blue) and SCA6^{84Q} mice (red) at 2 Hz. **(C and D)** OKR gain and phase (mean±SEM) plotted as a function of frequency for SCA6^{84Q} mice and WT mice. OKR gains at 0.2 and 0.4 Hz were significantly reduced in SCA6^{84Q} mice with no change in phase. **(E and F)** VORl gain and phase (mean±SEM) plotted as a function of frequency for SCA6^{84Q} mice and WT mice. VORl gains at all frequencies were significantly reduced in SCA6^{84Q} mice with no change in phase. Comparisons were two-way ANOVA with post hoc *Bonferroni*'s test. *P<0.05, **P<0.01, ***P<0.001.

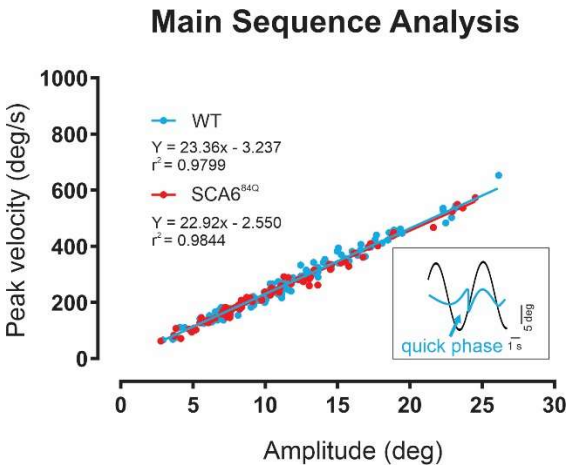

Figure 2. Nystagmus dynamics are comparable between wild-type **and SCA6^{84Q} mice.** Peak velocity vs. amplitude relationship for fast phases of vestibular nystagmus for wild-type (WT, blue dots) and SCA6^{84Q} mice (red dots). Regression lines are superimposed. There is no significant difference between the two slopes (p=0.2797).

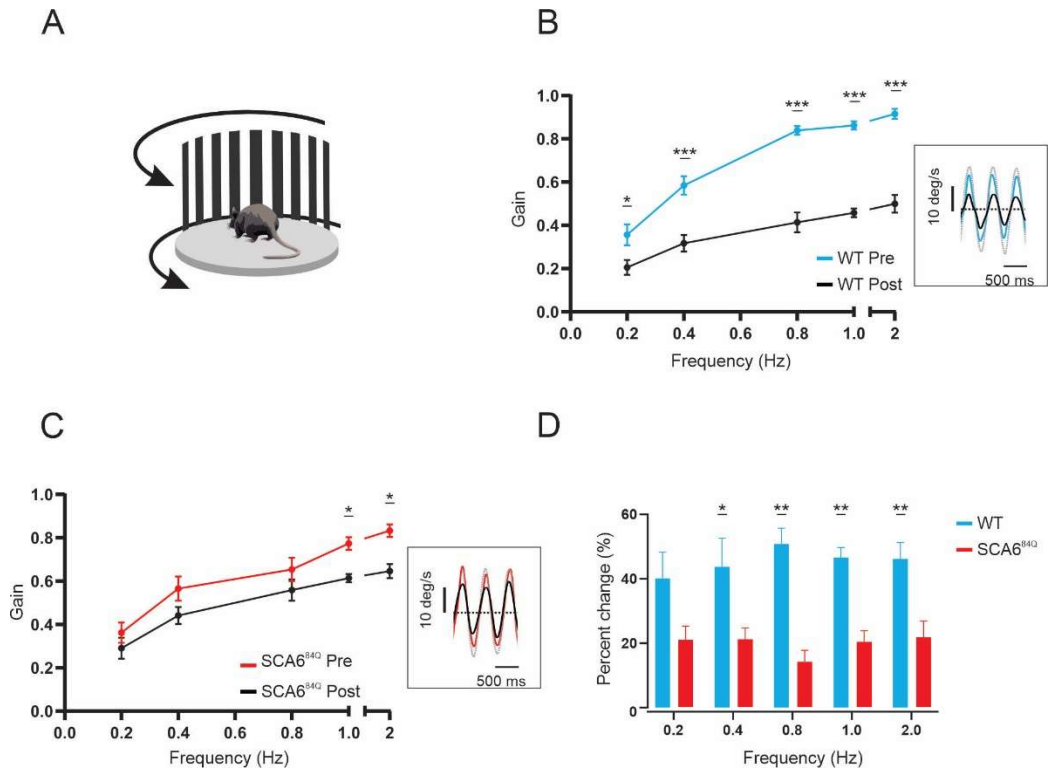

Figure 3. VOR learning is impaired in SCA6^{84Q} mice. (A) Schematic of the experimental setup. **(B)** VORd gain (mean±SEM) before and after the VOR gain-down training plotted as a function of frequency for wild-type (WT) mice (n=6). Inset, example of eye- and head-velocity (grey) traces before (blue) and after training (black) at 2 Hz **(C)** VORd gain (mean±SEM) before and after the VOR gain-down training plotted as a function of frequency for SCA6^{84Q} mice (n=7). Inset, example of eye- and head-velocity (grey) traces before (red) and after training (black) at 2 Hz **(D)** Percent change in VOR gain for WT and SCA6^{84Q} mice. Comparisons were made with Two-way ANOVA with post hoc Bonferroni's test. *P<0.05, **P<0.01, ***P<0.001.

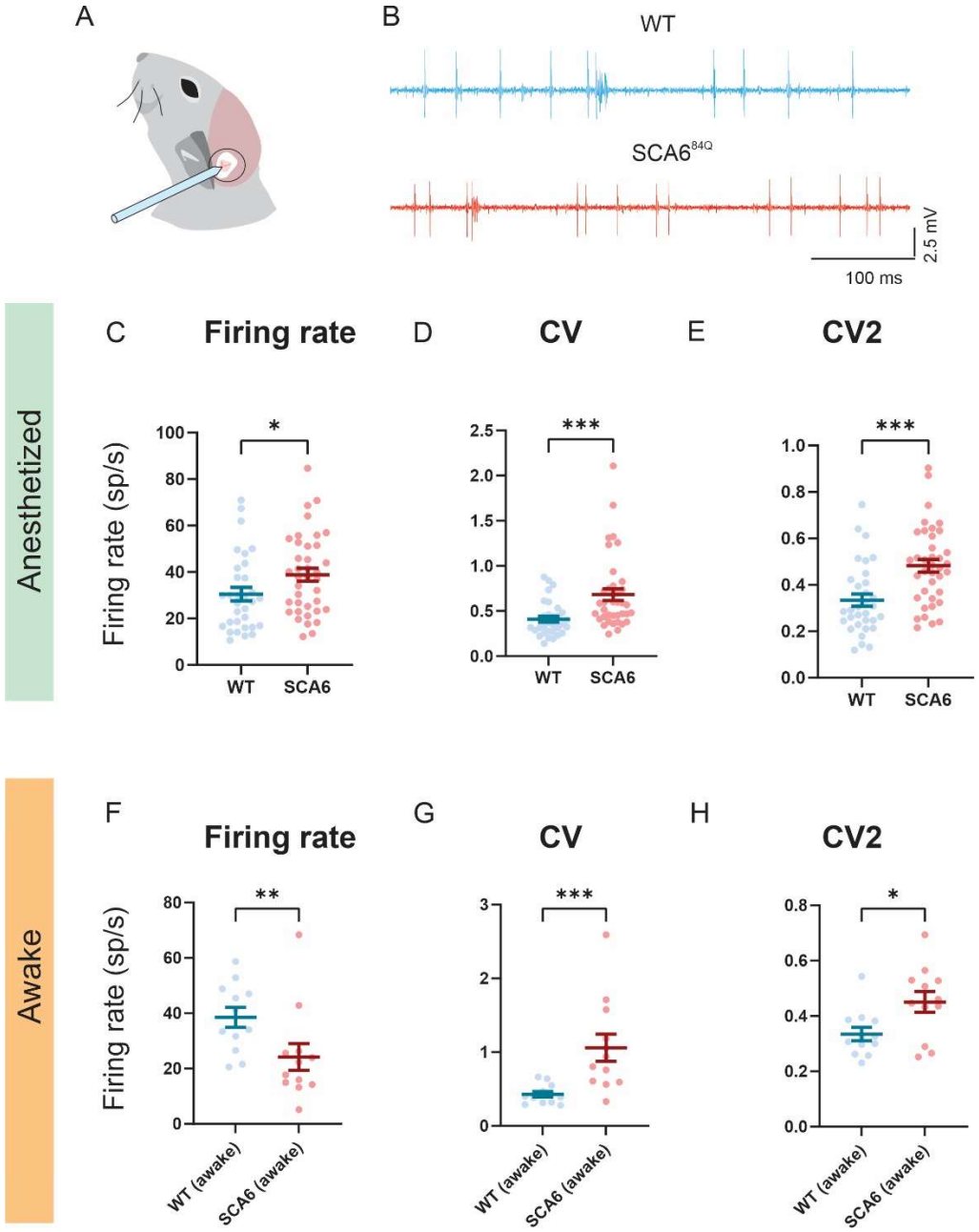

Figure 4. Firing precision is altered in SCA6^{84Q} mice. (A) Schematic of the experimental setup. **(B)** Sample recordings from anesthetized wild-type (WT, blue) and SCA6^{84Q} mice (red). **(C-E)** Comparison of firing rate, CV, and CV2 of simple spikes in the anesthetized state. Firing rate **(C)** is increased in SCA6^{84Q} mice (WT: frequency=30.49±2.89 sp/s; SCA6^{84Q} mice: frequency =38.83±2.81 sp/s). CV **(D)** is increased in SCA6^{84Q} mice (WT:CV=0.41±0.03; SCA6^{84Q} mice: CV =0.68±0.07). CV2 **(E)** is increased in SCA6^{84Q} mice (WT:CV2=0.33±0.03; SCA6^{84Q} mice:CV2 =0.48±0.03). N=32 cells for WT; N =38 cells for SCA6^{84Q} mice **(F-H)** Comparison of firing rate, CV, and CV2 of simple spikes in the awake state. Firing rate **(F)** is decreased in SCA6^{84Q} mice

(WT:frequency=38.49±3.58 sp/s; SCA6^{84Q} mice:frequency= 24.22±4.84 sp/s). CV **(G)** is increased in SCA6^{84Q} mice (WT:CV=0.43±0.04; SCA6^{84Q} mice: CV= 1.06±0.18). CV2 **(H)** is increased in SCA6^{84Q} mice (WT:CV2=0.33±0.03; SCA6^{84Q} mice:CV2= 0.45±0.03). Comparisons were made with a non-parametric Mann-Whitney U-test. *P<0.05, **P<0.01, ***P<0.001.

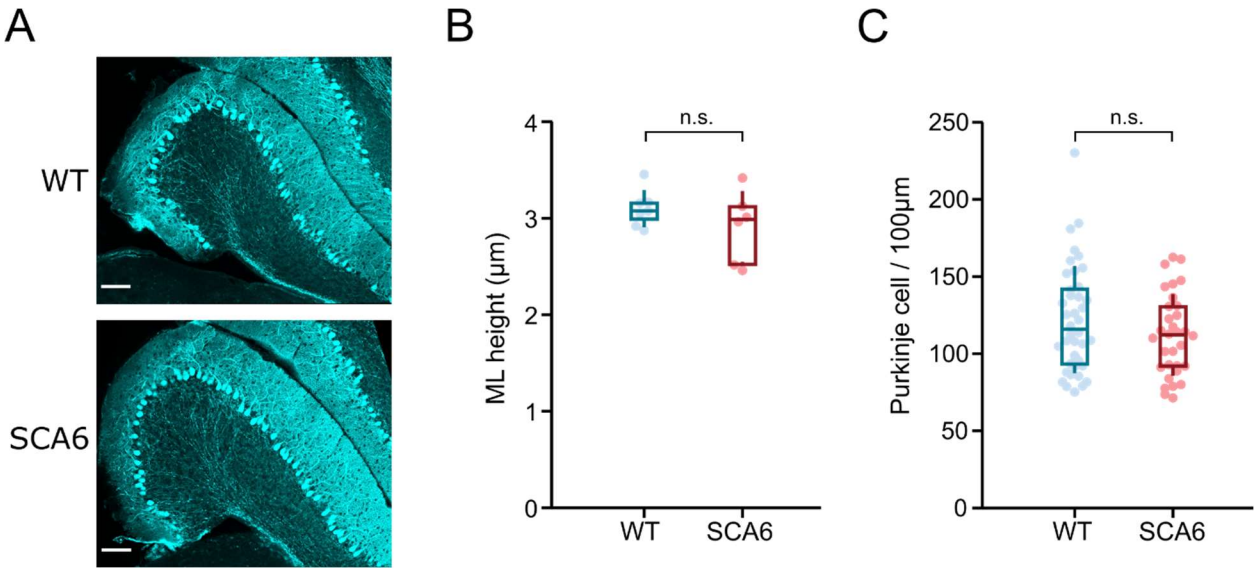

Figure 5. Flocculus morphology appears normal in SCA6$^{84Q/84Q}$ mice. (A) Anti-calbindin immunohistochemistry in the flocculus of wild-type (WT) and SCA6 animals at 7.5 months. Stained Purkinje cells and showed normal flocculus morphology in SCA6^{84Q} mice. **(B)** Measurement of molecular layer height showed no change in SCA6^{84Q} flocculus, and Purkinje cell density was also unchanged **(C)**. Comparisons were made with a non-parametric Mann-Whitney U-test.

Chapter 4

Loss of alpha-9 nicotinic acetylcholine receptor subunit predominantly results in impaired postural stability rather than gaze stability

4.1 Abstract

The functional role of the mammalian efferent vestibular system (EVS) is not fully understood. One proposal is that the mammalian EVS plays a role in the long-term calibration of central vestibular pathways, for example during development. Here to test this possibility, we studied vestibular function in mice lacking a functional α9 subunit of the nicotinic acetylcholine receptor (nAChR) gene family, which mediates efferent activation of the vestibular periphery. We focused on an α9 (-/-) model with a deletion in exons 1 and 2 (Morley et al., 2017). First, we quantified gaze stability by testing vestibulo-ocular reflex (VOR, 0.5-3Hz) responses of both α9 (-/-) mouse models in dark and light conditions. VOR gains and phases were comparable for both α9 (-/-) mutants and wild-type controls. Second, we confirmed the lack of an effect from the α9 (-/-) mutation on central visuo-motor pathways/eye movement pathways via analyses of the optokinetic reflex (OKR) and quick phases of the VOR. We found no differences between α9 (-/-) mutants and wild-type controls. Third and finally, we investigated postural abilities during instrumented rotarod and balance beam tasks. Head movements were quantified using a 6D microelectromechanical systems (MEMS) module fixed to the mouse's head. Compared to wild-type controls, we found head movements were strikingly altered in α9 (-/-) mice, most notably in the pitch axis. We confirmed these later results in another α9 (-/-) model, with a deletion in the exon 4 region (Vetter et al., 1999). Overall, we conclude that the absence of the α9 subunit of nAChRs predominately results in an impairment of posture rather than gaze.

4.2 Introduction

The mammalian efferent vestibular system (EVS) projects from the brainstem to the inner ear and thus is theoretically well placed to modulate the afferent output of the peripheral vestibular organs (reviewed in Cullen and Wei, 2021). The somas of mammalian EVS neurons are situated within a structure called 'group-e" located lateral to the abducens and genu of the facial nerve. The primary neurotransmitter of the efferent system is acetylcholine, although a diverse expression of other neuromodulators including calcitonin gene-related peptide (CGRP), 5'-triphosphate (ATP), GABA, and neuronal nitric oxide synthase (nNos) are also present at the synapse (reviewed in Holt et al., 2011; Soto and Vega, 2010; Yamashita et al., 1993). There are two primary cholinergic receptor types found in the vestibular labyrinth: nicotinic (nAChRs) and muscarinic (mAChRs). In mammals, vestibular hair cells are characterized by α9 and α10 containing nAChRs (Elgoyhen et al., 2001; Hiel et al., 1996; Anderson et al., 1997; Luebke et al. 2005; Morley et al., 2017). When activated, α9/10 nAChRs open calcium-dependent potassium (SK) channels, which then hyperpolarizes the hair cell to inhibit neurotransmitter release (Im, 2012; Kong et al., 2008; Turcan et al., 2010).

Despite its well-understood anatomy and synaptic mechanism, the functional role of the mammalian EVS in everyday life remains poorly understood. To date, several hypotheses of functional roles of the mammalian EVS have been proposed. One longstanding view was the mammalian EVS would differentiate between active and passive movements at the periphery by transmitting motor-related signals to the vestibular periphery that modulate its head motion coding range during active movement (Goldberg et al., 2000). However, this view has not been supported by experiments in monkeys as it was found that the EVS is not involved in either extra-vestibular sensory integration or context-dependent information encoding (Cullen and Minor 2002; Sadeghi et al. 2007; Jamali et al., 2009; Mackrous et al., 2019). It has also been proposed that the efferent vestibular system plays a slow modulatory role in shaping the functional connectivity/efficacy of the peripheral organs during maturation (Holt et al., 2011). Consistent with this idea, CGRP null mice demonstrate a substantial reduction in the efficacy of their vestibulo-ocular reflex (Luebke et al., 2014).

One of the readily available tools to investigate the functional role of the mammalian EVS is a transgenic mouse model. As noted above, α9 and α10 containing nAChRs are widely expressed

in the vestibular / auditory hair cells of the vertebrate inner ear and have not reported to exist in brain (Elgoyhen et al., 1994, 2001; Hiel et al., 1996; Simmons and Morley, 1998, 2011; Morley and Simmons, 2002). Accordingly, these nAChRs have become a popular target for deletion in studies aimed at understanding the functional role of the mammalian EVS. To date, most studies of the EVS have targeted α9 containing nAChRs and quantified the VOR in α9 (-/-) mutants (Hübner et al., 2015; Hübner et al., 2017, Eron et al., 2015). Moreover, the vestibular system plays a vital role in ensuring postural as well as gaze stability. However, to date, postural deficits in the α9 (-/-) mice, contrary to their VOR phenotype, have not been extensively studied. Accordingly, here we quantified both VOR and postural stability in α9 (-/-) mutant mice and compared performance to wild-type controls (Morley et al., 2017). Additionally, we compared optokinetic reflex (OKR) responses and VOR quick phases in α9 (-/-) mutant mice and their wild type counterparts. Finally, we objectively characterized postural stability during instrumented rotarod and balance beam tasks in these mice using an approach that has been previously shown to identify postural deficits in other transgenic mice (Ono et al., 2020), namely quantifying head motion using a 6D microelectromechanical systems (MEMS) module.

Overall, we did not identify deficits in the VOR of α9 (-/-) mice. Likewise, our analyses of quick phases and Optokinetic reflex (OKR) responses also suggested that the α9 (-/-) mutation did not affect central visuo-motor pathways/eye movement pathways. Importantly, however, α9 (-/-) mice did show significant impairments in performance on the balance beam and rotarod tests. Moreover, our quantitative analysis of head motion further revealed altered movement dynamics for α9 (-/-) mice as compared to their wildtype counterparts in each task, particularly in the pitch and fore-aft axes. Finally, we confirmed these later results in another α9 (-/-) model (Vetter et al., 1999) and likewise found comparable changes in the head motion in these same axes. Thus, taken together, our results suggest the loss of the α9 subunit of nAChRs largely affected postural rather than gaze stability.

4.3 Methods

4.3.1 Animals

We focused on two distinct α9 (-/-) models, with a deletion of exons 1 and 2 (*Chrna9*^{tm1Bjmy}, MGI:5787807, Morley et al., 2018) and the region of exon4 (*Chrna9*^{tm1Bev}, MGI:2158742, Vetter et al., 1999) of the *Chrna9* gene. The α9 nAChR KO mouse model with exons 1 and 2 deleted was generated by (Genoway, Inc., Lyon, France) and was back-crossed at the Boys Town National Research Hospital (BTNRH) to C57Bl/6J mice. For the studies reported here, mice were bred and housed at BTNRH until weaned and then transported to Johns Hopkins University. The BTNRH IACUC approved the transport and use of the animals for the studies reported here. Mice with the deletion of the exon 4 region, originally reported by Vetter et al. (1999), were obtained from The Jackson Laboratory and backcrossed to the C57Bl/6J mice at Johns Hopkins University. All animal experiments were conducted under the approved animal protocols at McGill University and Johns Hopkins University. The experimenter was blind to genotype during data collection as well as analysis for each of the tests detailed below.

4.3.2 Quantification of VOR and OKR

Surgical techniques and experimental setup have been previously described (Beraneck and Cullen, 2007). Eye movement data were collected using an infrared video system (ETL-200, ISCAN system). The rotational velocity of the turntable (head velocity) was measured using a MEMS sensor (MPU-9250, SparkFun Electronics). Eye movements during OKR were evoked by sinusoidal rotations of a visual surround (vertical black and white stripes, visual angle width of 5°) placed around the turntable at frequencies 0.2, 0.4,0.8, 1, 2, and 3 Hz with peak velocities of ±16◦/s. To record VOR responses, the turntable was rotated at sinusoidal frequencies 0.2, 0.4,0.8, 1, 2, and 3 Hz with peak velocities of ±16◦/s in both light and dark. In the light condition, the visual surround remained stationary, whereas, in the dark condition, both the visual surround and turntable rotated in phase. Head and eye movement signals were low-passed filtered at 125 Hz, and sampled at 1kHz. Eye position data were differentiated to obtain velocity traces. Cycles of data with quick phases were excluded from the analysis. Least-square optimization determined the VOR and OKN gains and phases plotted as mean ± standard error of the mean (SEM) against all frequencies for all mice.

4.3.3 Rotarod

Mice were trained with trials of 5, 10, 20 rpm for 120 seconds each with 15 minutes rest periods between trials and a 1-minute acclimation period. Mice were allowed to acclimate for 5 minutes on the rotarod during training and test trials. For each test trials, the rotarod accelerated from 4 rpm to 40 rpm with a ramp of 300 seconds.

Head movements in six dimensions were also recorded using a miniature head motion sensor (MPU-9250, SparkFun Electronics, Niwot, CO) affixed on the top of the skull, which comprises a three-dimensional (3D) accelerometer (measures linear acceleration; fore/aft, lateral, and vertical) and 3D gyroscope (measures angular velocity: roll, pitch, and yaw). Data was acquired at 200 Hz using windows-based CoolTerm software. We then computed the power spectral densities (pwelch function, MATLAB, MathWorks) using Welch's averaged periodogram with nfft =4096 and a Bartlett window (4096 ms duration) for all six dimensions of movement.

4.3.4 Balance beam

A 6-mm-wide and 40-cm-long beam was used for balance beam testing. Mice traverse 40 cm. Walking speed was measured by recording the time the mouse took to reach the goal box from the opposite end of the beam. Mice were scored ‘’time out" when failed to reach the endpoint in 2 min. Head movements in six dimensions were also recorded (See rotarod).

4.3.5 Air righting, tailing hanging and contact inhibition of righting tests

Air righting test –Mouse was picked up by the tail and lowered into a container so that all four feet were touching the bottom. The container was quickly inverted at a height of 30-40 cm so mouse fell supine. How mouse lands onto a foam cushion were observed and rated as below (Rabbath et al., 2001):

0 = the animal lands on its feet (normal).

1 = the animal lands on its side (mild deficit).

2 = the animal lands on its back (severe deficit).

Tail hanging test–Mouse was picked up by the tail and lowered to an even surface. Mouse's posture was rated using the following scale (Rabbath et al., 2001):

0 = straight body posture with extension of forelimbs towards the earth (normal).

1 = slightly bending the body ventrally (intermediate response).

2 = persistently bending the body (severe response).

Contact inhibition of righting test–Mouse was picked up by the tail and lowered into a container so that all four feet are touching the bottom. The container was quickly inverted so the mouse was supine while a surface was touching the soles of the mouse's feet. The mouse's reflex was rated using the following scale (Rabbath et al., 2001):

0 = animal rights successfully (normal).

1 = partial righting (intermediate response).

2 = complete loss of righting (severe response).

4.3.6 Swimming

A large container (26.25 x 16.25 x14.38') was filled with water (24-26°C) at the height of at least 15 cm. The mouse was placed into the water and observed for up to one minute. Its preformation was rated using the following scale (Hughes et al., 2010):

0 = swims, body elongated, and tail propels in flagella-like motion.

1 = immobile floating.

2 = underwater tumbling.

4.3.7 Resting head movement

Mice were placed in a cylinder (9 cm diameter and 21.5 cm height) that limited their motion, so mice maintained their steady posture. Head movements in six dimensions were recorded (See rotarod).

4.3.8. Statistical analysis

Data are reported as the mean ± SEM. Nonparametric Mann-Whitney U-test was performed to test significance for time to traverse (balance beam) between two groups. Two-way repeated-measures ANOVA followed by Bonferroni post hoc comparison tests was used for the following data: (1) the VOR data across frequencies and; (2) the latency to fall off the rotarod for 5 consecutive days. Non-normal distributed data were transformed to [Log (X 1)] to meet the

requirements of the ANOVA model. For the main sequence analysis, the extra sum-of-squares F test was used to compare two slopes. For power spectra analysis, we used an independent sample permutation test to test significant differences between the two groups. Prism 9 (GraphPad) or MATLAB was used for statistical analyses.

4.4 Results

4.4.1 VOR and OKR responses are normal in α9 (-/-) mice

We first measured VOR responses in - α9 (-/-) mice and their wild-type counterparts (Morley et al., 2017). We applied sinusoidal rotations at 0.2, 0.4,0.8,1,2 and 3 Hz with a peak velocity of 16 °/s. VOR responses were tested in the dark (referred to as VORd). The gain and phase of the eye movements generated during VORd testing were then quantified for each frequency of rotation. The robust compensatory eye movements generated by wild-type mice during VORd testing increased with frequency reaching fully compensatory gains (~unity) for stimulation ~0.8 Hz and higher (**Fig 1A,** blue trace). Similarly, α9 (-/-) mice generated robust compensatory eye movements across this frequency range. Indeed, VORd gains and phases were comparable to those of wild-type mice (**Fig 1A,** compare red and blue traces; $P>0.5$, $P>0.5$).

The optokinetic reflex (OKR) is a visually driven reflex that generates eye movements in response to a moving visual scene. During self-motion, the OKR complements the VOR to minimize visual motion on the retina to provide gaze stability at lower frequencies (reviewed in Cullen et al., 2019). Notably, the OKR shares premotor circuity with the VORd (for review, see Cullen and Van Horn, 2011). Thus, we measured OKR responses as a control for testing whether there are any deficits resulting from non-vestibular effects in the VOR circuitry. During OKR testing, the visual surround was rotated sinusoidally using the same stimulus as that used for VORd testing (i.e., 0.2, 0.4,0.8,1,2 and 3 Hz; peak velocity of 16 °/s). Quantification of the eye movements evoked by OKR testing revealed no difference in the response gains or phases of α9 (-/-) mice compared to their wild-type counterparts (**Fig 1B;** $P>0.5$, $P>0.5$).

Finally, during actual self-motion in the light, both the VOR and OKN work synergistically to stabilize gaze (reviewed in Cullen et al., 2019). Accordingly, we applied sinusoidal rotations at 0.2, 0.4,0.8,1,2 and 3 Hz with a peak velocity of 16 °/s. VOR responses in the light (referred to as VORl). Consistent with the lack of difference found during VORd and OKN testing, quantification of the eye movements evoked by VORl testing revealed no difference in the response gains or

phases of α9 (-/-) mice compared to their wild-type counterparts (**Fig 1C;** $P>0.5$, $P>0.5$). Thus, taken together, our results demonstrate that the loss of the α9 subunit of nAChRs did not alter gaze stability in the frequency range between 0.1- 3Hz.

4.4.2 Quick phase eye movement dynamics are not changed in α9 (-/-) mice

To further investigate whether eye movement control was altered in α9 (-/-) mice, we next quantified the relationship between the peak velocity and amplitude of quick phases evoked during rotational stimulation (i.e., main sequence relationship). In agreement with previous studies, this relationship was linear for our wild-type mice (**Fig 2**, blue symbols; $R^2 = 0.94$). Similarly, a similarly robust linear relationship was also observed for α9 (-/-) mice (**Fig 2,** red symbols; $R^2 = 0.93$). Furthermore, the slope of the main sequence relationship in α9 (-/-) mice and their wild-type mice counterparts were comparable (slope 37.9 versus 40.0 respectively; $P=0.0978$). Thus, together with the results in Figure 1 above, our findings suggest that the loss of α9 loss does not alter vestibularly driven VOR eye movements, visually driven OKR eye movements, stabilizing eye movements generated by the integration of the vestibular and visual inputs, or quick phase eye movements.

4.4.3 α9 (-/-) mice show impaired postural control on a rotarod

As noted above, to date, whether the loss of α9 results in postural deficits has not been well studied. Accordingly, we next tested whether α9 (-/-) mice demonstrate any postural impairments. We first conducted standard behavioral testing that included: (1) tail hanging test, (2) air righting, (3) contact inhibition of righting, and (4) swimming. All mice, regardless of their genotype, scored 0 (normal) on all listed behavioral tests (data not shown). We then subjected mice to an accelerating rotarod. All mice were subjected to 3 training sessions with 3 different constant rpm settings (at 5, 10, and 20 rpm). During the testing sessions, the rotarod was set to increase its rpm from 4 to 40 in 300 seconds. The time to fall from the rotarod was used to quantify their performance. The trial was repeated for 5 consecutive days. Overall, we found that α9 (-/-) mice showed poorer performance than their wild-type counterparts. Specifically, α9 (-/-) mice fell significantly earlier from the first day of testing (day 1) to the last day (day 5) (**Fig 3A**) (day 1, $P=0.0183$; day 2, $P=0.0435$; day 3, $P=0.0390$; day 4, $P=0.00481$; day 5, $P=0.0011$).

4.4.4 α9 (-/-) mice show different head movement dynamics compared to wild-type mice on a rotarod.

Given the poorer performance of α9 (-/-) mice on a rotarod, we hypothesized that α9 (-/-) mice should exhibit different head movement dynamics while balancing on the rotarod compared to wild-type mice. Accordingly, we quantified their head motion using a 6D MEMS module consisting of three gyroscopes and three linear accelerometers affixed to the animal's head post. All head movement was collected during day 5 of testing (**Fig 3B**). Power spectra of head movements revealed significantly lower power in α9 (-/-) mice as compared to their wild-type counterparts in the fore-aft and pitch axes at lower (0.1 to 1 Hz) frequencies (**Fig 3B,** compare red and blue traces; fore-aft, P=0.021; pitch, P=0.021). Significantly lower power was also found in the pitch axis in the mid (e.g., 1-5 Hz) frequencies range (pitch, P=0.0064). Thus, together, the altered head movement dynamics of α9 (-/-) mice in the fore-aft and pitch axes coupled with their and poorer scored performance indicates that their ability to maintain balance while completing the task was impaired. We further consider this point below in the Discussion.

4.4.5 α9 (-/-) mice are slower and show different head movement dynamics compared to wild-type mice on a balance beam

To further test whether the loss of α9 results in postural deficits, we tested the ability of our mice on a challenging balance test in which they locomoted across a narrow 6-mm balance beam. Overall, we found that the performance of our α9 (-/-) mice were markedly impaired during this task. Notably- α9 (-/-) mice took significantly longer to cross the balance beam compared to their wild-type counterparts (**Fig 4A**; P=0.0322). Accordingly, this result, together with our above results quantifying performance on the rotarod, is further indicative of impaired balance in α9 (-/-) mice.

As α9 (-/-) mice generally showed lower power in fore-aft and pitch axes while balancing on the rotarod, we hypothesized that mouse head movement dynamics on the balance beam would exhibit similar trends. Accordingly, we measured head movement in mice while they traversed the narrow 6-mm balance beam. Indeed, our power spectra analysis of the head motion generated during this testing revealed lower power in the low-frequency range (fore-aft, P=0.041; vert, P =0.021; pitch, P=0.0067; yaw, P=0.05) and mid and high-frequency ranges (mid-frequency: 1-5 Hz; vert, P=0.039; pitch, P=0.0028; High frequency: yaw, P=0.035) (**Fig 4C**). This consistent pattern of

lower power in fore-aft and pitch axes coupled with longer crossing times is consistent with the observed impairment in the ability of α9 (-/-) mice to maintain postural stability during rotarod testing. We further discuss the implications of these results below in the Discussion.

4.4.6 Exploratory and Resting head movement dynamics are comparable for α9 (-/-) mice and wild-type mice

Given that the mutant mice took longer to cross the balance beam (**Fig 3** above) we next investigated whether this might be explained by hypo-activity. Notably, our subjective visual inspection of these mice in the cage did not reveal any signs of hypo-activity. In addition, we placed both groups of mice within a cylinder and objectively quantified their activity levels, using two approaches. First, we quantified the number of times that the mice touch the wall of cylinder. We found no difference between two groups. Secondly, we plotted and compare power spectra of the animal's head movement during their time within the cylinder and found no significant differences in any motion dimension. Thus, these results suggest that impaired balance rather than hypo-activity in knockout mice led to longer transverse time on the balance beam.

Additionally, it is noteworthy that mutant mice strain with vestibular dysfunction can demonstrate head movement tremors/oscillations while at rest (see for example, Ono et al., 2020). To rule out the possibility the significant differences in head movement dynamics observed during balance beam and rotarod testing were due to the difference that is already present at rest, we reanalyzed the head movement data recorded when the mouse was placed in a cylinder, focused solely on epochs of time where mice i) did not make exploratory head movement, and ii) where their bodies remained stationary. No difference was observed in any axes between α9 (-/-) and control wild-type mice, indicating the lack of significant head tremors/oscillations while at rest in α9 (-/-) mice. Taken together, these results further strengthen our conclusion that postural stability is impaired in α9 (-/-) mice.

4.4.7 Postural phenotypes are similarly altered in a second α9 (-/-) mouse model

Finally, because the question of whether the loss of α9 results in postural deficits had not been well investigated prior to this study, we also completed the same rotarod and balance beam testing shown above in Figures 3 and 4 in another α9 (-/-) mouse model (Vetter et al., 1999, see

Methods). Similar to our results above, we found that these α9 (-/-) mice also fell significantly earlier than their wild-type counterparts, beginning on day 2 to day 5 (**Fig 5A**; day 2, *P*=0.0157; day 3, *P*=0.0218; day 4, *P*=0.0186; day 5, *P*=0.0155). Furthermore, a comparable quantification of 6-dimensional head motion during the rotarod test (**Fig 5B**) revealed that these α9 (-/-) mice likewise demonstrated a reduction in power in the fore-aft and pitch axes in both the low (fore-aft, *P*=0.017; pitch, *P*=0.025) and mid (fore-aft, *P*=0.05; pitch, *P*=0.045) frequency ranges, and significant differences were further found in this range for the roll and yaw axes (low frequency: roll, *P*=0.018; yaw, *P*=0.00075; mid-frequency: roll, *P*=0.0058; yaw, *P*=0.00045). Moreover, differences were seen in several axes in the high-frequency range (roll, *P*=0.0019; pitch, *P*=0.0038; yaw, *P*=0.0011). Correspondingly, we found that these same α9 (-/-) mice also took significantly longer to transverse the narrow balance beam compared to their wild-type counterparts (**Fig 5C**; *P*=0.023) and showed lower head motion power in fore-aft and pitch axes for the low-frequency range (**Fig 5D**; fore-aft, *P*=0.037; pitch, *P*=0.041). Thus, overall, the loss of α9 resulted in similar postural deficits in both α9 (-/-) mouse models tested in our study.

4.5 Discussion

Summary

In this study, we tested the vestibular function of mice lacking the α9 subunit of nicotinic acetylcholine receptors (nAChRs). Specifically, we tested both VOR and postural stability in an α9 (-/-) mouse model developed by Morley et al. (2017). We first quantified vestibular function by measuring the eye movements generated by the vestibulo-ocular reflex (VOR), which functions to ensure gaze stability during head motion (reviewed in Goldberg et al., 2012). The gain and phase of the compensatory VOR eye movements were quantified during rotations in both dark and light conditions. We found that VOR function was unimpaired in α9 knockout mice as compared to wild-type controls. Likewise, analysis of the relationship between quick phase amplitude and velocity evoked during rotational stimulation revealed a robust linear relationship that was unchanged from their wild-type counterparts. We also quantified the gaze stabilizing eye movements generated in response to a moving visual (versus vestibular) surround (optokinetic responses (OKR)). We found that OKR response gains and phases were comparable to those measured in wild-type controls, indicating that VOR pathway function was not altered at subsequent levels of central processing.

In contrast, our analysis of postural stability and motor control revealed deficits in these same α9 (-/-) mice. Notably, we scored performance during 3 tasks: standard rotarod testing, the balance beam test, and swimming test. In addition, head movements were quantified using a 6D microelectromechanical systems (MEMS) module fixed to the animal's head during rotarod testing, balance beam testing, and for resting head movements when the animal was stationary. Overall, we found impaired performance during rotarod testing; the time to fall was shorter for α9 (-/-) mice as compared to their wild-type counterparts. Likewise, we found impaired performance during balance beam testing; the crossing time was longer for α9 (-/-) mice. Furthermore, quantitative analysis of head motion during rotarod and balance beam testing consistently revealed altered head motion power – including a decrease in fore-aft and pitch axes rotation. Thus, overall, the ability of α9 (-/-) mice was impaired during both tasks, and in turn, head movement power was lower in α9 (-/-) mice compared to their wild-type counterparts. We further confirmed these later results in a second α9 (-/-) model (Vetter et al., 1999). Our results suggest that mutant mice were more restrained in their movements due to compromised vestibular function, and as such their ability to generate robust compensatory movements to remained balanced was reduced relative to wild-type

mice. We speculate that the most significantly impacted dimensions of motion (i.e., fore-aft and pitch axes rotation) corresponded to those for which the neural/biomechanical challenge to the balance system was the greatest during rotarod and balance beam tasks. Thus, taken together, our results provide strong evidence that the absence of the α9 nAChR subunit predominately results in impairments in postural rather than gaze stability.

4.5.1 Relationship to the existing VOR literature

Prior to the present study, our understanding of how the loss of the α9 subunit of the nicotinic acetylcholine receptor (nAChRs) alters vestibular function had been based largely on the measurement and quantification of VOR responses. Here, we first reported the VOR and postural responses of the same α9 knockout mice (Morley et al., 2017). We found that these mice show no difference in their vestibular driven eye movements as compared to wild-type controls over the frequency range tested (rotations up to 3Hz). The gains and phases of the compensatory VOR were unchanged in α9 (-/-) mice. Notably, this result is not consistent with those of previous studies reporting significantly reduced gain of the compensatory VOR evoked by stimulations >1Hz (Hübner et al., 2015). One possible difference is the genetic background of the mice used in our studies and in the Hübner studies. It is not uncommon for a gene on different genetic backgrounds to produce a different phenotype. The mice used in the studies reported here are on C57BL/6J mice while the Hübner studies were obtained from The Jackson Laboratory (JAX) and originated from the mice described by Vetter et al. (1999). The mice were originally on a CBA/CaJ X 129Sv background and maintained on an equivalent mixed strain. Additionally, Hübner et al., (2015) used an independent colony of hybrid CBA/CaJ x 129/SvEv as their control rather than using litter-mate controls, which could also potentially contribute to the differences reported in this study.

In addition, our analysis of the VOR quick phases responses (i.e., main sequence analysis) revealed that no change in the eye movements generated by α9 knockout mice as compared to their wild-type controls, consistent with (Hübner et al., 2015, but see Eron et al., 2015). In addition to ACh, the neuroactive peptide calcitonin-gene-related peptide (CGRP) acts at efferent synapses. Thus, it is noteworthy that, in contrast to α9 knockout mice, CGRP knockout mice demonstrate a profound (50%) reduction in the efficacy of their vestibulo-ocular reflex (Luebke et al., 2014). It has thus been proposed that the CGRP may play a slow modulatory role in shaping the functional connectivity/efficacy of the VOR pathways during maturation.

4.5.2 α9 and the efferent vestibular system: Implications for vestibular pathway modulation

The cell bodies of the mammalian efferent vestibular system are located in the group-e nucleus, situated just dorsal to the genu of the facial nerve and just medial to the VI (abducens) nucleus. Stimulation of the mammalian "group-e" nucleus evokes excitatory responses in both ipsilateral and contralateral vestibular afferents (Goldberg and Fernandez, 1980; Marlinski et al., 2004; McCue and Guinan, 1994), characterized by fast and slow responses with activation time constants of 100ms versus seconds, respectively (Goldberg and Fernandez, 1980; Sadeghi et al., 2009). Acetylcholine (ACh) is the primary neurotransmitter at the efferent vestibular synapses across vertebrate classes (reviewed in Holt et al. 2011, Goldberg et al., 2012). In mammals, nicotinic ACh receptors (nAChRs) are found in the vestibular labyrinth (Elgoyhen et al., 2001; Hiel et al., 1996; Luebke et al. 2014), and the efferent-mediated release of ACh activates these α9/α10 nicotinic AChRs (reviewed in Jordan et al. 2013, Poppi et al., 2020).

Mammalian vestibular afferent fibers originating in both the semicircular canals and otoliths vary in their resting discharge regularity and are commonly characterized as either "regular" or "irregular" (reviewed in Cullen 2019). Recent studies have established that regular and irregular afferents provide two parallel streams of sensory input to mammalian central vestibular pathways (reviewed in Cullen 2019). Regular afferents better encode information about head motion compared to irregular afferents (Sadeghi et al., 2007), whereas irregular afferents are more dynamic and better discriminate between head motion stimuli using precise (~6 ms) spike timing (Jamali et al., 2016, 2009). Importantly, stimulation of neurons in the mammalian "group-e" nucleus evoked markedly greater responses in irregular than regular afferents (reviewed in Cullen and Wei 2021). Furthermore, the application of nicotinic and muscarinic AChR antagonists preferentially block the fast versus slow components of the excitatory efferent-mediated responses evoked in these afferents (Schneider et al., 2021).

In this context, it is noteworthy that vestibular afferents with more irregular resting discharges (i.e., irregular afferents) are more likely to project to central vestibular nuclei neurons that comprise the vestibulo-spinal pathways, whereas those with more regular resting discharges (i.e., regular afferents) are more likely to project to central vestibular nuclei neurons that comprise the pathway generating the VOR (Goldberg et al., 1987; Sato and Sasaki, 1993). This difference in projections is consistent with studies showing that the VOR is unchanged following functional ablation of irregular afferents (Minor and Goldberg 1991; Angelaki and Perachio 1993). Thus,

given that experimental activation of the efferent vestibular system (EVS) produces a markedly larger effect on the responses of irregular than regular afferents, one logical hypothesis is that the EVS play a more significant role modulating vestibulo-spinal vs. vestibulo-ocular reflex pathways. Interestingly, this proposal is consistent with our present results, where we found significant differences in the postural performance of two distinct α9 (-/-) mouse models, while VOR eye movements for stimulation up to 3Hz were not altered.

As noted above prior studies have reported a significant reduction of VOR gain in α9 (-/-) mice for higher frequencies of stimulation (up to 10 Hz; Hübner et al., 2015). Additionally, this same group reported that the adaptation of the VOR that normally occurs in mice following visual-vestibular motor learning is significantly impaired in α9 (-/-) mice. Indeed, while there are reasons to believe that while regular afferents make the primary contribution to the VOR at lower frequencies of stimulation, the irregular afferents are important for VOR motor learning. In particular, the results of human and monkey studies have led to the proposal that a central pathway comprising phasic neurons, which predominately receive irregular afferent input, is highly modifiable and thus mediates visually induced VOR motor learning (Clendaniel et al. 2001, 2002) as well as compensation following peripheral vestibular loss (Lasker et al. 1999, 2000). In contrast, a central pathway comprising more tonic neurons that predominately receive regular afferent input mediates the direct unmodified VOR. Additionally, the influence of irregular afferents on the direct unmodified VOR itself should become more significant at higher frequencies. This is because the high-pass nature of their response dynamics will result in increasing larger gains compared to their regular counterparts. Given that most central neurons receive a mix of regular and irregular inputs (Goldberg et al., 1987; Sato and Sasaki, 1993), the relative contribution of irregular would then increase for VOR and vestibulo-spinal pathways as a function of frequency. Thus, it is possible that further testing with higher frequency stimulation (>3Hz) may reveal a significant reduction of VOR in the α9 (-/-) mice that were the focus of the present study.

4.5.3 Specificity of α9 to the periphery and directions for future research

There is much evidence that the cerebellum plays an essential role in ensuring balance (reviewed in Cullen 2016) and that intact VOR learning in mice is dependent on cerebellar innervation of brain stem vestibular nuclei (Beraneck et al. 2004). In this context, it is noteworthy that a recent study Lykhmus et al. (2017) reported that α9 transcript may be present in mitochondria

in cells in the brain, most notably in the vestibular nuclei and cerebellum. The possibility of a contribution of these cells cannot currently be excluded, although methodological issues regarding these studies have been raised (Morley et al., 2018). Indeed, our present findings that OKR responses are normal in α9 (-/-) mutant models demonstrated a lack of non-vestibular deficits at the level of the oculomotor circuitry. Notably, OKR responses are produced by a premotor circuit which involved the cerebellum (for review, see Cullen and Van Horn, 2011). Thus, our finding that OKR response gains and phases were comparable for both α9 (-/-) mouse models and their control mice is consistent with the general consensus that α9 is not present in the brain (Elgoyhen et al., 1994; Morley et al., 2018). Finally, it is noteworthy that the present focused on the role of the EVS on reflex and motor function. Recent studies have demonstrated impairments in multisensory attention in α9 (-/-) mice during a visual selective attention task with auditory distractors (Terreros et al., 2016; Jorratt et al., 2017). It is possible that the EVS likewise contributes to higher-order functions, for example reducing impulsivity during decision making during self-motion. Further studies are required to test this interesting possibility.

Figures

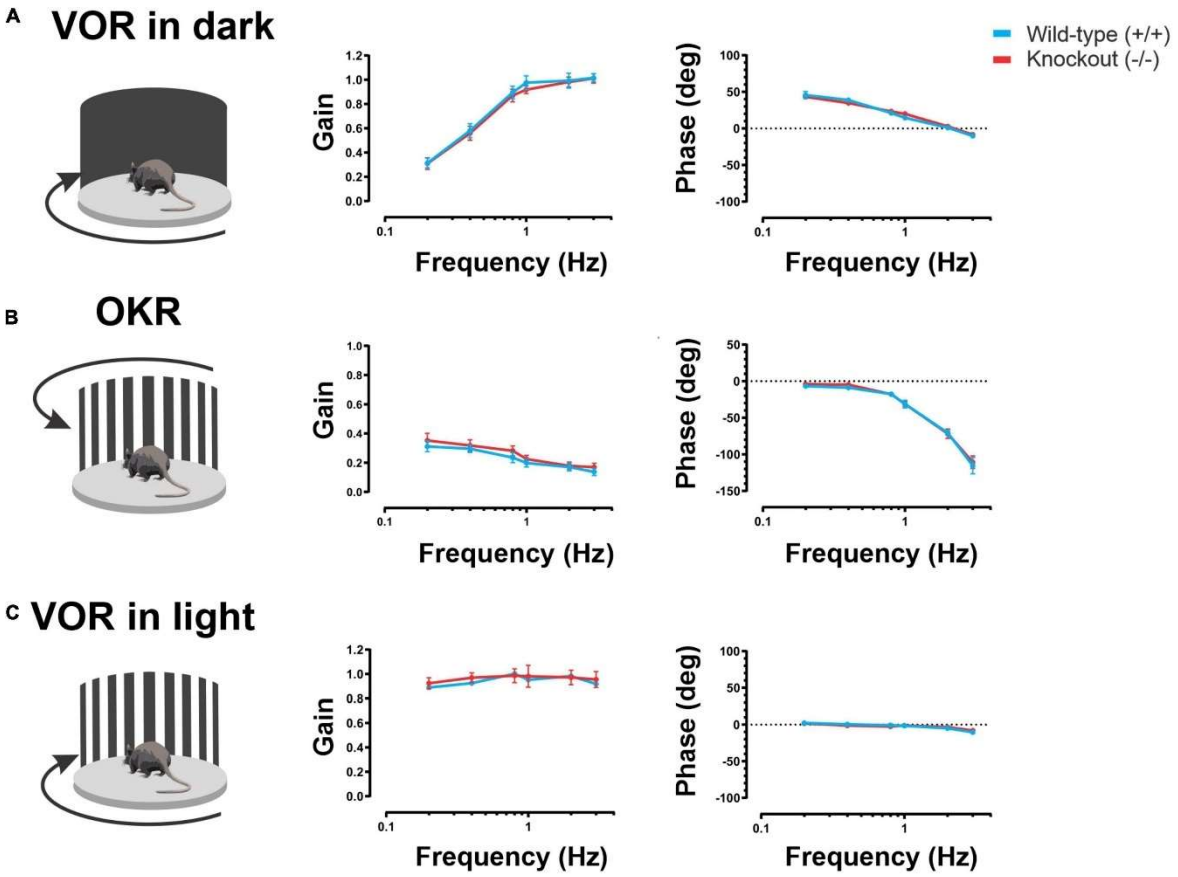

Figure 1. VOR and OKR responses are normal in α9(-/-) mice. (**A**) VORd gain and phase (mean±SEM) plotted as a function of frequency for wild-type and α9 (-/-) mice. N is 7 and 8 for both wild-type (blue) and α9 (-/-) (red) mice respectively for the model with a deletion in exon 1 and 2. (**B**) OKR gain and phase (mean±SEM) plotted as a function of frequency wild-type and α9 (-/-) mice. **(C)** VORl gain and phase (mean±SEM) plotted as a function of frequency for wild-type and α9 (-/-) mice.

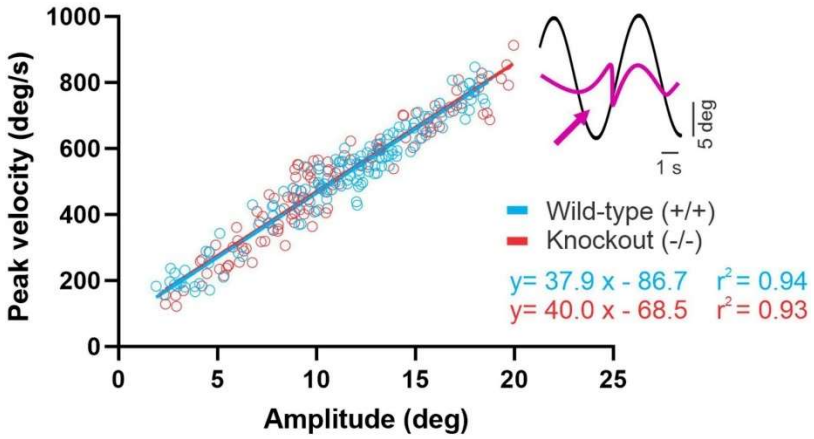

Figure 2. Quick phase eye movement dynamics are not changed in α9(-/-) mice. Peak velocity vs. amplitude relationship for quick phases of the VOR of wild-type and α9 (-/-) mice. Regression lines are superimposed. There is no significant difference between the two slopes.

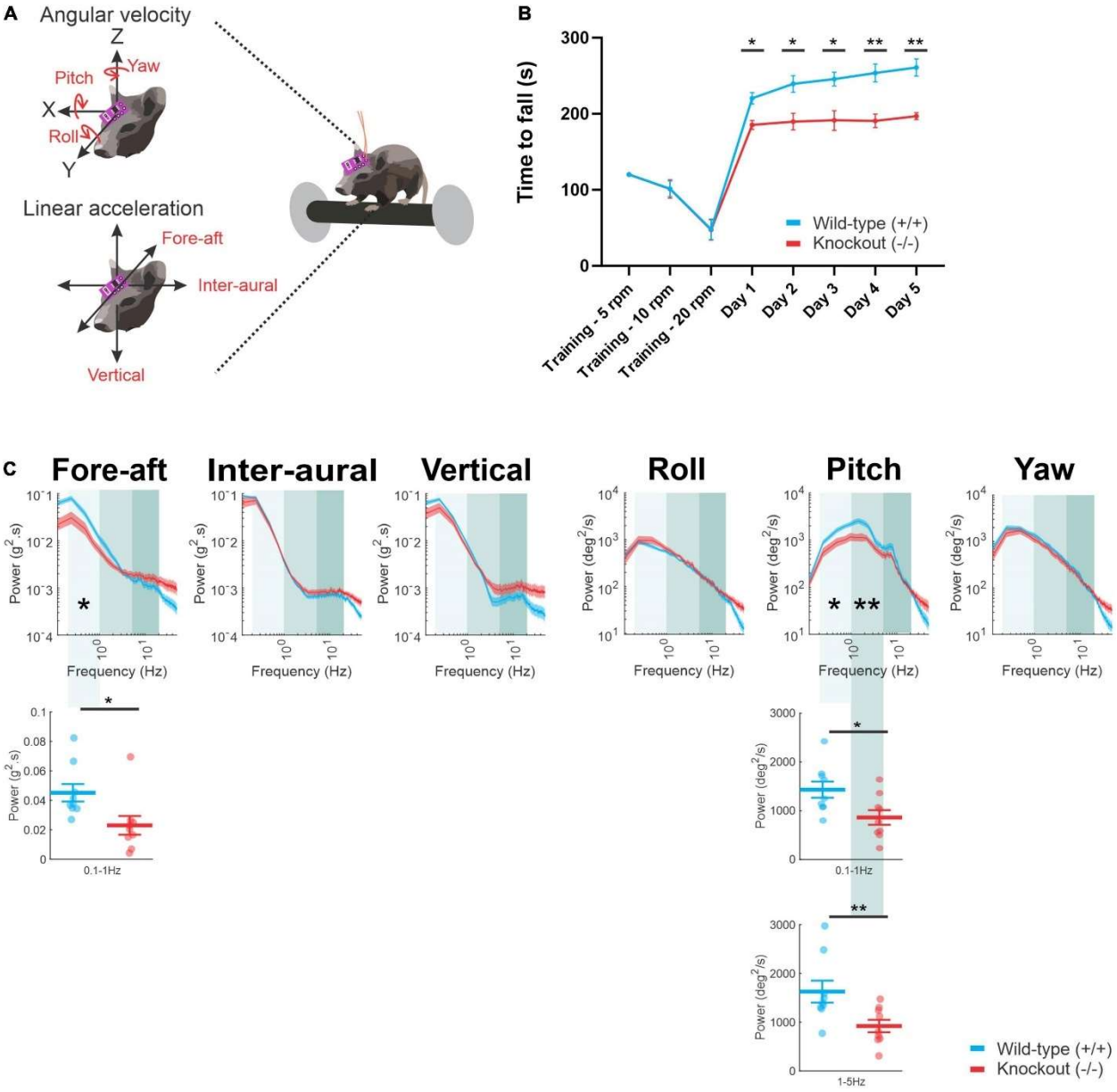

Figure 3. α9(-/-) mice showed impaired postural control on a rotarod. (A) A schematic of an accelerating rotarod assay. **(B)** Time to fall measured each day (mean±SEM) for wild-type (blue) mice and α9 (-/-) mice (red) **(C)** Comparison of power spectra density of head movements during rotarod in translational axes and rotational axes between wild-type mice and α9 (-/-) mice. N is 9 and 9 for both wild-type and α9 (-/-) mice. Error bars: SEM. *P<0.05, **P<0.01.

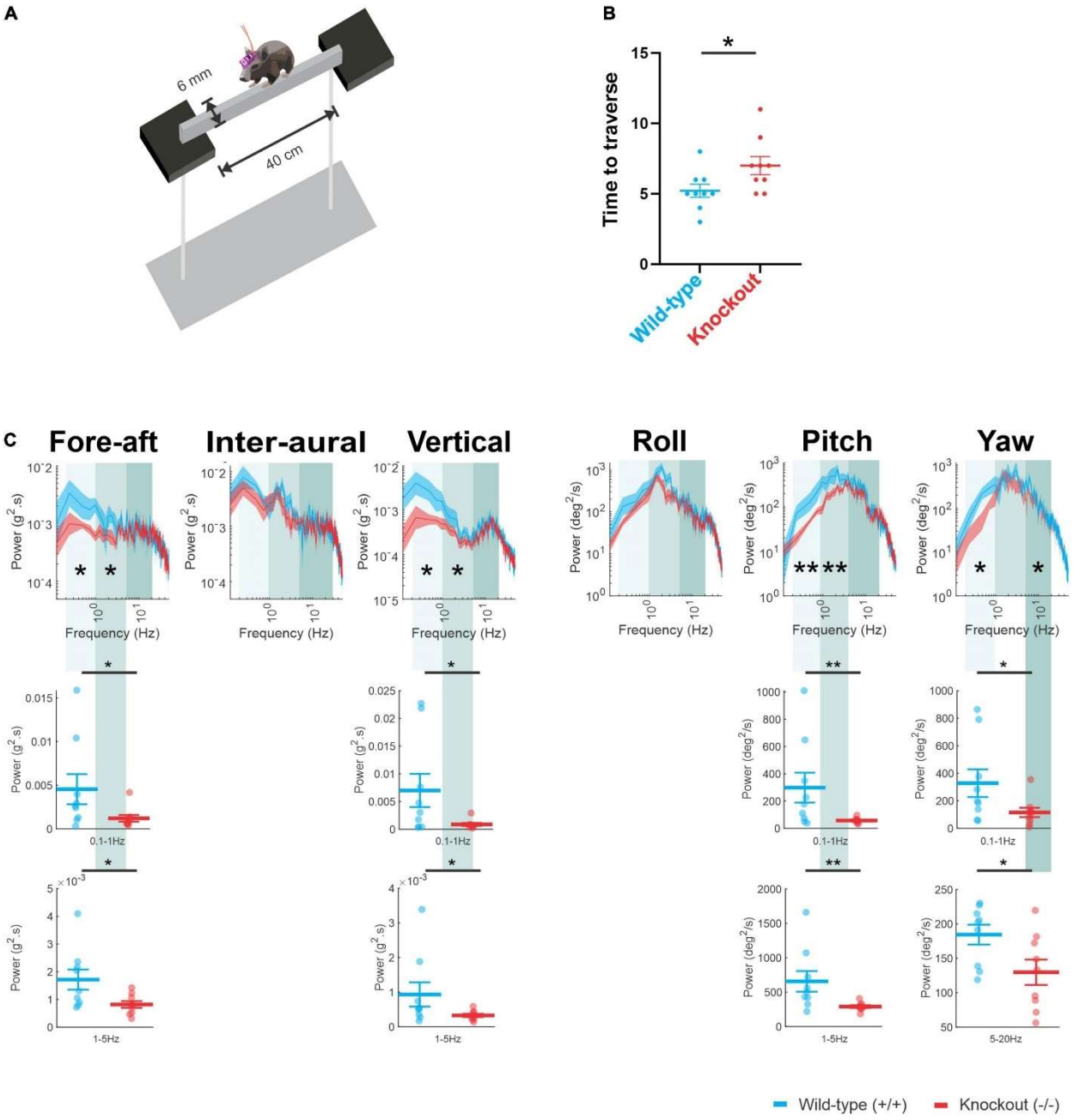

Figure 4. α9(-/-) mice showed impaired postural control on a balance beam. (A) A schematic of a narrow balance bean assay **(B)** Time taken to traverse the balance beam (mean±SEM) for wild-type mice (blue) and α9 (-/-) mice (red) **(C)** Comparison of power spectra density of head movements during balance beam in translational axes and rotational axes between wild-type mice and α9 (-/-) mice. N is 9 and 9 for both wild-type and α9 (-/-) mice. Error bars: SEM. *P<0.05, **P<0.01.

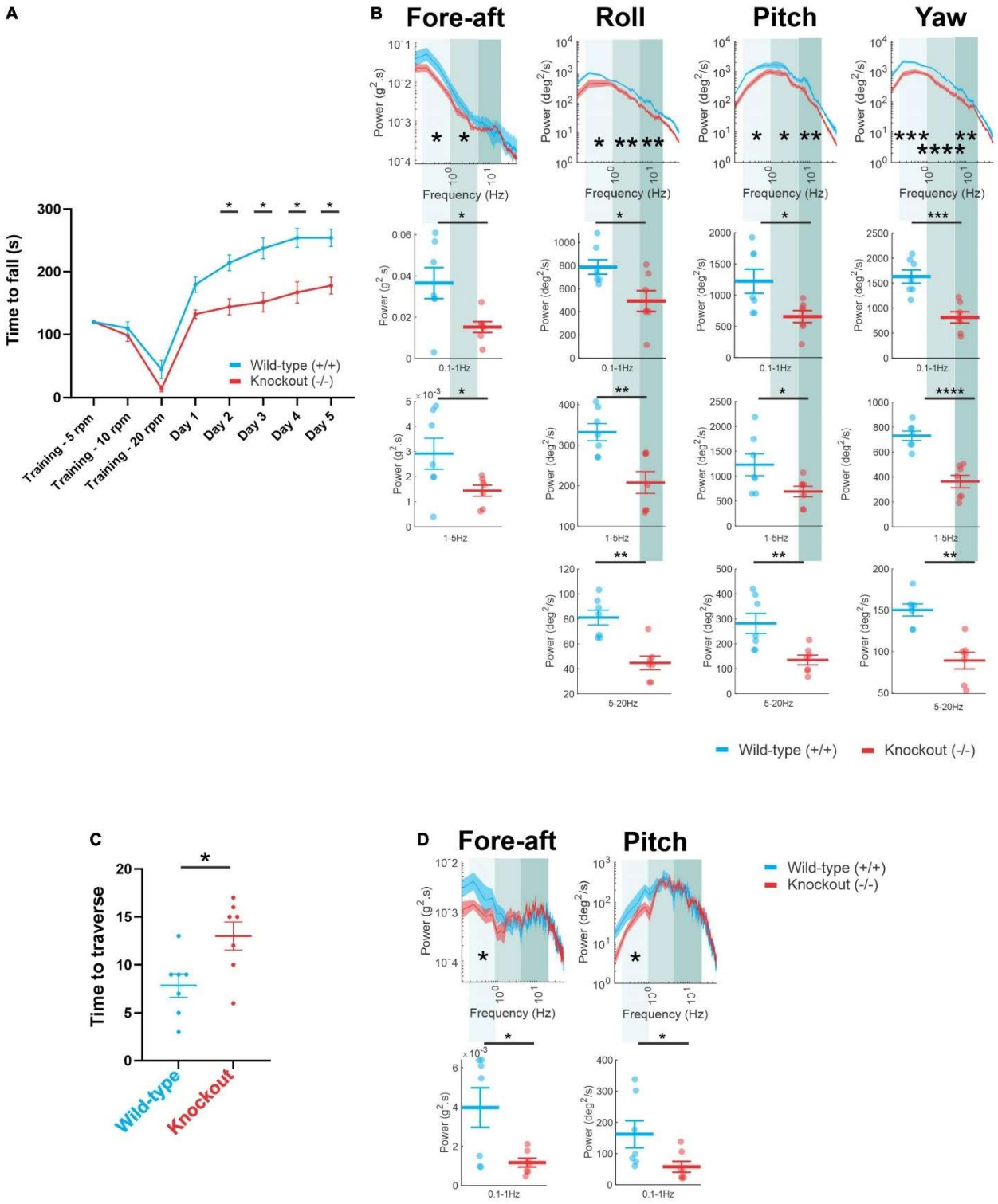

Figure 5. (A) Time to fall measured each day (mean±SEM) for wild-type mice (blue) and α9 (-/-) mice (red). **(B)** Comparison of power spectra density of head movements during rotarod in fore-aft, roll, pitch, and yaw axes between wild-type mice and α9 (-/-) mice. **(C)** Time taken to traverse the balance beam (mean±SEM) for wild-type mice and α9 (-/-) mice. **(D)** Comparison of power

spectra density of head movements during balance beam in fore-aft and pitch axes between wild-type mice and α9 (-/-) mice. N is 7 and 7 for both wild-type and α9 (-/-) mice. Error bars: SEM. *P<0.05, **P<0.01.

Chapter 5
General summary and discussion

The vestibular system, despite being a sense that often go unnoticed, plays a crucial role in our daily lives. The system conveys information about our head motion and orientation with respect to gravity to the brain, that is necessary for the generation of appropriate reflexes and accurate perception of self-motion. In addition, the vestibular system is highly plastic as it interacts with various parts of the brain, such as the cerebellum and the efferent vestibular system. While the progress made toward a systematic understanding of how the vestibular system functions has employed many different animal models, the use of mice has become increasingly important. Thus, in my doctoral research, I focused on the vestibular system in mice and performed a quantitative analysis of vestibular pathways and behaviors. In particular, I considered three vestibular pathways in my thesis: (1) the ascending vestibular pathway that contributes to the sense of direction, (2) the vestibulo-cerebellar pathways that ensure the maintenance of balance, posture, and gaze stability (3) the efferent vestibular pathway that transmits central information back to the peripheral vestibular system.

In my first experimental study, I showed that the nucleus prepositus hypoglossi (NPH), a region that is primarily an oculomotor area, does not relay head motion information per se to ascending vestibular pathways. The NPH receives direct projections from the vestibular nuclei and projects to the network of areas containing neurons that are tuned to a specific static head direction referred to as head direction (HD) cells. A common view had been that the NPH in rodents relays vestibular information to the HD network for computation of direction and spatial orientation. In contrast, prior studies in cat and nonhuman primates have established that the NPH serves as the oculomotor integrator – a structure that integrates (in the mathematical sense) eye velocity commands in the brain to provide the eye position signal required for accurate eye movements. Accordingly, to directly investigate this apparent discrepancy, I designed an experimental setup that provided the ability to dissociate eye and head movements while recording the activity of individual NPH neurons in mice. I found that NPH neurons displayed the same eye-movement-related behavior previously demonstrated in cats and nonhuman primates. Specifically, the responses of mouse NPH neurons can be accounted for across eye and head movement conditions

based solely on their sensitivities to eye position and velocity. Accordingly, during head motion, prepositus neurons did not encode additional vestibular information. Instead, their modulation could be explained based on their sensitivity to eye motion. Taken together, the results establish that the NPH in mice, as in other mammalian species, serves as the oculomotor neural integrator and suggests that eye movement, not head movement, information is relayed to HD cells.

In my second experimental study, I showed that vestibular function was impaired in a mouse model of spinocerebellar ataxia type 6 (SCA6). To do this, I quantified vestibular functions in SCA6 mice versus their littermate controls and linked functional changes to altered cerebellar firing rate behavior. Specifically, I first established deficits in vestibulo-ocular reflex (VOR) and VOR adaptation in SCA6 mice. I then completed single-unit recordings in the flocculus of the cerebellum. My results demonstrate that the firing regularity of Purkinje cells is greatly reduced in SCA6 mice at the onset of their ataxic phenotype. Taken together, these results provide new insights into the pathophysiology of SCA6 by revealing widespread effects across areas of the cerebellum, which extend beyond those regions commonly associated with gait deficits of SCA6.

Finally, in my last experimental study, I investigated the role of the efferent vestibular system. To do this, I tested gaze and postural stability in mice lacking an α9 subunit of the nicotinic acetylcholine receptor (nAChRs). α9 containing nAChRs are highly expressed in the mammalian efferent vestibular system (EVS), and both VOR and postural control assays were used to understand the functional roles of the mammalian EVS. Quantification of VOR responses revealed no effect of loss of the α9 subunit on gaze stability, but the ability to maintain balance and posture in α9 knockout mice was significantly reduced. These results reveal the predominant influence of the mammalian EVS on postural rather than gaze stability.

5.1 Eye movement encoding of the nucleus prepositus (NPH) and its contribution to spatial orientation

The first focus of this thesis was to test the recently proposed hypothesis that the nucleus prepositus hypoglossi (NPH) relays vestibular signals to the HD network necessary for generating the HD signal. In *Chapter 2*, I tested the responses of individual neurons in the NPH to see if they encode eye and/or head movement-related signals during a series of behavioral conditions that dissociated these two signals. In addition to establishing that NPH neurons only encode eye-movement-related information, I further discovered that the mouse NPH neurons non-linearly

encode eye movement. Specifically, eye movement coding is amplitude-dependent, with eye position and velocity sensitivities decreasing with increasing amplitude.

More specifically, my results presented in *Chapter 2* provide strong evidence that the nucleus prepositus predominately encodes eye movement information and does not relay distinct vestibular (i.e., head movement) information to the HD network. I show that the firing rates of individual prepositus neurons can be sufficiently described and predicted by a linear model with mean firing rate, eye position, and eye velocity parameters. Further, the addition of head position, velocity, and or acceleration to these models did not improve the ability to describe neuronal responses during vestibular stimulation. Thus, my findings overturn the prevailing view by showing that the nucleus prepositus does not convey vestibular information to the HD network as previously hypothesized (Brown et al., 2005). It is notable that the findings presented in this thesis are consistent with what has been found in the NPH of nonhuman primate during head movements (Dale and Cullen, 2013). This suggests that despite heavier reliance on vision to navigate the environment, nonhuman primates share this functional pathway with rodents (reviewed in Mitchell and Leopold, 2015). HD cells in the anterior thalamus of nonhuman primates are only recently have been functionally characterized (Laurens et al., 2016). However, similarly to previous rodent studies, no simultaneous recording of eye movements was performed. I speculate that neurons classified as "HD cells" are actually gaze-encoding cells. The lack of eye movement recording in previous rodent studies made it impossible to distinguish between gaze vs. head encoding cells. Indeed, this has been suggested by the existence of "visual place cells" in the hippocampus that the spatial representation is more driven by gaze than actual head direction (Rolls et al., 1999).

5.1.1 Possible sources of vestibular information to the HD network

As mentioned in *Chapter 2*, there are other potential sources for vestibular signals to the HD network. First, the supragenual nucleus is one candidate because of its projections between the vestibular nuclei and the dorsal tegmental nucleus (DTN) (Biazoli et al., 2006; Mehlman et al., 2021). However, no electrophysiological studies have yet been performed to confirm this. Recently, Mehlman et al. (2021) have shown that anatomical projections to the DTN and oculomotor neurons (i.e., abducens nucleus) arise from separate cell populations in the NPH. Therefore, it is also plausible that there is a subgroup in the NPH that relays vestibular information. However, no such cells were recorded in the current dataset presented.

My findings, in addition to a recently published nonhuman primate study, suggest a more prominent role of gaze encoding in the computation of spatial orientation. Indeed, to date, simultaneous recording of eye movements has not been performed in studies involving HD cells, so how dominant eye movement-related signals relate to the tuning of the spatially turned cells still needs to be addressed.

5.2 Altered Purkinje cell firing and its consequences on behavior

In *Chapter 3*, I tested to see if the mutant mouse model of SCA6 exhibits oculomotor and motor learning deficits in addition to their ataxic behavior. Human SCA6 patients have reported oculomotor deficits such as nystagmus and changes in their VOR and OKR gains. Indeed, $SCA6^{84Q/84Q}$ mice display reduced VOR and OKR gains, and their VOR adaptation efficacy was also significantly reduced.

In a prior study, we recorded Purkinje cells in the anterior vermis (i.e., lobule 3) in $SCA6^{84Q/84Q}$ mice at the onset of their ataxic behavior (Jayabal et al., 2016). We found that the firing rate and precision of Purkinje cells were greatly reduced in $SCA6^{84Q/84Q}$ mice. Given the association between the change in firing properties and ataxic behavior, I predicted that I would see an altered firing pattern in floccular Purkinje cells as the flocculus of the cerebellum control generation of VOR and OKR and VOR learning. These changes can partially explain oculomotor motor learning deficits observed in $SCA6^{84Q/84Q}$ mice. Accordingly, I recorded floccular regions of the cerebellum and found that firing rate regularity in this region is also significantly affected.

5.2.1 Significance of Purkinje cell dysfunction in behaviors

As sole output neurons in the cerebellum, it is indisputable that altered Purkinje cell intrinsic firing has a devastating effect on cerebellar functions. The results presented in *Chapter 3* support that cellular deficit of Purkinje cells, demonstrated by altered firing precision, largely accounts for motor deficits in $SCA6^{84Q/84Q}$ mice. Indeed, ataxic behaviors in a mouse model of EA2 (Walter et al., 2006), SCA1 (Hourez et al., 2011), SCA2 (Kasumu and Bezprozvanny, 2012), SCA3 (Shakkottai et al., 2011), SCA5 (Perkins et al., 2010), and $SCA6^{CT\text{-}27Q}$ (Mark et al., 2015), SCA7 (Stoyas et al., 2020), SCA13 (Hurlock et al., 2008), SCA27 (Shakkottai et al., 2009; Bosch et al., 2015) are all found to be associated with firing rate and/or firing precision deficits. This is noteworthy considering the diversity of genetic mutation that leads to these different ataxias. These

studies also suggest targeting changes in intrinsic activity (i.e., firing rate and precision) as treatment options for different ataxias. Indeed, efforts to restore abnormal intrinsic activity, such as counteracting disrupted calcium homeostasis and manipulation of potassium channel activity via viral reintroduction all led to the reduction of PC intrinsic firing deficits (reviewed in Cook et al., 2021). Notably, a broad-spectrum potassium channel blocker, 4-aminopyridine (4-AP) rescued PC intrinsic firing deficits in a mouse model of EA2 (Alviña and Khodakhah, 2010), SCA1 (Haurez et al., 2011) and SCA6 (Jayabal et al., 2016). These results suggest targeting changes in intrinsic activity can be applicable as a treatment strategy to multiple diseases.

5.2.2 Treatment options for SCA6 using a mouse model of SCA6

A voltage-gated potassium channel blocker, 4-AP rescued loss of firing precision and motor deficits in SCA6$^{84Q/84Q}$ mice. Indeed, using 4-AP restored firing precision and firing rate in a mouse model of EA2 (Alviña and Khodakhah, 2010), SCA1 (Hourez et al., 2011), and SCA6 (Jayabal et al., 2016), respectively. This iterates the close relationships between firing properties and cerebellar functions. In humans, 4-AP along with 3,4-diaminopyridine (3,4-DAP) have been tested for efficacy in alleviating ataxia. For example, both 4-AP and 3,4- have been used in patients with multiple sclerosis and have been shown to be effective in treating ataxic symptoms (Polman et al., 1994). 4-AP also alleviates ataxic symptoms in patients with EA2 (Strupp et al., 2004; Strupp et al., 2011). 4-AP has also been used in a short-term trial treating ataxia in SCA6 patients (Giordano et al., 2013). However, to date, all studies in both mouse models and human patients have been performed over a relatively short time span (~ 2 weeks). Further evaluation of the long-term effects of 4-AP is required to test the feasibility of 4-AP in treating SCA6 and other ataxic symptoms.

5.3 Functional roles of the rodent efferent vestibular system (EVS)

Despite being intact and operational, the function of the mammalian efferent vestibular system remains poorly understood. Accordingly, in *Chapter 3*, I investigated whether the mammalian EVS might play a more important role in shaping the efficacy of vestibular motor pathways involved in postural responses rather than gaze stability. To do this, I took advantage of a mouse mutant model lacking α9 subunit-containing nAChRs and quantified postural control using rotarod and balance beam testing. α9-knockout mice showed poorer performances on both

behavior assays. In addition, my head movement recordings in six dimensions revealed altered movement dynamics for α9-knockout mice in the pitch and fore-aft axis. Notably, these results were found to be consistent in another α9-knockout mice model.

5.3.1 Implication of studies in α9 knockout mice: plasticity vs. ensuring functional efficacy during development

nAChRs of the mammalian EVS almost exclusively express α9 and α10 subunits (Elgoyhen et al., 1994; Morley et al., 2018). The α9 subunit is particularly important because α10 subunits can only form functional heteromeric assemblies with α9 subunits (Elgoyhen et al., 2001; Vetter et al., 2007). Given the predominant localization of ACh and its associated receptors in terminals of efferent fibers, mouse mutant models lacking α9 subunit-containing nAChRs have been widely utilized to investigate the functional role of the mammalian EVS. For instance, α9-knockout mice have been used as a model to study the role of mammalian EVS in plasticity and compensation of the VOR. Prior studies have reported impaired VOR gains in α9 nAChR knockout mice, particularly at higher frequencies (e.g., > 1 Hz; Hübner et al., 2015). Furthermore, in a VOR visually-induced adaptation study, motor learning was reduced by ~70% in α9 nAChR knockout mice (Hübner et al., 2015). However, there has been a recent report that the α9 subunit may not only be present in the vestibular periphery but also in the cerebellum (Lykhmus et al., 2017). The methodology of this study has been questioned. However, if it holds true, then it is possible that the deficits observed are related to the cerebellum's known contribution to VOR motor learning rather than the EVS.

The results from my research further our understanding of the possible role of the EVS by demonstrating for the first time that impairments in postural control are actually more marked than those observed for the VOR. I further show this for two specific strains of α9 nAChR knockout mice, namely a model with a deletion in exon 1 and 2 and a model with a deletion in exon 4. Thus, my thesis findings strongly suggest that the EVS has the predominant influence on postural control rather than on gaze stability. Interestingly, this result is consistent with the fact that irregular afferents, which are affected more significantly by EVS stimulation than their regular counterparts (reviewed in Cullen and Wei, 2021), preferentially project to vestibular nuclei that mediate vesitbulo-spinal pathways. Additionally, irregular afferents are thought to make a more significant contribution to higher frequency VOR responses (Sadeghi et al., 2007). Thus, my work and prior

reports that VOR gains are more impaired in α9 nAChR knockout mice at higher versus lower frequencies (Chapter 5, and Hübner et al., 2015) are also consistent with the fact that the EVS predominately influences central pathways that are targeted by irregular afferents.

5.3.2 Implication of studies in another knockout mouse model targeting the EVS: ensuring functional efficacy during development

A second neurotransmitter that is essential in EVS function through its neuromodulatory role in acetylcholine release is calcitonin gene-related peptide (CGRP). CGRP is believed to increase the signal-to-noise ratio of cholinergic nicotinic signal transmission (Di Angelantonio et al., 2003). The majority of CGRP-positive neurons in the vestibular periphery are also labeled positive for ChAT, suggesting co-localization of ACh and CGRP in the same efferent terminal (reviewed in Ohno et al., 1993). Thus, a mouse model with a targeted deletion of αCGRP has been developed to understand the functional role of rodent EVS. Interestingly, αCGRP knockout mice showed a significant reduction of VOR gain by ~50% compared to WT mice, even at lower frequencies (Luebke et al., 2014). Given the CGRP functions in concert with ACh, this demonstrates its role in shaping the functional efficacy of VOR pathways. It is notable that, in contrast, α9 knockout mice do not typically demonstrate a reduction of VOR gain at lower stimulation frequencies (Chapter 5, and Hübner et al., 2015). One possible explanation is that, since CGRP is also known to be expressed in vestibular nuclei that project to the EVS, this deficit is due to changes in central rather than peripheral vestibular function (Wackym et al., 1993; Chi et al., 2007; Ahn et al., 2009). Thus, it is likely that CGRP knockout mice not only have impaired EVS function but also impaired central processing. Thus, it may be expected that they would demonstrate greater vestibular motor impairment than α9 knockout mice in which impaired function is potentially more directly targeted to the EVS.

Finally, to date, no study has assessed postural control in αCGRP knockout mice. Quantifying such postural control will further enhance understanding of the functional role of rodent EVS and characterize the difference between the effects of two major neurotransmitters in the system. Given the fact that postural control is significantly altered in α9 knockout mice, I predict that αCGRP knockout mice would also show poor performance on behavioral assays such as balance beam and rotarod. Further, since as mentioned above, CGRP may affect central vestibular function, I further predict that the loss of αCGRP compared to α9 will have an even more severe effect on postural

control. In order to gain a better understanding of the function of the mammalian EVS using knockout mice, the development of new mutant mice strains will be required. A current limitation is that animals are born with a gene deficit, and the deficit is not tissue specific. In the case of αCGRP knockout mice, site-specific recombination to generate conditional gene knockouts specifically in the vestibular periphery, will eliminate the confounding factor that CGRP is expressed in the central pathway. In recent years, significant progress in using *Cre-loxP* technology for conditional gene expression in the inner ear has been made so that Cre expression can be narrowed down to the vestibular organs (reviewed in Cox et al., 2012). Future work utilizing this tool will make the αCGRP mutant mouse model more ideal and feasible enough to compare with α9 knockout mice.

5.4 Conclusion and future directions

Taken together, the results of my research have contributed to furthering our understanding of the basic physiology and functions of the mouse vestibular system. Specifically, I first recorded individual burst-tonic prepositus neurons during head motion to overturn the prevailing view that prepositus neurons relay vestibular information to the HD network via the ascending vestibular pathway. Second, I quantified VOR responses and VOR adaptive capacity in a mouse model of SCA6, and then recorded individual floccular Purkinje cells to understand pathophysiological alteration associated with observed impairments in VOR responses and adaptation. Overall, the result of this study revealed similarities in the pathological phenotypes of human SCA6 patients and our mouse model as well as a possible cerebellar-based mechanism underlying the pathophysiology of SCA6. Finally, I quantified gaze and postural control in α9-knockout mice to understand the functional role of the mammalian EVS. Overall, these mice predominately demonstrated vestibular motor impairments in their postural rather than gaze stability. Importantly, this finding furthers our understanding of the vital role of the EVS in shaping the functional efficacy of vestibular pathways. Below, I end my discussion by reviewing some limitations of my studies and unanswered questions that require further investigation.

5.4.1 Gaze encoding of prepositus and its implication for the generation of an HD signal

Chapter 3 of this thesis provides evidence that prepositus neurons transmit eye-related information to the HD network during head motion. Thus, this finding strongly implies that an eye

movement signal is, in turn, sent to the HD cell network. One limitation of my work was that the mice were head-fixed, and head movements were passively applied via whole-body rotations. It is well established that early vestibular pathways differentially encode active versus passive head movements (reviewed in Cullen 2019). Furthermore, during active orienting and navigation, mice generate head movements far more robust than those applied here (>1300 deg/s and up to 20 Hz; Carriot et al, 2017). Thus, future studies in which recordings are made in the nucleus prepositus and HD cell network are needed to understand the encoding of eye versus head motion during active orienting and navigation behaviors. In *Chapter 3*, I showed a prototype of a training procedure to study such neuronal responses during active orienting head movement behaviors in mice.

A major limitation of previous studies investigating HD cells is that while head movements were measured, eye movement was never taken into consideration. In this context, one possible finding could be that nucleus prepositus neurons encode eye-movement-related information across all behaviors, including during active orienting and navigation. In this case, the transmission of eye movement signals to the head direction (HD) network would be a major discovery. My present results demonstrate that this is the case for passive head motion, and I anticipate similar results will be found for active head movements. If this is the case, it would overturn the prevailing view in the field by showing that the main contribution of the vestibular system to the generation of an HD signal is actually an eye rather than a head movement signal. My present findings already beg the question of whether HD cells are purely "head-direction" sensitive. Simultaneous recording of the activity of HD cells and eye movements during active movements is essential to confirm what is represented by the HD network in more natural conditions.

5.4.2 Change in the intrinsic firing vs. morphology in SCA6$^{84Q/84Q}$ mice

In *Chapter 4*, I compared the simple spike firing of floccular Purkinje cells in WT vs. SCA6 mice. In addition, morphological changes in the Purkinje cells were also studied, yet we found no difference between SCA6$^{84Q/84Q}$ mice and their controls at the onset of ataxia. Likewise, a prior study compared the simple spike firing of anterior vermis Purkinje cells in WT vs. SCA6 mice and found altered firing pattern but no morphological change at the early stage of SCA6 (Jayabal et al., 2015; 2016). These results imply the dominance of the altered firing pattern in the manifestation of abnormal phenotypes in SCA6$^{84Q/84Q}$ mice. Notably, these studies measure morphological

changes, including molecular layer height and Purkinje cell density. Further studies are required to determine whether other more specific changes in morphology might exist, such as dendritic length, an overall loss of terminal branches, presence of swelling of the Purkinje cell axon (i.e., Torpedoes). Nevertheless, the results imply the dominance of the altered firing pattern in the manifestation of abnormal phenotypes in SCA6$^{84Q/84Q}$ mice.

It should be noted that the Purkinje cell produces two distinct forms of actional potential output, namely simple and complex spikes. Complex spikes are driven by climbing fiber input and are believed to serve as an instructive signal in the cerebellar cortex during VOR adaptation. Though there are many hypotheses concerning the roles of complex spikes, it is an essential part of the cerebellar output. Our preliminary observations (not shown) examining firing properties of complex spikes such as firing rate, pause duration, number of spikelets, and firing regularity in SCA6 mice, indicated a decrease in the complex spike firing rate. Presynaptic climbing fibers to Purkinje cells synapses were labeled with VGLUT2 - a selective market for climbing fiber. The total number of VGLUT2-labeled puncta was calculated, and no significant difference was observed. However, it is still premature to conclude a possible alteration of complex spike firing patterns without physical changes based on our preliminary observation. Further evaluation looking at other measures such as the terminal axonal arborization of climbing fibers (i.e., height, number of branches, and width) is required for further characterization of possible morphological differences.

5.4.3 Role of mammalian EVS in shaping functional connectivity/efficacy during development vs. real-time

Previous developmental studies have demonstrated that the efferent innervation of the vestibular organs is established early in the development (reviewed in Highstein 1991). I speculate that the EVS plays a major role in fine tuning the efficacy of vestibular pathways during the development. In this context, the α9 knockout mouse model used in my study was born with the mutation and so both the development of vestibular pathways was likely affected, as would be any real-time modulation by the EVS. To dissociate between the two possibilities, future studies employing time-specific stimulation such as optogenetics would be useful. Turning on and off the EVS in wildtype mice during behavior tests such as rotarod or balance beam will help to test the possibility that the EVS calibrates the functional efficacy in real-time. For example, if wildtype mice do not

show significant difference in the time taken to traverse the balance beam when the EVS is active vs. transiently inhibited via optogenetics, this would provide that the EVS does not affect the vestibular pathways in real-time. In other words, the poorer performance observed in α9 knockout mice would be primarily due to improper calibration of functional connectivity/efficacy during development. Thus, I propose future use of optogenetics in the mouse model will be useful in furthering our understanding the functional role of the EVS.

Appendix A

Retinoic acid degradation shapes zonal development of vestibular organs and sensitivity to transient linear accelerations

A.1 Abstract

Each vestibular sensory epithelium in the inner ear is divided morphologically and physiologically into two zones, called the striola and extrastriola in otolith organ maculae, and the central and peripheral zones in semicircular canal cristae. We found that formation of striolar/central zones during embryogenesis requires Cytochrome P450 26b1 (Cyp26b1)-mediated degradation of retinoic acid (RA). In *Cyp26b1* conditional knockout mice, formation of striolar/central zones is compromised, such that they resemble extrastriolar/peripheral zones in multiple features. Mutants have deficient vestibular evoked potential (VsEP) responses to jerk stimuli, head tremor and deficits in balance beam tests that are consistent with abnormal vestibular input, but normal vestibulo-ocular reflexes and apparently normal motor performance during swimming. Thus, degradation of RA during embryogenesis is required for formation of highly specialized regions of the vestibular sensory epithelia with specific functions in detecting head motions.

A.2 Introduction

Sense of balance and heading is mediated by integration of vestibular, visual, and proprioceptive inputs. While unilateral vestibular deficits can largely be compensated by sensorimotor reorganization, bilateral loss of vestibular inner ear function, such as caused by aminoglycoside ototoxicity, cannot be fully compensated (Ahmed et al., 2012). As a consequence, patients with chronic bilateral vestibulopathy are disabled by imbalance and oscillopsia. Understanding how vestibular inputs are encoded by vestibular organs to maintain gaze and head stability is important from basic science and therapeutic perspectives.

Vestibular sensory epithelia comprise the maculae of the utricle and saccule, which detect linear acceleration, and the three canal cristae, which detect angular acceleration. Each sensory epithelium contains type I and type II mechanosensitive hair cells (HCs), which are surrounded by supporting cells (SCs) and innervated by afferent neurons of the vestibular ganglion (**Fig 1a**). Type I and II HCs are contacted by different afferent synaptic terminals: large calyceal endings on type I HCs and small bouton endings on type II HCs. The mechanosensitive stereociliary (hair) bundles of HCs couple to an otolithic membrane in the maculae and to a cupula in the cristae. Head accelerations deflect these accessory structures and the coupled hair bundles, modulating mechanotransduction channels in the bundles and ultimately changing the firing rate of afferent neurons (Jones et al., 2015).

Each vestibular organ has near its center a conserved, specialized region called the striola in the maculae and the central zone in the cristae (Eatock et al., 2011; Desai et al., 2005a; Desai et al., 2005b). Striolar/central zones may have evolved in land-based vertebrates as an adaptation to changes required for locomotion, including large independent head movements with high-frequency components (Baird et al., 1988; Straka et al., 2016). Striolas and central zones differ from extrastriolas and peripheral zones in many features, including hair bundle morphology, ion channel expression, and otoconia size (Lysakowski et al., 2011; Lim et al., 1984; Li et al., 2008). Additionally, afferents form complex calyces around multiple type I HCs in greater proportion in striolar/central zones (**Fig 1a**; Desai et al., 2005a; Desai et al., 2005b; Fernandez et al., 1990; Fernandez et al., 1988). Such differences give rise to afferent nerve populations with very different spontaneous and evoked physiological responses. Striolar/central zone afferents have more

irregular spike timing and are more sensitive to higher-frequency head motion than extrastriolar/peripheral afferents (Baird, et al., 1988; Goldberg et al., 1990; Eatock, 2018). Higher densities of low-voltage-activated K (K_{LV}) channels are expressed in striolar/central zone afferents, making them less excitable—less likely to fire in response to small currents—which contributes to their irregular firing patterns (Kalluri et al., 2010). By virtue of their different regularities, afferents from the two zones encode head motion into spike trains by different strategies: temporal pattern of spikes for the striolar/central zones vs. spike rate for extrastriolar/peripheral zones (Jamali et al., 2016) which are optimal for different kinds of sensory information. The formation of these regional specializations and their significance in mediating vestibular functions such as the vestibulo-ocular and vestibulo-spinal reflexes (VOR and VSR) are not known. Nevertheless, several lines of indirect evidence implicate irregular afferents, which innervate the striola, in generating the vestibular-evoked potential (VsEP) (Jones et al., 2015; Jones et al., 2011; Lee et al., 2017; Curthoys et al., 2017), a potential recorded in vivo that reflects activation of macular afferents by linear head motions (Jones et al., 2011; Jones et al., 2004; Dulon et al., 2009).

Here, we show that formation of the striolar/central zones of vestibular organs requires degradation of retinoic acid (RA) by the zone-specific expression of *Cyp26b1*, a gene encoding a RA degradation enzyme. RA, an important morphogen during embryogenesis (Rhinn and Dolle, 2012; Ross et al., 2000), is the bioactive form of vitamin A (retinol), which binds to RA receptors in the nucleus to regulate transcription. The availability of RA during embryogenesis is controlled by restricted expression of RA-synthesizing enzymes such as class 1A aldehyde dehydrogenases (Aldh1a), as well as degradation enzymes such as Cyp26s (Rhinn and Dolle, 2012). The complementary expression patterns of these enzymes during embryogenesis are important in patterning many tissues including the anterior–posterior axis of the inner ear (Bok et al., 2011; da Silva and Cepko, 2017; Dubey et al., 2018; Cunningham and Duester, 2015). We show that *Cyp26b1* conditional knockout (cKO) mice exhibit a severe reduction of striolar/central zones as manifested by a number of morphological, molecular, and physiological properties. These mice have normal horizontal angular vestibular-ocular reflexes (aVOR), driven by horizontal canal cristae, and normal responses to off-vertical axis rotation (OVAR), driven by the macular organs, but they lack VsEP and have head tremor and deficits during balance beam tests. These results suggest that striolas and central zones are not essential for mediating VORs, but are important for

responding to changes in linear acceleration and are likely important for controlling head stability and performing challenging vestibulomotor activities.

A.3 Methods

A.3.1 Mice and genotyping

The following mouse strains were used in the study: *Aldh1a3*$^{+/-}$ (maintained in a mixed C57BL/6J and CD1 background) (Molotkov et al., 2006), *Cyp26b*$^{flox/flox}$ (RIKEN BRC (RBRC04333), maintained in a C57BL/6J background), and *Foxg1*^{Cre} (Hebert and McConnell, 2000) (RRID:IMSR_JAX:004337, maintained in C57BL/6J background). In addition, *Cyp26b1*$^{+/-}$ mice were generated by breeding *Cyp26b1*$^{flox/flox}$ mice with a ubiquitous cre line, *Actin*^{Cre}, and maintained in a C57BL/6J background after recombination and removal of the *cre* allele. *Foxg1*^{Cre}*;Cyp26b1*$^{flox/-}$ were produced by crossing *Foxg1*^{Cre}*;Cyp26b1*$^{+/-}$ males with *Cyp26b1*$^{flox/flox}$ females. Genotyping for mouse strains used in this study was conducted by Transnetyx Inc. All animal experiments were conducted under the approved animal protocols at the NIH, University of Chicago, University of Nebraska -Lincoln, and Johns Hopkins University, and according to NIH animal user guidelines.

A.3.2 Tissue preparation

Timed pregnant females or postnatal mice were harvested and whole heads were hemi-sected, brain is removed, and fixed in 4% paraformaldehyde overnight. For anti-osteopontin staining, the specimens were fixed in Glyo-Fixx (Thermo Scientific) overnight. Then, half-heads were washed, cryo-preserved, and stored in −80 °C until processed for cryo-sectioning or whole-mount dissection subsequently.

A.3.3 In situ hybridization

In situ hybridization was conducted as previously described (Morsli et al, 1998). Digoxigenin-labeled RNA probes were generated for *Cyp26b1* (GenBank: AW049789), β-tectorim (Rau and Richardson., 1999), and *Aldh1a3* (Zhao et al., 2009) as described.

A.3.4 Whole-mount immunohistochemistry

Dissected saccules or utricles with anterior cristae and lateral cristae attached were blocked with PBS containing 4% normal donkey serum and 0.2% Triton X (PBT). Then, specimens were treated with primary antibodies diluted with blocking solution overnight at 4 °C. The primary antibodies used were as follows: goat polyclonal anti-Ocm (1:300, Santa Cruz Biotech, #sc-7446), rabbit polyclonal anti-β-tectorin (1:1000, a gift from Guy Richardson, Universtiy of Sussex), rabbit polyclonal anti-Myosin7a (1:1000, Proteus, #25-6790), mouse monoclonal anti-Myosin7a (1:50, Santa Cruz, sc-74516), rabbit polyclonal anti-calbindin (1:1000, Millipore, #AB1778), mouse monoclonal anti-βIII-tubulin (1:500; R&D, #MAB1195), mouse anti-βII spectrin (1:500; BD Bioscience, #612562), rabbit polyclonal anti-αII spectrin (1:500; Invitrogen, #PA5-35383), goat polyclonal anti-Jag1 (1:200; Santa Cruz, #sc-6011), goat polyclonal anti-Sox2 (1:500; Santa Cruz Biotech, #sc-17320), mouse monoclonal anti-Sox2 (1:150; Santa Cruz, sc-365823), goat polyclonal anti-osteopontin (1:500; R&D Systems, #AF808), rabbit polyclonal anti-Aldh1a3 (1:150; Millipore, #ABN427), and mouse monoclonal anti-acetylated tubulin (1:1000; Sigma-Aldrich, #T6793). Alexa Fluor 647-conjugated phalloidin was used to label actin-based stereocilia (Thermo Fisher Scientific, #A22287).

Following primary antibody incubation, samples were washed with PBT extensively before incubating with appropriate secondary antibodies conjugated with fluorescent proteins: donkey anti-mouse, rabbit, or goat IgG (H + L) antibody (Thermo Fisher Scientific) for 1 h at 4 °C. Then, samples were washed extensively with PBT before mounting with ProLong Gold Antifade (Invitrogen) and imaged with a Zeiss LSM780 confocal microscope. All low-power immunostaining pictures are composite of images taken at ×40 magnification.

A.3.5 Scanning electron microscopy

The preparation of samples for SEM was conducted as described (Forge et al., 2017). Briefly, the utricles and cristae were quickly dissected from harvested animals and submerged in fresh fixative consisting of 2.5% glutaraldehyde (Electron Microscopy Sciences), 2% formaldehyde (EMS), 3 mM calcium chloride, and 0.1 M cacodylate. Two hours after fixation at room temperature, the otoconia was exposed and then tissues were post fixed with osmium-thiocarbohydrazide-osmium method. Specimens were then dehydrated with a series of ethanol,

followed by critical point drying. After spattering with platinum for coating, pictures were taken using electron microscope (SU4800, Hitachi).

A.3.6 Measurement of otoconial size

SEM images were used to measure the length of each otoconia in control and mutant utricles ($n = 2$ for each genotype). To identify the central region in *Cyp26b1* cKO, the striola was identified in control utricles based on the smaller size of the otoconia. Then, a comparable region in the two mutant utricles was compared to that of the controls. The length of the otoconial crystals in the middle of striolar (4 mm^2) and MES region were measured by using the ImageJ (1.52 h) software.

A.3.7 Measurement of cilia length and K/S ratio

P3–P10 utricle samples ($n = 4$ for each genotype) were fixed and labeled with conjugated phalloidin, anti-acetylated tubulin (for kinocilium), and anti-αII spectrin antibodies. A composite picture of confocal images taken at ×40 magnification was generated and LPR was drawn based on hair bundle orientations. Then, regions lateral (lateral extrastriola) and immediately medial (striola) to the LPR in the center of the utricle were selected for stacked confocal images taken at the thickness of 0.2 μm. Length of the kinocilium and the tallest stereocilium were measured using the slice function of the Imaris software. Ratio of the height of the kinocilium (K) to the height of the tallest stereocilia (S) was calculated for 3–5 HCs in each region.

A.3.8 RA treatment of timed pregnant females

Viable *Aldh1a3*$^{-/-}$ mice was generated as described (Dupe et al., 2003). Briefly, RA powder (Sigma) was suspended in ethanol (5 mg/ml), and then 1 ml of RA solution was mixed with 50 mg of normal chow (5015, LabDiet) and administered to pregnant females ad libitum from E8.5 to E14.5.

A.3.9 Measurement of HC density and osteopontin-labeled HCs

HC density in the utricle was measured as described (Jiang et al., 2017). Briefly, a straight line across the widest region of an utricle was drawn along the anterior–posterior (A–P) axis. Then, two lines perpendicular to the A–P line, which mark the middle-third region of the utricle were drawn. This middle region was divided into two equal halves along the medial–lateral axis, and

the posterior half was further sub-divided into four equal regions marked as 1, 2, 3, and 4, representing LES, striola, and two MES regions, respectively. The number of HCs per 0.01 mm^2 area within areas 1 and 2 were counted.

A.3.10 Quantification of complex calyces

Whole-mount utricles of *Cyp26b1* cKO and littermate controls at P30–45 were immunolabelled with anti-Tuj1 and anti-calbindin antibodies ($n = 3$/group). Z-stacked images were taken using a laser scanning confocal microscope (Zeiss LSM780). Tuj1-positive calyces that surround two or three HC bodies in each utricle were scored manually by examining individual confocal stacks.

A.3.11 Whole-cell patch clamp recordings

Data shown here are from 21 littermates: 11 control mice (*Foxg1^{Cre};Cyp26b1$^{lox/+}$*, ages P17–P97, median P21) and 10 mutant mice (*Cyp26b1* cKO, $n = 10$, P12–P100, median P20.5). Tissue preparation was conducted as described (Songer and Eatock, 2013). For each electrophysiological experiment, a mouse was anesthetized deeply by exposure to isoflurane and decapitated. The utricle plus the superior division of the vestibular ganglion and distal part of the vestibular nerve were excised, trimmed, and secured in a recording chamber with the exposed apical surface of the epithelium facing up, as described (Songer and Eatock, 2013; Rüsch and Eatock, 1996).

Whole-cell recordings were made at room temperature (23–25 °C) using pipettes with resistances between 3 and 7 MΩ in standard solutions. The bath (external) solution was Leibovitz-15 (L15) medium, supplemented with 10 mM HEPES, ~315 mmol kg^{-1} and pH 7.4. The pipette (internal) solution comprised (in mM): 135 KCl, 0.1 $CaCl_2$, 3.5 $MgCl_2$, 3 Na_2ATP, 5 creatine phosphate (Na^+ salt), 0.1 Na-cAMP, 0.1 Li-GTP, 5 EGTA, and 5 HEPES. The solution was brought to pH 7.3 and ~300 mmol kg^{-1} by adding ~28 mM KOH. Sulforhodamine 101 (1 mg/100 ml; Invitrogen) was added to the internal solution to label the recorded HC or calyx.

Whole-cell, GΩ-seal recordings were made from visually identified HCs or calyceal afferent terminals within the semi-intact epithelium as described (Songer and Eatock, 2013). The

EPC-10 (HEKA) patch clamp amplifier was controlled by Patchmaster software (HEKA Electronik GmbH). In voltage clamp mode, we recorded currents evoked by iterated voltage steps with the amplifier's 4-pole low-pass corner frequency at 6 kHz and a sampling interval of 5–25 µs. Series resistances ranged from 4 to 32 MΩ (mean 10.4 ± 0.6 MΩ, $n = 57$) and were compensated during recordings by 80.1 ± 0.3%. Capacitive currents were nulled on-line with Patchmaster. We also recorded voltages evoked by iterated current steps in current clamp mode. Potentials are corrected for a liquid junction potential of 4 mV, calculated with the JPCalc software (Barry, 1994) as implemented by Clampex 10 (Molecular Devices). Cells were held at –64 mV (in voltage clamp) and resting potential (in current clamp), unless otherwise noted. For steady-state analyses of voltage-dependent properties, command potentials were corrected for series resistance errors.

Data were analyzed with OriginPro 2017 (OriginLab, Northampton MA). Results are presented as means ± SE. Comparisons were made with two-factor ANOVA, with one factor being genotype (control vs. mutant) and the other epithelial zone (striolar vs. extrastriolar), followed by Tukey's means comparisons. Effect size was estimated by Hedge's *g* statistic.

A.3.12 VsEP measurements

VsEP was measured in *Cyp26b1*$^{lox/+}$ ($n = 5$), *Foxg1*^{Cre}*;Cyp26b1*$^{lox/+}$ ($n = 10$) and *Cyp26b1* cKO ($n = 9$) mice. VsEP recordings were the same as methods published previously (Vijayakumar et al., 2015;2017; Mock et al., 2011). The first positive (P1) and negative (N1) response peaks of the VsEP waveform were scored for each intensity level. Thresholds (measured in dB re: 1.0 g/ms) were also obtained from the scored VsEP waveforms.

A.3.13 aVOR measurements

We measured eye movements of alert *Foxg1*^{Cre}*;Cyp26b1*$^{lox/+}$ ($n = 5$) and *Cyp26b1* cKO ($n = 5$) mice in response to transient (3000°/s^2 constant acceleration to peak/plateau velocity of 300°/s lasting 0.8–1.0 s, then −3000°/s^2 deceleration for 100 ms to rest at 90° from the starting position) yaw, whole-body head rotations in darkness using a fiducial-tracking, binocular 3D video-oculographic method and data analysis procedure identical to that described in detail previously (Migliaccio et al., 2005), except that the image acquisition rate was performed using new cameras with higher image resolution and framerate (180 frame/s). Sinusoidal stimuli were

0.02–10 Hz at peak velocity 100°/s for ≥10 cycles per trial. Eye rotation data were converted to rotation vectors in head coordinates and analyzed as described previously (Migliaccio et al., 2005). Yaw (horizontal) head angular velocity data were inverted prior to gain calculation. For transient stimuli, we restricted analysis to slow-phase nystagmus responses during the 100 ms constant-acceleration time segment after onset of each stimulus. For each trial, response latency was computed as the time difference between the zero-velocity-intercept times for lines fit in a least-mean-square sense to eye and head velocity during the constant-acceleration stimulus portion of the stimulus. Using the slopes of the same fitted lines, we computed "constant-acceleration segment gain" G_A as the mean over all cycles of the ratio of eye acceleration to head acceleration. For sinusoidal stimuli, we removed quick phases and saccades manually prior to further analysis of slow-phase nystagmus data, for which ≥10 cycles per trial were averaged and used to compute gain and phase of the yaw eye angular velocity response relative to the head angular velocity stimulus. Positive phase lead denotes a rightward slow-phase nystagmus response leading a leftward head rotation stimulus. Sinusoidal frequency response data were further parameterized by fitting a first-order high-pass filter to each animal's data. The resulting gain and corner frequency parameters were used for statistical comparison between mouse groups. Gain and latency data were analyzed using a Mann–Whitney U test with significance set at $P = 0.05$.

A.3.14 OVAR measurements

Foxg1^{Cre};*Cyp26b1*$^{lox/+}$ controls ($n = 6$) and *Cyp26b1* cKO mice ($n = 6$), ranging between 6 and 7 months old, were used. Techniques employed for measurement of eye movements during OVAR in alert mice were described elsewhere (Beraneck et al., 2012). Briefly, recordings made after fixating mice on a rotating platform, which was tilted 17° with respect to the ground. Platforms speed was increased from 0 to 50°/s in 500 ms and maintained its constant velocity for 72 s (10 complete rounds) before being stopped. Eye movements were measured using video occular-graphy (iScan). Quick phases were identified as previously described (Beraneck et al., 2008) and excluded from subsequent analysis. We then estimated the time constant of the OVAR slow-phase eye velocity response decay, as well as the amplitude and phase of its sinusoidal modulation using a linear regression approach (Cullen et al., 1996).

A.3.15 Open-field test

Three-month-old *Foxg1*^{Cre};*Cyp26b1*$^{lox/+}$ control ($n = 6$) and *Cyp26b1* cKO mice ($n = 5$) were used. Each mouse was placed in an open arena. Two minutes after habituation, subject was video recorded for 5 min. Trace of each mouse was visualized followed by analysis with Topscan software (3.0, Clever Sys Inc.).

A.3.16 Rotarod test

Foxg1^{Cre};*Cyp26b1*$^{lox/+}$ controls ($n = 10$) and *Cyp26b1* cKO mice ($n = 9$), ranging from 2 to 5 months old, were used. Each mouse was placed on a motorized rotating rod (ROTA ROD, Panlab, Harvard Apparatus) that gradually accelerated from 5 to 40 r.p.m. in 5 min, and the time required for the mouse to fall off the rotarod was scored. Each mouse underwent tests for three consecutive days with 5 trials per day. First day was considered to be the training day. Averaged score for each day was processed for statistical analysis.

A.3.17 Balance beam test

Foxg1^{Cre};*Cyp26b1*$^{lox/+}$ control ($n = 5$) and *Cyp26b1* cKO mice ($n = 6$), ranging between 6 and 7 months old, were used. The balance beam apparatus consisted of a 60-cm-long and 20-mm-wide beam that was positioned 70 cm above ground with an escape box on one end. Walking speed was measured by recording the time the animal took to reach the escape box from the opposite end of the beam. When 6-mm-wide beam was used, mice were placed at the midpoint of the 80-cm-long beam and the time taken to reach the endpoint on either side (time to traverse 40 cm) was measured. Mice were scored ‘’time out” when failed to reach the endpoint in 2 min.

A.3.18 Head-tremor measurements of P9 pups

P9 controls ($n = 8$) and *Cyp26b1* cKO ($n = 6$) pups were placed in an open arena. Their motor activities and behavior were video recorded for 10 min. The total distance traversed, the number of bouts per 100 mm traveled, and duration of each bout episode were measured using the Topscan software.

A.3.19 Head-tremor measurements of adult mice

Control ($n = 6$) and *Cyp26b1* cKO mice ($n = 6$) between 6 and 7 months old were used. Mice were placed in a cylinder (9 cm diameter and 21.5 cm height) that limited their motion, so mice maintained their steady posture. Head movements in six dimensions were recorded using a miniature head motion sensor (MPU-9250, SparkFun Electronics, Niwot, CO) affixed on the top

of the skull, which comprises a three-dimensional (3D) accelerometer (measures linear acceleration; right/left, fore/aft, and up/down) and 3D gyroscope (measures angular velocity: pitch, roll, and yaw). Data were acquired at 200 Hz using windows-based CoolTerm software. We then computed the power spectral densities (pwelch function, MATLAB, MathWorks) using Welch's averaged periodogram with nfft = 128 and a Bartlett window (128 ms duration) for all six dimensions of movement.

A.3.12 Statistical analysis

T test was used for comparison of two samples, and either one- or two-way ANOVA, followed by Tukey's multiple comparison tests was used for more than two samples. Data distribution was assumed to be normal, but not formally tested. All statistics were conducted by Prism 7 (GraphPad Inc.), except in cases described separately. All data are shown as average ± SEM.

A.4 Results

A.4.1 Expression of *Cyp26b1* and *Aldh1a3* in the vestibular organs

We observed complementary expression patterns of transcripts for the RA-degrading enzyme Cyp26b1 and the RA-synthesizing enzyme Aldh1a3 in developing vestibular organs that were not described previously. During embryogenesis, the sensory epithelia of the utricle (**Fig 1 b-d**), saccule (**Fig 1b**) and cristae (**Fig 1 b-d**) show *Cyp26b1* expression in the center surrounded by *Aldh1a3* expression in the periphery. The *Cyp26b1* expression domain in the maculae appears comparable to that of β-tectorin, a striolar SC marker (**Fig 1 b-d**; Rau et al., 1999). Adjacent cryo-sections processed for in situ hybridization confirmed the complementary relationships among *Aldh1a3*, *Cyp26b1*, and β-tectorin in both maculae and the lateral crista (**Fig 1f-h**). *Cyp26b1* hybridization signals appear to be concentrated basally in striolar SCs, but *Aldh1a3* distribution is broad in the extrastriola/central zone at E15.5 (**Fig 1f-h**). Similar results were obtained with immunostaining using anti-Aldh1a3 antibodies. As the sensory epithelium matures, Aldh1a3 immunoreactivity is localized to both HCs and SCs in the extrastriola and some HCs in the striola by postnatal day 0 (P0). Overall, these expression patterns suggest that differential expression of RA could establish the central and peripheral zones of vestibular organs.

A.4.2 Formation of the striolar/central zone requires *Cyp26b1*

To test the hypothesis that striolar/central zone formation in each vestibular sensory organ requires RA degradation, we analyzed vestibular organs in gain and loss of RA function mutants, *Cyp26b1*$^{-/-}$ and *Aldh1a3*$^{-/-}$ embryos, respectively, between E17.5 and E18.5, and these mutants survive until birth (Dupe et al., 2003; Yashiro et al., 2004). Total HC number is increased by 13% in *Cyp26b1*$^{-/-}$ utricles, but unchanged in *Aldh1a3*$^{-/-}$ utricles, compared to controls (**Fig 2j**). The Ca^{2+}-binding protein oncomodulin (Ocm) is expressed only in the type I HCs located within the striolar/central zone (**Fig 2a**; Simmons et al., 2010). In *Cyp26b1*$^{-/-}$ inner ears, Ocm expression is reduced in both maculae and cristae (**Fig 2b**). Percentages of Ocm^+ HCs are decreased in *Cyp26b1*$^{-/-}$ utricles (**Fig 2k**). Similar decreases in Ocm + HCs were observed in saccules and lateral cristae (**Fig 2l**).

In *Aldh1a3*$^{-/-}$ mutants, in which RA synthesis is reduced, the Ocm expression domain is increased in the maculae but not cristae (**Fig 2c**). In *Aldh1a3*$^{-/-}$ utricles, the expression domain of Ocm expands towards the medial extrastriolar (MES) region (**Fig 1a**), but not the lateral extrastriolar (LES) region of utricles (**Fig 2c**); in *Aldh1a3*$^{-/-}$ saccules, in contrast, the Ocm expression domain is broadly expanded.The percentages of Ocm^+ HCs are increased per utricle (**Fig 2k**) and saccule, compared to controls. In contrast, no increase in Ocm^+ HCs is evident for the lateral crista (**Fig 2l**), suggesting the presence of other compensatory sources of RA in the cristae. Nevertheless, these combined results (**Table 1**) suggest that formation of the striolar/central zone-specific HCs in vestibular organs is regulated by Cyp26b1-mediated degradation of RA.

We next examined whether the identity of SCs in the striolar/central zone of vestibular organs is also affected in mutants deficient for enzymes in the RA pathway. In normal maculae, β-tectorin is specifically expressed in striolar SCs (**Fig 2d** and m; Rau and Richardson, 1999). Consistent with the changes in Ocm expression by HCs, the extent of β-tectorin expression is reduced in *Cyp26b1*$^{-/-}$ utricles (**Fig 2e and m**) and increased in *Aldh1a3*$^{-/-}$ utricles (**Fig 2f and m**). These results show that striolar SC identity in the utricle requires the decrease in striolar RA levels that is mediated by Cyp26b1. In the saccule, in contrast, no significant difference in the β-

tectorin-positive region was detected in either *Cyp26b1*$^{-/-}$ or *Aldh1a3*$^{-/-}$ ears (**Table 1**), suggesting that changes in RA levels may not affect SC formation in the saccule. In cristae, which have different accessory structures than the maculae, β-tectorin is not expressed (**Fig 2d**) and there is no known SC marker for the central zone, preventing the evaluation of RA effects on SC identity.

Many regional differences in the vestibular organ develop postnatally. For example, osteopontin, an extracellular matrix protein, is found in extrastriolar type I HCs at birth (McInturff et al., 2018). Another prominent feature of mammalian vestibular epithelia is the postnatal development of afferent nerve endings (calyces) encasing single or multiple type I HC bodies (**Fig 1a;** Lysakowski et al., 2011; Fernandez et al., 1990; 1988). In order to investigate the role of RA in postnatal differentiation, we bypassed the lethality of *Cyp26b1*$^{-/-}$ and *Aldh1a3*$^{-/-}$ mice (Dupe et al., 2003; Yashiro et al., 2004) by first generating cKO of *Cyp26b1* (*Foxg1*^{Cre};*Cyp26b1*$^{lox/-}$) using *Foxg1*^{Cre}, which is expressed in tissues such as the otic placode and forebrain during early embryogenesis (Hebert and McConnell, 2000). We also generated viable *Aldh1a3*$^{-/-}$ mice by supplementing maternal RA during embryonic day (E) 8.5 to E14.5 of development (*Aldh1a3*$^{-/-}$ (em RA)). This RA supplementation has been demonstrated to rescue the RA requirements of *Aldh1a3*$^{-/-}$ mice during early embryogenesis without reducing the inner ear defects, which develop later (Dupe et al., 2003; Romand et al., 2013). In *Cyp26b1* cKO mice, reduction of Ocm and β-tectorin expression patterns are similar to those of the *Cyp26b1* KOs). Additionally, we investigated the nature of the Ocm^{-} type I HCs in the striola of *Cyp26b1* cKO utricles using anti-osteopontin antibodies, which labels extrastriolar type I HCs postnatally (McInturff et al.,2018). *Cyp26b1* cKO utricles lack normal striolar identifying features and we delineated a comparable region to the control striola (see Methods) for comparison to controls. Our results showed that there is an upregulation of osteopontin immunoreactivity in *Cyp26b1* cKO striolas.Together, these results suggest that the type I HCs are present in the *Cyp26b1* mutant striola, but they have acquired some extrastriolar type I HC properties.

Additionally, we used calbindin-D28K immunoreactivity to selectively stain for striolar/central zone afferents (Leonard and Kevetter., 2002) in control and mis-regulated RA mutants at P40 or P45. Similar to what was observed for HCs and SCs, the calbindin expression domain is decreased in all *Cyp26b1* cKO vestibular sensory organs compared to controls (**Fig**

2g,h,n, and o). These results indicate that the development of calyceal-bearing afferents of striolar/central zones requires relatively lower levels of RA signaling regulated by *Cyp26b1*.

In *Aldh1a3*$^{-/-}$ (em RA) mice, the calbindin-expressing domain is increased in the utricle but not in the lateral crista (**Fig 2i,n, and o**, Table 1), consistent with the expanded striolar region in the *Aldh1a3*$^{-/-}$ mutants. Together, these results suggest that formation of the striolar/central zone in the vestibular organs requires Cyp26b1 enzyme to degrade the RA emanating from the surrounding sensory tissue, which is largely generated by Aldh1a3 in the maculae, although not in the cristae (**Table 1**).

A.4.3 *Cyp26b1* deletion affects anatomical features of the striola

Next, we investigated the mature anatomy of the striola in *Cyp26b1* cKO utricles as a result of altered RA signaling during embryogenesis. A significant characteristic of the maculae is the presense of the otoconia, mineralized calcium carbonate crystals embedded above the otolithic membrane (**Fig 1a**; Lim, 1984). Under low magnification, the otoconial layer in the utricle is more transparent in the striola than the rest of the organ due to the smaller size and number of otoconia (Figs. 1a and 3a). This clear zone is absent in *Cyp26b1* cKO utricles (**Fig 3b**). Scanning electron micrographs (SEMs) of control utricles show smaller otoconia and more extensive perforations of the underlying meshwork otoconia in the striola (**Fig 3c-c";** Lim, 1984) compared to the MES (**Fig 3c"**'). In *Cyp26b1* cKO utricles, SEM revealed no regional differences in otoconial crystals (**Fig 3d-d"**), consistent with low-power brightfield images (**Fig 3b**). Crystals throughout *Cyp26b1* cKO utricles were of similar size to control MES crystals (**Fig 3e**), indicating that the zonal difference in otoconial size was absent in the *Cyp26b1* cKO utricles.

At the sensory epithelium level, the striola has a lower density of HCs (number per surface area) than in the rest of the sensory organ4, reflecting larger apical cell surfaces. To investigate whether this regional marker is also affected by RA signaling, the density of HCs in the striolar region was compared between controls and *Cyp26b1* cKO mutants. In *Cyp26b1* cKO utricles, which lack normal striolar identifying features, we delineated a comparable region to the control striola (see Methods) for comparison. In control utricles, HC density was lower in striola than in LES. This regional difference in HC density was not detected in mutant utricles. Striolar HC

density in *Cyp26b1* cKO mutant epithelia was significantly higher than in control striola and comparable to HC density in control-LES.

In control utricles, the kinocilium length is shorter in the striola than extrastriola (Li et al., 2008). Consequently, the ratio of the length of the kinocilium to that of the tallest stereocilium (K/S ratio) is also significantly smaller in the striola than extrastriola (Li et al., 2008).We therefore measured whether RA signaling affected these properties. For this analysis, we referenced hair bundle location to the line of polarity reversal (LPR) of hair bundles, which is closely associated with the striola in macular organs (**Fig 1a**), and hair bundle orientation was identified by phalloidin staining of actin-filled stereocilia or anti-spectrin staining of the cuticular plate in which stereocila insert (Deans et al., 2007). In the mouse, the utricular striola is largely medial to the LPR, whereas the saccular striola straddles the LPR (**Fig 1a**; Jiang et al., 2017). We determined that the relative position of the LPR was not altered in either the mutant utricle or saccule. In utricles, the K/S ratio in the *Cyp26b1* cKO striola was comparable to its value in the control extrastriola, but not the control striola. These results suggest that the zonal difference in the K/S ratio is absent in the *Cyp26b1* cKO utricles.

Visual inspection of living utricular epithelia with differential contrast microscopy suggested that complex calyces, a prominent feature of the striolar/central zone (Desai et al., 2005a; 2005b; Li et al., 1990), were less numerous in *Cyp26b1* cKO utricles. To quantitatively examine this impression, we stained neurons with Tuj1 antibody and counted calyces in control and *Cyp26b1* cKO utricular striolas.

Complex calyces encasing two or three type I HCs (double or triple calyces, respectively) were present in significantly higher numbers in control striolas (**Fig 4a and c**) than in *Cyp26b1* cKO striolar regions (**Fig 4b and c**).

Together, our results showed that the lack of *Cyp26b1* during embryogenesis affects many mature features of the striola, including the otoconia, expression of Ca^{2+}-binding proteins, HC density, hair bundle morphology, and incidence of complex calyces, suggesting that striolar maturation depends on low levels of RA signaling.

A.4.4 Striola physiology is affected in *Cyp26b1* cKO mice

To assess whether zonal differences in physiology were affected by the mutation, we recorded from HCs and afferent calyces in both control and *Cyp26b1* cKO mice using a semi-intact preparation of the utricle and distal nerve. We visualized the epithelium's apical surface with differential-interference-contrast optics, which allow resolution of hair bundles, HC bodies, and calyceal afferent terminals. Because the *Cyp26b1* cKO utricles had lost the zonal markers that we usually use (hair bundle size, HC density as viewed from above, the proportion of calyces that are complex), we relied on the LPR, assigning recordings in the first 10 HC rows medial to the LPR as "striolar." We performed the whole-cell recording configuration on visually identified type I or type II HCs or on calyceal afferent terminals that surround type I HCs, and measured voltage-gated currents in voltage clamp mode and resting potential and step-evoked voltage changes in current clamp mode. Recorded HCs and calyceal terminals were filled with fluorescent dye, allowing their visualization with fluorescence optics.

In HCs ($n = 64$, from 21 mice), there were no obvious effects of the *Cyp26b1* cKO manipulation on whole-cell voltage-sensitive conductances, as revealed by currents evoked by voltage steps or voltage responses to current steps. Wild-type type I and type II cells from mice and other amniotes (Contini et al., 2017) have outwardly rectifying K^+ currents with very different voltage dependence: the voltage of half-maximal activation ($V_{1/2}$) is 40–70 mV more negative in type I HCs compared to type II HCs. The unusually negative voltage dependence of the type I-specific K^+ conductance ($g_{K,L}$) has significant consequences for the size and speed of the receptor potential and appears to be essential for non-quantal transmission at type I–calyx synapses (Contini et al., 2017). This key difference was preserved in the striolar zones of *Cyp26b1* cKO utricles: three-factor analysis of variances (ANOVAs) on $V_{1/2}$ for HC type (I vs. II), genotype, and epithelial zone yielded a highly significant difference for HC type ($F(1,46) = 1348.33$, $P = 0$), but for no other comparison. Thus, the *Cyp26b1* cKO mutation did not grossly affect the electrophysiological differentiation of type I and type II HCs.

Differences were seen, however, when we compared spiking activity of striolar and LES calyx-bearing afferents in *Cyp26b1* cKO and $Foxg1^{Cre};Cyp26b1^{lox/+}$ controls. In the LES, calyx-

bearing afferents are dimorphic afferents (forming both calyx and bouton terminals, **Fig 1a**). In the striola, calyx-bearing afferents are either dimorphic or pure-calyx afferents. We measured spiking activity of dimorphic afferents or pure-calyx vestibular afferents via ruptured-patch recordings from their calyceal terminals (spikes initiate on the afferent neurite below the base of the calyx (Lysakowski et al., 2011). Striolar afferent neurons were more excitable in *Cyp26b1* cKO mice compared to $Foxg1^{Cre};Cyp26b1^{lox/+}$ controls, as measured by lower current threshold for spiking and tendency to fire a longer train of spikes in response to supra-threshold current steps. Threshold current was defined as the lowest current at which spiking occurred when currents were incremented in 50-pA steps (red traces, **Fig 5a-c**). Threshold currents were significantly larger for striolar afferents than for control-LES afferents and any other afferent class, including *Cyp26b1* cKO striolar afferents (**Fig 5d**). Threshold currents did not differ significantly between *Cyp26b1* cKO striolar afferents and *Cyp26b1* cKO-LES afferents or control-LES afferents. Thus, *Cyp26b1* cKO manipulation reduced threshold current for spiking in striolar afferents to levels typical for extrastriolar afferents.

Afferent firing patterns were classified for current steps 2–3 times threshold current as either transient (1–3 onset spikes) or sustained (>4 spikes). The tendency of isolated neurons to respond to injected current steps with transient or sustained responses correlates with their tendency to fire more irregularly or more regularly in vivo, when they are driven by synaptic inputs from HCs (Kalluri et al., 2010). In control utricles, striolar afferents were more likely to have transient than sustained responses and extrastriolar afferents were more likely to have sustained than transient responses (**Fig 5e**), consistent with previous data from rat vestibular ganglion neurons (Kalluri et al., 2010) and calyceal terminals (Songer and Eatock, 2013). In *Cyp26b1* cKO utricles, the normal zonal difference in firing pattern disappeared: most striolar afferents, like extrastriolar afferents, had sustained responses to current steps (**Fig 5e**).

These changes in excitability in the *Cyp26b1* cKO zone corresponding to the striola (reduced current threshold, more sustained firing) likely involve loss of striolar-specific ion channel expression. Candidates include low-voltage-activated K (K_{LV}) channels, which reduce neuronal excitability by increasing K^+ conductance around resting potential, such that more current is required to depolarize to spike threshold. In normal utricular afferents, K_{LV} channels are

expressed more in striola than extrastriola (Lysakowski et al., 2011; Kalluri et al., 2010; Songer and Eatock, 2013; Lwasaki et al., 2008). *Cyp26b1* cKO afferents may lack this zonal difference in K_{LV} expression, based on measurements of K_{LV} current that is on at –65 mV and turned off by stepping membrane voltage to –125 mV. In Cyp26b1 cKO utricles, K_{LV} current per afferent calyx recording did not differ significantly across zones (striola: 870 ± 114 pA, $n = 16$; extrastriola:1192 ± 151 pA, $n = 6$; $P = 0.14$). Thus, *Cyp26b1* cKO utricles showed changes in afferent physiology that are consistent with a loss of striolar identity.

A.4.5 Absent VsEP in *Cyp26b1* cKO mice

To assess the functional consequences of losing the striola in vivo, we recorded with scalp electrodes the VsEP, which represent summed far-field afferent responses to transient linear accelerations, in control and *Cyp26b1* cKO mice. Control mice (*Cyp26b1*$^{lox/+}$ and *Foxg1*^{Cre}*;Cyp26b1*$^{lox/+}$ heterozygous animals) had normal VsEP responses, whereas *Cyp26b1* cKO mice showed either absent or deficient VsEP responses (**Fig 6a**). VsEP thresholds for *Cyp26b1*$^{lox/+}$ and *Foxg1*^{Cre}*;Cyp26b1*$^{lox/+}$ heterozygotes were similar (**Fig 6b**). There were also no differences in VsEP response activation latencies (P1, N1) or amplitude (P1–N1) at the highest stimulus level (+6 dB re: 1 g/ms) across the two genotypes. Taken together, these data show that VsEP was severely affected in *Cyp26b1* cKO mice, indicating that loss of the striola effectively abolishes most, if not all, VsEP response, supporting the hypothesis (Jones et al., 2015) that the VsEP is a summated potential reflecting activity of striolar afferents and their downstream targets.

A.4.6 Normal VOR and OVAR in *Cyp26b1* cKO mice

Next, we tested whether the VOR was also affected in the *Cyp26b1* cKO mutants based on the hypothesis that striola and central zones are important for vestibular-reflex function (Eatock, 2018; Curthoys et al., 2017). The VOR plays an important role in ensuring gaze stabilization during everyday activities by producing compensatory eye movements in the direction opposite of the head movement (Stahl, 2004). Because the dynamic response properties (i.e., gain and phase) of the VOR can be precisely quantified, it has also become a valuable tool for assessing vestibular function in mice. The best characterized VOR is the aVOR, which counter-rotates eyes in the horizontal plane and is largely driven by signals from horizontal canal cristae. As a control for eye

muscle function, we also examined the optokinetic reflex (OKR), which uses visual signals to control eye motion, allowing tracking of a moving visual scene or objects. Normally, OKR functions in concert with VOR and vestibular neck reflexes to achieve the correct head and eye motion to stabilize visual field (Stahl, 2004). Both the *Foxg1*^{Cre}*;Cyp26b1*$^{lox/+}$ heterozygotes and *Cyp26b1* cKO mice showed robust OKR responses. Although aVOR gain increased and aVOR phase decreased systematically with increasing frequency of stimulus, there were no significant differences between *Foxg1*^{Cre}*;Cyp26b1*$^{lox/+}$ heterozygotes and *Cyp26b1* cKO mice in gain, phase change, model gain, or model time constant up to 10 Hz (Fig 7a-e; $P > 0.05$ for all comparisons).

Next, to detect reflex responses derived from macular organs, OVAR testing was conducted (Beraneck et al., 2012). For this purpose, we analyzed the recorded eye movements from the mice with heads fixed to a rotating platform (50°/s constant velocity), tilted 17° with respect to the ground (**Fig 7f**). The eye velocity comprises two different responses: (1) a transient canal-mediated response that initially increases then gradually decays and (2) an otolith-mediated steady-state response in which eye velocity oscillates around a constant bias with a sinusoidal waveform. We quantified differences between the two groups by comparing the amplitudes and time constants of transient responses and the amplitudes and biases of steady-state responses. Similar to aVOR results, both transient and steady-state OVAR responses were comparable for *Cyp26b1* cKO vs. controls (**Fig 7f and g**). Together, these results indicate that despite the loss of striolar/central zone identity in vestibular sensory organs, horizontal aVOR and OVAR responses were normal by these assays in the *Cyp26b1* cKO mice, at least up to the maximal testable frequencies, which largely span the physiologically relevant range of head motion for mice in their natural environments (Carriot et al., 2017).

A.4.7 Vestibular balance test of *Cyp26b1* cKO mice

The vestibular system plays a vital role in balance control. To ensure stable body posture, VSRs produce compensatory movements of the neck and body to maintain the head in an upright position. Thus, we next tested *Cyp26b1* cKO mutants on a number of vestibular tasks used to test for balance and postural defects in mice. First, we found that these mice did not exhibit either circling or head tilting behaviors that are often associated with loss of vestibular function in rodents.

Additionally, open-field testing revealed no hyperactivity in *Cyp26b1* cKO mutants, and the swimming ability of mutants was not affected under either light or dark conditions. We further subjected animals to rotarod testing (Tun et al., 2014) and quantified their performance based on the time the animal remained on the rotating rod with increasing acceleration. *Cyp26b1* cKO and $Foxg1^{Cre};Cyp26b1^{lox/+}$ controls exhibited similar motor performance on day 1 of the trial (**Fig 8a**). However, *Cyp26b1* cKO mutants performed better (took longer time to fall) than controls on the second and third days (**Fig 8a**). Whether this improved performance on the rotarod is due to replacement of striolar/central zone with extrastriolar/peripheral zone tissue or other mechanisms is not clear. Nevertheless, these collective behavioral results support the conclusion that the *Cyp26b1* cKO mutants exhibit no balance deficits during many of the tests commonly used to access balance and motor control functions in mice.

The balance beam test can detect subtle deficits in motor skills and balance that may not be detected by other standard motor and balance tests such as the rotarod test (Luong et al., 2011). Accordingly, we tested the performance of *Cyp26b1* cKO mice on the balance beam. We found that *Cyp26b1* cKO mice walked slower than controls on a 20-mm-wide beam over 60 cm length (**Fig 8b**). On a narrower beam (6 mm) over a distance of 40 cm, *Cyp26b1* cKO mice tended to freeze and stop walking (3 out of 6 vs. 1 out of 5 in controls) or moved slower than controls (**Fig 8c**). These results indicate that *Cyp26b1* cKO mice show a deficit in coordinating challenging vestibulomotor functions

.

A.4.8 Increased head tremor in *Cyp26b1* cKO mice

Despite normal aVOR, OVAR, and performance for all standard motor and balance tests other than balance beam testing, we observed that it was possible to distinguish *Cyp26b1* cKO mice from controls in their cages, because the former demonstrated head tremor. This distinctive feature of *Cyp26b1* cKO mice was particularly obvious at early postnatal ages. Quantitative analysis at P9 showed that the incidence of head tremor per 100 mm distance traveled was higher in mutants than controls (**Fig 9a**) and each head-tremor episode also lasted longer in mutants (**Fig 9b**). These head tremor became less noticeable during normal activities in a cage as the mutants matured, suggesting some level of compensation. To quantify head tremor in adult *Cyp26b1* cKO mutants, we affixed a 6D MEMS module consisting of three gyroscopes and three linear

accelerometers to the mouse's head implant. We confirmed that, when mice were not actively moving through their environment, *Cyp26b1* cKO adults exhibit head tremor (**Fig 9c and d**). Power spectra of head movements revealed higher power for *Cyp26b1* cKO mutants than controls at high frequency (5–20 Hz) for all six dimensions (**Fig 9e and f**). For mid-frequency (1–5 Hz), *Cyp26b1* cKO mutants have higher power for yaw and roll head velocity (**Fig 9f**). Taken together, these results indicate that the ability to maintain head stabilization in *Cyp26b1* cKO mice is compromised.

A.5 Discussion

Based on molecular, cellular, and physiological evidence, we demonstrated that striolar/central zones of vestibular sensory organs in the *Cyp26b1* mutants (gain of RA signaling) are severely reduced. We concluded that reduced RA signaling mediated by the expression of *Cyp26b1* in the prospective striolar/central zones is required for this regional formation. This conclusion is supported by results from a complementary mouse model, *Aldh1a3*$^{-/-}$ mice, in which endogenous RA signaling is reduced in the peripheral region of sensory organs and striolar HCs are expanded in the two maculae (**Fig 2**). The expansion of Ocm^{+} HC in the central zone is not observed in the cristae (**Fig 2c**). We attributed this difference between maculae and cristae to possible functional redundancy provided by *Aldh1a1* and *Aldh1a2*, which are expressed in the adjacent nonsensory tissues or in the roof of the sensory organs (Romand et al., 2006). Additionally, the extent of expansion of Ocm^{+} HCs is different between the utricle and saccule (**Fig 2c**). Therefore, it is possible that intrinsic molecular differences across different regions of a sensory organ could also affect the response to the loss of RA signaling.

It is unclear how lower RA signaling mediates the unique cellular and anatomical features of the central regions during development. *Cyp26b1* is not detectable in the developing vestibular ganglion at E13.5 and P0 using in situ hybridization. Based on the concentrated expression of *Cyp26b1* in SCs of striolar/central zones, one possibility is that Cyp26b1 in SCs degrades RA and provides a niche for the afferent nerve endings to form calyces. Receptors of RA are known to be expressed in the otic vesicle and neural-sensory epithelium of the inner ear (Dolle et al., 1994; Romand et al., 2002; Shen et al., 2015). Alternatively, the reduced RA in striolar SCs could regulate downstream genes within SCs, which indirectly affect the development of HCs and their

afferents. Previous results have suggested such a function for SCs (Gomez-Casati et al., 2010). Activated erbB receptors in SCs of the utricle lead to production of BDNF, which promotes synaptogenesis between HCs and afferent neurons.

VsEP measure utricular and saccular function and are produced in response to transient changes in linear head acceleration (jerk) (Jones et al., 2004; Dulon et al., 2009). Several lines of evidence have implicated the irregular afferents of the striola in the generation of VsEP. First, the phase-locking and transient firing properties of irregular neurons render them the most likely candidates to respond in a synchronized manner to linear jerk stimuli and produce the signature compound action potentials (Jones et al., 2015; Curthoys et al., 2017). Second, VsEP is impaired by inhibitors of KCNQ (Kv7) channels, which are most abundant in the calyceal endings of the striola (Lee et al., 2017). Third, the linear pulse stimuli used to evoke VsEP are likely to activate irregular, striolar, afferents based on experiments with sound and bone vibration stimuli in the 500–1000 Hz range (Curthoys et al., 2017; McCue and Cuinand, 1994).

Our results provide strong evidence that the VsEP originates in the striola. The loss of morphological and physiological features in the striola of *Cyp26b1* cKO mice together with the loss of VsEP suggests that the striola is necessary for the generation of VsEP. In control otolith organs, mechanical input to HCs in different zones is differentially shaped by striking differences in otoconia, otolithic gel layers, hair bundle morphology, and bundle coupling to the otoconia9. These differences are likely to contribute to the greater sensitivity of striolar afferents to high-frequency and transient head motion, including the linear pulse stimuli used to evoke VsEPs. In *Cyp26b1* cKO mice, otoconia are present but have extrastriolar-like properties throughout the epithelium. Other likely factors are the zonal differences in calcium-binding proteins, afferent calyceal synapses, and excitability, all absent in *Cyp26b1* cKO.

Given the larger cell bodies, higher conduction velocities (Lysakowski et al., 1995; Goldberg and Fernandez (Lysakowski et al., 1995; Goldberg and Fernandez, 1977) and greater phase advances of evoked firing (Hullar et al., 2005; Kim et al., 2011; Sadeghi et al., 2007) of irregular neurons in striolar/central zones than regular neurons in extrastriolar/peripheral zones, these regions have been postulated to be important for mediating short-latency vestibular reflexes

(Huterer and Cullen, 2002). The aVOR in mice is fast with a latency as low as <7 ms (Hübner et al., 2017). However, we did not detect any deficit in aVOR and OVAR in *Cyp26b1* cKO mutants when lateral cristae and macular organs, respectively, were inertially stimulated, suggesting that the striolar/central zones of vestibular organs (innervated by irregular afferents) are dispensable for these functions, at least in the adults. We cannot rule out the possibility that vestibular reflexes at a younger age or stimulations beyond frequencies tested (10 Hz in the case of aVOR) may require normal function of the central zones. These results further suggest that regular afferents concentrated in the extrastriolar/peripheral zones of vestibular organs are important for mediating VOR. It was reported that *Aldh1a3*$^{-/-}$ (em RA) mice show absence of aVOR and OVAR responses (Romand et al., 2013), and our results show that the striolar/central zones in the vestibular organs are expanded based on Ocm staining (**Fig 2**). Thus, these results are consistent with previous evidence that extrastriolar/peripheral zones are more important than striolar/central zones for aVOR and OVAR—for example, when irregular afferents in squirrel monkeys were selectively affected with galvanic currents, aVOR was not changed (Minor and Goldberg, 1991). Together, these results suggest that regular afferents in extrastriolar/peripheral zones rather than irregular afferents in striolar/central zones are more important for mediating angular and linear VOR in mice.

A long-standing hypothesis is that irregular afferents, which innervate the striolar/central zone, preferentially contribute to VSR (Goldberg and Fernandez, 1971; Bilotto et al., 1982). Our finding that loss of striolar/central zones leads to a deficit in coordinating challenging postural control on the balance beam is consistent with this proposal Goldberg and Fernandez, 1971; Bilotto et al., 1982). Surprisingly, however, *Cyp26b1* cKO mice performed well on other less sensitive tests commonly used for assessing changes in balance and motor control function in vestibularly deficient mice. Further, we did not observe common vestibular behavioral deficits such as head tilt and circling in the *Cyp26b1* cKO mutants. Together, these two observations suggest that the extrastriolar/peripheral zones, which constitute 75–80% of the sensory epithelia (Desai et al., 2005a;2005b, Baird et al., 1988; Goldberg et al., 1990) and are innervated by regular afferents, play a critical role in vestibulo-spinal as well as vestibulo-ocular reflexes in mice. In support of this hypothesis, regular afferents with their sustained firing properties are thought to be more

important in conveying head positional information in steady state such as head tilts (Fernandez and Goldberg, 1976).

A distinguishing characteristic of *Cyp26b1* cKO mice was that they demonstrated head tremor. Similar head-movement behaviors have been reported in both primates and humans with compromised vestibular function. For example, squirrel monkeys show transient head tremor and postural instability after plugging one of the lateral semicircular canals (Paige, 1983). Patients with chronic bilateral vestibular loss who exhibit gaze variability and oscillopsia also show unusually pronounced head oscillations in response to weighted head mass (Saglam et al., 2014). These head tremors are attributed to failure of vestibular input that is normally required to maintain head stability (Goldberg and Cullen, 2011; Angelaki and Cullen, 2008) and ensure movement accuracy during active goal-directed behaviors (Saglam et al., 2014; Sylvestre and Cullen, 2006). It is tempting to speculate that in the *Cyp26b1* cKO mouse, abnormal vestibular inputs from striolar/central regions cause head tremor, and affect challenging activities that require rapid vestibular input to motor centers, such as traversing a narrow balance beam. This phenotype is consistent with the postulated temporal precision of head-movement detection by the striolar/central zones (Straka et al., 2016; Jamali et al., 2016). One caveat is that *Cyp26b1* is also expressed in the cortex and brainstem (Zhang et al., 2003), and *Cyp26b1* cKO mice show some loss of expression in the brain, raising the possibility that the behavioral phenotype reflects central in addition to peripheral *Cyp26b1* loss.

In summary, using a genetic approach we generated a viable mouse mutant that largely lacks the striolar/central zone of vestibular organs. By disrupting RA signaling during embryogenesis, the entire axis of this specialized zone failed to develop properly, including associated components such as the otoconia and innervating neurons. The loss of this highly specialized and conserved region (Lysakowski and Goldberg, 2004) selectively affected the ability of vestibular afferents to respond to transient changes in linear acceleration, as shown by VsEP recordings, and produced some behavioral effects manifested as head tremor and balance beam deficits. A better understanding of the striolar/central zone-specific function has clinical and therapeutic relevance as HCs in this region are more susceptible to ototoxic insults in animal models (Lindeman, 2009).

Low levels of RA signaling mediated by two of the RA degradation enzymes, Cyp26a1 and Cyp26c1, are also required for the formation of the retinal fovea (da Silva and Cepko, 2017). Similar to *Cyp26b1* cKO effects on the entire striolar/central zone axis (accessory structure–HC–neurons), perturbation of RA signaling in the developing retina disrupts multiple foveal features, including photoreceptor distribution, ganglion cell density, and interneuron organization. Therefore, the same developmental strategy generates regional specialization and functional diversity in two sensory systems.

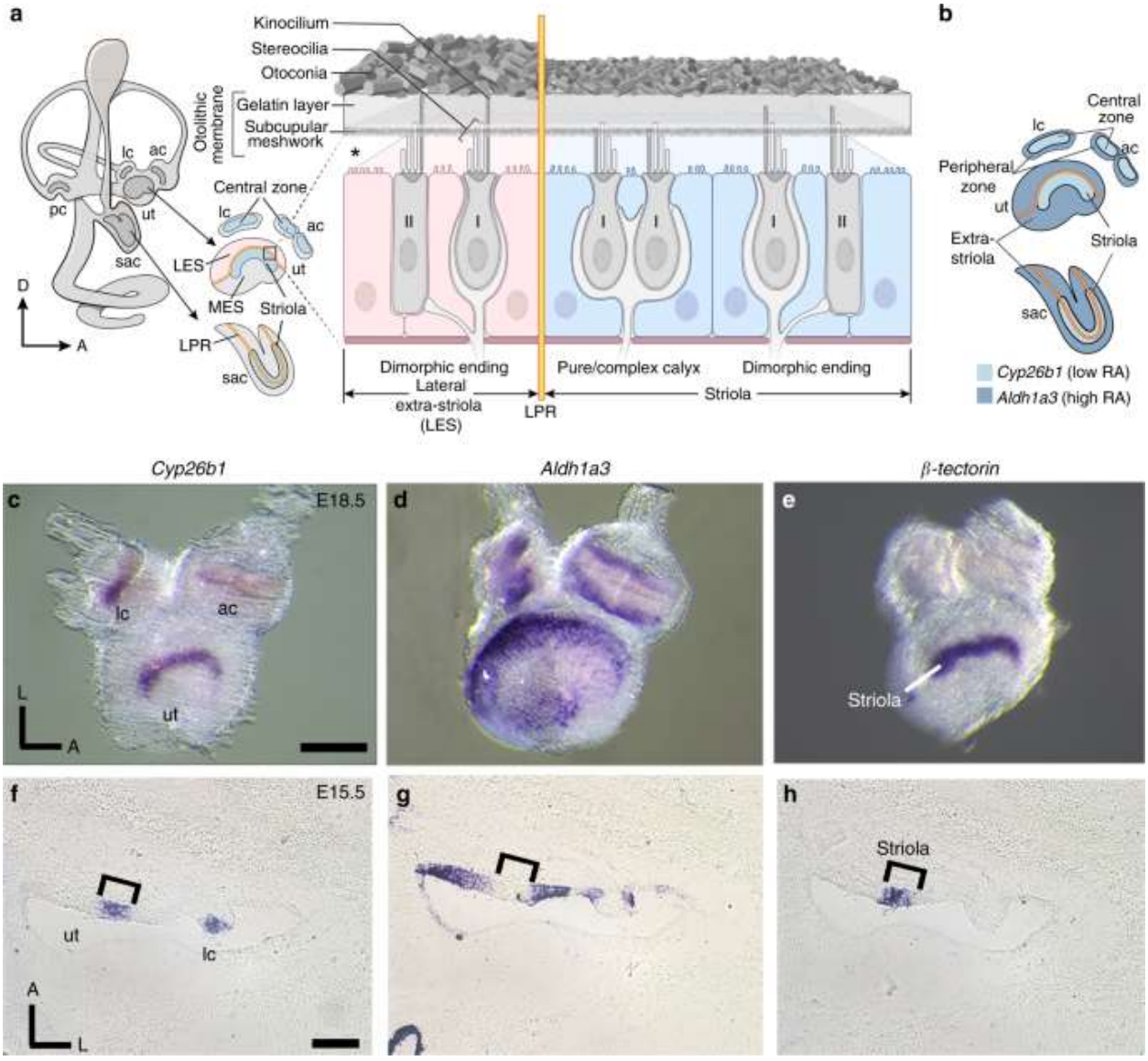

Figure A1. Complementary expression pattern of *Cyp26b1* and *Aldh1a3*. (**a)** Schematic illustration of the inner ear and sectional view of the utricle (ut) across the striola and lateral extrastriola region (LES). Pear-shaped type I HCs are innervated by calyces and cylindrical-shaped type II HCs are innervated by bouton type endings. Pure/complex calyces are exclusively present in the striolar/central zone, whereas dimorphic nerve endings are found across the entire organ. Otoconia are smaller in size and less abundant in striola than extrastriola of the utricle. Asterisk indicates that the relationship between hair bundles and the otoconial membrane is not clear, but evidence suggests that hair bundles of striolar HCs are less firmly embedded in the otolithic membrane than their counterparts in the extrastriolar region (Lim et al., 1984; Spoon et al., 2011). Yellow line represents the line of polarity reversal (LPR), which separates each macula into two regions with opposite hair bundle orientations: 1) striola and MES (medial extrastriola): 2) LES. The striola of maculae and the central zone of anterior (ac) and lateral cristae (lc) are in blue color. The LPR is at the lateral edge of the striola in the ut but it bisects the striola in the saccule (sac). (**b)** Schematic summary of the expession pattern of *Cyp26b1* (light blue) and *Aldh1a3* (dark blue) described in (**c**–**h)**. (**c**–**e)** Whole-mount in situ hybridization analysis of *Cyp26b1*, *Aldh1a3*, and β-*tectorin* transcripts at E18.5 mouse ut, ac, and lc. Expression of *Cyp26b1* (**c**) is restricted to the central zone of the two cristae and striola of the ut that is β-*tectorin* positive **e**, whereas *Aldh1a3* (**d**) is predominantly expressed in the peripheral regions. (**f**–**h)** Adjacent tissue sections at the levels of ut and lc at E15.5. **f** *Cyp26b1* expression is concentrated in the supporting cell (SC) layer of the central zone of the lc and striola of the ut, comparable to the β-tectorin domain (**h**, bracket). (**g)** *Aldh1a3* expression is largely complementary to *Cyp26b1* (**f**) in each organ. Scale bars: 200 μm. RA, retinoic acid; D, dorsal; A, anterior; L, lateral; pc, posterior crista. **a**, **b** Drawn by NIH Medical Arts.

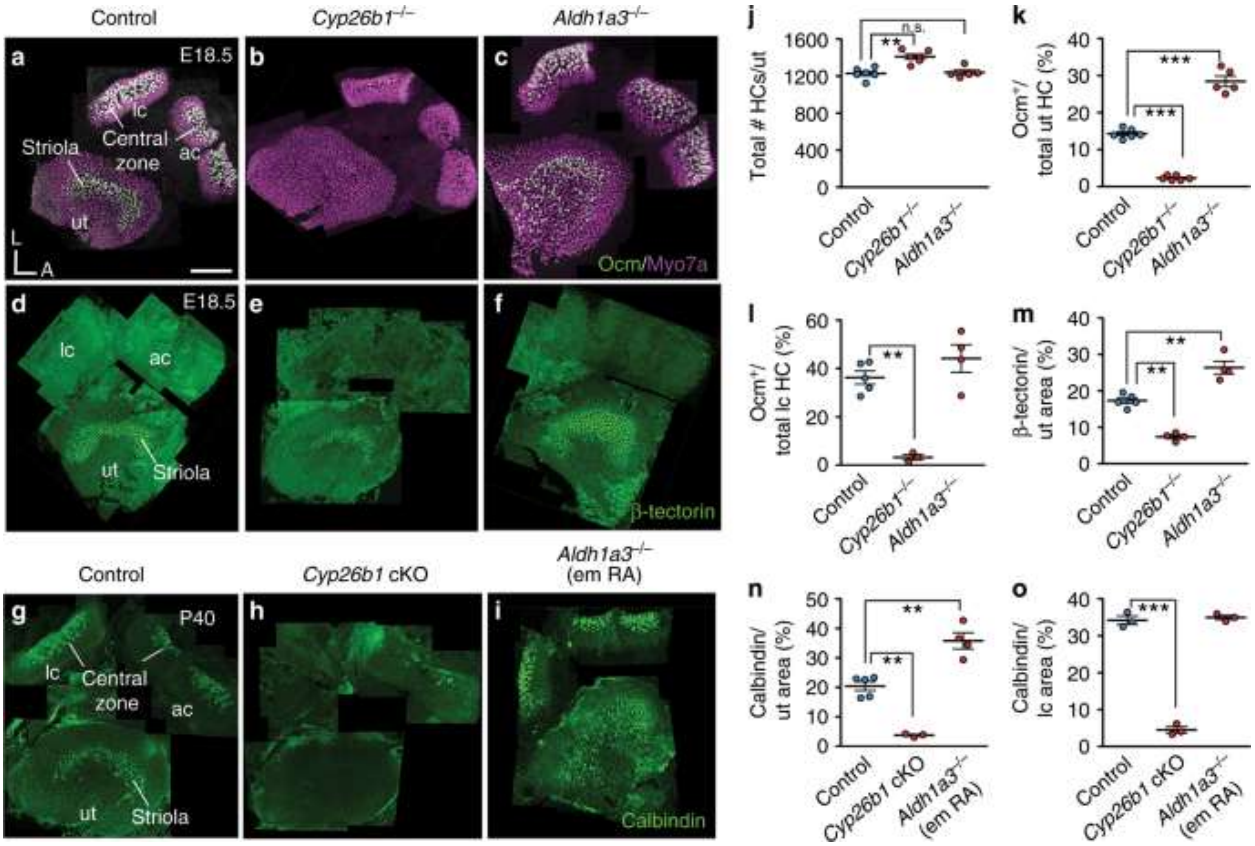

Figure A2. Disruption of RA signaling alters striolar/central zone formation. **(a)** Oncomodulin (Ocm) is expressed in type I HCs in striolar/central zones, whereas all HCs are positive for Myosin7a of controls. (**b**, **c**, **j)** Total HC number is increased in *Cyp26b1*$^{-/-}$ (1394 ± 39, $P = 0.014$, $n = 6$), but unchanged in *Aldh1a3*$^{-/-}$ utricles (1285 ± 28, $P = 0.419$, $n = 5$), compared to controls (1229 ± 30, $n = 6$). (**b**, **c**, **k)** Percentages of Ocm^{+} HCs (14.3 ± 0.5 in controls, $n = 6$) are decreased in *Cyp26b1*$^{-/-}$ (2.3 ± 0.2, $n = 6$, $p < 0.0001$) and increased in *Aldh1a3*$^{-/-}$ utricles (28.4 ± 1.4, $n = 5$, $P < 0.0001$). (**b**, **c**, **l)** Percentages of Ocm^{+} HCs in lateral cristae (lc, 36.2 ± 2.7 in controls, $n = 5$) are reduced in *Cyp26b1*$^{-/-}$ (3.2 ± 1.1, $n = 3$, $P = 0.0005$), but unchanged in *Aldh1a3*$^{-/-}$ mutants (44.1 ± 5.6, $n = 4$, $P = 0.302$). (**d)** Anti-β-tectorin labels SCs in striolas of utricles. (**e**, **f**, **m)** β-tectorin^{+} domain, as % of total utricular macular area (17.4 ± 0.9 in controls, $n = 5$), is reduced in *Cyp26b1*$^{-/-}$ (7.4 ± 0.6, $n = 4$, $P = 0.0002$) and increased in *Aldh1a3*$^{-/-}$ (26.4 ± 1.7, $n = 4$, $P = 0.0003$) utricles. **g** Anti-calbindin labels calyceal nerve endings in striolar/central zones. (**h**, **i**, **n**, **o)** Expression and percentage of calbindin-positive area is reduced in utricles (3.8 ± 0.3, $n = 3$, $P = 0.0005$) and cristae (4.7 ± 1.4, $n = 3$, $P < 0.0001$) of *Cyp26b1* cKO, but increased in utricles (36.0 ± 6.6, $n = 4$, $P = 0.0006$) and unchanged in cristae

(34.4 ± 0.5, $n = 3$, $P = 0.3021$) of *Aldh1a3*$^{-/-}$ (em RA) mutants, compared to respective controls (**n**, 19.7 ± 1.7, $n = 5$; **o**, 34.2 ± 1.1, $n = 3$). Error bars: SEM. Significance was assessed by one-way ANOVA for all panels. A, anterior; L, lateral. $^{**}P < 0.01$ and $^{***}P < 0.001$. n.s., not significant. Scale bar: 200 μm.

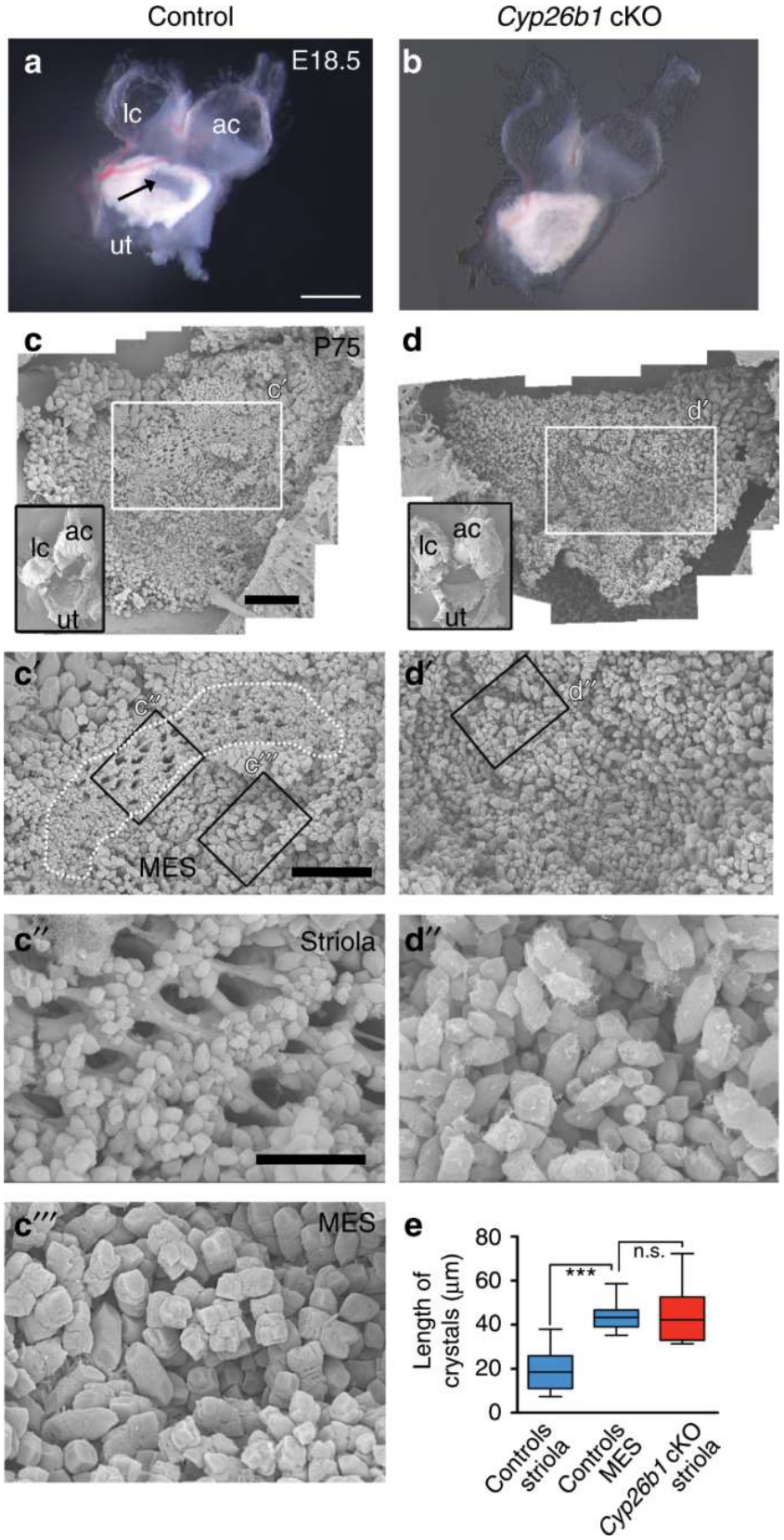
Control
Cyp26b1 cKO
a
E18.5
lc
ac
ut
b
c
P75
c′
lc
ac
ut
d
d′
lc
ac
ut
c′
c″
c‴
MES
d′
d″
c″
Striola
d″
c‴
MES
e
Length of crystals (µm)
80
60
40
20
0
***
n.s.
Controls striola
Controls MES
Cyp26b1 cKO striola

Figure A3. Loss of regional differences in the otoconia of *Cyp26b1* utricles. (a, b) A dissected utricle (ut), anterior (ac), and lateral cristae (lc) of $Foxg1^{Cre};Cyp26b1^{lox/+}$ control (**a**) and *Cyp26b1* cKO (**b**) ears at E18.5. In control utricle, the striola region shows a clearance of the otoconia (arrow in **a**), which is missing in *Cyp26b1* cKO utricles. **c–e** SEM of otoconia in $Foxg1^{Cre};Cyp26b1^{lox/+}$ controls (**c–c‴**) and *Cyp26b1* cKO (**d–d″**) utricles at P75. Insets show low-power views of respective utricles. In controls (**c′**, **c″**, **c‴**), the striolar region (dotted outline) shows otoconia with smaller crystals (**c″**, **e**, 19.7 ± 1.5 μm, $n = 22$ crystals) and perforated holes in the subcupular meshwork layer (**c″**), whereas the medial extrastriolar region (MES) shows larger otoconia (**c‴**, **e**, 40.2 ± 2.2 μm, $n = 23$, $P < 0.0001$). There is no clear regional difference in the size of the otoconia in the *Cyp26b1* cKO mutant utricle (**d**, **d′**), and the otoconia crystals in the presumptive striolar region are larger in size (**d″**, **e**, 42.9 ± 3.1 μm, $n = 21$), comparable to those found in MES of controls (**c‴**, $P = 0.6509$). The one-way ANOVA with multiple comparisons was applied. In the box plots, bounds of box span from 25 to 75% percentile, center line represents the median, and whiskers represent the minimum and maximum of the data points. ***$P < 0.001$. Scale bars: 200 μm for **a**, **b**, 300 μm for **c**, **d**, and **c′**, **d′**, and 100 μm for **c″**, **c‴**, **d″**. n.s., not significant.

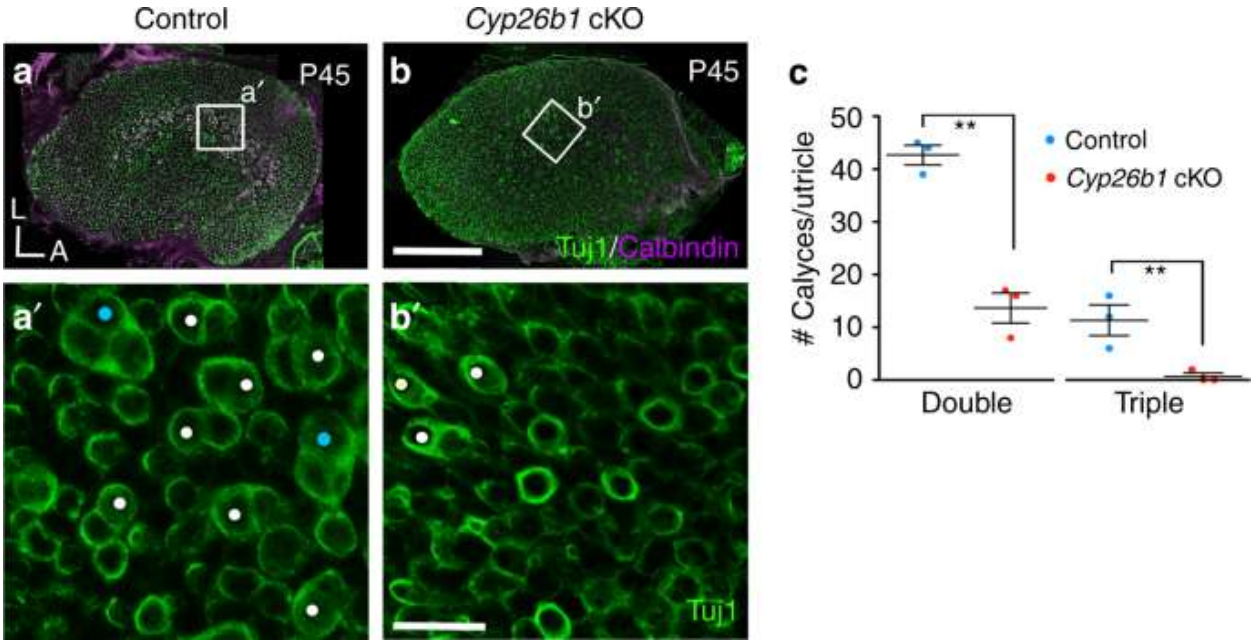

Figure A4. Pure/complex calyces are reduced in *Cyp26b1* cKO mice. (a–c) P45 whole-mount utricles from controls (**a**, **a′**) and *Cyp26b1* cKO (**b**, **b′**) immunolabeled with anti-Tuj1 (green) and anti-calbindin (magenta) antibodies. (**a**, **b)** Maximum intensity projection of the entire utricle. (**a′**, **c)** Enlarged, single plane image of the rectangular region in control striola (**a**), showing the presence of large number of double (white circles, 42.6 ± 1.8 double calyces/utricle) and triple (cyan circles, 10.0 ± 2.0 triple/utricle, $n = 3$ utricles) calyces at the cell body level. (**b′**, **c)** Fewer double calyces (white circles, 13.6 ± 2.8 double calyces/utricle, $P = 0.001$, unpaired t test) and no triple calyx (0.6 ± 0.6 triple calyces/utricle, $P = 0.006$, $n = 3$) are found in the corresponding region of *Cyp26b1* cKO mutants. Scale bars: 200 µm for **a**, **b**; 30 µm for **a′**, **b′**. $^{**}P < 0.01$. A, anterior; L, lateral. Error bars: SEM.

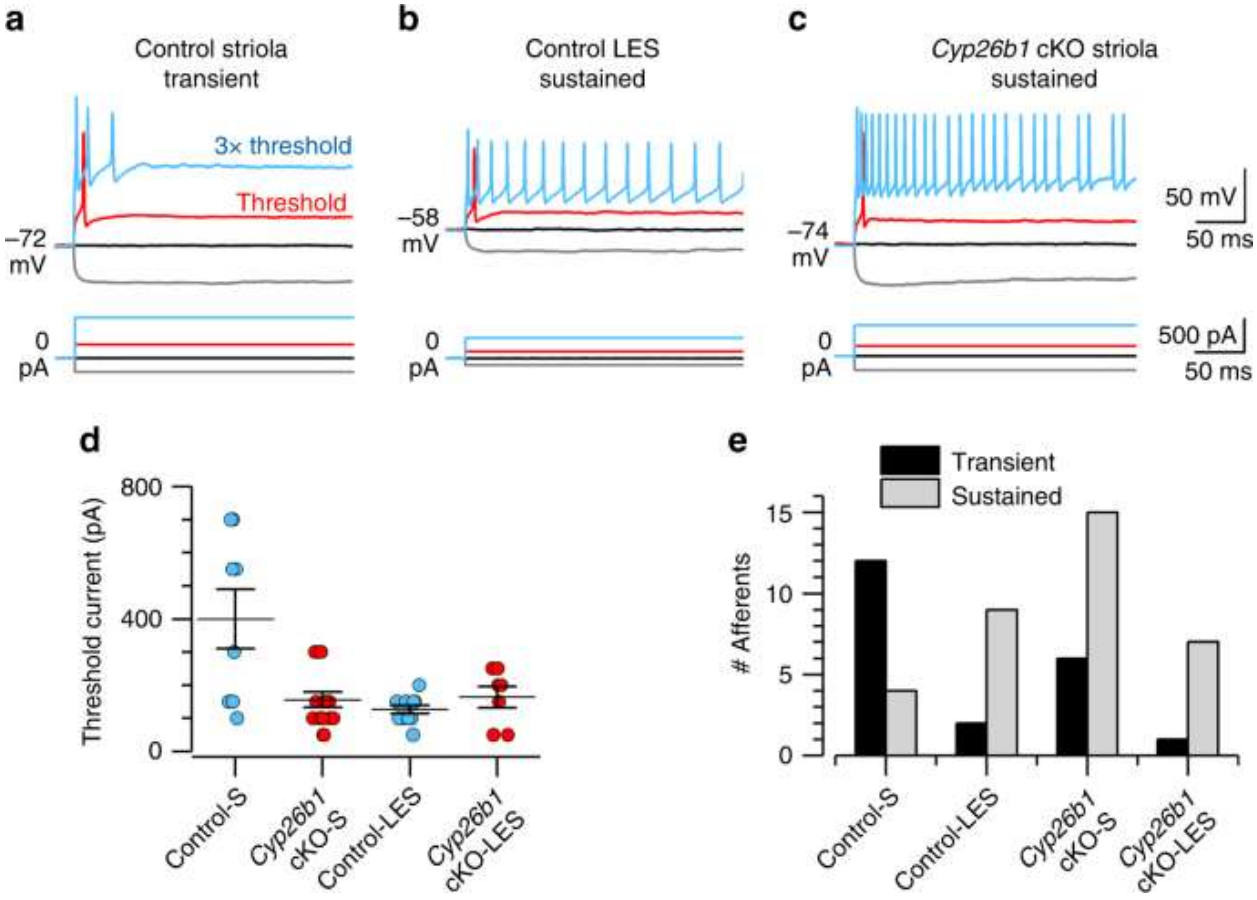

Figure A5. Neural activity in the striola of *Cyp26b1* cKO mice is extrastriolar-like. (a–d) *Cyp26b*1 cKO striolar afferents, like control extrastriolar afferents, were more excitable than control striolar afferents, as shown by their tendency to fire more spikes and by reduced current thresholds for spiking. **(a–c)** Whole-cell current clamp records from patched calyces of a control striolar (Control-S) afferent (**a**), control lateral extrastriolar (Control-LES) afferent (**b**), and

a *Cyp26b1* cKO striolar (*Cyp26b1* cKO-S) afferent (**c**). Five hundred-millisecond current steps were delivered in 50-pA increments from –200 pA to >1 nA relative to zero holding current; a subset is shown including the response at threshold current (red). Three times (3×) threshold current- (blue) evoked transient spiking in the control striolar afferent, but sustained spiking in the control-LES afferent and *Cyp26b1* cKO-S afferent. **(d)** Mean threshold current to activate spikes was significantly higher in Control-S calyces than in all other categories—that is, the *Cyp26b1* cKO-S calyces resembled *Cyp26b1* cKO lateral extrastriolar (*Cyp26b1* cKO-LES) calyces and Control-LES calyces. Two-way ANOVA showed main effects of genotype (control vs. *Cyp26b1* cKO, $F(1,41) = 6.1$, $P = 0.02$), zone (striola vs. LES, $F(1,41) = 10.0$, $P = 0.003$) and their interaction ($F(1,41) = 11.2$, $P = 0.002$). Control-S afferents (400 ± 90 pA, $n = 8$) differed significantly from each other category, including control-LES afferents (127.3 ± 12 pA, $n = 11$; $P = 0.0003$, effect size 1.9) and *Cyp26b1* cKO-S afferents (156.3 ± 23 pA, $n = 16$; $P = 0.0005$, effect size 1.6). *Cyp26b1* cKO-S afferents did not differ from control-LES afferents ($P = 0.94$) or *Cyp26b1* cKO-LES afferents (164 ± 32 pA, $n = 7$, $P > 0.99$). **(e)** Transient firing was more common than sustained firing in Control-S afferents; sustained firing was more common in Control-LES, *Cyp26b1* cKO-S, and *Cyp26b1* cKO-LES afferents. Error bars: SEM.

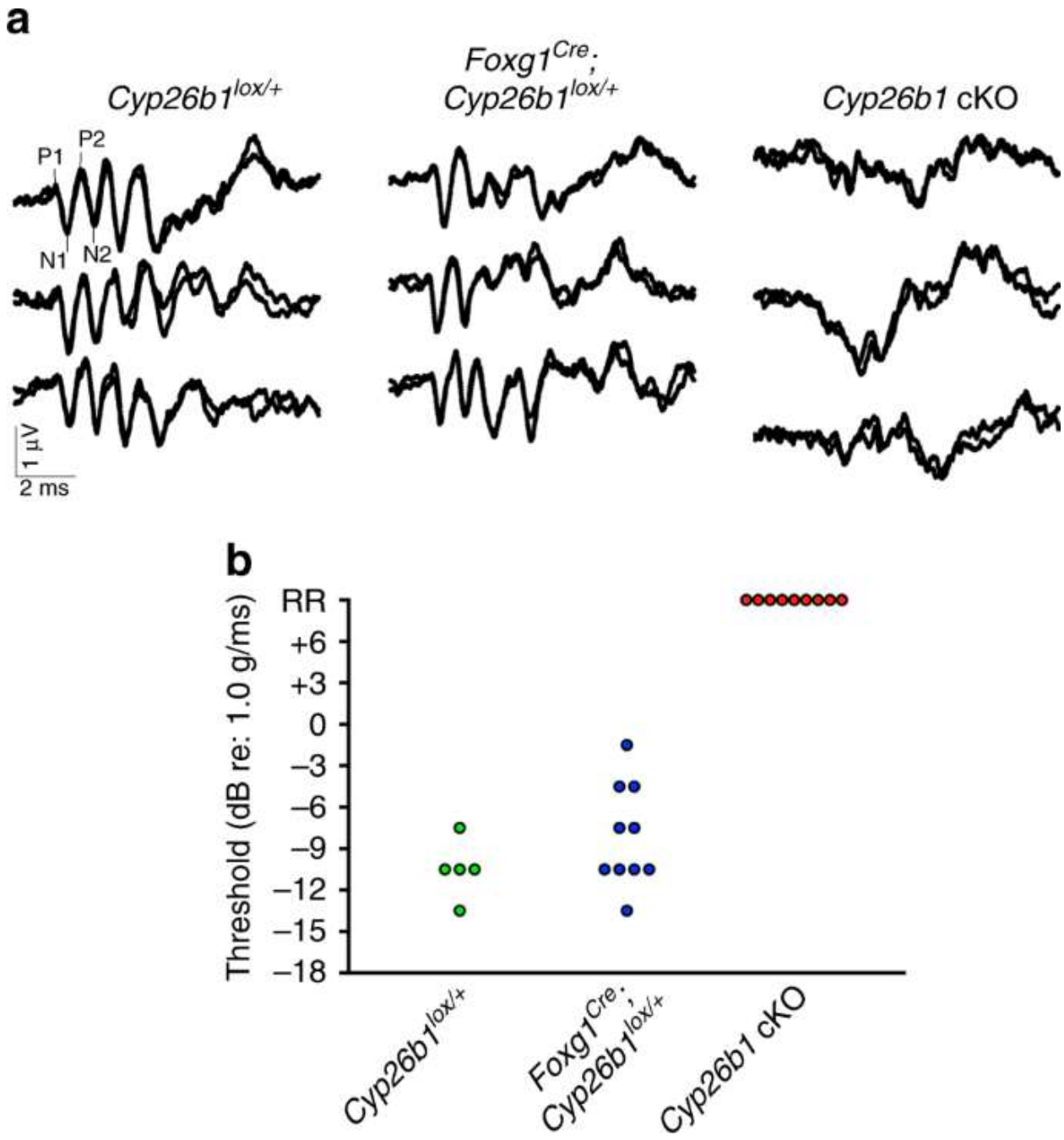

Figure A6. Absence of linear vestibular-evoked potential (VsEP) in *Cyp26b1* cKO mice. **(a)** Three representative VsEP waveforms for each genotype recorded at maximal jerk stimulus (+6 dB). In the *Cyp26b1* cKO mutants, distinct peaks of P1–P2 and N1–N2 are not detectable. **(b)** Summary of thresholds for VsEP determined by various jerk magnitudes. There was no significant difference in VsEP thresholds between the $Cyp26b1^{lox/+}$ (−10.5 ± 1.34 dB re: 1 g/ms, $n = 5$) and $Foxg1^{Cre};Cyp26b1^{lox/+}$ heterozygotes (−8.1 ± 1.17 dB re:

1 g/ms; $n = 10$, $P = 0.1026$, unpaired t test). *Cyp26b1* cKO mutants generated only a remnant response (RR).

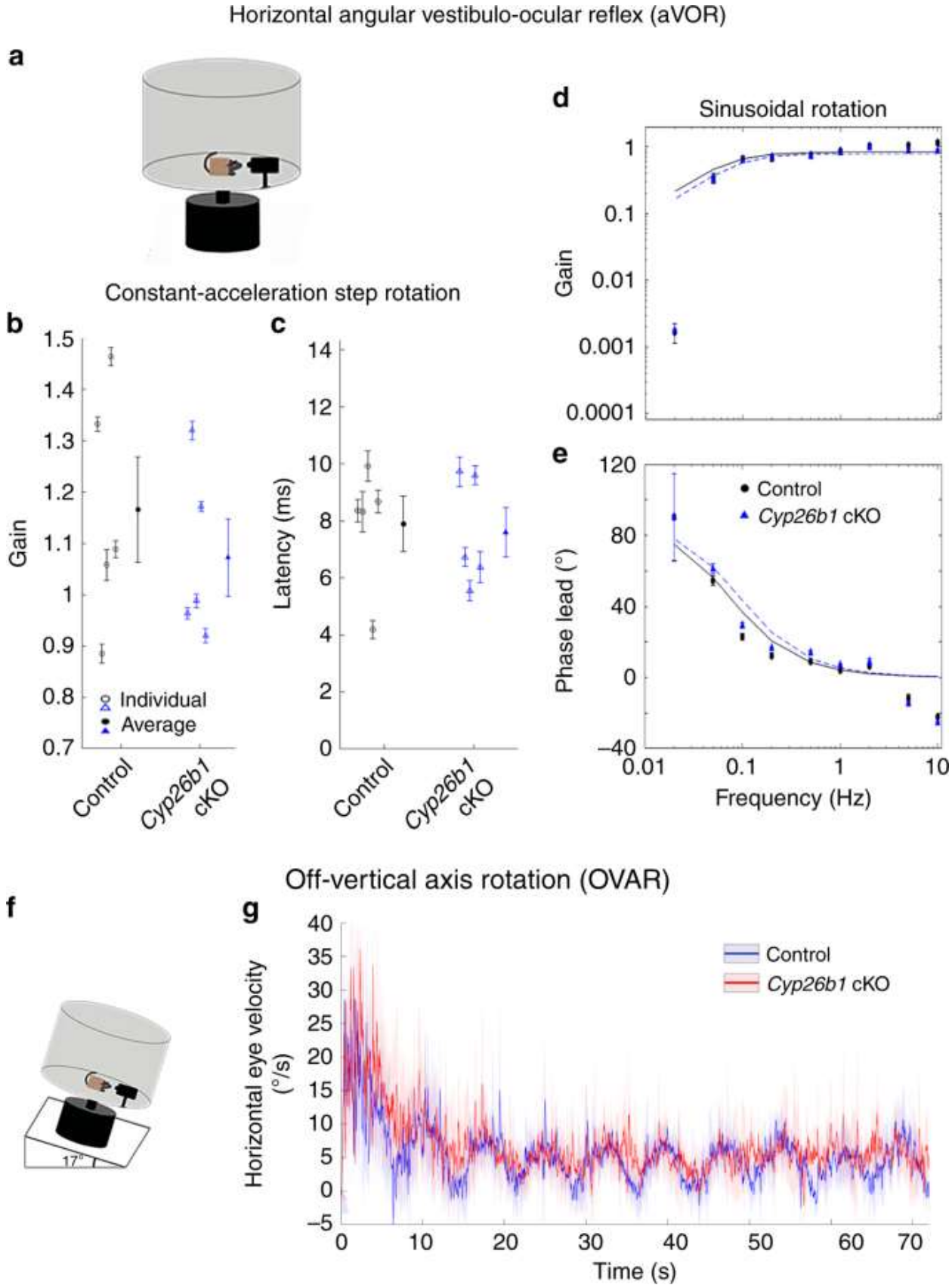
Horizontal angular vestibulo-ocular reflex (aVOR)
a
Constant-acceleration step rotation
b
Gain
Individual
Average
Control
Cyp26b1 cKO
c
Latency (ms)
Control
Cyp26b1 cKO
d
Sinusoidal rotation
Gain
e
Phase lead (°)
Control
Cyp26b1 cKO
Frequency (Hz)
Off-vertical axis rotation (OVAR)
f
17°
g
Horizontal eye velocity (°/s)
Control
Cyp26b1 cKO
Time (s)

Figure A7. Normal aVOR and OVAR responses in *Cyp26b1* cKO mice. (a) Schematic view of aVOR apparatus. Constant-acceleration step gain G_A **(b)** and latency **(c)** for aVOR responses to whole-body, 3000°/s^2 whole-body passive yaw rotations in darkness about an Earth-vertical axis through the head. Open markers denote individual mice; thick markers and lines show mean ± SEM. Gain **(d)** and phase lead **(e)** for yaw slow-phase aVOR responses to 0.02–10 Hz, 100°/s peak velocity sinusoidal, whole-body passive yaw rotations. Solid and dashed lines show first-order high-pass filter model fits to control and *Cyp26b1* cKO mouse population data, respectively. The high variability of phase and 0.02 Hz and relatively poor fit to gain data at 0.02 Hz are due to the small amplitude of responses at that frequency. Differences between control and *Cyp26b1* cKO mice were not significant for G_A, latency, model gain, or model time constant ($P < 0.05$ for all comparisons, Mann–Whitney *U* test). **(f)** Schematic view of apparatus for off-vertical axis rotation (OVAR). Pitch of the table was maintained at 17°. **(g)** No significant difference in the eye velocity was observed between control and *Cyp26b1* cKO mice during transient response (~20 s; amplitude: 43.8 ± 8.3 vs. 38.7 ± 7.4° ($P = 0.66$, unpaired *t* test), time constant: 4.1 ± 1.1 vs. 5.1 ± 2.3 s ($P = 0.68$, unpaired *t* test), when both semicircular canal and otolith organs are stimulated, and steady-state response (~20 s; amplitude: 5.3 ± 0.72 vs. 5.8 ± 0.75° ($P = 0.64$, unpaired *t* test), bias: 10.5 ± 1.3 vs. 8.5 ± 1.3 ($P = 0.33$, unpaired *t* test), time when only responses from otolith organs are expected to be measured.

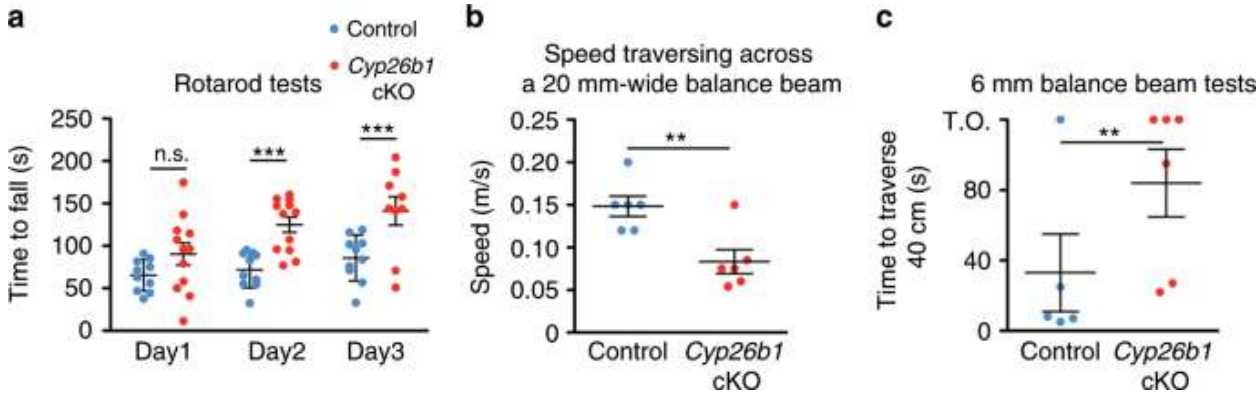

Figure A8. Impaired coordination of *Cyp26b1* cKO mice on balance beam. **(a)** Quantification of rotarod tests. Each mouse was placed on a rotating rod, which accelerated from 5 to 40 r.p.m. over a 5-min period. *Cyp26b1* cKO and $Foxg1^{Cre};Cyp26b1^{lox/+}$ controls exhibited similar motor performance on day 1 of the trial (90.3 ± 15.9 s in mutants, $n = 10$, vs. 65.3 ± 6.5 s in controls, $n = 10$, $P = 0.2573$). *Cyp26b1* cKO mutants were able to stay on rod longer than controls on the second day of testing (123.3 ± 11.0 s mutants vs. 71.7 ± 7.5 s controls, $P = 0.0003$) and third day (141.2 ± 17.8 s mutants vs. 85.7 ± 9.5 s controls, $P = 0.0037$). The two-way ANOVA with multiple comparisons was applied. **(b)** Quantification of speed to traverse 60 cm distance on a 20-mm-wide beam. *Cyp26b1* cKO mutants moved slower (0.083 ± 0.014 m/s, $n = 6$) than controls (0.148 ± 0.011 m/s, $n = 5$, $P = 0.0056$, unpaired *t* test). **(c)** Quantification of time taken to cross 40 cm distance on a 6-mm-wide beam. Half of *Cyp26b1* cKO mutants failed to traverse the beam in 2 min (3/6), whereas most of controls reached the endpoints within 30 s (4/5). By assigning 2 min for all the mice that failed to complete the 40 cm distance, *Cyp26b1* cKO mutants moved slower (taking 84.0 ± 19.24 s to traverse the beam) than controls (33.0 ± 22.04 s for controls, $P = 0.0099$, unpaired *t* test). Error bars: SEM. $^{**}P < 0.01$ and $^{***}P < 0.001$. TO, time out; n.s., not significant.

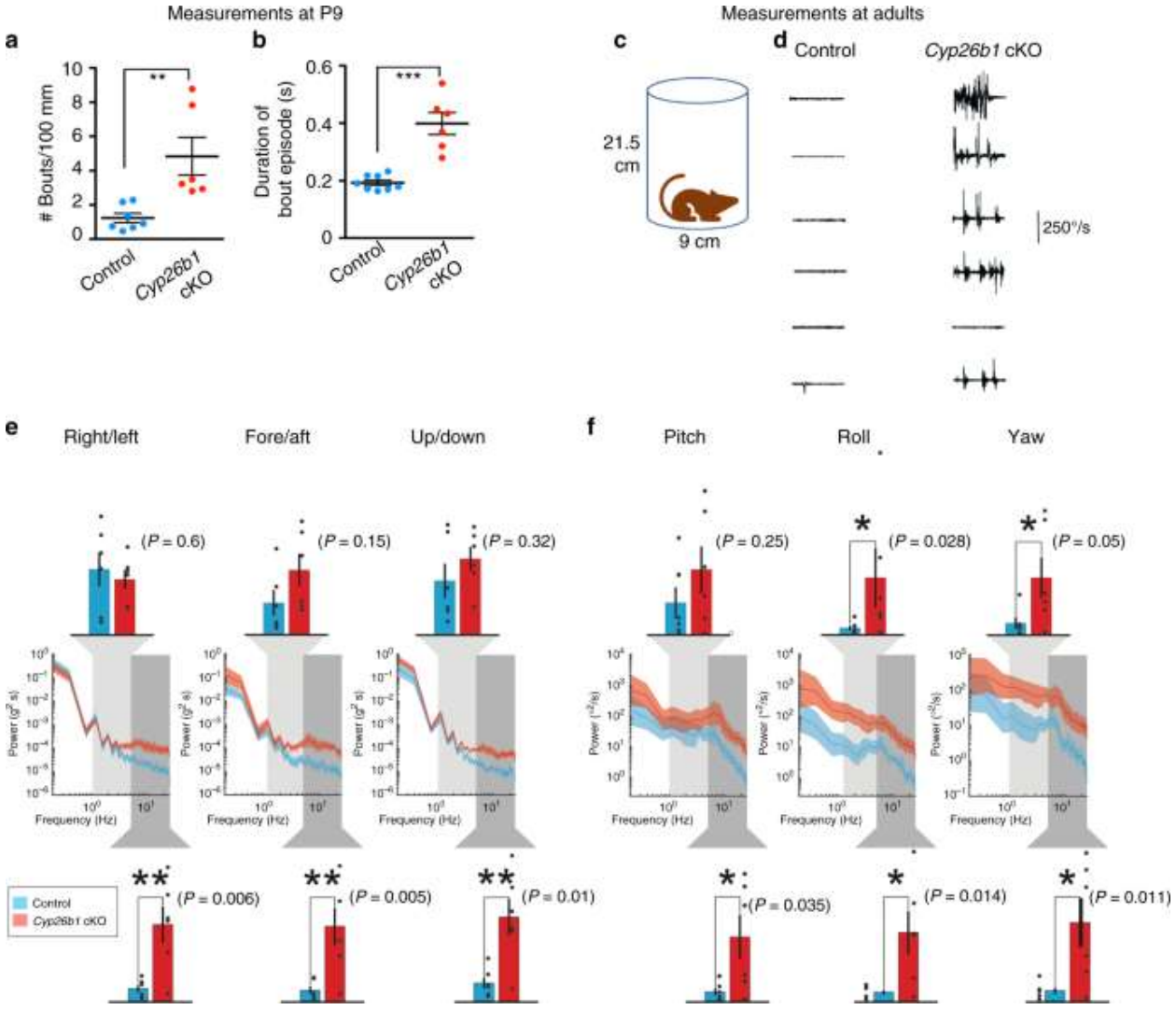

Figure A9. Increased head tremor in *Cyp26b1* cKO mice. (a, b) Quantification of head tremor for P9 pups. The number of bouts normalized over a 100 mm distance traveled **(a)** and average duration of each head-tremor episode over a 10-min period are shown (**b**). *Cyp26b1* cKO pups showed more frequent (**a**, 4.8 ± 1.1 in mutants, $n = 6$, vs. 1.2 ± 0.2 in controls, $n = 8$, $P = 0.0059$) and longer duration (**b**, 398 ± 38 ms in mutants vs. 192 ± 9 ms in controls, $n = 8$, $P < 0.0001$) head tremor, compared to $Foxg1^{Cre};Cyp26b1^{lox/+}$ controls. **c** Schematic of the apparatus for measuring head tremor of an adult mouse at rest with a miniture head motion sensor affixed on the top of the skull. **(d)** *Cyp26b1* cKO showed characteristic head tremor (5/6), which were not present in controls. **(e, f)** Comparison of power spectra density of head movements in translational axes **(e)** and rotational axes **(f)** between controls (blue) and *Cyp26b1* cKO mutants (red). *Cyp26b1* cKO

exhibit siginificantly higher power than controls at high frequencies (5–20 Hz, $P = 0.006$ for right/left, $P = 0.005$ for fore/aft, $P = 0.01$ for up/down, $P = 0.035$ for pitch, $P = 0.014$ for roll, and $P = 0.011$ for yaw axis, $n = 6$/group). Angular head velocity for yaw and roll axes of *Cyp26b1* cKO also had significantly higher power for frequencies between 1 and 5 Hz (upper graphs, $P = 0.05$ for yaw and $P = 0.028$ for roll axis). Unpaired *t* test was applied for all panels. Error bars: SEM. *$P < 0.05$, **$P < 0.01$, and ***$P < 0.001$.

Table 1. Phenotypic summary of *Cyp26b1* cKO and *Aldh1a3* (em RA) KO.

	utricle		saccule		cristae	
	Cyp26b1 cKO	*Aldh1a3* KO	*Cyp26b1* cKO	*Aldh1a3* KO	*Cyp26b1* cKO	*Aldh1a3* KO
Ocm (HC)	↓	↑	↓	↑	↓	no change
β-tectorin (SC)	↓	↑	no change	no change	N/A	N/A
Calbindin (afferent)	↓	↑	↓	N/D	↓	no change

N/D - not determined
N/A - not applicable

References

Ahmed, R. M., Hannigan, I. P., MacDougall, H. G., Chan, R. C. & Halmagyi, G. M. (2012) Gentamicin ototoxicity: a 23-year selected case series of 103 patients. *Med. J. Aust.* 196, 701–704 (2012).

Ahn, S. K., Khalmuratova, R., Jeon, S. Y., Kim, J. P., Park, J. J., Hur, D. G., & Balaban, C. D. (2009). Colocalization of 5-HT1F receptor and calcitonin gene-related peptide in rat vestibular nuclei. *Neuroscience letters*, *465*(2), 151-156.

Alviña, K., & Khodakhah, K. (2010). The therapeutic mode of action of 4-aminopyridine in cerebellar ataxia. *Journal of Neuroscience,* 30(21), 7258–7268.

Anderson, A. D., Troyanovskaya, M., and Wackym, P. A. (1997). Differential expression of α2–7, α9 and β2–4 nicotinic acetylcholine receptor subunit mRNA in the vestibular end-organs and Scarpa's ganglia of the rat. *Brain Res* 778, 409–413. doi:10.1016/s0006-8993(97)01121-9.

Angelaki, D. E. & Cullen, K. E. Vestibular system: the many facets of a multimodal sense. *Annu. Rev. Neurosci.* **31**, 125–150 (2008).

Angelaki, D. E., & Hess, B. J. (1995). Lesion of the nodulus and ventral uvula abolish steady-state off-vertical axis otolith response. *Journal of Neurophysiology*, *73*(4), 1716-1720.

Angelaki, D. E., and Perachio, A. A. (1993). Contribution of irregular semicircular canal afferents to the horizontal vestibuloocular response during constant velocity rotation. *J Neurophysiol* 69, 996–999. doi:10.1152/jn.1993.69.3.996.

Angelaki, D. E., McHenry, M. Q., Dickman, J. D., Newlands, S. D., & Hess, B. J. (1999). Computation of inertial motion: neural strategies to resolve ambiguous otolith information. *Journal of Neuroscience*, *19*(1), 316-327.

Arnold, D. B., Robinson, D. A., & Leigh, R. J. (1999). Nystagmus induced by pharmacological inactivation of the brainstem ocular motor integrator in monkey. *Vision research*, *39*(25), 4286-4295.

Arts, M. P., De Zeeuw, C. I., Lips, J., Rosbak, E., & Simpson, J. I. (2000). Effects of nucleus prepositus hypoglossi lesions on visual climbing fiber activity in the rabbit flocculus. *Journal of Neurophysiology*, *84*(5), 2552–2563.

Ashizawa, T., Öz, G., & Paulson, H. L. (2018). Spinocerebellar ataxias: prospects and challenges for therapy development. *Nature Reviews Neurology*, *14*(10), 590-605.
Baird, R. A., Desmadryl, G., Fernandez, C. & Goldberg, J. M. (1988).The vestibular nerve of the chinchilla. II. Relation between afferent response properties and peripheral innervation patterns in the semicircular canals. *J. Neurophysiol.* 60, 182–203.

Barmack, N. H., & Shojaku, H. (1992). Vestibularly induced slow oscillations in climbing fiber responses of Purkinje cells in the cerebellar nodulus of the rabbit. *Neuroscience*, *50*(1), 1-5.

Barmack, N. H., & Shojaku, H. (1995). Vestibular and visual climbing fiber signals evoked in the uvula-nodulus of the rabbit cerebellum by natural stimulation. *Journal of neurophysiology*, *74*(6), 2573-2589.

Barmack, N. H., & Yakhnitsa, V. (2013). Modulated discharge of Purkinje and stellate cells persists after unilateral loss of vestibular primary afferent mossy fibers in mice. *Journal of neurophysiology*, *110*(10), 2257-2274.

Barry, P. H. (1994). JPCalc, a software package for calculating liquid junction potential corrections in patch-clamp, intracellular, epithelial and bilayer measurements and for correcting junction potential measurements. *J. Neurosci. Methods* 51, 107–116.

Bassett, J. P., & Taube, J. S. (2001). Neural correlates for angular head velocity in the rat dorsal tegmental nucleus. *Journal of Neuroscience*, *21*(15), 5740-5751.

Bassett, J. P., Tullman, M. L., & Taube, J. S. (2007). Lesions of the tegmentomammillary circuit in the head direction system disrupt the head direction signal in the anterior thalamus. *Journal of Neuroscience*, *27*(28), 7564–7577.

Belknap, D. B., & McCrea, R. A. (1988). Anatomical connections of the prepositus and abducens nuclei in the squirrel monkey. *Journal of Comparative Neurology*, *268*(1), 13–28.

Belknap, D. B., & McCrea, R. A. (1988). Anatomical connections of the prepositus and abducens nuclei in the squirrel monkey. *Journal of Comparative Neurology*, *268*(1), 13-28.

Beraneck, M., & Cullen, K. E. (2007). Activity of vestibular nuclei neurons during vestibular and optokinetic stimulation in the alert mouse. *Journal of Neurophysiology*, *98*(3), 1549–1565.

Beraneck, M., Bojados, M., Le Seac'h, A., Jamon, M. & Vidal, P. P. (2012). Ontogeny of mouse vestibulo-ocular reflex following genetic or environmental alteration of gravity sensing. *PLoS ONE* 7, e40414.

Beraneck, M., Idoux, E., Uno, A., Vidal, P.-P., Moore, L. E., and Vibert, N. (2004). Unilateral Labyrinthectomy Modifies the Membrane Properties of Contralesional Vestibular Neurons. *J Neurophysiol* 92, 1668–1684. doi:10.1152/jn.00158.2004.

Beraneck, M., McKee, J. L., Aleisa, M. & Cullen, K. E. (2008) Asymmetric recovery in cerebellar-deficient mice following unilateral labyrinthectomy. *J. Neurophysiol.* 100, 945–958.

Bilotto, G., Goldberg, J. M., Peterson, B. W. & Wilson, V. J. (1982). Dynamic properties of vestibular reflexes in the decerebrate cat. *Exp. Brain Res.* 47, 343–352.

Blair, H. T., Cho, J., & Sharp, P. E. (1999). The anterior thalamic head-direction signal is abolished by bilateral but not unilateral lesions of the lateral mammillary nucleus. *Journal of Neuroscience*, *19*(15), 6673–6683.

Blazquez, P. M., Hirata, Y., Heiney, S. A., Green, A. M., & Highstein, S. M. (2003). Cerebellar signatures of vestibulo-ocular reflex motor learning. *Journal of Neuroscience*, *23*(30), 9742-9751.

Bok, J. et al. (2011). Transient retinoic acid signaling confers anterior-posterior polarity to the inner ear. *Proc. Natl. Acad. Sci. USA* 108, 161–166.

Bosch, M. K., Carrasquillo, Y., Ransdell, J. L., Kanakamedala, A., Ornitz, D. M., & Nerbonne, J. M. (2015). Intracellular FGF14 (iFGF14) is required for spontaneous and evoked firing in cerebellar Purkinje neurons and for motor coordination and balance. *Journal of Neuroscience*, *35*(17), 6752-6769.

Boyle, R., & Highstein, S. M. (1990). Efferent vestibular system in the toadfish: action upon horizontal semicircular canal afferents. *Journal of Neuroscience*, *10*(5), 1570-1582.

Boyle, R., Carey, J. P., & Highstein, S. M. (1991). Morphological correlates of response dynamics and efferent stimulation in horizontal semicircular canal afferents of the toadfish, Opsanus tau. *Journal of neurophysiology*, *66*(5), 1504-1521.

Boyle, R., Rabbitt, R. D., & Highstein, S. M. (2009). Efferent control of hair cell and afferent responses in the semicircular canals. *Journal of neurophysiology*, *102*(3), 1513-1525.

Brodal, P. (1979). The pontocerebellar projection in the rhesus monkey: an experimental study with retrograde axonal transport of horseradish peroxidase. *Neuroscience*, *4*(2), 193-208.

Brooks, J. X., & Cullen, K. E. (2013). The primate cerebellum selectively encodes unexpected self-motion. *Current Biology*, *23*(11), 947-955.

Brown, J. E., Card, J. P., & Yates, B. J. (2005). Polysynaptic pathways from the vestibular nuclei to the lateral mammillary nucleus of the rat: substrates for vestibular input to head direction cells. *Experimental brain research*, *161*(1), 47-61.

Butler, W. N., & Taube, J. S. (2015). The nucleus prepositus hypoglossi contributes to head direction cell stability in rats. *Journal of Neuroscience*, *35*(6), 2547–2558.
Butler, W. N., Smith, K. S., van der Meer, M. A., & Taube, J. S. (2017). The head-direction signal plays a functional role as a neural compass during navigation. *Current Biology*, *27*(9), 1259-1267.

Buttner, N., Geschwind, D., C.jen, J., Pcrlman, S., Pulst, S. M., & Baloh, R. W. (1998). Oculomotor phenotypes in autosomal dominant ataxias. *Archives of Neurology*, 55(10), 1353–1357.

Büttner, U., & Grundei, T. (1995). Gaze-evoked nystagmus and smooth pursuit deficits: their relationship studied in 52 patients. *Journal of neurology*, *242*(6), 384-389.

Buttner, U., Fuchs, A. F., Markert-Schwab, G., & Buckmaster, P. (1991). Fastigial nucleus activity in the alert monkey during slow eye and head movements. *Journal of neurophysiology*, *65*(6), 1360-1371.

Büttner-Ennever, J. A., & Horn, A. K. E. (1996). Pathways from cell groups of the paramedian tracts to the floccular region a. *Annals of the New York Academy of Sciences*, *781*(1), 532-540.

Cannon, S. C., & Robinson, D. A. (1987). Loss of the neural integrator of the oculomotor system from brain stem lesions in monkey. *Journal of Neurophysiology*, *57*(5), 1383–1409.

Cao, Y. Q., & Tsien, R. W. (2005). Effects of familial hemiplegic migraine type 1 mutations on neuronal P/Q-type Ca2+ channel activity and inhibitory synaptic transmission. *Proceedings of the National Academy of Sciences*, *102*(7), 2590-2595.

Carleton, S. C., & Carpenter, M. B. (1983). Afferent and efferent connections of the medial, inferior and lateral vestibular nuclei in the cat and monkey. *Brain Research*, *278*(1–2), 29–51.

Carriot, J., Jamali, M., Chacron, M. J., & Cullen, K. E. (2014). Statistics of the vestibular input experienced during natural self-motion: implications for neural processing. *Journal of Neuroscience*, *34*(24), 8347-8357.

Carriot, J., Jamali, M., Chacron, M. J., & Cullen, K. E. (2017). The statistics of the vestibular input experienced during natural self-motion differ between rodents and primates. *The Journal of physiology*, *595*(8), 2751-2766

Catterall, W. A. (2000). From ionic currents to molecular mechanisms: the structure and function of voltage-gated sodium channels. *Neuron*, *26*(1), 13-25.

Cheron, G., Escudero, M., & Godaux, E. (1996). Discharge properties of brain stem neurons projecting to the flocculus in the alert cat. I. Medical vestibular nucleus. *Journal of Neurophysiology*, *76*(3), 1759-1774.

Cheron, G., Gillis, P., & Godaux, E. (1986). Lesions in the cat prepositus complex: effects on the optokinetic system. *The Journal of Physiology*, *372*(1), 95–111.

Cheron, G., Godaux, E., Laune, J. M., & Vanderkelen, B. (1986). Lesions in the cat prepositus complex: effects on the vestibulo-ocular reflex and saccades. *The Journal of Physiology*, *372*(1), 75–94.

Chi, F. L., Jiao, Y., Liu, H. J., Wang, J., Shi, Y., & Barr, J. J. (2007). Retrograde neuron tracing with microspheres reveals projection of CGRP-immunolabeled vestibular afferent neurons to the vestibular efferent nucleus in the brainstem of rats. *Neuroendocrinology*, *85*(3), 131-138.

Chopra, R., Bushart, D. D., Cooper, J. P., Yellajoshyula, D., Morrison, L. M., Huang, H., ... & Shakkottai, V. G. (2020). Altered Capicua expression drives regional Purkinje neuron vulnerability through ion channel gene dysregulation in spinocerebellar ataxia type 1. *Human molecular genetics*, *29*(19), 3249-3265.

Christova, P., Anderson, J. H., & Gomez, C. M. (2008). Impaired eye movements in presymptomatic spinocerebellar ataxia type 6. *Archives of neurology*, *65*(4), 530-536.

Clark, B. J., & Taube, J. S. (2012). Vestibular and attractor network basis of the head direction cell signal in subcortical circuits. *Frontiers in Neural Circuits*, *6*(FEBRUARY), 1–12.

Clendaniel, R. A., Lasker, D. M., & Minor, L. B. (2001). Horizontal vestibuloocular reflex evoked by high-acceleration rotations in the squirrel monkey. IV. Responses after spectacle-induced adaptation. *Journal of neurophysiology*, *86*(4), 1594-1611.

Clendaniel, R. A., Lasker, D. M., and Minor, L. B. (2002). Differential Adaptation of the Linear and Nonlinear Components of the Horizontal Vestibuloocular Reflex in Squirrel Monkeys. *J Neurophysiol* 88, 3534–3540. doi:10.1152/jn.00404.2002.

Contini, D., Price, S. D. & Art, J. J. (2017). Accumulation of K(+) in the synaptic cleft modulates activity by influencing both vestibular hair cell and calyx afferent in the turtle. *J. Physiol.* 595, 777–803.

Cook, A. A., Fields, E., & Watt, A. J. (2021). Losing the beat: contribution of Purkinje cell firing dysfunction to disease, and its reversal. *Neuroscience*, *462*, 247-261.

Cox, B. C., Liu, Z., Lagarde, M. M. M., & Zuo, J. (2012). Conditional gene expression in the mouse inner ear using Cre-loxP. *Journal of the Association for Research in Otolaryngology*, *13*(3), 295-322.

Cristobal, R., Wackym, P. A., Cioffi, J. A., Erbe, C. B., Roche, J. P., & Popper, P. (2005). Assessment of differential gene expression in vestibular epithelial cell types using microarray analysis. *Molecular brain research*, *133*(1), 19-36.

Cullen, K. E. (2012). The vestibular system: multimodal integration and encoding of self-motion for motor control. *Trends in neurosciences*, *35*(3), 185-196.

Cullen, K. (2016). Visuomotor integration. In *Neuroscience in the 21st Century: From Basic to Clinical, Second Edition* (pp. 961-1005). Springer New York.

Cullen, K. E. (2019). Vestibular processing during natural self-motion: implications for perception and action. *Nat. Rev. Neurosci.* 20, 346–363. doi:10.1038/s41583-019-0153-1.

Cullen, K. E., & Taube, J. S. (2017). Our sense of direction: Progress, controversies and challenges. *Nature Neuroscience*, *20*(11), 1465–1473.

Cullen, K. E., and Horn, M. R. (2011). The neural control of fast vs. slow vergence eye movements. *The European journal of neuroscience* 33, 2147–54. doi:10.1111/j.1460-9568.2011.07692.x.

Cullen, K. E., and Minor, L. B. (2002). Semicircular canal afferents similarly encode active and passive head-on-body rotations: implications for the role of vestibular efference. *The Journal of neuroscience : the official journal of the Society for Neuroscience* 22, RC226.

Cullen, K. E., Chen-Huang, C., & McCrea, R. A. (1993). Firing behavior of brain stem neurons during voluntary cancellation of the horizontal vestibuloocular reflex. II. Eye movement related neurons. *Journal of Neurophysiology*, *70*(2), 844–856.

Cullen, K. E., Rey, C. G., Guitton, D. & Galiana, H. L. (1996). The use of system identification techniques in the analysis of oculomotor burst neuron spike train dynamics. *J. Comput. Neurosci.* 3, 347–368.

Cunningham, T. J. & Duester, G. (2015). Mechanisms of retinoic acid signalling and its roles in organ and limb development. *Nat. Rev. Mol. Cell. Biol.* 16, 110–123.

Curthoys, I. S., MacDougall, H. G., Vidal, P. P. & de Waele, C. (2017). Sustained and transient vestibular systems: a physiological basis for interpreting vestibular function. *Front. Neurol.* 8, 117.

da Silva, S. & Cepko, C. L. (2017). Fgf8 expression and degradation of retinoic acid are required for patterning a high-acuity area in the retina. *Dev. Cell* 42, 68–81 e66 (2017).

Dale, A., & Cullen, K. E. (2013). The nucleus prepositus predominantly outputs eye movement-related information during passive and active self-motion. *Journal of Neurophysiology*, *109*(7), 1900–1911.

De Zeeuw, C. I., Wylie, D. R., Stahl, J. S., & Simpson, J. I. (1995). Phase relations of Purkinje cells in the rabbit flocculus during compensatory eye movements. *Journal of Neurophysiology*, *74*(5), 2051–2064.

Deans, M. R. et al. (2007). Asymmetric distribution of prickle-like 2 reveals an early underlying polarization of vestibular sensory epithelia in the inner ear. *J. Neurosci.* 27, 3139–3147 (2007).

Delgado-García, J. M., Vidal, P. P., Gómez, C., & Berthoz, A. (1989). A neurophysiological study of prepositus hypoglossi neurons projecting to oculomotor and preoculomotor nuclei in the alert cat. *Neuroscience*, *29*(2), 291–307.

Denier, C., Ducros, A., Vahedi, K. A., Joutel, A., Thierry, P., Ritz, A., ... & Tournier–Lasserve, E. (1999). High prevalence of CACNA1A truncations and broader clinical spectrum in episodic ataxia type 2. *Neurology*, *52*(9), 1816-1816.

Desai, S. S., Ali, H. & Lysakowski, A. (2005). Comparative morphology of rodent vestibular periphery. II. Cristae ampullares. *J. Neurophysiol.* 93, 267–280.

Desai, S. S., Zeh, C. & Lysakowski, A. (2005). Comparative morphology of rodent vestibular periphery. I. Saccular and utricular maculae. *J. Neurophysiol.* 93, 251–266.

Di Angelantonio, S., Giniatullin, R., Costa, V., Sokolova, E., & Nistri, A. (2003). Modulation of neuronal nicotinic receptor function by the neuropeptides CGRP and substance P on autonomic nerve cells. *British journal of pharmacology*, *139*(6), 1061-1073.

Dieringer, N. (1987). The role of compensatory eye and head movements for gaze

Dolle, P., Fraulob, V., Kastner, P. & Chambon, P. (1994). Developmental expression of murine retinoid X receptor (RXR) genes. *Mech. Dev.* 45, 91–104.

Du, X., Wang, J., Zhu, H., Rinaldo, L., Lamar, K. M., Palmenberg, A. C., ... & Gomez, C. M. (2013). Second cistron in CACNA1A gene encodes a transcription factor mediating cerebellar development and SCA6. *Cell*, *154*(1), 118-133.

Dubey, A., Rose, R. E., Jones, D. R. & Saint-Jeannet, J. P. (2018). Generating retinoic acid gradients by local degradation during craniofacial development: one cell's cue is another cell's poison. *Genesis* 56.

Ducros, A., Denier, C., Joutel, A., Cecillon, M., Lescoat, C., Vahedi, K., ... & Tournier-Lasserve, E. (2001). The clinical spectrum of familial hemiplegic migraine associated with mutations in a neuronal calcium channel. *New England Journal of Medicine*, *345*(1), 17-24.

Dulon, D., Safieddine, S., Jones, S. M. & Petit, C. (2019). Otoferlin is critical for a highly sensitive and linear calcium-dependent exocytosis at vestibular hair cell ribbon synapses. *J. Neurosci.* 29, 10474–10487.

Dumont, M., Wall, C. E., Botton-Divet, L., Goswami, A., Peigné, S., & Fabre, A. C. (2016). Do functional demands associated with locomotor habitat, diet, and activity pattern drive skull shape evolution in musteloid carnivorans?. *Biological Journal of the Linnean Society*, *117*(4), 858-878.

Dupe, V. et al. (2003). A newborn lethal defect due to inactivation of retinaldegyde dehydrogenase type 3 is prevented by maternal retinoic acid treatment. *Proc. Natl. Acad. Sci. USA* 100, 14036–14041.

Eatock, R. A. & Songer, J. E. (2011). Vestibular hair cells and afferents: two channels for head motion signals. *Annu. Rev. Neurosci.* 34, 501–534.

Eatock, R. A. (2018). Specializations for fast signaling in the amniote vestibular inner ear. *Integr. Comp. Biol.* 58, 341–350.

Elgoyhen, A. B., Johnson, D. S., Boulter, J., Vetter, D. E., and Heinemann, S. (1994). α9: An acetylcholine receptor with novel pharmacological properties expressed in rat cochlear hair cells. *Cell* 79, 705–715. doi:10.1016/0092-8674(94)90555-x.

Elgoyhen, A. B., Vetter, D. E., Katz, E., Rothlin, C. V., Heinemann, S. F., and Boulter, J. (2001). α10: A determinant of nicotinic cholinergic receptor function in mammalian vestibular and cochlear mechanosensory hair cells. *Proc National Acad Sci* 98, 3501–3506. doi:10.1073/pnas.051622798.

Eron, J. N., Davidovics, N., and Santina, C. C. D. (2015). Contribution of vestibular efferent system alpha-9 nicotinic receptors to vestibulo-oculomotor interaction and short-term vestibular compensation after unilateral labyrinthectomy in mice. *Neurosci Lett* 602, 156–161. doi:10.1016/j.neulet.2015.06.060.

Escudero, M., Cheron, G., & Godaux, E. (1996). Discharge properties of brain stem neurons projecting to the flocculus in the alert cat. II. Prepositus hypoglossal nucleus. *Journal of Neurophysiology*, *76*(3), 1775–1785.

Fernandez, C. & Goldberg, J. M. (1976). Physiology of peripheral neurons innervating otolith organs of the squirrel monkey. I. Response to static tilts and to long-duration centrifugal force. *J. Neurophysiol.* 39, 970–984.

Fernandez, C., Baird, R. A. & Goldberg, J. M. (1988). The vestibular nerve of the chinchilla. I. Peripheral innervation patterns in the horizontal and superior semicircular canals. *J. Neurophysiol.* 60, 167–181.

Fernandez, C., Goldberg, J. M. & Baird, R. A. (1990). The vestibular nerve of the chinchilla III. Peripheral innervation patterns in the utricular macula. *J. Neurophysiol.* 63, 767–780.

Fernández, C., Lysakowski, A. N. N. A., & Goldberg, J. M. (1995). Hair-cell counts and afferent innervation patterns in the cristae ampullares of the squirrel monkey with a comparison to the chinchilla. *Journal of neurophysiology*, *73*(3), 1253-1269.

Fletcher, C. F., Lutz, C. M., O'Sullivan, T. N., Shaughnessy Jr, J. D., Hawkes, R., Frankel, W. N., ... & Jenkins, N. A. (1996). Absence epilepsy in tottering mutant mice is associated with calcium channel defects. *Cell*, *87*(4), 607-617.
Fletcher, G. F., Balady, G., Blair, S. N., Blumenthal, J., Caspersen, C., Chaitman, B., ... & Pollock, M. L. (1996). Statement on exercise: benefits and recommendations for physical activity programs for all Americans: a statement for health professionals by the Committee on Exercise and Cardiac Rehabilitation of the Council on Clinical Cardiology, American Heart Association. *Circulation*, *94*(4), 857-862.

Forge, A., Taylor, R. R., Dawson, S. J., Lovett, M. & Jagger, D. J. (2017).Disruption of SorCS2 reveals differences in the regulation of stereociliary bundle formation between hair cell types in the inner ear. *PLoS Genet.* 13, e1006692.

Frens, M. A., Mathoera, A. L., & van der Steen, J. (2001). Floccular complex spike response to transparent retinal slip. *Neuron*, *30*(3), 795-801.

Fuchs, A. F., Robinson, F. R., & Straube, A. N. D. R. E. A. S. (1993). Role of the caudal fastigial nucleus in saccade generation. I. Neuronal discharge pattern. *Journal of neurophysiology*, *70*(5), 1723-1740.

Fushiki, H., & Barmack, N. H. (1997). Topography and reciprocal activity of cerebellar Purkinje cells in the uvula-nodulus modulated by vestibular stimulation. *Journal of Neurophysiology*, *78*(6), 3083-3094.

Fyhn, M., Molden, S., Witter, M. P., Moser, E. I., & Moser, M. B. (2004). Spatial representation in the entorhinal cortex. *Science*, *305*(5688), 1258–1264.

Gacek, R. R. (1960). Efferent component of the vestibular nerve. In *Neural mechanisms of the auditory and vestibular systems* (pp. 276-284). Springfield, Ill.: Thomas.

Gan, S. R., Wang, J., Figueroa, K. P., Pulst, S. M., Tomishon, D., Lee, D., ... & Kuo, S. H. (2017). Postural tremor and ataxia progression in spinocerebellar ataxias. *Tremor and Other Hyperkinetic Movements*, *7*.

Gardner, E. P., & Fuchs, A. F. (1975). Single-unit responses to natural vestibular stimuli and eye movements in deep cerebellar nuclei of the alert rhesus monkey. *Journal of neurophysiology*, *38*(3), 627-649.

Ghelarducci, B., Ito, M., & Yagi, N. (1975). Impulse discharge from flocculus Purkinje cells of alert rabbits during visual stimulation combined with horizontal head rotation. *Brain research*, *87*(1), 66-72.

Gioanni, H. (1988). Stabilizing gaze reflexes in the pigeon (Columba livia). *Experimental Brain Research*, *69*(3), 567-582.

Giordano, I., Bogdanow, M., Jacobi, H., Jahn, K., Minnerop, M., Schoels, L., ... & Klockgether, T. (2013). Experience in a short-term trial with 4-aminopyridine in cerebellar ataxia. *Journal of neurology*, *260*(8), 2175-2176.
Godaux, E., Mettens, P., & Chéron, G. (1993). Differential effect of injections of kainic acid into the prepositus and the vestibular nuclei of the cat. *The Journal of physiology*, *472*(1), 459-482.

Goldberg, J. M. & Cullen, K. E. (2011). Vestibular control of the head: possible functions of the vestibulocollic reflex. *Exp. Brain Res.* 210, 331–345.

Goldberg, J. M. & Fernandez, C. (1977). Conduction times and background discharge of vestibular afferents. *Brain Res.* 122, 545–550.

Goldberg, J. M. & Fernandez, C. (1971). Physiology of peripheral neurons innervating semicircular canals of the squirrel monkey. III. Variations among units in their discharge properties. *J. Neurophysiol.* 34, 676–684.

Goldberg, J. M. (2000). Afferent diversity and the organization of central vestibular pathways. *Exp Brain Res* 130, 277–297. doi:10.1007/s002210050033.

Goldberg, J. M., & Cullen, K. E. (2011). Vestibular control of the head: possible functions of the vestibulocollic reflex. *Experimental brain research*, *210*(3), 331-345.

Goldberg, J. M., and Fernandez, C. (1980). Efferent vestibular system in the squirrel monkey: anatomical location and influence on afferent activity. J Neurophysiol 43, 986–1025. doi:10.1152/jn.1980.43.4.986

Goldberg, J. M., Desmadryl, G., Baird, R. A. & Fernandez, C. (1990).The vestibular nerve of the chinchilla. V. Relation between afferent discharge properties and peripheral innervation patterns in the utricular macula. *J. Neurophysiol.* 63, 791–804.

Goldberg, J. M., Highstein, S. M., Moschovakis, A. K., and Fernandez, C. (1987). Inputs from regularly and irregularly discharging vestibular nerve afferents to secondary neurons in the vestibular nuclei of the squirrel monkey. I. An electrophysiological analysis. *J Neurophysiol* 58, 700–718. doi:10.1152/jn.1987.58.4.700.

Goldberg, J. M., Wilson, V. J., Cullen, K. E., Angelaki, D. E., Broussard, D. M., Buttner-Ennever, J., ... & Minor, L. B. (2012). *The vestibular system: a sixth sense*. Oxford University Press.

Goldberg, J., & Peterson, B. W. (1986). Reflex and mechanical contributions to head stabilization in alert cats. *Journal of neurophysiology*, *56*(3), 857-875.

Gomez, C. M., Thompson, R. M., Gammack, J. T., Perlman, S. L., Dobyns, W. B., Truwit, C. L., ... & Anderson, J. H. (1997). Spinocerebellar ataxia type 6: gaze-evoked and vertical nystagmus, Purkinje cell degeneration, and variable age of onset. *Annals of Neurology:*

Official Journal of the American Neurological Association and the Child Neurology Society, *42*(6), 933-950.

Gomez-Casati, M. E. et al. (2010). Nonneuronal cells regulate synapse formation in the vestibular sensory epithelium via erbB-dependent BDNF expression. *Proc. Natl. Acad. Sci. USA* 107, 17005–17010.

Goodridge, J. P., & Taube, J. S. (1995). Preferential Use of the Landmark Navigational System by Head Direction Cells in Rats. *Behavioral Neuroscience*, *109*(1), 49–61.

Graf, W. E. R. N. E. R., Simpson, J. I., & Leonard, C. S. (1988). Spatial organization of visual messages of the rabbit's cerebellar flocculus. II. Complex and simple spike responses of Purkinje cells. *Journal of Neurophysiology*, *60*(6), 2091-2121.

Gruart, A., & Delgado-Garcia, J. M. (1994). Signalling properties of identified deep cerebellar nuclear neurons related to eye and head movements in the alert cat. *The Journal of Physiology*, *478*(1), 37-54.

Hafting, T., Fyhn, M., Molden, S., Moser, M. B., & Moser, E. I. (2005). Microstructure of a spatial map in the entorhinal cortex. *Nature*, *436*(7052), 801–806.

Handler, H. P., Man, L. J., Dansithong, W., Scoles, D. R., Pulst, S. M., Orr, H. T., & Shakkottai, V. G. (2020). Altered Capicua expression drives regional Purkinje neuron vulnerability through ion channel gene dysregulation in spinocerebellar ataxia type 1. *Human Molecular Genetics*, 29(19), 3249–3265.

Haque, A., & Dickman, J. D. (2005). Vestibular gaze stabilization: different behavioral strategies for arboreal and terrestrial avians. *Journal of neurophysiology*, *93*(3), 1165-1173.

Hardisty-Hughes, R. E., Parker, A., and Brown, S. D. M. (2010). A hearing and vestibular phenotyping pipeline to identify mouse mutants with hearing impairment. *Nat. Protoc.* 5, 177–190. doi:10.1038/nprot.2009.204.

Hayakawa, T., & Zyo, K. (1985). Afferent connections of gudden's tegmental nuclei in the rabbit. *Journal of Comparative Neurology*, *235*(2), 169–181.

Hebert, J. M. & McConnell, S. K. (2000). Targeting of cre to the Foxg1 (BF-1) locus mediates loxP recombination in the telencephalon and other developing head structures. *Dev. Biol.* 222, 296–306.

Hiel, H., Elgoyhen, A. B., Drescher, D. G., and Morley, B. J. (1996). Expression of nicotinic acetylcholine receptor mRNA in the adult rat peripheral vestibular system. *Brain Res* 738, 347–352. doi:10.1016/s0006-8993(96)01046-3.

Highstein, S. M. (1991). The central nervous system efferent control of the organs of balance and equilibrium. *Neuroscience research*, *12*(1), 13-30.

Highstein, S. M., & Baker, R. (1985). Action of the efferent vestibular system on primary afferents in the toadfish, Opsanus tau. *Journal of neurophysiology*, *54*(2), 370-384.

Highstein, S. M., Goldberg, J. M., Moschovakis, A. K., & Fernandez, C. (1987). Inputs from regularly and irregularly discharging vestibular nerve afferents to secondary neurons in the vestibular nuclei of the squirrel monkey. II. Correlation with output pathways of secondary neurons. *Journal of neurophysiology*, *58*(4), 719-738.

Hillman, D., Chen, S., Aung, T. T., Cherksey, B., Sugimori, M., & Llinas, R. R. (1991). Localization of P-type calcium channels in the central nervous system. *Proceedings of the National Academy of Sciences*, *88*(16), 7076-7080.

Holt, G. R., & Douglas, J. (2022). Comparison of Discharge Variability Visual Cortex Neurons In Vitro and In Vivo in Cat. *Journal of Neurophysiology*, 75(5).

Holt, J. C., Lysakowski, A., & Goldberg, J. M. (2011). The efferent vestibular system. *Auditory and vestibular efferents*, 135-186..

Holt, J. C., Lysakowski, A., and Goldberg, J. M. (2010). Auditory and Vestibular Efferents. Spr Hdb Aud, 135–186. doi:10.1007/978-1-4419-7070-1_6.

Hourez, R., Servais, L., Orduz, D., Gall, D., Millard, I., de Kerchove d'Exaerde, A., ... & Schiffmann, S. N. (2011). Aminopyridines correct early dysfunction and delay neurodegeneration in a mouse model of spinocerebellar ataxia type 1. *Journal of Neuroscience*, *31*(33), 11795-11807.

Hübner, P. P., Khan, S. I., and Migliaccio, A. A. (2015). The mammalian efferent vestibular system plays a crucial role in the high-frequency response and short-term adaptation of the vestibuloocular reflex. *Journal of neurophysiology* 114, 3154–65. doi:10.1152/jn.00307.2015.

Hübner, P. P., Khan, S. I., and Migliaccio, A. A. (2017). The mammalian efferent vestibular system plays a crucial role in vestibulo-ocular reflex compensation after unilateral labyrinthectomy. *J Neurophysiol* 117, 1553–1568.

Huh, Y. E., Kim, J. S., Kim, H. J., Park, S. H., Jeon, B. S., Kim, J. M., ... & Zee, D. S. (2015). Vestibular performance during high-acceleration stimuli correlates with clinical decline in SCA6. *The Cerebellum*, *14*(3), 284-291.

Hullar, T. E. et al. (2005). Responses of irregularly discharging chinchilla semicircular canal vestibular-nerve afferents during high-frequency head rotations. *J. Neurophysiol.* 93, 2777–2786.

Hurlock, E. C., McMahon, A., & Joho, R. H. (2008). Purkinje-cell-restricted restoration of Kv3. 3 function restores complex spikes and rescues motor coordination in Kcnc3 mutants. *Journal of Neuroscience*, *28*(18), 4640-4648.

Huterer, M. & Cullen, K. E. (2002).Vestibuloocular reflex dynamics during high-frequency and high-acceleration rotations of the head on body in rhesus monkey. *J. Neurophysiol.* 88, 13–28 .

Im, G. J. (2012). Role of Nicotinic Acetylcholine Receptor on Efferent Inhibition in Cochlear Hair Cell. *Korean J Audiology* 16, 108–113. doi:10.7874/kja.2012.16.3.108.

Indriati, D. W., Kamasawa, N., Matsui, K., Meredith, A. L., Watanabe, M., & Shigemoto, R. (2013). Quantitative localization of Cav2. 1 (P/Q-type) voltage-dependent calcium channels in Purkinje cells: somatodendritic gradient and distinct somatic coclustering with calcium-activated potassium channels. *Journal of Neuroscience*, *33*(8), 3668-3678.

Ishikawa, K., Watanabe, M., Yoshizawa, K., Fujita, T., Iwamoto, H., Yoshizawa, T., ... & Mizusawa, H. (1999). Clinical, neuropathological, and molecular study in two families with spinocerebellar ataxia type 6 (SCA6). *Journal of Neurology, Neurosurgery & Psychiatry*, *67*(1), 86-89.

Ito, M. (1972). Cerebellar control of the vestibular neurones: physiology and pharmacology. *Progress in brain research*, *37*, 377-390.

Iwasaki, H., Kani, K., & Maeda, T. (1999). Neural connections of the pontine reticularformation, which connects reciprocally with the nucleus prepositus hypoglossi in the rat. *Neuroscience*, *93*(1), 195–208.

Iwasaki, S., Chihara, Y., Komuta, Y., Ito, K. & Sahara, Y. (2008). Low-voltage-activated potassium channels underlie the regulation of intrinsic firing properties of rat vestibular ganglion cells. *J. Neurophysiol.* 100, 2192–2204.

Jamali, M., Carriot, J., Chacron, M. J., and Cullen, K. E. (2019). Coding strategies in the otolith system differ for translational head motion vs static orientation relative to gravity. Elife 8, e45573. doi:10.7554/elife.45573.

Jamali, M., Chacron, M. J., and Cullen, K. E. (2016). Self-motion evokes precise spike timing in the primate vestibular system. Nature communications 7, 13229. doi:10.1038/ncomms13229.

Jamali, M., Sadeghi, S. G., and Cullen, K. E. (2009). Response of vestibular nerve afferents innervating utricle and saccule during passive and active translations. *Journal of neurophysiology* 101, 141–9. doi:10.1152/jn.91066.2008.

Jayabal, S., Chang, H. H. V., Cullen, K. E., & Watt, A. J. (2016). 4-aminopyridine reverses ataxia and cerebellar firing deficiency in a mouse model of spinocerebellar ataxia type 6. *Scientific reports*, *6*(1), 1-12.

Jayabal, S., Ljungberg, L., Erwes, T., Cormier, A., Quilez, S., El Jaouhari, S., & Watt, A. J. (2015). Rapid onset of motor deficits in a mouse model of spinocerebellar ataxia type 6 precedes late cerebellar degeneration. *Eneuro*, *2*(6).

Jiang, T., Kindt, K. & Wu, D. K. (2017). Transcription factor Emx2 controls stereociliary bundle orientation of sensory hair cells. *Elife* 6.

Jones, S. M., Erway, L. C., Johnson, K. R., Yu, H. & Jones, T. A. (2004). Gravity receptor function in mice with graded otoconial deficiencies. *Hear Res.* 191, 34–40.

Jones, T. A. et al. (2011). The adequate stimulus for mammalian linear vestibular evoked potentials (VsEPs). *Hear Res.* 280, 133–140.

Jones, T. A., Lee, C., Gaines, G. C. & Grant, J. W. (2015). On the high frequency transfer of mechanical stimuli from the surface of the head to the macular neuroepithelium of the mouse. *J. Assoc. Res. Otolaryngol.* 16, 189–204.

Jordan, P. M., Parks, X. X., Contini, D., & Holt, J. C. (2013). A review of synaptic mechanisms of vestibular efferent signaling in turtles: extrapolation to efferent actions in mammals. *Journal of Vestibular Research*, *23*(3), 161-175.

Jorratt, P., Delano, P. H., Delgado, C., Dagnino-Subiabre, A., and Terreros, G. (2017). Difference in perseverative errors during a visual attention task with auditory distractors in alpha-9 nicotinic receptor subunit wild type and knock-out mice. Front. Cell. Neurosci. 11, 1–9. doi:10.3389/fncel.2017.00357.

Jun, K., Piedras-Rentería, E. S., Smith, S. M., Wheeler, D. B., Lee, S. B., Lee, T. G., ... & Shin, H. S. (1999). Ablation of P/Q-type Ca2+ channel currents, altered synaptic transmission, and progressive ataxia in mice lacking the α1A-subunit. *Proceedings of the National Academy of Sciences*, *96*(26), 15245-15250.

K., Gehring, K., Mckinney, R. A., Shoubridge, E. A., Mcpherson, P. S., Durham, H. D., & Brais, B. (2015). Sacs knockout mice present pathophysiological defects underlying autosomal recessive spastic ataxia of charlevoix-saguenay. *Human Molecular Genetics*, 24(3), 727–739.

Kahlon, M., & Lisberger, S. G. (2000). Changes in the responses of Purkinje cells in the floccular complex of monkeys after motor learning in smooth pursuit eye movements. *Journal of neurophysiology*, *84*(6), 2945-2960.

Kalluri, R., Xue, J. & Eatock, R. A. (2010). Ion channels set spike timing regularity of mammalian vestibular afferent neurons. *J. Neurophysiol.* 104, 2034–2051.

Kaneko, C. R. (1997). Eye movement deficits after ibotenic acid lesions of the nucleus prepositus hypoglossi in monkeys. I. Saccades and fixation. *Journal of neurophysiology*, *78*(4), 1753-1768.

Kaneko, C. R. S. (1999). Eye movement deficits following ibotenic acid lesions of the nucleus prepositus hypoglossi in monkeys II. Pursuit, vestibular, and optokinetic responses. *Journal of Neurophysiology*, *81*(2), 668–681.

Kasumu, A., & Bezprozvanny, I. (2012). Deranged calcium signaling in Purkinje cells and pathogenesis in spinocerebellar ataxia 2 (SCA2) and other ataxias. *The Cerebellum*, *11*(3), 630-639.

Katoh, A., Jindal, J. A., & Raymond, J. L. (2007). Motor deficits in homozygous and heterozygous p/q-type calcium channel mutants. *Journal of neurophysiology*.

Kim, K. S., Minor, L. B., Della Santina, C. C. & Lasker, D. M. (2011). Variation in response dynamics of regular and irregular vestibular-nerve afferents during sinusoidal head rotations and currents in the chinchilla. *Exp. Brain Res.* 210, 643–649.

Klockgether, T., Mariotti, C., & Paulson, H. L. (2019). Spinocerebellar ataxia. *Nature reviews Disease primers*, *5*(1), 1-21. Chopra, R., Bushart, D. D., Cooper, J. P.,

Knierim, J. J., & Zhang, K. (2012). Attractor dynamics of spatially correlated neural activity in the limbic system. *Annual Review of Neuroscience*, *35*, 267–285.

Koeppen, A. H. (2005). The pathogenesis of spinocerebellar ataxia. *Cerebellum*, 4(1), 62–73.

Kong, J., Adelman, J. P., and Fuchs, P. A. (2008). Expression of the SK2 calcium-activated potassium channel is required for cholinergic function in mouse cochlear hair cells. *J Physiology* 586, 5471–5485. doi:10.1113/jphysiol.2008.160077.

Korte, G. E., & Mugnaini, E. (1979). The cerebellar projection of the vestibular nerve in the cat. *Journal of Comparative Neurology*, *184*(2), 265-277.

Kulik, Á., Nakadate, K., Hagiwara, A., Fukazawa, Y., Luján, R., Saito, H., ... & Shigemoto, R. (2004). Immunocytochemical localization of the α1A subunit of the P/Q-type calcium channel in the rat cerebellum. *European Journal of Neuroscience*, *19*(8), 2169-2178.

Langer, T., Fuchs, A. F., Scudder, C. A., & Chubb, M. C. (1985). Afferents to the flocculus of the cerebellum in the rhesus macaque as revealed by retrograde transport of horseradish peroxidase. *Journal of Comparative Neurology*, *235*(1), 1-25.

Langer, T., Kaneko, C. R. S., Scudder, C. A., & Fuchs, A. F. (1986). Afferents to the abducens nucleus in the monkey and cat. *Journal of Comparative Neurology*, *245*(3), 379–400.

Lariviere, R., Gaudet, R., Gentil, B. J., Girard, M., Conte, T. C., Minotti, S., ... & Brais, B. (2015). Sacs knockout mice present pathophysiological defects underlying autosomal recessive spastic ataxia of Charlevoix-Saguenay. *Human molecular genetics*, *24*(3), 727-739.

Lasker, D. M., Backous, D. D., Lysakowski, A., Davis, G. L., and Minor, L. B. (1999). Horizontal Vestibuloocular Reflex Evoked by High-Acceleration Rotations in the Squirrel Monkey. II. Responses After Canal Plugging. *J Neurophysiol* 82, 1271–1285. doi:10.1152/jn.1999.82.3.1271.

Lasker, D. M., Hullar, T. E., and Minor, L. B. (2000). Horizontal Vestibuloocular Reflex Evoked by High-Acceleration Rotations in the Squirrel Monkey. III. Responses After Labyrinthectomy. *J Neurophysiol* 83, 2482–2496. doi:10.1152/jn.2000.83.5.2482.

Lee, C., Holt, J. C. & Jones, T. A. (2017). Effect of M-current modulation on mammalian vestibular responses to transient head motion. *J. Neurophysiol.* 118, 2991–3006.

Lemos, J., & Manto, M. (2022). Pharmacotherapy of cerebellar and vestibular disorders. *Current Opinion in Neurology*, 35(1), 118–125.

Leonard, R. B. & Kevetter, G. A. (2002). Molecular probes of the vestibular nerve I. Peripheral termination patterns of calretinin. *Brain Res.* 928, 8–17.

Li, A., Xue, J. & Peterson, E. H. (2008). Architecture of the mouse utricle: macular organization and hair bundle heights. *J. Neurophysiol.* 99, 718–733.

Lim, D. J. (1984). Otoconia in health and disease. A review. *Ann. Otol. Rhinol. Laryngol. Suppl*. 112, 17–24.

Lindeman, H. H. (2009). Regional differences in sensitivity of the vestibular sensory epithelia to ototoxic antibiotics. *Acta Oto-Laryngol.* 67, 177–189.

Lisberger, S. G., Miles, F. A., & Zee, D. S. (1984). Signals used to compute errors in monkey vestibuloocular reflex: possible role of flocculus. *Journal of neurophysiology*, *52*(6), 1140-1153.

Lisberger, S. G., Pavelko, T. A., & Broussard, D. M. (1994). Responses during eye movements of brain stem neurons that receive monosynaptic inhibition from the flocculus and ventral paraflocculus in monkeys. *Journal of Neurophysiology*, *72*(2), 909-927.

Liu, R., Chang, L., & Wickern, G. (1984). The dorsal tegmental nucleus: an axoplasmic transport study. *Brain Research*, *310*(1), 123–132.

Lopez-Barneo, J., Darlot, C., Berthoz, A., & Baker, R. (1982). Neuronal activity in prepositus nucleus correlated with eye movement in the alert cat. *Journal of Neurophysiology*, *47*(2), 329–352.

Lorente de Nó, R. (1933). Studies on the struture of the cerebral cortex I: The area entorhinalis. *J. Psychol. Neurol.(Leipzig)*, *45*, 381-438.

Luebke, A. E., Holt, J. C., Jordan, P. M., Wong, Y. S., Caldwell, J. S., & Cullen, K. E. (2014). Loss of α-calcitonin gene-related peptide (αCGRP) reduces the efficacy of the vestibulo-ocular reflex (VOR). *Journal of Neuroscience*, *34*(31), 10453–10458.

Luebke, A. E., Maroni, P. D., Guth, S. M., and Lysakowski, A. (2005). Alpha-9 nicotinic acetylcholine receptor immunoreactivity in the rodent vestibular labyrinth. *J Comp Neurol* 492, 323–333. doi:10.1002/cne.20739.

Lukas, C., Schöls, L., Bellenberg, B., Rüb, U., Przuntek, H., Schmid, G., ... & Suchan, B. (2006). Dissociation of grey and white matter reduction in spinocerebellar ataxia type 3 and 6: a voxel-based morphometry study. *Neuroscience letters*, *408*(3), 230-235.

Luong, T. N., Carlisle, H. J., Southwell, A. & Patterson, P. H.(2011). Assessment of motor balance and coordination in mice using the balance beam. *J. Vis. Exp.* https://doi.org/10.3791/2376.

Lykhmus, O., Voytenko, L. P., Lips, K. S., Bergen, I., Krasteva-Christ, G., Vetter, D. E., et al. (2017). Nicotinic Acetylcholine Receptor α9 and α10 Subunits Are Expressed in the Brain of Mice. *Front Cell Neurosci* 11, 282. doi:10.3389/fncel.2017.00282.

Lysakowski, A., & Goldberg, J. M. (2004). Morphophysiology of the vestibular periphery. In *The vestibular system* (pp. 57-152). Springer, New York, NY.

Lysakowski, A. et al. (2011). Molecular microdomains in a sensory terminal, the vestibular calyx ending. *J. Neurosci.* 31, 10101–10114 (2011).

Lysakowski, A., Minor, L. B., Fernandez, C. & Goldberg, J. M. (1995). Physiological identification of morphologically distinct afferent classes innervating the cristae ampullares of the squirrel monkey. *J. Neurophysiol.* 73, 1270–1281.

Mackrous, I., Carriot, J., Jamali, M., and Cullen, K. E. (2019). Cerebellar Prediction of the Dynamic Sensory Consequences of Gravity. *Curr Biol*. doi:10.1016/j.cub.2019.07.006.

Maekawa, K. Y. O. J. I., & Simpson, J. L. (1973). Climbing fiber responses evoked in vestibulocerebellum of rabbit from visual system. *Journal of Neurophysiology*, *36*(4), 649-666.

Maklad, A., & Fritzsch, B. (2003). Partial segregation of posterior crista and saccular fibers to the nodulus and uvula of the cerebellum in mice, and its development. *Developmental brain research*, *140*(2), 223-236.

Manzoni, D., Andre, P., & Pompeiano, O. (2004). Proprioceptive neck influences modify the information about tilt direction coded by the cerebellar anterior vermis. *Acta oto-laryngologica*, *124*(4), 475-480.

Manzoni, D., Pompeiano, O., & Andre, P. (1998). Neck influences on the spatial properties of vestibulospinal reflexes in decerebrate cats: role of the cerebellar anterior vermis. *Journal of Vestibular Research*, *8*(4), 283-297.

Manzoni, D., Pompeiano, O., Bruschini, L., & Andre, P. (1999). Neck input modifies the reference frame for coding labyrinthine signals in the cerebellar vermis: a cellular analysis. *Neuroscience*, *93*(3), 1095-1107.

Marini, G., Provini, L., & Rosina, A. (1976). Gravity responses of Purkinje cells in the nodulus. *Experimental Brain Research*, *24*(3), 311-323.

Mark, M. D., Krause, M., Boele, H. J., Kruse, W., Pollok, S., Kuner, T., ... & Herlitze, S. (2015). Spinocerebellar ataxia type 6 protein aggregates cause deficits in motor learning and cerebellar plasticity. *Journal of Neuroscience*, *35*(23), 8882-8895.

Marlinski, V., & McCrea, R. A. (2009). Self-motion signals in vestibular nuclei neurons projecting to the thalamus in the alert squirrel monkey. *Journal of neurophysiology*, *101*(4), 1730-1741.

Marlinski, V., Plotnik, M., & Goldberg, J. M. (2004). Efferent actions in the chinchilla vestibular labyrinth. *Journal of the Association for Research in Otolaryngology*, *5*(2), 126-143.

Marlinski, V., Plotnik, M., and Goldberg, J. M. (2004). Efferent Actions in the Chinchilla Vestibular Labyrinth. J Assoc Res Otolaryngology 5, 126–143. doi:10.1007/s10162-003-4029-7.

Mathews, M. A., Camp, A. J., & Murray, A. J. (2017). Reviewing the role of the efferent vestibular system in motor and vestibular circuits. *Frontiers in physiology*, *8*, 552.

Matsushita, K., Wakamori, M., Arii, T., Oda, S. I., Mori, Y., & Imoto, K. (2002). Bidirectional Alterations in Cerebellar Synaptic Transmission oftottering and rollingCa2+ Channel Mutant Mice. *Journal of Neuroscience*, *22*(11), 4388-4398.

McCrea, R. A., & Baker, R. (1985). Anatomical connections of the nucleus prepositus of the cat. *Journal of Comparative Neurology*, *237*(3), 377–407.

McCrea, R. A., & Horn, A. K. (2006). Nucleus prepositus. *Progress in brain research*, *151*, 205-230.

McCue, M. P. & Guinand, J. J. (1994). Acoustically responsive fibers in the vestibular nerve of the cat. *J. Neurosci.* 14, 6058–6070 (1994).

Mccue, M. P., & Guinan, J. J. (1994). Influence of efferent stimulation on acoustically responsive vestibular afferents in the cat. *Journal of Neuroscience*, *14*(10), 6071-6083.

McFarland, J. L., & Fuchs, A. F. (1992). Discharge patterns in nucleus prepositus hypoglossi and adjacent medial vestibular nucleus during horizontal eye movement in behaving macaques. *Journal of Neurophysiology*, *68*(1), 319–332.

McInturff, S., Burns, J. C. & Kelley, M. W. (2018). Characterization of spatial and temporal development of type I and type II hair cells in the mouse utricle using new cell-type-specific markers. *Biol. Open* 7.

McKinney, R. A., & Watt, A. J. (2021). Molecular Identity and Location Influence Purkinje Cell Vulnerability in Autosomal-Recessive Spastic Ataxia of Charlevoix-Saguenay Mice. *Frontiers in Cellular Neuroscience*, 15(December), 1–15.

Mehlman, M. L., Marcroft, J. L., & Taube, J. S. (2021). Anatomical projections to the dorsal tegmental nucleus and abducens nucleus arise from separate cell populations in the nucleus prepositus hypoglossi, but overlapping cell populations in the medial vestibular nucleus. *Journal of Comparative Neurology*, *529*(10), 2706–2726.

Meng, H., May, P. J., Dickman, J. D., & Angelaki, D. E. (2007). Vestibular signals in primate thalamus: properties and origins. *Journal of Neuroscience*, *27*(50), 13590-13602.

Meredith, F. L. & Rennie, K. J. (2016). Channeling your inner ear potassium: K(+) channels in vestibular hair cells. *Hear Res* 338, 40–51.

Mettens, P., Godaux, E., Chéron, G., & Galiana, H. L. (1994). Effect of muscimol microinjections into the prepositus hypoglossi and the medial vestibular nuclei on cat eye movements. *Journal of neurophysiology*, *72*(2), 785-802.

Migliaccio, A. A., Macdougall, H. G., Minor, L. B. & Della Santina, C. C. (2005). Inexpensive system for real-time 3-dimensional video-oculography using a fluorescent marker array. *J. Neurosci. Methods* 143, 141–150.

Miles, F. A., & Braitman, D. J. (1980). Long-term adaptive changes in primate vestibuloocular reflex. II. Electrophysiological observations on semicircular canal primary afferents. *Journal of neurophysiology*, *43*(5), 1426-1436.

Miles, F. A., & Lisberger, S. G. (1981). Plasticity in the vestibulo-ocular reflex: a new hypothesis. *Annual review of neuroscience*, *4*(1), 273-299.

Miles, F. A., Fuller, J. H., Braitman, D. J., & Dow, B. M. (1980). Long-term adaptive changes in primate vestibuloocular reflex. III. Electrophysiological observations in flocculus of normal monkeys. *Journal of Neurophysiology*, *43*(5), 1437-1476.

Miller, R. J. (1992). Voltage-sensitive Ca2+ channels. *The Journal of biological chemistry (Print)*, *267*(3), 1403-1406.

Minor, L. B., and Goldberg, J. M. (1991). Vestibular-nerve inputs to the vestibulo-ocular reflex: a functional-ablation study in the squirrel monkey. *J Neurosci*, *11*, 1636-1648.

Mintz, I. M., Adams, M. E., & Bean, B. P. (1992). P-type calcium channels in rat central and peripheral neurons. *Neuron*, *9*(1), 85-95.

Mintz, I. M., Venema, V. J., Swiderek, K. M., Lee, T. D., Bean, B. P., & Adams, M. E. (1992). P-type calcium channels blocked by the spider toxin ω-Aga-IVA. *Nature*, *355*(6363), 827-829.

Mitchell, J. F., & Leopold, D. A. (2015). The marmoset monkey as a model for visual neuroscience. *Neuroscience research*, *93*, 20-46.

Mock, B., Jones, T. A. & Jones, S. M. (2011). Gravity receptor aging in the CBA/CaJ strain: a comparioson to auditory aging. *JARO* 12.

Molotkov, A., Molotkova, N. & Duester, G. (2006). Retinoic acid guides eye morphogenetic movements via paracrine signaling but is unnecessary for retinal dorsoventral patterning. *Development* 133, 1901–1910.

Money, K. E., Landolt, J. P., Correia, M. J., & Laufer, J. (1974). Anatomical and physiological investigations of the vestibular system of birds. *Brain, Behavior and Evolution*, *10*(1-3), 212-227.

Mori, Y., Friedrich, T., Kim, M. S., Mikami, A., Nakai, J., Ruth, P., ... & Numa, S. (1991). Primary structure and functional expression from complementary DNA of a brain calcium channel. *Nature*, *350*(6317), 398-402.

Mori, Y., Wakamori, M., Oda, S. I., Fletcher, C. F., Sekiguchi, N., Mori, E., ... & Imoto, K. (2000). Reduced Voltage Sensitivity of Activation of P/Q-Type Ca2+ Channels is Associated with the Ataxic Mouse MutationRolling Nagoya (tgrol). *Journal of Neuroscience*, *20*(15), 5654-5662.

Morley B.J., Whiteaker, P., Elgoyhen, A.B. (2018).Commentary: Nicotinic Acetylcholine Receptor α9 and α10 Subunits Are Expressed in the Brain of Mice. (2018). *Front Cell Neurosci*, 2, 104. doi: 10.3389/fncel.2018.00104.

Morley, B. J., Dolan, D. F., Ohlemiller, K. K., & Simmons, D. D. (2017). Generation and Characterization of α9 and α10 Nicotinic Acetylcholine Receptor Subunit Knockout Mice on a C57BL/6J Background. *Front Neurosci*, *11*, 516. doi:10.3389/fnins.2017.00516.

Morsli, H., Choo, D., Ryan, A., Johnson, R. & Wu, D. K. (1998). Development of the mouse inner ear and origin of its sensory organs. *J. Neurosci.* 18, 3327–3335.

Murata, Y., Kawakami, H., Yamaguchi, S., Nishimura, M., Kohriyama, T., Ishizaki, F., ... & Nakamura, S. (1998). Characteristic magnetic resonance imaging findings in spinocerebellar ataxia 6. *Archives of neurology*, *55*(10), 1348-1352.

Mustari, M. J., Fuchs, A. F., Langer, T. P., Kaneko, C., & Wallman, J. (1988). The role of the primate lateral terminal nucleus in visuomotor behavior. *Progress in brain research*, *75*, 121-128.

Nagao, S. (1992). Different roles of flocculus and ventral paraflocculus for oculomotor control in the primate. *Neuroreport*, *3*(1), 13-16.

Nagao, S., & Kitazawa, H. (2003). Effects of reversible shutdown of the monkey flocculus on the retention of adaptation of the horizontal vestibulo-ocular reflex. *Neuroscience*, *118*(2), 563-570.Oman, C. M., Marcus, E. N., & Curthoys, I. S. (1987).

Nakamura, S. (1998). Characteristic magnetic resonance imaging findings in spinocerebellar ataxia 6. *Archives of neurology*, *55*(10), 1348-1352.

O'Keefe, J. (1976). Place units in the hippocampus of the freely moving rat. *Experimental Neurology*, *51*(1), 78–109.

O'Keefe, J., & Dostrovsky, J. (1971). The hippocampus as a spatial map: Preliminary evidence from unit activity in the freely-moving rat. In *Brain Research* (Vol. 34, pp. 171–175). Elsevier Science.

Ohno, K., Takeda, N., Tanaka-tsuji, M., & Matsunaga, T. (1993). Calcitonin gene-related peptide in the efferent system of the inner ear: a review. *Acta Oto-Laryngologica*, *113*(sup501), 16-20.

Oman, C. M., Marcus, E. N., & Curthoys, I. S. (1987). The influence of semicircular canal morphology on endolymph flow dynamics: An anatomically descriptive mathematical model. *Acta oto-laryngologica*, *103*(1-2), 1-13.

Ono, K., Keller, J., López Ramírez, O., González Garrido, A., Zobeiri, O. A., Chang, H. H. V., et al. (2020). Retinoic acid degradation shapes zonal development of vestibular organs and sensitivity to transient linear accelerations. *Nat. Commun.* 11, 1–15. doi:10.1038/s41467-019-13710-4.

Ophoff, R. A., Terwindt, G. M., Vergouwe, M. N., Van Eijk, R., Oefner, P. J., Hoffman, S. M., ... & Frants, R. R. (1996). Familial hemiplegic migraine and episodic ataxia type-2 are caused by mutations in the Ca2+ channel gene CACNL1A4. *Cell*, *87*(3), 543-552.

Osanai, R., Nagao, S., Kitamura, T., Kawabata, I., & Yamada, J. (1999). Differences in mossy and climbing afferent sources between flocculus and ventral and dorsal paraflocculus in the rat. *Experimental Brain Research*, *124*(2), 248-264.

Pachitariu, M., Steinmetz, N., Kadir, S., Carandini, M., & Harris, K. (2016). Fast and accurate spike sorting of high-channel count probes with KiloSort. *Advances in Neural Information Processing Systems*, *Nips*, 4455–4463.

Paige, G. D. (1983). Vestibuloocular reflex and its interactions with visual following mechanisms in the squirrel monkey. II. Response characteristics and plasticity following unilateral inactivation of horizontal canal. *J. Neurophysiol.* 49, 152–168.

Paige, G. D., & Seidman, S. H. (1999). Characteristics of the VOR in response to linear acceleration. *Annals of the New York Academy of Sciences*, *871*(1), 123-135.

Parks, X. X., Contini, D., Jordan, P. M., & Holt, J. C. (2017). Confirming a role for α9nAChRs and SK potassium channels in type II hair cells of the turtle posterior crista. *Frontiers in Cellular Neuroscience*, *11*, 356.

Perkins, E. M., Clarkson, Y. L., Sabatier, N., Longhurst, D. M., Millward, C. P., Jack, J., ... & Jackson, M. (2010). Loss of β-III spectrin leads to Purkinje cell dysfunction recapitulating the behavior and neuropathology of spinocerebellar ataxia type 5 in humans. *Journal of Neuroscience*, *30*(14), 4857-4867.

Pietrobon, D. (2002). Calcium channels and channelopathies of the central nervous system. *Molecular neurobiology*, *25*(1), 31-50.

Polman, C. H., Bertelsmann, F. W., de Waal, R., van Diemen, H. A., Uitdehaag, B. M., van Loenen, A. C., & Koetsier, J. C. (1994). 4-Aminopyridine is superior to 3, 4-diaminopyridine in the treatment of patients with multiple sclerosis. *Archives of neurology*, *51*(11), 1136-1139.

Poppi, L. A., Holt, J. C., Lim, R., & Brichta, A. M. (2020). A review of efferent cholinergic synaptic transmission in the vestibular periphery and its functional implications. *Journal of Neurophysiology*, *123*(2), 608-629.

Precht, W., Simpson, J. I., & Llinás, R. (1976). Responses of Purkinje cells in rabbit nodulus and uvula to natural vestibular and visual stimuli. *Pflügers Archiv*, *367*(1), 1-6.

Rabbath, G., Necchi, D., De Waele, C., Gasc, J. P., Josset, P., and Vidal, P. P. (2001). Abnormal vestibular control of gaze and posture in a strain of a waltzing rat. *Exp. Brain Res.* 136, 211–223. doi:10.1007/s002210000568.

Rabbitt, R. D., Boyle, R., & Highstein, S. M. (2010). Mechanical amplification by hair cells in the semicircular canals. *Proceedings of the National Academy of Sciences*, *107*(8), 3864-3869.

Rabbitt, R. D., Damiano, E. R., & Grant, J. W. (2004). Biomechanics of the semicircular canals and otolith organs. In *The vestibular system* (pp. 153-201). Springer, New York, NY.

Raman, I. M., & Bean, B. P. (1999). Ionic currents underlying spontaneous action potentials in isolated cerebellar Purkinje neurons. *Journal of Neuroscience*, *19*(5), 1663-1674.

Ranck, J. B. (1985). Head direction cells in the deep cell layer of dorsolateral pre-subiculum in freely moving rats. *Electrical activity of the archicortex*. Barmack, N. H.,

Fagerson, M., & Errico, P. (1993). Cholinergic projection to the dorsal cap of the inferior olive of the rat, rabbit, and monkey. *Journal of Comparative Neurology*, *328*(2), 263–281.

Rau, A., Legan, P. K. & Richardson, G. P. (1999). Tectorin mRNA expression is spatially and temporally restricted during mouse inner ear development. *J. Comp. Neurol.* 405, 271–280.

Raymond, J. L., Lisberger, S. G., & Mauk, M. D. (1996). The cerebellum: a neuronal learning machine?. *Science*, *272*(5265), 1126-1131.

Redish, A. D., Elga, A. N., & Touretzky, D. S. (1996). A coupled attractor model of the rodent Head Direction system. *Network: Computation in Neural Systems*, *7*(4), 671–685.

Restituito, S., Thompson, R. M., Eliet, J., Raike, R. S., Riedl, M., Charnet, P., & Gomez, C. M. (2000). The polyglutamine expansion in spinocerebellar ataxia type 6 causes a β subunit-specific enhanced activation of P/Q-type calcium channels in Xenopus oocytes. *Journal of Neuroscience*, *20*(17), 6394-6403.

Rhinn, M. & Dolle, P. (2012). Retinoic acid signalling during development. *Development* 139, 843–858.

Robinson, D. A. (1970). Oculomotor unit behavior in the monkey. *Journal of neurophysiology*, *33*(3), 393-403.

Robinson, D. A. (1976). Adaptive gain control of vestibuloocular reflex by the cerebellum. *Journal of neurophysiology*, *39*(5), 954-969.

Robinson, F. R., Phillips, J. O., & Fuchs, A. F. (1994). Coordination of gaze shifts in primates: Brainstem inputs to neck and extraocular motoneuron pools. *Journal of Comparative Neurology*, *346*(1), 43–62.

Rochester, L., Galna, B., Lord, S., Mhiripiri, D., Eglon, G., & Chinnery, P. F. (2014). Gait impairment precedes clinical symptoms in spinocerebellar ataxia type 6. *Movement Disorders*, *29*(2), 252-255.

Rolfs, A., Koeppen, A. H., Bauer, I., Bauer, P., Buhlmann, S., Topka, H., Schöls, L., & Riess, O. (2003). Clinical features and neuropathology of autosomal dominant spinocerebellar ataxia (SCA17). *Annals of Neurology*, 54(3), 367–375.

Romand, R. et al. (2006). Dynamic expression of retinoic acid-synthesizing and -metabolizing enzymes in the developing mouse inner ear. *J. Comp. Neurol.* 496, 643–654.

Romand, R. et al. (2013). Retinoic acid deficiency impairs the vestibular function. *J. Neurosci.* 33, 5856–5866.

Romand, R. et al. (2002). The retinoic acid receptors RARa and RARg are required for inner ear development. *Mech. Dev.* 119, 213–223.

Ross, S. A., McCaffery, P. J., Drager, U. C. & De Luca, L. M. (2000). Retinoids in embryonal development. *Physiol. Rev*. 80.

Rüsch, A. & Eatock, R. A. (1996). A delayed rectifier conductance in type I hair cells of the mouse utricle. *J. Neurophysiol.* 76.

Sadeghi, S. G., Goldberg, J. M., Minor, L. B., & Cullen, K. E. (2009). Efferent-mediated responses in vestibular nerve afferents of the alert macaque. *Journal of neurophysiology*, *101*(2), 988-1001.

Sadeghi, S. G., Goldberg, J. M., Minor, L. B., and Cullen, K. E. (2009). Effects of canal plugging on the vestibuloocular reflex and vestibular nerve discharge during passive and active head rotations. *Journal of neurophysiology* 102, 2693–703. doi:10.1152/jn.00710.2009.

Sadeghi, S. G., Minor, L. B. & Cullen, K. E. (2007). Response of vestibular-nerve afferents to active and passive rotations under normal conditions and after unilateral labyrinthectomy. *J. Neurophysiol.* 97, 1503–1514.

Sadeghi, S. G., Minor, L. B., & Cullen, K. E. (2006). Dynamics of the horizontal vestibuloocular reflex after unilateral labyrinthectomy: response to high frequency, high acceleration, and high velocity rotations. *Experimental brain research*, *175*(3), 471-484.

Saglam, M., Glasauer, S. & Lehnen, N. (2014). Vestibular and cerebellar contribution to gaze optimality. *Brain* 137, 1080–1094.

Sasaki, H., Kojima, H., Yabe, I., Tashiro, K., Hamada, T., Sawa, H., ... & Nagashima, K. (1998). Neuropathological and molecular studies of spinocerebellar ataxia type 6 (SCA6). *Acta neuropathologica*, *95*(2), 199-204.

Sato, F., and Sasaki, H. (1993). Morphological correlations between spontaneously discharging primary vestibular afferents and vestibular nucleus neurons in the cat. *J Comp Neurol* 333, 554–566. doi:10.1002/cne.903330408.

Sato, H., & Noda, H. (1992). Saccadic dysmetria induced by transient functional decoration of the cerebellar vermis. *Experimental brain research*, *88*(2), 455-458.

Satoh, J. I., Tokumoto, H., Yukitake, M., Matsui, M., Matsuyama, Z., Kawakami, H., ... & Kuroda, Y. (1998). Spinocerebellar ataxia type 6: MRI of three Japanese patients. *Neuroradiology*, *40*(4), 222-227.

Schindelin, J., Arganda-Carreras, I., Frise, E., Kaynig, V., Longair, M., Pietzsch, T., … Cardona, A. (2012). Fiji: an open-source platform for biological-image analysis. *Nature Methods*, *9*(7), 676–682.

Schneider, G. T., Lee, C., Sinha, A. K., Jordan, P. M., and Holt, J. C. (2021). The mammalian efferent vestibular system utilizes cholinergic mechanisms to excite primary vestibular afferents. *Sci Rep-uk* 11, 1231. doi:10.1038/s41598-020-80367-1.

Schöls, L., Krüger, R., Amoiridis, G., Przuntek, H., Epplen, J. T., & Riess, O. (1998). Spinocerebellar ataxia type 6: genotype and phenotype in German kindreds. *Journal of Neurology, Neurosurgery & Psychiatry*, *64*(1), 67-73.

Shakkottai, V. G., do Carmo Costa, M., Dell'Orco, J. M., Sankaranarayanan, A.Wulff, H., & Paulson, H. L. (2011). Early changes in cerebellar physiology accompany motor dysfunction in the polyglutamine disease spinocerebellar ataxia type 3. *Journal of Neuroscience*, *31*(36), 13002-13014.

Shakkottai, V. G., Xiao, M., Xu, L., Wong, M., Nerbonne, J. M., Ornitz, D. M., & Yamada, K. A. (2009). FGF14 regulates the intrinsic excitability of cerebellar Purkinje neurons. *Neurobiology of disease*, *33*(1), 81-88.

Shanidze, N., Lim, K., Dye, J., & King, W. M. (2012). Galvanic stimulation of the vestibular periphery in guinea pigs during passive whole body rotation and self-generated head movement. *Journal of neurophysiology*, *107*(8), 2260-2270.

Sharp, P. E., Blair, H. T., & Cho, J. (2001). The anatomical and computational basis of the rat head-direction cell signal. *Trends in neurosciences*, *24*(5), 289-294.

Sheliga, B. M., Yakushin, S. B., Silvers, A., Raphan, T., & Cohen, B. (1999). Control of spatial orientation of the angular vestibulo-ocular reflex by the nodulus and uvula of the vestibulocerebellum. *Annals of the New York Academy of Sciences*, *871*(1), 94-122.

Shen, J., Scheffer, D. I., Kwan, K. Y. & Corey, D. P. (2015). SHIELD: an integrative gene expression database for inner ear research. *Database (Oxf.)* 2015, bav071

Shinder, M. E., Purcell, I. M., Kaufman, G. D., & Perachio, A. A. (2001). Vestibular efferent neurons project to the flocculus. *Brain research*, *889*(1-2), 288-294.

Shojaku, H., Barmack, N. H., & Mizukoshi, K. (1991). Influence of vestibular and visual climbing fiber signals on Purkinje cell discharge in the cerebellar nodulus of the rabbit. *Acta Oto-Laryngologica*, *111*(sup481), 242-246.

Stoyas, C. A., Bushart, D. D., Switonski, P. M., Ward, J. M., Alaghatta, A., Tang, M. B., ... & La Spada, A. R. (2020). Nicotinamide pathway-dependent Sirt1 activation restores calcium homeostasis to achieve neuroprotection in spinocerebellar ataxia type 7. *Neuron*, *105*(4), 630-644.

Siebold, C., Glonti, L., Glasauer, S., & Buttner, U. (1997). Rostral fastigial nucleus activity in the alert monkey during three-dimensional passive head movements. *Journal of neurophysiology*, *77*(3), 1432-1446.

Simmons, D. D., Tong, B., Schrader, A. D. & Hornak, A. J. Oncomodulin identifies different hair cell types in the mammalian inner ear. *J. Comp. Neurol.* 518, 3785–3802 (2010).

Skaggs, W., Knierim, J., Kudrimoti, H., & McNaughton, B. (1994). A model of the neural basis of the rat's sense of direction. *Advances in neural information processing systems*, *7*.

Slemmer, J. E., Haasdijk, E. D., Engel, D. C., Plesnila, N., & Weber, J. T. (2007). Aldolase C-positive cerebellar Purkinje cells are resistant to delayed death after cerebral trauma and AMPA-mediated excitotoxicity. *European Journal of Neuroscience*, *26*(3), 649-656.

Solodkin, A., & Gomez, C. M. (2012). Spinocerebellar ataxia type 6. In Handbook of Clinical Neurology (1st ed., Vol. 103). Elsevier B.V.

Songer, J. E. & Eatock, R. A. (2013). Tuning and timing in mammalian type I hair cells and calyceal synapses. *J. Neurosci.* 33, 3706–3724.

Soto, E., and Vega, R. (2010). Neuropharmacology of Vestibular System Disorders. *Curr Neuropharmacol* 8, 26–40. doi:10.2174/157015910790909511.

Spoon, C., Moravec, W. J., Rowe, M. H., Grant, J. W. & Peterson, E. H. (2011). Steady-state stiffness of utricular hair cells depends on macular location and hair bundle structure. *J. Neurophysiol.* 106, 2950–2963.

Stahl, J. S. (2004). Eye movements of the murine P/Q calcium channel mutant rocker, and the impact of aging. *Journal of neurophysiology*, *91*(5), 2066-2078.

Stahl, J. S. (2004). Using eye movements to assess brain function in mice. *Vis. Res* 44, 3401–3410.

Stahl, J. S., & Thumser, Z. C. (2012). Dynamics of abducens nucleus neurons in the awake mouse. *Journal of Neurophysiology*, *108*(9), 2509–2523.

Stahl, J. S., & Thumser, Z. C. (2014). Flocculus Purkinje cell signals in mouse Cacna1a calcium channel mutants of escalating severity: an investigation of the role of firing irregularity in ataxia. *Journal of neurophysiology*, *112*(10), 2647-2663.

Stahl, J. S., James, R. A., Oommen, B. S., Hoebeek, F. E., & De Zeeuw, C. I. (2006). Eye movements of the murine P/Q calcium channel mutant tottering, and the impact of aging. *Journal of neurophysiology*, *95*(3), 1588-1607.

Stone, L. S., & Lisberger, S. G. (1990). Visual responses of Purkinje cells in the cerebellar flocculus during smooth-pursuit eye movements in monkeys. I. Simple spikes. *Journal of neurophysiology*, *63*(5), 1241-1261.

Stoyas, C. A., Bushart, D. D., Switonski, P. M., Ward, J. M., Alaghatta, A., Tang, M. B., ... & La Spada, A. R. (2020). Nicotinamide pathway-dependent Sirt1 activation restores calcium homeostasis to achieve neuroprotection in spinocerebellar ataxia type 7. *Neuron*, *105*(4), 630-644.

Straka, H., Zwergal, A. & Cullen, K. E. (2015). Vestibular animal models: contributions to understanding physiology and disease. *J. Neurol.* 263(Suppl. 1), S10–S23.

Strick, P. L. (1985). The Cerebellum: The Cerebellum and Neural Control. Masao Ito. Raven, New York, 1984. xviii, 580 pp., illus. $75. *Science*, *229*(4713), 547-547.

Strupp, M., Kalla, R., Claassen, J., Adrion, C., Mansmann, U., Klopstock, T., ... & Jahn, K. (2011). A randomized trial of 4-aminopyridine in EA2 and related familial episodic ataxias. *Neurology*, *77*(3), 269-275.

Strupp, M., Kalla, R., Dichgans, M., Freilinger, T., Glasauer, S., & Brandt, T. (2004). Treatment of episodic ataxia type 2 with the potassium channel blocker 4-aminopyridine. *Neurology*, *62*(9), 1623-1625.

Suzuki, D. A., & Keller, E. L. (1982). Vestibular signals in the posterior vermis of the alert monkey cerebellum. *Experimental Brain Research*, *47*(1), 145-147

Suzuki, D. A., & Keller, E. L. (1988). The role of the posterior vermis of monkey cerebellum in smooth-pursuit eye movement control. I. Eye and head movement-related activity. *Journal of Neurophysiology*, *59*(1), 1-18.

Swensen AM, Bean BP (2003) Ionic mechanisms of burst firing in dissociated Purkinje neurons. Journal of Neuroscience 23:9650-9663.

Sylvestre, P. A. & Cullen, K. E. (2006). Premotor correlates of integrated feedback control for eye-head gaze shifts. *J. Neurosci.* 26, 4922–4929.

Sylvestre, P. A., Choi, J. T. L., & Cullen, K. E. (2003). Discharge dynamics of oculomotor neural integrator neurons during conjugate and disjunctive saccades and fixation. *Journal of Neurophysiology*, *90*(2), 739–754.

Takeichi, N., Fukushima, K., Sasaki, H., Yabe, I., Tashiro, K., & Inuyama, Y. (2000). Dissociation of smooth pursuit and vestibulo-ocular reflex cancellation in SCA-6. *Neurology*, *54*(4), 860-866.

Taube, J. S. (1998). Head direction cells and the neurophysiological basis for a sense of direction. *Progress in Neurobiology*, *55*(3), 225–256.

Taube, J. S. (2007). The head direction signal: Origins and sensory-motor integration. *Annual Review of Neuroscience*, *30*, 181–207.

Taube, J. S., Muller, R. U., & Ranck, J. B. (1990). Head-direction cells recorded from the postsubiculum in freely moving rats. I. Description and quantitative analysis. *Journal of Neuroscience*, *10*(2), 420–435.

Terreros, G., Jorratt, P., Aedo, C., Elgoyhen, A. B., and Delano, P. H. (2016). Selective attention to visual stimuli using auditory distractors is altered in alpha-9 nicotinic receptor subunit knock-out mice. J. Neurosci. 36, 7198–7209. doi:10.1523/JNEUROSCI.4031-15.2016.

Terwindt, G. M., Ophoff, R. A., Haan, J., Frants, R. R., Ferrari, M. D., & DMGRG. (1996). Familial hemiplegic migraine: a clinical comparison of families linked and unlinked to chromosome 19. *Cephalalgia*, *16*(3), 153-155.

Thier, P., & Möck, M. (2006). The oculomotor role of the pontine nuclei and the nucleus reticularis tegmenti pontis. *Progress in brain research*, *151*, 293-320.

Toscano-Márquez, B., Cook, A. A., Rice, M., Smileski, A., Vieira-Lomasney, K., Charron, F., ... & Watt, A. J. (2021). Molecular identity and location influence Purkinje cell vulnerability in ARSACS mice. *Frontiers in cellular neuroscience*, 485.

Tottene, A., Conti, R., Fabbro, A., Vecchia, D., Shapovalova, M., Santello, M., ... & Pietrobon, D. (2009). Enhanced excitatory transmission at cortical synapses as the basis for facilitated spreading depression in CaV2. 1 knockin migraine mice. *Neuron*, *61*(5), 762-773.

Tu, L., Poppi, L., Rudd, J., Cresswell, E. T., Smith, D. W., Brichta, A., et al. (2017). Alpha-9 nicotinic acetylcholine receptors mediate hypothermic responses elicited by provocative motion in mice. *Physiol Behav* 174, 114–119.

Tung, V. W., Burton, T. J., Dababneh, E., Quail, S. L. & Camp, A. J. (2014). Behavioral assessment of the aging mouse vestibular system. *J. Vis. Exp.* https://doi.org/10.3791/51605.

Turcan, S., Slonim, D. K., & Vetter, D. E. (2010). Lack of nAChR activity depresses cochlear maturation and up-regulates GABA system components: temporal profiling of gene expression in α9 null mice. *PloS one*, *5*(2), e9058.

Unno, T., Wakamori, M., Koike, M., Uchiyama, Y., Ishikawa, K., Kubota, H., ... & Watase, K. (2012). Development of Purkinje cell degeneration in a knockin mouse model reveals lysosomal involvement in the pathogenesis of SCA6. *Proceedings of the National Academy of Sciences*, *109*(43), 17693-17698.

Usowicz, M. M., Sugimori, M., Cherksey, B., & Llinás, R. (1992). P-type calcium channels in the somata and dendrites of adult cerebellar Purkinje cells. *Neuron*, *9*(6), 1185-1199.

Vetter, D. E., Liberman, M. C., Mann, J., Barhanin, J., Boulter, J., Brown, M. C., ... & Elgoyhen, A. B. (1999). Role of α9 nicotinic ACh receptor subunits in the development and function of cochlear efferent innervation. *Neuron*, *23*(1), 93-103.

Vijayakumar, S. et al. Rescue of peripheral vestibular function in Usher syndrome mice using a splice-switching antisense oligonucleotide. *Hum. Mol. Genet.* 26, 3482–3494 (2017).

Vijayakumar, S. et al. (2015). Vestibular dysfunction, altered macular structure and trait localization in A/J inbred mice. *Mamm. Genome* 26, 154–172.

Voogd, J., & Bigaré, F. (1980). The inferior olivary nucleus: anatomy and physiology.

Voogd, J., Jaarsma, D., & Marani, E. (1996). The cerebellum: chemoarchitecture and anatomy. *Handbook of chemical neuroanatomy*, *12*, 1-369.

Wackym, P. A., Popper, P., & Micevych, P. E. (1993). Distribution of calcitonin gene-related peptide mRNA and immunoreactivity in the rat central and peripheral vestibular system. *Acta oto-laryngologica*, *113*(5), 601-608.

Waespe, W., Büttner, U., & Henn, V. (1981). Input-output activity of the primate flocculus during visual-vestibular interaction. *Annals of the New York Academy of Sciences*, *374*, 491-503.

Waespe, W., Büttner, U., & Henn, V. (1981). Visual-vestibular interaction in the flocculus of the alert monkey. *Experimental Brain Research*, *43*(3), 337-348.

Walter, J. T., Alviña, K., Womack, M. D., Chevez, C., & Khodakhah, K. (2006). Decreases in the precision of Purkinje cell pacemaking cause cerebellar dysfunction and ataxia. *Nature Neuroscience*, 9(3), 389–397.

Watanabe, E. (1984). Neuronal events correlated with long-term adaptation of the horizontal vestibulo-ocular reflex in the primate flocculus. *Brain research*, *297*(1), 169-174.

Watase, K., Barrett, C. F., Miyazaki, T., Ishiguro, T., Ishikawa, K., Hu, Y., ... & Zoghbi, H. Y. (2008). Spinocerebellar ataxia type 6 knockin mice develop a progressive neuronal dysfunction with age-dependent accumulation of mutant CaV2. 1 channels. *Proceedings of the National Academy of Sciences*, *105*(33), 11987-11992.

Wearne, S., Raphan, T., & Cohen, B. (1996). Nodulo-Uvular Control of Central Vestibular Dynamics Determines Spatial Orientation of the Angular Vestibulo-Ocular Reflex a. *Annals of the New York Academy of Sciences*, *781*(1), 364-384.

Wearne, S., Raphan, T., & Cohen, B. (1998). Control of spatial orientation of the angular vestibuloocular reflex by the nodulus and uvula. *Journal of neurophysiology*, *79*(5), 2690-2715.

Westenbroek, R. E., Sakurai, T., Elliott, E. M., Hell, J. W., Starr, T. V., Snutch, T. P., & Catterall, W. A. (1995). Immunochemical identification and subcellular distribution of the alpha 1A subunits of brain calcium channels. *Journal of Neuroscience*, *15*(10), 6403-6418.

Wiest, G., Tian, J. R., Baloh, R. W., Crane, B. T., & Demer, J. L. (2001). Otolith function in cerebellar ataxia due to mutations in the calcium channel gene CACNA1A. *Brain*, *124*(12), 2407-2416.

Womack M, Khodakhah K (2002) Active contribution of dendrites to the tonic and trimodal patterns of activity in cerebellar Purkinje neurons. Journal of Neuroscience 22:10603- 10612.

Womack MD, Khodakhah K (2003) Somatic and dendritic small-conductance calcium-activated potassium channels regulate the output of cerebellar Purkinje neurons. Journal of Neuroscience 23:2600-2607.

Womack, M. D., Chevez, C., & Khodakhah, K. (2004). Calcium-activated potassium channels are selectively coupled to P/Q-type calcium channels in cerebellar Purkinje neurons. *Journal of Neuroscience*, *24*(40), 8818-8822.

Womack, M., & Khodakhah, K. (2002). Active contribution of dendrites to the tonic and trimodal patterns of activity in cerebellar Purkinje neurons. *Journal of Neuroscience*, *22*(24), 10603-10612

Yakusheva, T. A., Shaikh, A. G., Green, A. M., Blazquez, P. M., Dickman, J. D., & Angelaki, D. E. (2007). Purkinje cells in posterior cerebellar vermis encode motion in an inertial reference frame. *Neuron*, *54*(6), 973-985.

Yamada, J., & Noda, H. (1987). Afferent and efferent connections of the oculomotor cerebellar vermis in the macaque monkey. *Journal of comparative neurology*, *265*(2), 224-241.

Yamashita, T., Ohnishi, S., Ohtani, M., and Kumazawa, T. (2009). Effects of Efferent Neurotransmitters on Intracellular Ca2+ Concentration in Vestibular Hair Cells of the Guinea Pig. *Acta Oto-laryngol* 113, 26–30. doi:10.3109/00016489309126173.

Yang, Q., Hashizume, Y., Yoshida, M., Wang, Y., Goto, Y., Mitsuma, N., ... & Mizusawa, H. (2000). Morphological Purkinje cell changes in spinocerebellar ataxia type 6. *Acta neuropathologica*, *100*(4), 371-376.

Yashiro, K. et al. (2004). Regulation of retinoic acid distribution is required for proximodistal patterning and outgrowth of the developing mouse limb. *Dev. Cell* 6.

Ying, S. H., Choi, S. I., Lee, M., Perlman, S. L., Baloh, R. W., Toga, A. W., & Zee, D. S. (2005). Relative atrophy of the flocculus and ocular motor dysfunction in SCA2 and SCA6. *Annals of the New York Academy of Sciences*, *1039*(1), 430-435.

Yoder, R. M., & Taube, J. S. (2014). The vestibular contribution to the head direction signal and navigation. *Frontiers in Integrative Neuroscience*, *8*(APR), 1–13.

Yu-Wai-Man, P., Gorman, G., Bateman, D. E., Leigh, R. J., & Chinnery, P. F. (2009). Vertigo and vestibular abnormalities in spinocerebellar ataxia type 6. *Journal of neurology*, *256*(1), 78-82.

Zhang, J., Smith, D., Yamamoto, M., Ma, L. & McCaffery, P. (2003). The meninges is a source of retinoic acid for the late-developing hindbrain. *J. Neurosci.* 23, 7610–7620.

Zhang, K. (1996). Representation of spatial orientation by the intrinsic dynamics of the head-direction cell ensemble: A theory. *Journal of Neuroscience*, *16*(6), 2112–2126.

Zhao, X. et al. (2009). Retinoic acid promotes limb induction through effects on body axis extension but is unnecessary for limb patterning. *Curr. Biol.* 19, 1050–1057.

Zhuchenko, O., Bailey, J., Bonnen, P., Ashizawa, T., Stockton, D. W., Amos, C., ... & Lee, C. C. (1997). Autosomal dominant cerebellar ataxia (SCA6) associated with small polyglutamine expansions in the α1A-voltage-dependent calcium channel. *Nature genetics*, *15*(1), 62-69.

Zugaro, M. B., Arleo, A., Berthoz, A., & Wiener, S. I. (2003). Rapid spatial reorientation and head direction cells. *Journal of Neuroscience*, *23*(8), 3478–3482.

Zwingman, T. A., Neumann, P. E., Noebels, J. L., & Herrup, K. (2001). Rocker is a new variant of the voltage-dependent calcium channel gene Cacna1a. *Journal of Neuroscience*, *21*(4), 1169-1178.